

# STUDIES OF THERAPEUTIC PROTEIN TARGET: ORNITHINE DECARBOXYLASE FROM *ENTAMOEBIA HISTOLYTICA*

## A THESIS

*Submitted in partial fulfilment of the  
requirements for the award of the degree*

*of*

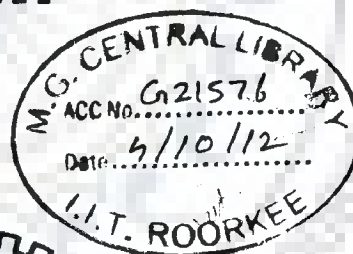
DOCTOR OF PHILOSOPHY

*in*

BIOTECHNOLOGY

*by*

**PREETI**



DEPARTMENT OF BIOTECHNOLOGY  
INDIAN INSTITUTE OF TECHNOLOGY ROORKEE  
ROORKEE-247 667 (INDIA)

APRIL, 2012



# INDIAN INSTITUTE OF TECHNOLOGY ROORKEE ROORKEE

## CANDIDATE'S DECLARATION

I hereby certify that the work which is being presented in the thesis entitled **STUDIES OF THERAPEUTIC PROTEIN TARGET: ORNITHINE DECARBOXYLASE FORM ENTAMOEBA HISTOLYTICA** in partial fulfilment of the requirements for the award of the Degree of Doctor of Philosophy and submitted in the Department of Biotechnology of the Indian Institute of Technology Roorkee, Roorkee is an authentic record of my own work carried out during a period from July 2007 to April 2012 under the supervision of Dr. Shailly Tomar, Assistant Professor, Department of Biotechnology, Indian Institute of Technology Roorkee, Roorkee.

The matter presented in this thesis has not been submitted by me for the award of any other degree of this or any other Institute.

*Preeti*  
(PREETI)

This is to certify that the above statement made by the candidate is correct to the best of my knowledge.

Dated: 12<sup>th</sup> April 2012

*Shailly Tomar*  
(Shailly Tomar)  
Supervisor

The Ph.D. Viva-Voce Examination of Ms. **PREETI**, Research Scholar, has been held on

..... 25.06.2012 .....

*Shailly Tomar*  
Signature of Supervisor

*S. S. Rastogi*  
25.06.2012  
Signature of Chairman SRC

*Puneet Kaur*  
Signature of External Examiner

*Shailly Tomar*  
Signature of Head of the Dept./Chairman ODC

## Abstract

*Entamoeba histolytica* is a single-celled parasitic protozoan responsible for causing amoebiasis. The parasite infects liver and intestine, which may cause mild diarrhea and life threatening abscessions. *E. histolytica* is responsible for over 50 million infections in tropical and temperate regions, and nearly 100,000 deaths worldwide each year. Polyamine biosynthesis pathway enzymes are potential drug targets in parasitic protozoan diseases. The first and rate-limiting step of this pathway is catalyzed by ornithine decarboxylase (ODC). ODC enzyme functions as an obligate homodimer and active site is located at the dimer interface. However, partially purified ODC from *E. histolytica* (*Eh*ODC) is reported to exist in a pentameric state. The drug  $\alpha$ -difluoromethylornithine (DFMO), a potent substrate analogue inhibitor of ODC, is widely used for the treatment of various diseases including *Trypanosoma brucei* infections. However, this drug is ineffective against *E. histolytica*. To analyze such differences we compared the sequence of *Eh*ODC enzyme with ODCs from wide range of organisms, which demonstrated the conservation of the sequence of *Eh*ODC at the active site and dimer interface. We re-investigated the oligomerization state of *Eh*ODC to identify and characterize the active oligomeric form of *Eh*ODC. Size-exclusion chromatography and mass spectrophotometry analysis revealed that *Eh*ODC enzyme exists in the dimeric form.

Further, computational model of *Eh*ODC dimer was generated. Molecular dynamic simulations were performed and the dimeric structure was found to be very stable with RMSD value  $\sim 0.327$  nm. We have generated different mutants by site-directed mutagenesis to determine that the dimeric state is the active form of *Eh*ODC and to study the role of residues at the dimer interface. These studies signifies that active *Eh*ODC is a functional homodimer where two active site pockets form at the interface due to some long and short range of interactions at the interface. The residues important for dimer formation present at the interface are responsible for keeping two monomers in close proximity. Disruption of dimer disfigured the active site pocket which results in the inactivation of *Eh*ODC enzyme. Further, realizing the importance of structure based drug designing, we determined the crystal structure of *Eh*ODC at 2.8 Å resolution. Structure was solved by molecular replacement method. The enzyme forms orthorhombic crystal exhibiting  $P2_12_12_1$  symmetry

with unit cell parameters  $a = 76.66$ ,  $b = 119.28$ ,  $c = 179.28$  Å. Structure, sequence and phylogenetic studies of *Eh*ODC reveal its evolutionary relationship with homologs of active and inactive ODC as well as structural modifications rendering its resistance towards DFMO.

This thesis is divided into five chapters and covers the characterization of therapeutically important protein: ornithine decarboxylase from *Entamoeba histolytica*, which is Pyridoxal 5' phosphate dependent enzyme of fold III group IV decarboxylase. Enzyme has been characterized on the basis of biochemical, mutational, *in silico* and 3D crystal structure analysis.

**Chapter 1** Reviews the literature; describes the life cycle and the genome organization of *Entamoeba histolytica*, metabolic pathways; polyamine biosynthetic pathway; role of polyamines in various life processes; regulation of polyamine biosynthesis by ornithine decarboxylase (ODC); pyridoxal 5' phosphate dependent enzymes; classification of ODC; reaction mechanism and Inhibition of ODC; regulation of ODC by antizyme and antizyme inhibitor; structural and mutational studies of ODC.

**Chapter 2** Describes the over-expression, purification and biochemical characterization of recombinant *Eh*ODC. The expression of *Eh*ODC enzyme was done in *E. coli* BL21 (DE3) cells transformed with pET30a-*Eh*ODC construct having enterokinase cleavage site. Protein was purified to homogeneity by two step procedure that employed metal ion affinity chromatography followed by gel filtration chromatography. Protein was found to be expressed best at 18 °C for 14 hours. Enzymatic activity of *Eh*ODC was determined spectrophotometrically by product (putrescine) detection colorimetric assay and found to be active in the presence of L-ornithine. Oligomeric state determination was done by various methods. 1) Crosslinking experiment was performed using 40 µl glutaraldehyde solution (12.5 % v/v) acidified with 1 µl 5 N HCl. The sample was analysed on 12 % SDS-PAGE and found to be crosslinked to form dimer of ~90 kDa. 2) The purified protein was applied onto a HiLoad 16/60 Superdex 200 gel filtration column and compared with elution volume of standard protein marker. It was confirmed to be a dimer of ~90 kDa. 3) Matrix-assisted laser desorption/ionization time of flight mass spectrometry (MALDI/TOF MS) was performed. The mass spectrometer revealed two peaks corresponding to molecular weight ~45 kDa and

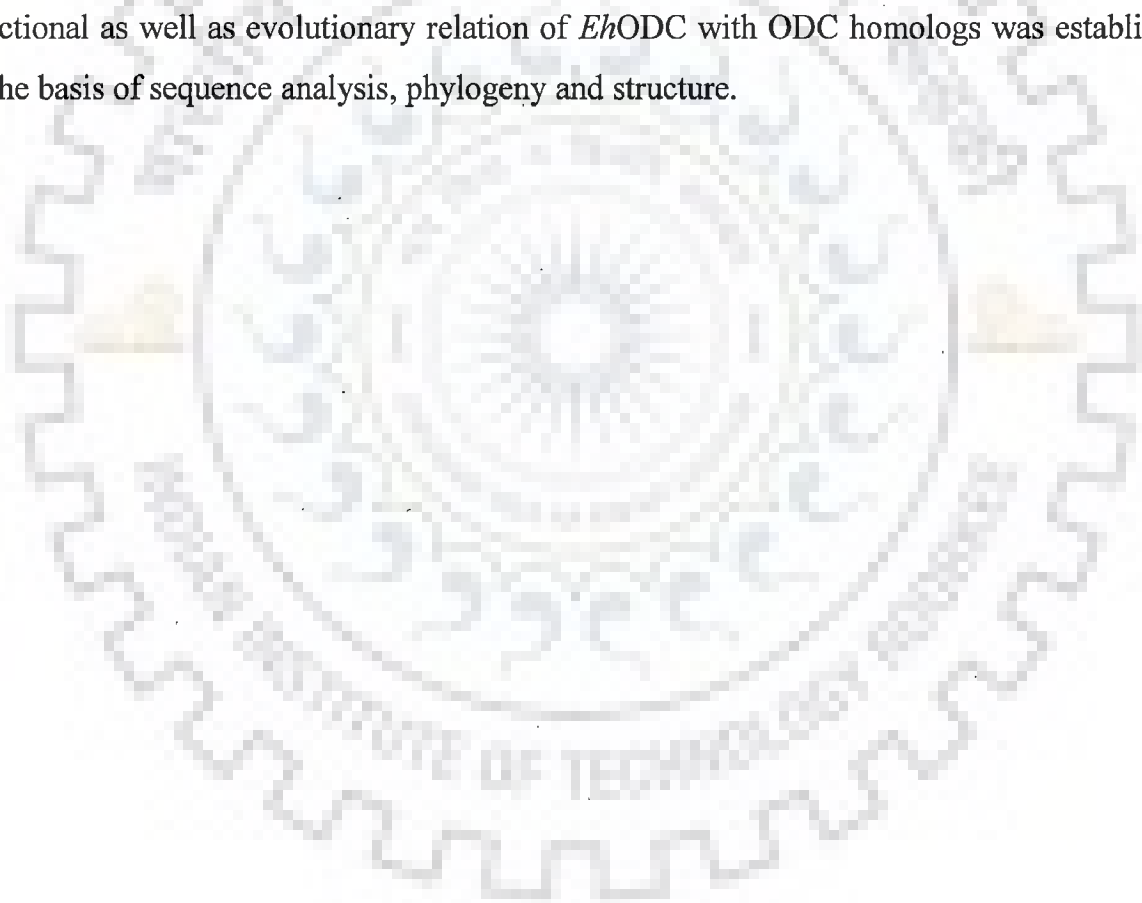


~90 kDa. **4)** The effect of urea and NaCl on oligomeric state of *Eh*ODC was determined at different concentrations (2 M or 4 M), and analyzed by loading on Hi-load 16/60 superdex 200 gel filtration column. The concentration of urea and NaCl were estimated to have adverse effect on the oligomeric state of protein and increase in concentration result in the disruption of the dimer to monomer. For secondary structure determination circular dichroism (CD) of protein was performed. The secondary structure content of *Eh*ODC was comparable to other well characterized ODC.

**Chapter 3** Describes the bioinformatics, computational analysis and molecular modeling of *Eh*ODC. Three-dimensional (3D) homology model of *Eh*ODC homodimer was generated by comparative modeling using MODELLER 9v8. Molecular dynamics (MD) simulation of dimeric model of *Eh*ODC was performed using GROMACS (v 4.5.4) package. The homodimer contains two separate active sites at the dimer interface with Lys57 and Cys334 residues of opposite monomers contributing to each active site. Molecular dynamic simulation was performed and the dimeric structure was found to be very stable with RMSD value ~0.327 nm.

**Chapter 4** Describes the site directed mutagenesis studies of *Eh*ODC. Residues playing critical role at the active site and at dimer interface were studied in detail. The residues present at the interface and responsible for dimer stability and active site residues responsible for catalysis were mutated. Expression, purification and enzymatic activity of different mutants were done using the same protocol as used for purification of wild type *Eh*ODC. The results revealed that mutation of Lys57Ala or Cys334Ala completely abolishes enzyme activity. Interestingly, partial restoration of the enzyme activity was observed when inactive Lys57Ala and Cys334Ala mutants were mixed confirming that the dimer is the active form. Gly361Tyr and Lys157Ala mutations at the dimer interface were found to abolish the enzyme activity. Gel filtration chromatography analysis revealed that Gly361Tyr mutant was showing two peaks at the elution volume corresponding to dimer (~90 kDa) and monomer (~46 kDa). Further, Gly361Tyr-Lys157Ala double mutant of *Eh*ODC was expressed at very high concentration of IPTG and found to very unstable during purification.

**Chapter 5** Describes the crystal structure of ornithine decarboxylase from *Entamoeba histolytica*. Cloning of the C-terminal truncated construct of *Eh*ODC was done in pET28c with TEV protease cleavage site. Expression, purification and enzymatic activity of  $15\Delta cEh$ ODC was done using the same protocol as used for purification of wild type *Eh*ODC. The crystals were grown at 20 °C by sitting drop vapor diffusion method using 2  $\mu$ l of protein solution mixed with 1  $\mu$ l of reservoir solution containing 20 % PEG 3350 in 0.2 M LiCl solution maintained at pH 6.8 as provided in Hampton PEG ION screen. All diffraction data were collected using rotating anode X-ray source and solved by molecular replacement method. The orthorhombic crystal exhibiting  $P2_12_12_1$  symmetry with unit cell parameters  $a = 76.66$ ,  $b = 119.28$ ,  $c = 179.28$  Å. Sequence analysis revealed that *Eh*ODC is an evolutionary bridge between functional ornithine decarboxylase and nonfunctional antizyme inhibitor. Functional as well as evolutionary relation of *Eh*ODC with ODC homologs was established on the basis of sequence analysis, phylogeny and structure.



## Acknowledgement

With immense pleasure, I would like to thank my heavenly father, who has stood by me and helped me along the way. I would also like to thank my family and all the people who have helped me in one way or other during my research tenure. I express my sincere gratitude towards my supervisor, **Dr. Shailly Tomar**, for her constructive criticism, excellent guidance and encouragement to bring the present work to conclusion.

My sincere thanks to Professor. Rentala Madhubala, School of Life Sciences, Jawaharlal Nehru University, New Delhi, India who believed in me and allowed me to work on her project. Without her able guidance I would have not been able to fill color in my thesis.

I am also thankful to Genomics and Proteomics Facility of TCGA (New Delhi, India) for their timely assistance in recording the spectra and sequencing of genes for various constructs. I endow special thanks to Dr. Pravindra Kumar, for helping me in understanding the realm of structure biology and bioinformatics. His advises and collaboration with my lab was so helpful, and I couldn't have succeeded without his esteemed presence. I am also thankful to Dr. Karthikeyan Subramanian for helpful discussion especially during crystallographic analysis of the protein. It is my great pleasure to thank Prof. Ritu Barthwal Coordinator, NMR facility at IIC of the institute, for help and support.

I would like to thank my committee members, Prof. G. S Randhawa, Dr. Sishir Sinha and Dr. Ashwini Kumar Sharma. Not only I have learned so much from them my research work, but also they have advised me in all aspects of my academic career. I am very fortunate to have such helpful committee members.

I am grateful to the faculty members Prof. R. P. Singh, Prof. Ritu Barthwal, Prof. H. S. Dhaliwal, Dr. R. Prasad, Dr. Partha Roy, Dr. Vikas Pruthi, Dr. Bijan Chaudhary, Dr. Sanjoy Ghosh, Dr. Naveen K. Navani, Dr. Ranjana Pathania and Dr. Maya Nair for their encouragement and helpful advises.

I am obliged to my group members Sushmita, Dipak, Shivendra, Aditya, Pramod, Manju, Sonali, Navneet, Deepankar, Saurabh, Girijesh, Prabhat, Bibekananda, Preeti, Nidhi, Anamika for their sincere efforts, amiable attitude and cooperation in the lab. I am greatly indebted to Manali, Satya, Selva, Megha, and Rajat who created an excellent work environment and understanding the frustrations of research and helped me in all possible ways for struggle through my difficult time.

I owe special thanks to my pals Manali, Vivek, Ashish, Adeel, Archana, Pankaj, Payal, and Rupal for their love and constant support. I am thankful to Manali for her support in broaching my career, believing in my capabilities and encouraging for pursuing my higher studies in this field. I am also grateful to Aruna, Neha, Nivedita, Rashmi, Prachi, Swati, Pradeep, Shweta, Charu and Geetu, for providing support and friendship that I needed. A million thanks to Satya, without him I would not have reached to this height of my career graph.

Last but not least, I thank my parents, Vinod Kumar and Sunita Rani, for giving me life, for blessing and unconditional love. They always encouraged me to pursue my interest while spending their life in tough time and working hard to fulfill all my needs. They are huge source of inspiration to me and my devotion and respect for them will be forever. I also want to acknowledge my grandparents Banarsi, Chandrakala, Perulal and Radha for their love and blessings. I am obliged to my sister Jyoti for her unconditional love and support, and for always believing in me. I have spent a quality time with her and my niece Divyansha whenever I felt low in my research. I thank my brothers Arun, Rahul and Vikram for their constant love and moral support. My words are insufficient to express my thanks to my brother Arun and Lokesh who helped me a lot to work on bioinformatics in Linux platform. I also thank my uncle and aunty and cousins for their love.

Finally I would like to thank to Council of Scientific & Industrial Research (CSIR), New Delhi India for financial assistance as (JRF and SRF).

**(PREETI)**

## LIST OF PUBLICATIONS

- 1) **Preeti**, Satya Tapas, Pravindra Kumar, Rantala Madhubala and Shailly Tomar. Biochemical, mutational and *in silico* structural evidence for a functional dimeric form of the ornithine decarboxylase from *Entamoeba histolytica*. *PLoS Neglected Tropical Diseases*. 2012, 6: e1559. doi:10.1371/journal.pntd.0001559.
- 2) Satya Tapas, Abhinav Kumar, Sonali Dhindwal, **Preeti**, Pravindra Kumar. Structural analysis of chorismate synthase from *Plasmodium falciparum*: A novel target for anti-malaria drug discovery. *International Journal of Biological Macromolecules*. 2011, 49: 767-777.
- 3) Sakshi Tomar, Dipak N. Patil, Manali Datta, Satya Tapas, **Preeti**, Ashwani K. Sharma, Shailly Tomar and Pravindra Kumar. Crystallization, and preliminary X-ray diffraction analysis of the complex of Kunitz-type tamarind trypsin inhibitor and porcine pancreatic trypsin. *Acta Cryst F*. 2009, 65: 1179-1181.
- 4) Dipak N. Patil, **Preeti**, Anshul Chaudhry, Ashwani K. Sharma, Shailly Tomar and Pravindra Kumar. Purification, crystallization and preliminary crystallographic studies of a Kunitz-type proteinase inhibitor from tamarind (*Tamarindus indica*) seeds. *Acta Cryst F*. 2009, 65: 736-738.
- 5) **Preeti**, Satya Tapas, Pravindra Kumar, Rantala Madhubala and Shailly Tomar. Structural basis for insensitive of *E. histolytica* ornithine decarboxylase towards DFMO and evolutionary relationship with antizyme inhibitors. (communicated).

# CONTENTS

Page No.

CANDIDATE'S DECLARATION	
DEDICATIONS	
ABSTRACT	i-iv
ACKNOWLEDGEMENTS	v-vi
LIST OF PUBLICATIONS	vii
CONTENTS	viii-xii
LIST OF FIGURES	xiii-xx
LIST OF TABLES	xxi-xxii
LIST OF ABBREVIATIONS USED	xxiii-xxiv
STRUCTURE AND MODELS SUBMITTED TO DATA BANK	xxv
INTRODUCTION	1-3

## CHAPTER 1

### REVIEW OF LITERATURE

1.1	Introduction	4
1.2	Life cycle of <i>Entamoeba histolytica</i>	4
1.3	Genome organization of <i>E. histolytica</i>	6
1.4	Metabolic pathways in <i>E. histolytica</i>	7
1.4.1	Polyamine metabolic pathway	8
1.5	Ornithine decarboxylase gene in the genome	9
1.6	Localization of <i>EhODC</i> within the cell	11
1.7	Polyamines (PAs)	11
1.7.1	Polyamine structure and location in the cell	11
1.7.1.1	Structure of PAs	11
1.7.1.2	Localization of PAs	12
1.7.2	Importance of PA metabolism	12
1.7.3	Physiological characteristics of PAs	13
1.7.3.1	Interaction of PAs with nucleic acids	13
1.7.3.1.1	PAs in DNA stabilization	13
1.7.3.1.2	PAs in RNA stabilization	14
1.7.3.2	PAs in protein synthesis	14
1.7.3.3	PAs in glycolysis	15
1.7.3.4	PAs in oxidative defense mechanism	15
1.7.3.5	PAs in signal transduction	15
1.7.3.6	PAs in mitochondrial metabolism	16
1.7.3.7	PAs in central nervous system	16
1.7.3.8	PAs in angiogenesis and cancer	17
1.7.4	PAs in plants	17
1.7.5	PAs in animal cell cycle	17
1.7.6	PAs in bacteria	19



1.7.7	PAs in protozoa	19
1.7.7.1	PAs in <i>Entamoeba histolytica</i>	20
1.8	Polyamine biosynthetic pathway	21
1.9	Ornithine decarboxylase (ODC)	22
1.9.1	ODC as regulatory enzyme of PA biosynthetic pathway	22
1.9.2	ODC as PLP dependent enzyme	22
1.9.3	Fold type III ODC available	24
1.9.4	Decarboxylase subfamily	24
1.10	Characteristic features of ODCs	25
1.11	Reaction mechanism of ODC	26
1.12	Regulation mechanisms of ODC	28
1.12.1	Antizyme mediated ODC regulation	28
1.12.2	Antizyme inhibitor (AZI) mediated ODC Regulation	29
1.13	Inhibition mechanism of ODC	31
1.13.1	Substrate analogues and derivative	31
1.13.1.1	Inhibition mechanism of substrate analogues	32
1.13.2	Product analogues	33
1.13.2.1	Inhibition mechanism of product analogues	35
1.13.3	Cofactor-substrate analogues	35
1.13.3.1	Inhibition mechanism of cofactor-substrate analogues	35
1.14	Structure of ODC	36
1.14.1	Crystal structures of ODC available	38
1.14.2	Basic structure of ODC from fold type I and III family	40
1.15	Mutational studies of ODC	43

## CHAPTER II

### EXPRESSION, PURIFICATION AND CHARACTERIZATION OF ORNITHINE DECARBOXYLASE FROM *ENTAMOEBEA HISTOLYTICA*

2.1	Abstract	45
2.2	Introduction	45
2.3	Materials and Methods	48
2.3.1	Reagents	48
2.3.2	Methodology	48
2.3.2.1	Expression and solubility of <i>Eh</i> ODC	48
2.3.2.2	Purification of <i>Eh</i> ODC	49
2.3.2.3	<i>Eh</i> ODC enzyme assay	50
2.3.3	Secondary structure analysis	51
2.3.3.1	Far-UV Circular Dichroism spectrum	52
2.3.4	Characterization of oligomeric state of <i>Eh</i> ODC	52
2.3.4.1	Chemical crosslinking	52
2.3.4.2	Molecular mass and oligomeric state determination	53

	2.3.4.3	Effect of Urea and NaCl on <i>Eh</i> ODC oligomerization	54
2.5		Results and Discussion	54
	2.5.1	Plasmid isolation and verification for <i>Eh</i> ODC insert	54
	2.5.2	Nucleotide along with the amino acid code of <i>Eh</i> ODC	56
	2.5.3	Strategy used for <i>Eh</i> ODC protein expression	57
	2.5.4	Expression and solubility of <i>Eh</i> ODC	58
	2.5.5	<i>Eh</i> ODC purification	58
	2.5.6	<i>Eh</i> ODC enzyme activity	61
	2.5.7	Secondary structure analysis of <i>Eh</i> ODC	62
	2.5.8	Characterization of oligomeric state of <i>Eh</i> ODC	63
	2.5.9	Biochemical and biophysical methods	63
	2.5.9.1	Crosslinking analysis	63
	2.5.9.1.1	Glutaraldehyde crosslinking	63
	2.5.9.1.2	DMS crosslinking	64
	2.5.9.2	Gel filtration and MALDI-TOF analysis of <i>Eh</i> ODC	65
	2.5.9.3	Effect of urea and NaCl on oligomeric state of <i>Eh</i> ODC	66
2.6		Conclusion	68

## CHAPTER III

### *IN SILICO* STRUCTURAL ANALYSIS

3.1		Abstract	69
3.2		Introduction	69
3.3		Hardware and software	71
3.4		Methods	72
	3.4.1	Sequence analysis	72
	3.4.2	Secondary structure prediction	72
	3.4.3	Molecular modeling	72
	3.4.4	Molecular dynamics simulation	73
3.5		Results and discussion	74
	3.5.1	Sequence analysis and phylogeny	74
	3.5.2	Secondary structure analysis	79
	3.5.3	Prediction of the disordered regions	81
	3.5.4	Disordered regions in <i>Eh</i> ODC sequence	81
	3.5.5	Generation and stability of 3D model of <i>Eh</i> ODC	83
	3.5.6	Structure analysis of <i>Eh</i> ODC monomeric subunit	84
	3.5.7	Structure analysis of dimeric <i>Eh</i> ODC	86
	3.5.8	Stability of the dimeric model of <i>Eh</i> ODC	87
3.6		Conclusion	89

## CHAPTER IV

### SITE DIRECTED MUTAGENESIS AND CHARACTERIZATION OF ACTIVE SITE AND DIMER INTERFACE RESIDUES

4.1	Abstract	91
4.2	Introduction	91
4.3	Materials and Methods	93
	4.3.1 Reagents	93
	4.3.2 Methodology	93
	4.3.2.1 Site directed mutagenesis	93
	4.3.2.2 Purification, activity and size exclusion chromatography of <i>Eh</i> ODC mutants	95
4.4	Results and discussion	95
	4.4.1 Site directed mutagenesis	95
	4.4.2 Plasmid map for mutant <i>Eh</i> ODC	97
	4.4.3 Analysis of mutated plasmid	97
	4.4.4 Strategy used for site directed mutagenesis of <i>Eh</i> ODC	98
	4.4.5 Purification, activity and size exclusion chromatography of <i>Eh</i> ODC mutants	99
	4.4.6 Characterization of active site mutant <i>Eh</i> ODC	101
	4.4.7 Characterization of interface mutant <i>Eh</i> ODC	103
4.5	Conclusion	106

## CHAPTER V

### CRYSTAL STRUCTURE OF ORNITHINE DECARBOXYLASE FROM *E. HISTOLYTICA* AND INSIGHT INTO BINDING MECHANISM OF DFMO

5.1	Abstract	108
5.2	Introduction	108
5.3	Materials and Methods	111
	5.3.1 Reagents	111
	5.3.2 Methodology	111
	5.3.2.1 Cloning of C-terminal truncated <i>Eh</i> ODC	111
	5.3.2.2 Plasmid map of 15 $\Delta$ c <i>Eh</i> ODC construct	112
	5.3.2.3 Strategy used for cloning and purification	114
	5.3.2.4 Expression and purification	115
	5.3.2.5 Enzymatic activity of 15 $\Delta$ c <i>Eh</i> ODC	115
	5.3.2.6 Gel filtration analysis	115
	5.3.2.7 Crystallization	116
	5.3.2.8 Data collection and structure determination	116
	5.3.2.9 Sequence analysis, model generation, and docking	117

5.4	Result and Discussion	118
5.4.1	Sequence analysis and cloning of 15 $\Delta$ c <i>Eh</i> ODC	118
5.4.2	Expression and purification of 15 $\Delta$ c <i>Eh</i> ODC	119
5.4.3	Oligomeric state analysis in solution	120
5.4.4	Activity of 15 $\Delta$ c <i>Eh</i> ODC	121
5.4.5	Crystal packing	121
5.4.6	Overall structure and folding	125
5.4.7	Active site of <i>Eh</i> ODC	126
5.5	Active site pattern revealing insensitivity towards DFMO	129
5.6	Sequence comparison with other ODC and AZI	132
5.7	Analysis of AZ binding sequence in <i>Eh</i> ODC	138
5.9	Conclusion	140

<b>REFERENCES</b>		141-172
-------------------	--	---------



## LIST OF FIGURES

Page No.

- Figure 1.1: Life cycle of *E. histolytica* showing two major stages: trophozoites and cyst.** 6
- Figure 1.2: The genome organization of *Eh*ODC.** The genome of *Eh*ODC from 5' terminal sequence 58455 to 3' end 59696 denoted in red color with gene marked as EHI\_100430. The stretch of the genome from 53182 bps to 63342 bps contain five protein coding genes out of which only two are known to have some structure- function relationships while other 3 are hypothetical proteins which have not been characterized. 10
- Figure 1.3: Structures of polyamines with their positively charged amino group (Blue color).** 12
- Figure 1.4: Schematic representation of various phases of the cell cycle and the mediators of cell cycle progression.** Progression of cell cycle depends upon different polyamines at different stages of growth. Arrow indicates PAs concentration in the direction of cell cycle progression. The abundancy of different polyamines are indicated by different colors. Presence of all PAs are indicated by green, and presence of spermidine and putrescine are indicated by orange, and absence of PAs are indicated in red. 18
- Figure 1.5: Biosynthetic pathway of polyamines putrescine and higher polyamines.** 1) Ornithine decarboxylase; 2) Spermidine synthase; 3) Spermine synthase. 21
- Figure 1.6: Classification of the Pyridoxal 5' phosphate dependent enzyme on the basis of sequences, secondary structure, biochemical information and hydrophobicity profile.** 22
- Figure 1.7: Classification of decarboxylases into subfamilies on the basis of sequence similarity.** 25
- Figure 1.8: Secondary structure elements and consensus sequence of PLP binding fold type III decarboxylase.** Strands are shown as arrows, helices as cylinders and loops as lines, dashed lines denoted the regions in the sequence that are not conserved (numbered as in mouse ODC). Schiff base is marked by circle. 27
- Figure 1.9: Reaction mechanism of ornithine decarboxylase.** Four steps:- 1) Transamination; 2) Decarboxylation; 3)  $\alpha$ -Protonation and 4) Second transamination. PLP is Pyridoxyl 5' phosphate; L-orn is substrate L-ornithine and Put is the product putrescine. 27
- Figure 1.10: Mechanism of regulation of ODC mediated by Antizyme (AZ) and Antizyme inhibitor (AZI).** AZ binds to recognition site (purple

color) of either ODC or AZI result in the formation of heterodimer complex of AZ-ODC and AZ-AZI. In addition, it also causes dissociation of dimers to monomer. The AZ-ODC complex undergoes degradation mediated by 26S proteasome (gray arrows). AZ-AZI complex formation allows the escape of ODC to undergo degradation and active enzyme catalyzes decarboxylation reaction (black arrows). 30

**Figure 1.11: Reaction mechanism of inhibition of ornithine decarboxylase enzyme (*Tb*ODC) in the presence of DFMO (*T. brucei*).** 34

**Figure 1.12: Structure of product substrate analogue. *N*-(4'-pyridoxal)-ornithine (BOC)-OMe.HCl (POB).** 35

**Figure 1.13: Cartoon diagram of human ODC.** Showing dimer with chain A, chain B in purple and blue color respectively. Structure start with N-terminal of Chain A and end with C-terminal of Chain B. Two active sites at the interface, the ligands shown in green and contacts are marked in red dots. 37

**Figure 1.14: Active site of human ODC.** Showing PLP in yellow color and surrounding residues in gray color, water molecule are indicated by green color interaction between enzyme and cofactor and water molecules have been represented by green color dashed lines. 38

**Figure 1.15: Structure of ODCs from different fold type comprised of common secondary structure and fold pattern of  $\alpha/\beta$ -barrel and  $\beta$ -sheet domain. A) Structure of *T. brucei* ODC B) human ODC, C) mouse ODC D) *Vibrio vulnificus* ODC and E) *Lactobacillus* (30a) ODC.** 41-42

**Figure 2.1: Schematic representation of enzymatic cleavage of substrate L-ornithine to product putrescine and colorimetric assay used to determine the product formation.** 51

**Figure 2.2: Plasmid pET30a-*Eh*ODC.** A) Gel showing cloned plasmid digested with restriction enzymes *Bam*HI and *Xho*I releasing an insert of 1,242 bps. Lane 1: DNA ladder; Lane 2: RE digested plasmid. B) Schematic representation of the vector map pET30a-with *Eh*ODC insert. The colored tag represents the specific antibiotic resistance gene, restriction sites, insert gene and promoter region. 55

**Figure 2.3: Nucleotide and derived amino acid sequence of *Eh*ODC.** 56

**Figure 2.4: Schematic representation of the strategy used for obtaining pure recombinant *Eh*ODC protein.** 57

**Figure 2.5: Gel profile of expression of *Eh*ODC at different temperatures.** Lane 1: supernatant (uninduced); Lane 2: supernatant (induced at 37 °C); Lane 3: supernatant (induced at 18 °C); Lane 4: pellet (uninduced); Lane 5: pellet (induced at 37 °C); Lane 6: pellet (induced at 18 °C). 58



**Figure 2.6: Purification of *Eh*ODC. A) Affinity purification of *Eh*ODC showing purified protein in 12 % SDS-PAGE. Lane 1: molecular weight marker (kDa); Lane 2-4: *Eh*ODC full length purified protein; Lane 5: Flow-through; Lane 6: Supernatant showing soluble fractions of *E. coli* lysate. B) 12 % SDS-PAGE gel showing purified *Eh*ODC His tag cleaved protein. Lane 1: Molecular weight marker; Lane 2: Purified *Eh*ODC-His tagged protein; Lane 3: Purified His tag cleaved protein with molecular weight ~46 kDa.**

59

**Figure 2.7: A) Size-exclusion chromatography profile. Elution profile of *Eh*ODC and 12 % SDS-PAGE (insert) analysis of major peak fractions. B) The elution profile of standard molecular weight markers through HiLoad 16/60 Superdex 200 column. The column void volume ( $V_0$ ) and molecular weight (kDa) of standard proteins are indicated.**

60

**Figure 2.8: The formation of antipyrylquinoneimine measured at 492nm with different concentration of substrate L-ornithine.**

61

**Figure 2.9: Circular Dichroism spectroscopy of *Eh*ODC. A Far-UV CD spectrum of 0.35 mg/ml *Eh*ODC protein. Data were analyzed using online K2d server for determining the secondary structure contents.**

62-63

**Figure 2.10: Gel showing chemical crosslinking in the presence of glutaraldehyde analyzed by 12 % SDS-PAGE. Lane 1: Molecular weight marker; Lane 2-3: Protein treated with glutaraldehyde showing two sharp bands corresponds to molecular weight of ~90 kDa and ~46 kDa respectively; Lane 4: Untreated purified protein. Arrow pointing to a sharp band represents the dimer of ~90 kDa.**

64

**Figure 2.11: Crosslinking in the presence of dimethyl suberimidate dihydrochloride (DMS). Lane 1: Untreated protein; Lane 2-8: Concentration of DMS (2-0.8 mg/ml); Lane 9: Molecular weight marker.**

64

**Figure 2.12: MALDI-TOF MS analysis of *Eh*ODC showing two peaks corresponding to ~44558.430 Da and ~90667.295 Da.**

66

**Figure 2.13: Effect of chaotropic agents on oligomeric property of *Eh*ODC. (A) & (B): Gel-filtration chromatogram showing the elution profile of *Eh*ODC protein treated with 2 M and 4 M NaCl respectively; (C) & (D): Gel filtration chromatogram showing the profile of protein treated with 2 M and 4 M urea respectively.**

67

**Figure 3.1: The enzymatic reaction catalyzed by ornithine decarboxylase. The pyridoxal 5' phosphate (PLP)-dependent ODC catalyzes decarboxylation of ornithine and produces putrescine.**

70

**Figure 3.2: Amino acid sequence of *Eh*ODC encoded for 413 residues with number of residues labeled.**

74

**Figure 3.3: Multiple sequence alignment of *Eh*ODC (AAX35675) with other ODC sequences.** The conserved residues are highlighted with black background color. The secondary structure elements and numbering of amino acid sequence of human ODC are presented above the aligned sequences. The signatory motifs PxxAVKC(N) (PLP binding motif) and WGPTCDGL(I)D (substrate binding motif) are highlighted in boxes where “x” signifies any amino acid and amino acids in brackets depict the option at a given position. Underlined sequence denotes the amino acids showing similarity with (1) Antizyme binding region (2) PEST like region. The circles under the amino acid indicate the residues interacting with cofactor PLP whereas triangles denote the substrate L-ornithine binding residues in the active site pocket. The residues denoted with cross mark are involved in the formation of salt bridges in between two monomers. The residues indicated with stars are present at the interface and form a stack of aromatic rings. Residue important for dimer formation and present away from the interface is denoted with a square. The motif A represents the interface residues of two monomers present very closer to each other. Alignments are obtained using ESPript.

76

**Figure 3.4: Phylogeny of ornithine decarboxylase from various sources.** The amino acid sequences of ODC were taken from plants *R. communis* (XP\_002510610.1), *N. glutinosa* (AAG45222.1), *C. annum* (AAL83709.1), *Z. mays* (AAM92262.1), *D. stramonium* (P50134.1); animals *X. laevis* (NP\_001079692.1), *R. norvegicus* (NP\_036747.1), *M. musculus* (P00860.2), *H. sapiens* (P11926.2); fungi *A. oryzae* (XP\_001825149.2) *M. circinelloides* (CAB61758.1), *E. festucae* (ABM55741.1), *P. brasiliensis* (AAF34583.1); *S. cerevisiae* (EDN60096.1) *F. solani* (ABC47117.1), *C. albicans* (AAC49877.1); protozoa *P. bursaria* (NP\_048554.1), *T. brucei* (P07805.2), *L. donovani* (P27116.1), *E. histolytica* (AAX35675) and bacteria *V. vulnificus* (YP\_004188159.1), *A. caulinodans* (YP\_001523249.1), *P. syringae* (AAO58018.1), *E. amylovora* (YP\_003539917.1), *S. scabiei* (YP\_003491041.1), *Azospirillum* (BAI72082.1), *E. coli* (BAE77028.1), *Lactobacillus* (P43099.2). Different clusters representing a particular group are highlighted in boxes whereas the representatives of protozoa ODC are highlighted by arrow marks.

78

**Figure 3.5: Secondary structure prediction from the primary sequence of *Eh*ODC by using PSIPred server.**

80

**Figure 3.6: Prediction of structurally disordered regions of *Eh*ODC.** The disordered regions are depicted in red and folded regions are depicted in green. Two regions found to be disordered has been denoted in red color and ranging from 242-TIKELEFPE-250, to 397-SIEC NSVPSLNGIP HYA-413. Predictions were done using DisEMBL 1.5.

82

**Figure 3.7: 3D structure of *Eh*ODC monomer. (A) Cartoon diagram of *Eh*ODC model generated using MODELLER 9v8. (B) Topological arrangement of secondary structures in *Eh*ODC monomer. Monomer of**

*Eh*ODC consists of two domains,  $\beta/\alpha$ -barrel shown in purple and sheet domain having sheet S1 in green, sheet S2 in blue and helices and turns in orange. The helices are presented by circles, strands are represented by triangles and the loops connecting these structures are represented as connecting lines.

85

**Figure 3.8: Schematic representation of dimer interface and active site of *Eh*ODC.** (A) Subunits of the dimer are arranged in head to tail manner where subunit A and B are shown in yellow and green colors respectively. (B) The residues critically important for dimer formation are presented in sticks and overall dimeric structure is presented in cartoon. Residues from opposite monomer are marked by apostrophe (') sign. (C) Surface view of monomeric chains highlighting the residues at the dimer interface in different colors. The monomers have been separated and rotated to 90° giving clear view of interface residues. Red and blue color indicates residues involved in salt bridge formation and orange color depicts hydrophobic interactions. (D) Closer view of residues at the interface forming salt bridge. (E) Aromatic residues at the interface arranged as a stack of ring structures forming amino acids zipper. (F) Residues at the active site interacting with cofactor PLP from each monomer are presented in sticks. Residues from subunit A and B are shown in yellow and green colors respectively.

87-88

**Figure 3.9: Molecular dynamics simulation profile.** RMSD of dimeric protein after molecular dynamics simulation for 8 ns relative to pre-MD dimeric structure.

89

**Figure 4.1: Amino acid sequence with nucleotide codons.** Residues in red font are showing the corresponding mutation site in the *Eh*ODC protein sequence.

96

**Figure 4.2: Schematic representation of the vector map pET30a-with *Eh*ODC.** The colored tag represents the specific restriction sites, insert gene and promoter region. The insert gene of *Eh*ODC with mutated site *Eh*ODC<sup>m</sup> in the sequence has been represented with red color.

97

**Figure 4.3: PCR product containing amplified mutant plasmid.** Lane 1: DNA ladder (1kb); Lane 2: PCR product containing mutant *Eh*ODC.

97

**Figure 4.4: Schematic representation of strategy used for creating mutant *Eh*ODC.**

98

**Figure 4.5: Purification of mutant proteins of *Eh*ODC.** A) Mutant K57A: Lane 1: Pellet; Lane 2: Supernatant; Lane 3: Flow-through; Lane 4: Washing; Lane 5-9: Purified fractions. B) Mutant C334A: Lane 1: Pellet; Lane 2: Supernatant; Lane 3: Flow-through; Lane 4-6: Purified fractions. C) Mutant K157A: Lane 1: Pellet; Lane 2: Supernatant; Lane 3: Flow-through; Lane 4: Washing; Lane 5-9: Purified fractions. D) Mutant G334D: Lane 1: Pellet; Lane 2: Supernatant; Lane 3: Flow-through; Lane 4-5: Purified fractions. E)

**Mutant G334Y:** Lane 1: Pellet; Lane 2: Supernatant; Lane 3: Flow-through; Lane 4-5: Purified fractions.

99-100

**Figure 4.6: Enzyme activity of wild type *Eh*ODC and its mutants.** Enzymatic activity of *Eh*ODC mutants relative to the activity of the wild-type enzyme. Cys334Ala, Lys57Ala Gly361Tyr and Lys157Ala are inactive. Cys334Ala and Lys57Ala mutants were mixed in 1:1 ratio and the mixture shows recovery of approximately 29 % of the wild-type enzyme activity. The plot represents the average of three measurements.

102

**Figure 4.7: Schematic representation of homodimers and heterodimers in the mixture of *Eh*ODC Cys334Ala and Lys57Ala mutants.** (A-C): Homodimer formation of wild-type and mutants of *Eh*ODC in individual solution. (D): Possible combinations of *Eh*ODC monomeric subunits in the mixture of Cys334Ala and Lys57Ala mutants forming heterodimer and homodimers.

103

**Figure 4.8: Gel filtration analysis of interface residue mutants.** Gel-filtration chromatogram of Gly361Asp mutant showing monomer peak corresponding the wild type *Eh*ODC (~90 kDa).

104

**Figure 4.9: Gel filtration analysis of interface residue mutants.** A) Gel-filtration chromatogram of Gly361Tyr mutant showing partial dissociation of dimers into monomers; B) Gel-filtration chromatogram of Lys157Ala mutant showing partial dimeric disruption.

106

**Figure 5.1: Schematic diagram of the cloned 15Δ*Eh*ODC construct map.** pET-28c expression vector with TEV protease cleavage site and *Eh*ODC of 1,197 bps was inserted in between *Nde*I-*Xho*I fragment red zone with T indicate the C-terminal part which has been deleted from the sequence.

113

**Figure 5.2: Schematic representation of the strategy used for the cloning of 15Δ*Eh*ODC from full-length *Eh*ODC construct.**

114

**Figure 5.3: Agarose gel profile of 15Δ*Eh*ODC:** Lane 1: Cloned plasmid containing the 15Δ*Eh*ODC with insert size 1,197 bps; Lane 2: 1kb DNA ladder; Lane 3: Cloned plasmid RE digested with *Nde*I and *Xho*I enzymes.

119

**Figure 5.4: 12% SDS-PAGE gel showing the expression and purification of 15Δ*Eh*ODC.** A) Lane 1: Induced pellet; Lane 2: Induced supernatant; Lane 3: Uninduced pellet; Lane 4: Uninduced supernatant. B) Lane 1: Molecular weight marker; Lane 2-5: Purified fractions. Arrow points to the protein of molecular weight ~44 kDa.

119

**Figure 5.5: The gel filtration chromatogram elution profile of the 15Δ*Eh*ODC protein.** The elution volume of 15Δ*Eh*ODC protein was compared with the standard molecular weight markers. The protein was eluted



at a volume of 74 ml corresponding to molecule weight of ~87 kDa. Insert showing the purified protein after gel filtration chromatography. 120

**Figure 5.6: Crystals of 15Δ*Eh*ODC along with the diffraction pattern. A)** Diamond shaped crystals in 20 % (v/v) PEG 3350, 0.2 M LiCl maintained at pH 6.8. **B)** Diffraction pattern of 15Δ*Eh*ODC crystal at 2.8 Å. 121

**Figure 5.7: Schematic representation of crystal packing and overall structure of the model obtained after molecular replacement. A)** Crystal packing of *Eh*ODC in an orthorhombic unit cell; O is the origin of the unit cell with four chains arranged on a, b and c axis in x, y and z direction. **B)** Cartoon diagram of tetrameric model of *Eh*ODC showing AB-CD, dimer-dimer interface; **C)** Tetrameric model rotated to 90° to insight into the center of the molecule. 123-124

**Figure 5.8: Crystal structure of *Eh*ODC monomeric subunit. A)** Cartoon diagram of the monomer showing arrangement of barrel and sheet domain. **B)** Topology diagram of monomer of *Eh*ODC where helices are represented with cylinder and sheets with the arrows connected with loops, dashed line indicates the sequence missing in the structure. 126

**Figure 5.9: Surface view diagram of active sites of functional ODC, nonfunctional antizyme inhibitor and *Eh*ODC. A)** Monomer of human ODC with active site colored in blue. **B)** monomer of *Eh*ODC showing active site residues identical to human ODC colored blue, identical to AZI colored green and unique to *Eh*ODC in red color. **C)** Monomer of AZI showing residues identical to human ODC in blue and those are mutated colored green. 128

**Figure 5.10: Active site of *Eh*ODC showing the difference between the interaction of substrate L-ornithine and substrate analogue DFMO.** Active site at the dimer interface orange color residues are of chain A and blue color residues of chain B. **A)** Interaction to PLP with L-ornithine (Cyan); **B)** Interaction of PLP attached to DFMO (violet). 131

**Figure 5.11: Multiple sequence alignment of ornithine decarboxylase and its homologues antizyme inhibitor to determine the conservation of sequence and mutation of active site and substrate binding residues.** Circles indicate the residues important for enzymatic activity. Numbering is according to *Eh*ODC. 136

**Figure 5.12: Phylogenetic relationship of *Eh*ODC with antizyme Inhibitor and ODC:** Sequence of ODC and their evolutionary related homologous were retrieved from various sources. **Antizyme inhibitor** of *Homo sapiens* (BAA23593.1), *Nomascus leucogenys* (XP\_003256127.1), *Macaca mulatta* (XP\_002805501.1), *Mus musculus* (AAB87464.1), *Rattus norvegicus* (BAA23594.1), *Monodelphis domestica* (XP\_001369332.1), *Xenopus laevis* (NP\_001087584.1), *Danio rerio* (BAB84695.1), *Tetraodon nigroviridis* (ENSTNIT00000008148.1), *Anolis carolinensis* (XP\_003219500.1), *Gallus*

*gallus* (NP\_001008729.1), *Ornithorhynchus anatinus* (XP\_001506230.1), *Canis familiaris* (XP\_849306.1), *Bos Taurus* (NP\_001076080.1), *Loxodonta africana* (XP\_003408472.1). **Ornithine decarboxylase sequence from *Aedes aegypti*** (EAT48998.1), *Entamoeba histolytica* (AAX35675.1), *Plasmodium falciparum* (AAF14518.1), *Leishmania donovani* (AAA29259.1), *Datura stramonium* (CAA61121.1), *Solanum lycopersicum* (NP\_001234616.1), *Glycine max* (CAD91349.1), *Chlamydomonas reinhardtii* (CAE46409.1), *Monodelphis domestica* (XP\_001371947.1), *Bos Taurus* (AAA92339.1), *Macaca mulatta* (NP\_001185615.1), *Homo sapiens* (NP\_002530.1), *Mus musculus* (NP\_038642.2), *Anolis carolinensis* (XP\_003215471.1), *Trypanosoma brucei* (AAA30219.1), *Xenopus laevis* (CAA39760.1).

137-138

**Figure 5.13: Antizyme binding sequence of human ODC (*HsODC*) is compared with *EhODC*.** Residues 117-140 in *HsODC*, *HsAZI* and other ODC were considered for comparative analysis. Antizyme binding region of *homo sapiens*, *Trypanosoma brucei*, *Paramecium bursaria*, *Leishmania donovani*, *Entamoeba histolytica* and *Plasmodium falciparum* were aligned by ClustalW.

139





## LIST OF TABLES

### Page No.

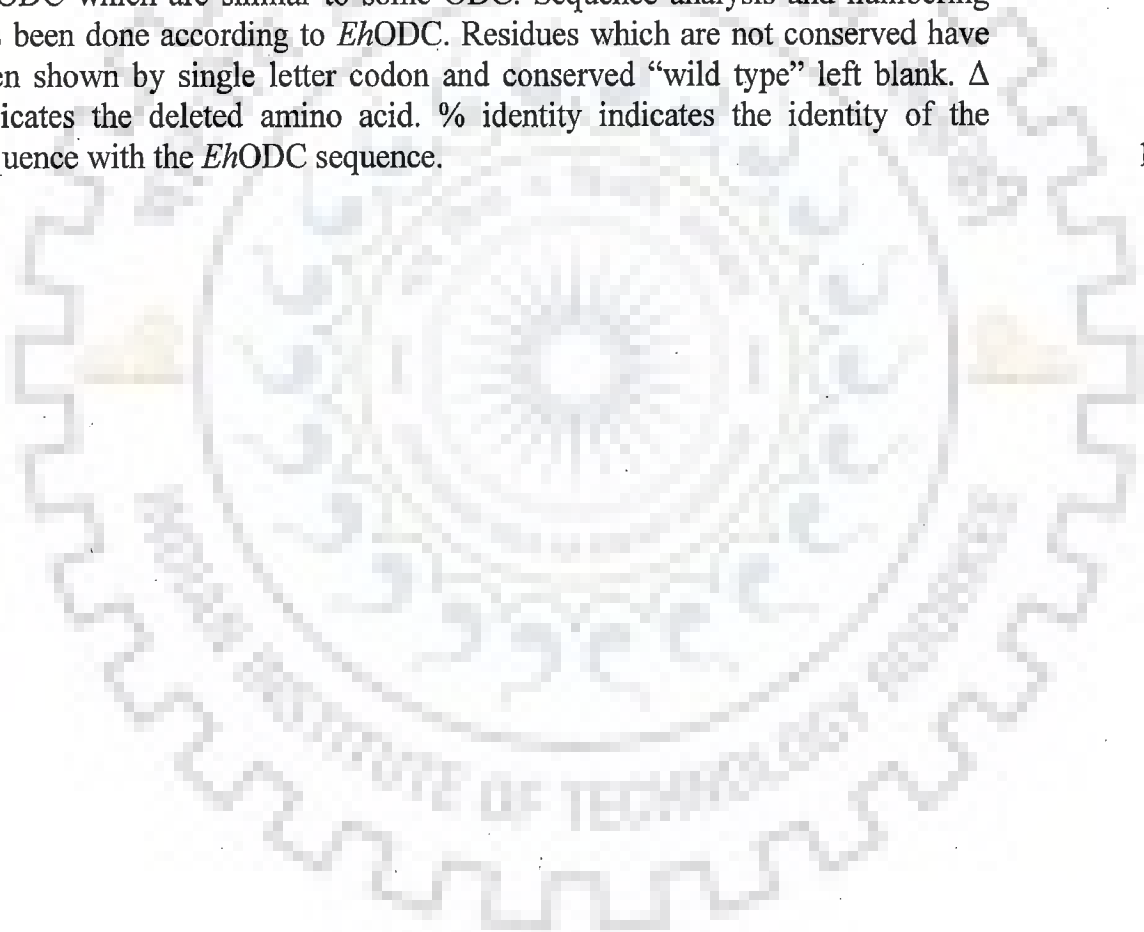
<b>Table 1.1: Genome organization of <i>Eh</i>ODC coding region.</b> The accession number with locus and gene ID has been given to locate the organization of <i>Eh</i> ODC within the whole genome.	10
<b>Table 1.2: Concentrations of polyamines in parasites.</b> <sup>e</sup> denotes the nmol/mg dry weight.	13
<b>Table 1.3: Polyamine concentration reported to be present in parasitic protozoa. In this table:</b> <sup>c</sup> is for concentration in milimolar; <sup>d</sup> is for concentration in pmol/10 <sup>6</sup> parasitized erythrocyte.	20
<b>Table 1.4: Pyridoxal 5' phosphate dependent enzymes fold types.</b> Show PLP dependent enzymes of fold-type I and III from eukaryotic and prokaryotic organisms.	23
<b>Table 1.5: Fold type III ODC which have been crystallized.</b>	24
<b>Table 1.6: Chemical structures of substrate analogues with different side chains.</b> The basic structure given above the table and different side chains are presented with the K <sub>d</sub> values.	32
<b>Table 1.7: Enzyme ODC structure data from eukaryotic and prokaryotic organisms.</b> Show the oligomeric state of ODCs from different groups of decarboxylases, with their PDB-ID and the space group. Data obtained from RCSB PDB.	39
<b>Table 1.8: Enzyme ODCs identified and characterized for studying the effect of inhibitors.</b>	40
<b>Table 1.9: Mutant and complex structure of ODC with substrate/inhibitor.</b>	43
<b>Table 2.1 Showing the comparative secondary structure content obtained by CD data analysis and SOPMA server.</b>	63
<b>Table 4.1: Sequences of mutagenic primers and annealing temperatures used for PCR amplification of mutant plasmids.</b> Mutated nucleotides are underlined. S: sense and An: antisense.	94
<b>Table 5.1: Statistical representation of data collection and structure refinement parameters along with quality of the model accessed by Ramachandran plot.</b> <sup>a</sup> value in parentheses are for the highest resolution shell.	123

**Table 5.2: Comparative glide score and energy for L-ornithine and DFMO for determining the binding efficiency of the ligand to dimer of EhODC.**

130

**Table 5.3: Sequence analysis of ODC and antizyme inhibitor, comparing the active site residues of ODC/AZI from various organisms. Abbreviation denoted:- C<sup>f</sup> for cofactor binding; B<sup>s</sup> salt bridge formation; S substrate binding residues; I<sup>f</sup> interface of dimer ; D<sup>i</sup> important for dimer formation. Species with the name of protein are shown on left side. Colour indication:- Violet columns signifies the mutation in AZI; Orange columns signifies the mutated residues in *E. histolytica* ODC which are similar to AZI; Gray shows the unique mutations in *Eh*ODC which is neither conserved in ODC nor in AZI; Blue indicate the mutation in *Eh*ODC which are rarely found in AZI and functional ODC; Olive color point out the mutations in *Eh*ODC which are similar to some ODC. Sequence analysis and numbering has been done according to *Eh*ODC. Residues which are not conserved have been shown by single letter codon and conserved "wild type" left blank. Δ indicates the deleted amino acid. % identity indicates the identity of the sequence with the *Eh*ODC sequence.**

133-134



## LIST OF ABBREVIATIONS USED

Å	Angstrom
α	Alpha
°C	Degree centigrade
β	Beta
BamH	<i>Bacillus amyloliquefaciens</i>
μl	Microlitre
μmole	Micromole
γ	Gamma
AADC	Amino acid decarboxylase
AMPA	α-Amino-3-hydroxy-5-methyl-4-isoxazolepropionic acid
AMP	Adenosine Monophosphate
ATP	Adenosine Triphosphate
bp	Base pair
B-factor	Debye-Waller factor/Temperature factor
CNS	Central nervous system
CO <sub>2</sub>	Carbon dioxide
cm	Centimeter
DNA	Deoxyribose nucleic acid
Dpn	<i>Diplococcus pneumoniae</i>
dNTPs	Deoxy nucleotide tri phosphates
EDTA	Ethylenediaminetetracetic acid
eg.	For example
EMBL	European Molecular Biology Lab
et al.	et alia
DTT	Dithiothreitol
F1	Filial 1
g	Gram
h	Hours
H <sub>2</sub> O <sub>2</sub>	Hydrogen peroxide
IITR	Indian Institute of Technology Roorkee
IPTG	Isopropyl β-D-thiogalactoside
K	Kelvin
kbp	Kilo bases
kDa	Kilo Daltons
L.	Liter
m	Meter
M	Molar
mg	Milligram
MgCl <sub>2</sub>	Magnesium chloride
min	Minute
ml	Millilitre
mm	Milli meter
mM	Millimolar

mRNA	messenger RNA
NCBI	National Center for Biotechnology Information
Nde	<i>Neisseria denitrificans</i>
ng	Nanogram
Ni	Nickel
nm	Nanometer
PCR	Polymerase chain reaction
PDB	Protein Data Bank
PFK	Phosphofructokinase
PK	Pyruvate Kinase
RE	Restriction endonuclease
R-factor	Residual-factor
RNA	Ribose nucleic acid
RNaseA	RibonucleaseA
rpm	Revolutions per minute
s	Seconds
Taq	<i>Thermus aquaticus</i>
USA	United States of America
UV	Ultraviolet
V	Volt
v/v	Volume /volume
Xho	<i>Xanthomonas holcicola</i>



## STRUCTURE AND MODELS SUBMITTED TO DATA BANK

- 1) PDB ID: 4AIB
- 2) PMDB ID: PM0077698 (monomer)
- 3) PMDB ID: PM0077699 (dimer)



## Introduction

*Entamoeba histolytica* is an anaerobic parasitic protozoan which infects humans and primates. It invades the intestine and liver, which may cause mild diarrhea and serious dysentery with bloody and mucoid stool. If untreated, the parasite can cause life-threatening haemorrhagic colitis and/or extra-intestinal abscesses. Polyamine biosynthetic pathway has been characterized as a potent therapeutic target in *T. brucei* along with many other protists. Identification of ornithine decarboxylase, the first enzyme of polyamine biosynthesis from *E. histolytica* opens an opportunity for the development of new chemotherapeutic agents against protozoan parasites.

The ornithine decarboxylase (ODC) enzyme has been reported to be present in various protozoa including *Leishmania*, *Trypanosoma*, *Giardia*, and *Plasmodium* and is a validated drug target in *Trypanosoma brucei* for treatment of African sleeping sickness. The ODC enzyme is an obligate homodimer which catalyzes the conversion of L-ornithine to putrescine. In addition to this, two active site pockets are present at the dimer interface. This enzyme has a very short half-life due to its ubiquitin-independent 26S proteasome mediated degradation which is stimulated by the binding to antizyme. The sequence analysis of ODCs from various sources revealed the presence of antizyme recognition sequence at N-terminal and P (Proline), E (Glutamate), S (Serine) T (Threonine) amino acid rich sequence at C-terminal which is a signaling sequence for 26S proteasome mediated degradation. Besides increase in ODC proteolysis, interaction of antizyme with ODC leads to catalytic inactivation of the enzyme by disrupting the enzymatically active ODC dimer. In addition, the antizyme binding loop and PEST sequence which is accessible in ODC monomer is found to be buried in the dimer of ODC that ultimately prevents it from degradation. Thus, dimer formation is not only important for its catalytic function but also for its protection against antizyme-dependent endoproteolysis.

Crystal structures of ODC enzyme from *T. brucei* (PDB ID: 1QU4), human (PDB ID: 2O00), and mouse (PDB ID: 7ODC) revealed that the monomeric subunits interact in head to tail manner and form two catalytic sites at the dimer interface. The structure of ODC in



complex with substrate and product analogues, including ornithine analog  $\alpha$ -difluoromethylornithine (DFMO) has been investigated. DFMO is a suicide inhibitor of ODC and has been reported to inhibit growth of various pathogenic protozoan parasites such as *Giardia lamblia*, *Plasmodium falciparum*, and various *Trypanosoma* species, but have relatively poor effect on more virulent strains as *T. brucei rhodesiense*.

Sequence and structure-function studies revealed the arise of a new homologue of ODC known as antizyme inhibitor (AZI) which has lost its ability of decarboxylation due to the mutation of critical residues in the active site. These homologues hold the ability to regulate various life processes including the protection of ODC from degradation due to antizyme. The AZI bind to the antizyme more efficiently as compared to ODC and result in its sequestration.

In *E. histolytica*, the only enzyme of polyamine biosynthesis reported to exist is ODC. The *Eh*ODC enzyme has been cloned and successfully characterized by Jhingran *et al.* (2008). Sequence homology revealed that *Eh*ODC has 36 % sequence identity with ODC from *Datura stramonium*. In addition to this, it also shares 33 % and 32% identity with human and *Trypanosoma brucei* ODC respectively. *Eh*ODC has been reported to exist as homopentamer. Furthermore, *Eh*ODC is insensitive to DFMO, a known inhibitor of ODC and DFMO has no inhibitory effect on the cell growth of the parasite. Therefore, it is necessary to develop an alternate strategy for inhibition of *Eh*ODC enzyme that leads to block parasite growth and proliferation.

In the present study, we are reinvestigating the oligomeric properties of *Eh*ODC under various physiological conditions. These studies revealed that *Eh*ODC exist in dimeric state in the solution and disruption of dimer to monomer occurs with the effect of different chaotropic agents. *In silico* studies were carried out to investigate the enzymatically active and energetically stable form of *Eh*ODC. Sequence analysis revealed its phylogenetic relation with ODC from other phyla. In addition, various interactions were found to be responsible for the active dimer formation and various disordered regions were identified that affects the stability of the protein.

The mutations were inserted at the active site and also at the dimer interface for those residues playing critical role either in the activity or in the stability of dimer. Mutational studies were carried out to investigate the effect of each mutation on the activity and stability of the *Eh*ODC dimer. Sequence analysis revealed that the *Eh*ODC possesses some disordered regions at the C-terminus. The C-terminal truncation of the full length *Eh*ODC was performed to remove 15 amino acid residues. The 15 C-terminal truncated *Eh*ODC protein was expressed and purified. The purified protein was used for crystallization and crystals were obtained. These crystals diffracted at 2.8 Å and exhibiting P2<sub>1</sub>2<sub>1</sub>2<sub>1</sub> symmetry with unit cell parameters  $a = 76.66 \text{ \AA}$ ,  $b = 119.28 \text{ \AA}$ ,  $c = 179.28 \text{ \AA}$ . 3D structure of *Eh*ODC was determined to insight into the active site pattern for determining the structural differences which are responsible for the insensitivity of *Eh*ODC towards DFMO. In addition to this, the sequence analysis and phylogenetic studies were performed to investigate the relationship of *Eh*ODC with functional ODC and nonfunctional antizyme inhibitor. These studies will allow us to understand the physiological characteristics of *Eh*ODC and also provide the alternate strategy for designing structure based inhibitors to inhibit the dimeric functional *Eh*ODC.



# **CHAPTER I**

## **REVIEW OF LITERATURE**

## 1.1 Introduction

*Entamoeba histolytica* is a single-celled parasitic protozoan responsible for causing amoebiasis. The parasite infects liver and intestine, which may cause mild diarrhea and life threatening abscessions (Haque *et al.*, 2003). *E. histolytica* is responsible for over 50 million infections in tropical and temperate regions, and nearly 100,000 deaths worldwide each year (Haque *et al.*, 2003; Rosas-Arreguín *et al.*, 2008; López-Vallejo *et al.*, 2011).

The parasite mainly infects humans and primates and 45-50 % infections are due to poor sanitation. *E. histolytica* infection is largely unknown during early stages as it remains asymptotically in the gastrointestinal tract for months before developing any symptom of disease (Gathiram *et al.*, 1987; Haque *et al.*, 2001). Its reproduction process involves two major stages: first stage is trophozoites which are large, wall-lacking cells and second stage is cysts which are small, thick walled cells. Mature cysts in the gastrointestinal track are the parasitic entities that play a critical role during infection. The infection is the consequence of excystation (release of trophozoites) and starts with the encroachment of intestinal lining causing colitis and dysentery (Stanley *et al.*, 1992). In severe infection, parasites travel through blood to different organs, primarily to liver causing abscesses and also to lungs, brain and spleen (Stanley, 2003).

## 1.2 Life cycle of *Entamoeba histolytica*

The life cycle of *Entamoeba histolytica* begins with ingestion of contaminated food and water into the host intestine. Mature cyst passes through the gut to the ileum of small intestine where excystation takes place (Shibayama *et al.*, 1998; Stanley, 2003). One trophozoite with four nuclei emerges, divides three times and each nucleus divides once to produce eight trophozoites from each cyst. Trophozoites migrate to large intestine where multiplication takes place by binary fission. Encystation of the freshly formed cell occurs in the large intestine. Immature cyst forms and undergoes nuclear division that results in the appearance of quadrinucleated mature cysts (Figure 1.1). Both trophozoites and cyst stages can pass through feces (Stanley, 2003).

Cysts can survive in the outer environment and are responsible for transmission to continue its life cycle. The newly appeared trophozoites can invade intestinal mucosa and bore into the wall causing bloody diarrhea and abdominal cramp (Espinosa-Cantellano *et al.*, 2000; Marinets *et al.*, 1997; Stanley *et al.*, 1992; Bhattacharya *et al.*, 1992). Trophozoites undergo two metabolically different states: noninvasive and invasive infections. The noninvasive infection remains confined to the intestine and individual become asymptomatic carrier by passing cysts to the stool (Gathiram *et al.*, 1987; Haque *et al.*, 2001). In invasive infections, trophozoites invade through the blood stream, reach to the other vital organs and infect them.

In *E. histolytica*, asexual reproduction is the only mode of propagation. Binary fission of cell occurs at the trophozoites state. Small protrusion or bud appears on the surface of the mother cell. Nuclear fission results in the formation of two nuclei, divided nucleus migrates to the small protrusion and consequent wall formation leads to the separation of the newly formed bud containing the divided nucleus from the mother cell (Aguilar-Díaz *et al.*, 2010). The evidences suggest that genotype does not vary from cell to cell due to asexual reproduction. General basis for evolution of novel genotype possibly linked to excystation of parasite in new host. However, the exact mechanism is still unknown (Argüello *et al.*, 1992; Aguilar-Díaz *et al.*, 2010).

*E. histolytica* is a colonel parasitic protozoan (Tibayrenc *et al.*, 1990). Strain can be maintained in laboratory either in the presence of bacteria (xenically) or in the absence of bacteria (axenically). Axenic strains are being used to investigate the parasitic virulence or gene expression analysis without host environment. An important property of axenic culture was observed that it contains DNA 10 folds higher than xenic culture. This DNA content of axenized parasites reduces relatively as bacterial load increases equivalent to xenic culture. A similar process of variation in DNA content observed during passage from cyst to trophozoite in *E. invadens*, a model organism for studying encystation mechanisms (Argüello *et al.*, 1992; Mukherjee *et al.*, 2009).



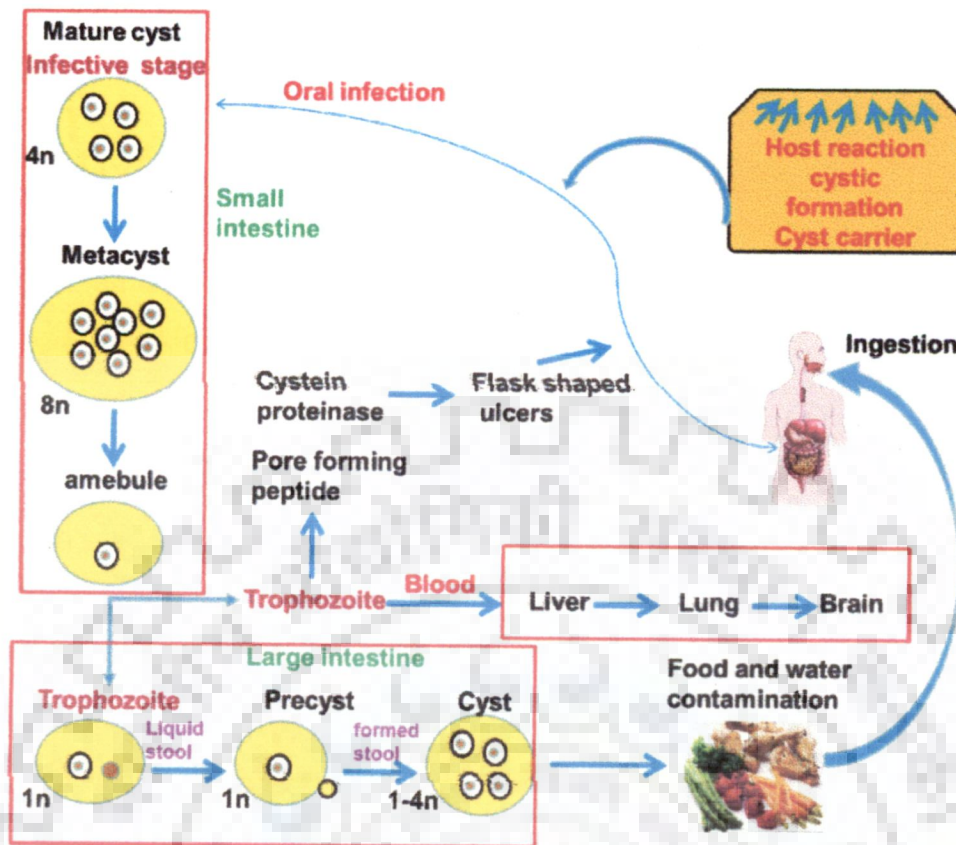


**Figure 1.1:** Life cycle of *E. histolytica* showing two major stages: trophozoites and cyst. (<http://www.dpd.cdc.gov/dpdx/HTML/Amebiasis.htm>)

These variations are the evidence to prove accumulation of multiple copies of the genome (polyploidy), although the expansion or contraction of specific regions of the genome or some other rearrangements could be possible. Xenic culture of parasite display increased virulence *in vitro* or in mouse model experiments. However, the reason for its increased virulence in xenic culture and change in the genome in axenic culture is still unknown (Clark *et al.*, 2007).

### 1.3 Genome organization of *E. histolytica*

The whole genome sequencing of *E. histolytica* was undertaken by Wellcome Trust Sanger Institute, Pathogen Sequencing Unit, in collaboration with **Graham Clark** at the London School of Hygiene and Tropical Medicine 2001. Another group, **The Institute of Genome Research (TIGR)** which was involved in sequencing of the half of the target genome (Project ID: 142) in Rockville, MD, USA. However, the genome sequence of *E. histolytica*



strain (HM1: IMSS) was largely unclosed with fragmented database till 2005. The genome sequence paints a clear picture of location of several enzymes of different pathways and regulatory elements (Mann, 2002; Loftus *et al.*, 2005). The identification of genomic regions encode for virulent factors such as cysteine proteases, amoebapores (Leippe *et al.*, 2004), proteinases (Tillack *et al.*, 2007) and lectins (Petri, 2000) etc., opens an opportunity for better analysis of pathogenesis. The complete sequence provides true evidences to answer why axenic strains are less virulent and responsible for the variable outcome of infection.

The complete genome of *E. histolytica* was predicted to be distributed on 20 linear chromosomes along with numerous episomes in the nucleus (Kumari *et al.*, 2011). Genome analysis revealed the presence of segmental duplications of up to 16 kb flanked inverse repeats. Some gene families found to be tightly associated with the transposable elements. From the detailed genome analysis, *E. histolytica* (HM-1: IMSS) was found to have 20,772,429 nucleotides DNA length containing 1,496 scaffolds. It encoded 8,163 genes of average 1.17 kbps in size which belong to total 897 protein families (Lorenzi *et al.*, 2010).

#### **1.4 Metabolic pathways in *E. histolytica***

Pathogen is a resident of human intestinal track which maintains symbiotic relationship with many bacteria and hosts and derives most of the preformed organic nutrients from them. *E. histolytica* genome sequence shares most of the characteristics with *Giardia lamblia* and *Trachomonas vaginalis* infesting human intestinal and urogenital tract respectively. The *de novo* synthesis of purine, pyrimidine and thymidylate has been eliminated from its genome and it relies on salvage pathway for nucleotide metabolism. *E. histolytica* has lost its ability to synthesize the fatty acid, however able to synthesize phospholipids (Zhang *et al.*, 1991, 1992). It lacks most of the amino acid biosynthetic pathways except serine and cysteine which are major intracellular thiols (Ariyanayagam *et al.*, 1999).

*E. histolytica* is a type I amitochondriate protist lacking both mitochondria and hydrogenosome. During evolution, *E. histolytica* has not only reduced or eliminated mitochondrial metabolic pathways but also acquired and carried near about 100 genes from the prokaryotic organisms (Tovar *et al.*, 1999; Leon-Avila *et al.*, 2004). This organism lacks aerobic metabolism including tricarboxylic acid (TCA) cycle and mitochondrial electron

transport chain (Clark *et al.*, 2007). It uses anaerobic metabolic pathways which are generally associated with bacteria. *Entamoeba* is incapable of converting organic substrates such as glucose, water etc. rather rely on various types of substrate level phosphorylation for its energy generation. (Reeves, 1984; Husain *et al.*, 2010; Vicente *et al.*, 2009; Pineda *et al.*, 2010).

#### 1.4.1 Polyamine metabolic pathway

Along with anabolic reactions, the catabolic reactions are also important for having many functional aspects. One is arginine catabolic pathway in which arginine can be converted to either ornithine or agmatine via corresponding enzymes arginase (EC 3.5.3.1) or arginine decarboxylase (EC 4.1.1.19) (Elnekave *et al.*, 2003). Arginine decarboxylation reaction utilizes protons and helps in providing acid resistance to the cysts while passing through the human stomach (Anderson *et al.*, 2005). Secondly arginine gets depleted as a substrate for the generation of human macrophages, preventing NO synthesis and amoebicidal activity (Elnekave *et al.*, 2003). Both arginase and arginine decarboxylase enzymes could be important for the generation of the polyamine putrescine. However, the enzymes S-adenosyl-L-methionine decarboxylase (EC 4.1.1.50), spermidine synthase (EC 2.5.1.16) and spermine synthase (EC 2.5.1.22) involved in the formation of higher polyamines were not identified in *E. histolytica* (Anderson *et al.*, 2005). The physiological significance of putrescine has been estimated by its high concentration in trophozoites which was demonstrated by NMR spectroscopy (9.5 mM) (Bakker-Grunwald *et al.*, 1995). However, the fate of this polyamine is still unknown as none of the higher polyamines have been demonstrated in *E. histolytica*.

Some evidences were found which clarified the facts about spermidine necessity for *E. histolytica*. These facts encourage us to consider spermidine as an essential trace nutrient which may be present either in some modified form or may be transported from the host along with other nutrients as spermidine transporters have been reported to exist in *E. histolytica* (Anderson *et al.*, 2005). The first evidence is the enzyme deoxyhypusine synthase found in *E. histolytica* which requires spermidine to produce deoxyhypusine on eIF5a (eukaryotic initiation factor 5a), a protein essential for cell proliferation (Park *et al.*, 1997). Secondly, trypanothione, a spermidine-containing thiol which is a major thiol in

*trypanosomes* and *leishmania*, (Fairlamb *et al.*, 1992) is a controversial issue regarding its presence or absence in *E. histolytica*. The first report in 1997 confirmed the presence of trypanothione in *E. histolytica* (Ondarza *et al.*, 1997). However, the report was contradicted later (Ariyanayagam *et al.*, 1999). Although the matter is still unresolved and a general agreement accepted cysteine as a major thiol in *E. histolytica* strain HM-1: IMSS (Fahey *et al.*, 1984). Further work on the characterization of genes as well as transporters involved in spermidine uptake may help in understanding the function of deoxyhypusine synthase.

Polyamine biosynthetic pathway has been characterized as a potent therapeutic target in *T. brucei* along with many other protists (Marton *et al.*, 1995; Seiler, 2003; Casero *et al.*, 2005). Identification of ornithine decarboxylase, the first enzyme of polyamine biosynthesis from *E. histolytica* opens an opportunity for the development of new chemotherapeutic agents against protozoa parasites. The ornithine decarboxylase (ODC) gene from *E. histolytica* encodes a 46 kDa protein similar to both plant and vertebrate enzymes and has been characterized biochemically (Arteaga-Nieto *et al.*, 1996, 2002). Further, recombinant *E. histolytica* ODC (*Eh*ODC) has been expressed in *E. coli* and purified to homogeneity. Interestingly, difluoromethylornithine (DFMO) which is a potent inhibitor of ODC enzyme is used as a therapeutic agent for African sleeping sickness caused by *T. brucei* (Bacchi *et al.*, 1980). However, DFMO found to be ineffective against *Eh*ODC (Gillin *et al.*, 1984; Jhingran *et al.*, 2008).

### **1.5 Ornithine decarboxylase gene in genome**

The genome organization of *Eh*ODC has revealed a double stranded DNA with EHI\_100430 gene coding for ornithine decarboxylase (Table 1.1). The average length of the nucleotides sequence includes 1,241 base pairs (58455-59696 from 5' end to 3' end) on positive strand DNA. The *Eh*ODC sequence is flanked by protein phosphatase at N-terminal end and a hypothetical protein at C-terminal end (Figure 1.2).

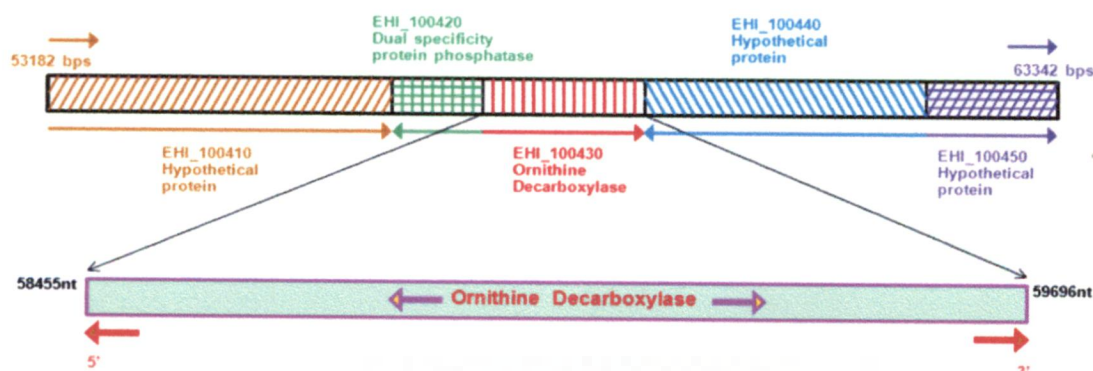


**Figure 1.2: The genome organization of *EhODC*.** The genome of *EhODC* from 5' terminal sequence 58455 to 3' end 59696 denoted in red color with gene marked as EHI\_100430. The stretch of the genome from 53182 bps to 63342 bps contain five protein coding genes out of which only two are known to have some structure- function relationships while other 3 are hypothetical proteins which have not been characterized (<http://www.ncbi.nlm.nih.gov/genome>).

Product name	Strand	Length	Accession No.	GeneID	Locus_tag
Ornithine decarboxylase	+	413	<u>XP</u> 655113.1	3409429	EHI_100430

**Table 1.1: Genome organization of *EhODC* coding region.** The accession number with locus and gene ID has been given to locate the organization of *EhODC* within the whole genome (<http://www.ncbi.nlm.nih.gov/genome/>).

The ornithine decarboxylase enzyme from *Entamoeba histolytica* which catalyzes the conversion of L-ornithine to putrescine was cloned (Jhingran *et al.*, 2008). Sequence homology revealed that *EhODC* has highest sequence similarity with *Datura stramonium*, human ODC and *Trypanosoma brucei* ODC which is 36 %, 33 % and 32 % respectively.

Further, amino acid sequence comparison helps in predicting the secondary structures of *EhODC* protein which revealed that only 380 residues have structural role. In this study, we elucidate the structural and functional aspects of *EhODC* and role of this enzyme as a therapeutic target.



## **1.6 Localization of *Eh*ODC within the cell**

*Eh*ODC found to be present in the cytoplasm as a soluble enzyme, also in the surrounding vesicles and the plasma membrane (Terán-Figueroa *et al.*, 2009). Extranuclear DNA, cytoplasmic structures kinetoplast-like organelles (*Ehk*Os) also appeared to be link with ODC. However, natural double-stranded DNA showed no traces of ODC interactions within the nucleus. The presence of *Eh*ODC in *Ehk*Os suggests role of polyamines in DNA packing within the organelles as found in other systems (Shayovits *et al.*, 1994; Wang *et al.*, 1999; Kilpeläinen *et al.*, 2000). More studies are required to understand the significance of such distribution of ODC in *E. histolytica*.

## **1.7 Polyamines (PAs)**

The polyamines (PAs) are organic compounds found ubiquitously in all living cells including bacteria, fungi, protozoa, plants and animals. These PAs provide immense contribution in wide variety of biological processes especially cell growth and differentiation (Pegg, 1986; Tabor *et al.*, 1984). Cells can undergo growth arrest, if PAs depleted to less than minimum required amount for the cell cycle progression (Balasundaram *et al.*, 1991, 1993). These PAs are primarily aliphatic amines with three or four methylene carbon chains connecting the amino and imino groups. The hydrophilicity and flexibility of these PAs increase as the charged amino groups increase in the structures which are responsible for positive charge at physiological pH.

### **1.7.1 Polyamines structure and location in the cell.**

#### **1.7.1.1 Structure of PAs**

PAs are organic compounds having two or more primary amino groups. Putrescine is a diamine, spermidine is a tri-amine and spermine with tetra-amine groups fully protonated at physiological pH. Unique properties of PAs are the distribution of positively charged amino groups at regular interval. The hydrocarbon chain in their structures provides flexibility and hydrophilic interactions to the aliphatic cations of interacting macromolecules (Marton *et al.*, 1995; Thomas *et al.*, 2001). Some other amine containing compounds as 1,3-diaminopropane

and cadaverine were also found to have similar properties and included in this category. Molecular formulation of these compounds has been given as follows (Figure 1.3).

Putrescine	$\text{NH}_3^+-(\text{CH}_2)_4-\text{NH}_3^+$
Spermidine	$\text{NH}_3^+-(\text{CH}_2)_3-\text{NH}^+-(\text{CH}_2)_3-\text{NH}_3^+$
Spermine	$\text{NH}_3^+-(\text{CH}_2)_3-\text{NH}^+-(\text{CH}_2)_3-\text{NH}^+-(\text{CH}_2)_3-\text{NH}_3^+$
Diaminopropane	$\text{NH}_3^+-(\text{CH}_2)_3-\text{NH}_3^+$
Cadaverine	$\text{NH}_3^+-(\text{CH}_2)_5-\text{NH}_3^+$

**Figure 1.3: Structures of polyamines with their positively charged amino group (Blue color).**

#### **1.7.1.2 Localization of PAs**

Most prokaryotes do not possess the spermine in the genetic structure but putrescine and spermidine are ubiquitous may be in very less concentration. *In vivo* PAs occur either as free cationic forms or bound in conjugation with many types of anionic cell constituents (Corley *et al.*, 1983; Datta *et al.*, 1987; Igarashi *et al.*, 1989). The PAs in the cell found to be associated with phenolic acids, proteins and phospholipids.

#### **1.7.2 Importance of PA metabolism**

Importance of polyamines can be estimated by relating their functions in cell signaling, regulation, synthesis, degradation, regeneration and maintenance of their own cellular concentration at certain level. In the cell system, these are found in minute quantities varying from micromoles to milimoles. Spermine and spermidine are found in the cells in slightly higher concentrations as compared to putrescine (Watanabe *et al.*, 1991). At different phases of cell cycle, the concentration of these cationic molecules fluctuates, and reaches to the highest level during proliferation phases and stress conditions. Polyamines content varies from species to species within a family. Estimated concentrations of polyamines in different organisms are presented below in the following table (Table 1.2) (Sharma *et al.*, 1989; Hamana *et al.*, 1995; Rathaur *et al.*, 1988; Gordon *et al.*, 1989; Wittich *et al.*, 1987).



Name of the parasite	Concentration of polyamines (nmol/mg) protein			
	Putrescine	Spermidine	Spermine	Putrescine/Spermine
<i>Brugia patei</i>	0.19	40.0	61.50	0.005
<i>Onchocerca volvulus</i>	0.60	4.0	31.0	0.02
<i>Nippostrongylus brasiliensis</i>	ND	9.82	2.35	–
<i>Romanomermis culicivorax</i> <sup>e</sup>	2.74	6.9	0.12	0.40
<i>Ancylostoma ceylanicum</i>	0.06	1.06	0.24	0.06
<i>Hymenolepsis diminuta</i>	0.32	3.25	19.30	0.10

**Table 1.2: Concentrations of polyamines in parasites.** <sup>e</sup> denotes the nmol/mg dry weight.

### 1.7.3 Physiological characteristics of PAs

#### 1.7.3.1 Interaction of PAs with nucleic acids

##### 1.7.3.1.1 PAs in stabilization of DNA

The polyamines possess most unique characteristic property of binding to nucleic acids, especially to DNA. Cationic nature of polyamines neutralizes the charges of phosphate groups of DNA and facilitates the interactions with bases and intercalation into grooves of double helices (Feuerstein *et al.*, 1986-1991; Deng *et al.*, 2000). These nonspecific electrostatic interactions render compactness and stability to the genome without disrupting the native structures. Polyamine-bound genomic DNA maintains the B-form structure even upon precipitation (condensation). PAs causes negligible structural changes to native B-DNA when bind in a thin condensed layer to the surface (Deng *et al.*, 2000). Spermidine and spermine have been confirmed by immunocytochemical studies, to be associated with highly compact mitotic chromosomes (Hougaard *et al.*, 1987; Sauve *et al.*, 1999). However the function of PAs during cell cycle may be responsible for stabilization rather than regulatory effect on the chromatin structure (Laitinen *et al.*, 1998; Hobbs *et al.*, 2000).

Polyamines have ability to prevent DNA fragmentation mediated by restriction endonucleases (Brüne *et al.*, 1991), alkylation agents (Mackintosh *et al.*, 2000), radiations (Douki *et al.*, 2000), and reactive oxygen species (ROS) (Ha *et al.*, 1998; Chattopadhyay *et al.*, 2006). Spermine and un-symmetrically alkylated polyamine analogues prohibit interaction of DNA with assaulting agents and prevent the cleavage of DNA strands.

PAs and their analogues contains amine group which is functionally similar to sodium azide a well-known scavenger of singlet oxygen. Spermine due to its evenly distributed multivalent cationic nature can only be attributed to bring out the stabilization of highly charged triplex DNA (Vertino *et al.*, 1987; Brahe *et al.*, 1995). PAs binding to DNA facilitate the negative charge neutralization, minimize energy requirements for bending and alleviate the protein-DNA interactions. The process of DNA bending is an important regulation process during transcription (Kerppola, 1998; Coulombe, 1999). Many proteins which are involved in tight regulation of transcriptional processes facilitate the cooperative bending of DNA.

#### **1.7.3.1.2 PAs in RNA stabilization**

PAs have the ability to regulate the transcription process and stimulate translation of preformed mRNA (Kuznetsov *et al.*, 2006). In animals, PAs are essential for maintaining the normal integrity of the intestinal epithelial cell. They asseverate the low level of nucleophosmin (NPM) and p53 mRNAs for the normal intestinal epithelial cell. Depletion of cellular PAs by inhibiting ornithine decarboxylase with alpha-difluoromethylornithine dramatically enhanced the cytoplasmic abundance of HuR. HuR is a RNA binding protein which binds and stabilizes these nucleophosmin (NPM), p53 mRNA that encodes for nucleophosmin (NPM), and p53 protein. The depletion of PAs results in high level of (NPM), p53 mRNA which leads to uncontrolled growth and proliferation of intestinal epithelial cells (Zou *et al.*, 2006).

#### **1.7.3.2 PAs in protein synthesis**

PAs bring about an increase in the efficiency of over-all protein synthesis. They exhibit differential effects on large number of proteins, by acting either at any or all of the stages of

translation namely- initiation, elongation, termination. Additionally, PAs also stimulate the charging of transfer RNA (tRNA). The overall rate of protein synthesis increases even if limiting concentration of a particular tRNA species is available. The PAs deficiency results in the formation of an impaired polysome (Höltkä *et al.*, 1985, 1986) that could be due to irregular initiation and/or elongation processes (Takemoto *et al.*, 1983). These outcomes confirmed the ability of polyamines to bind and influence secondary structures of mRNA, tRNA and rRNA (Kusama-Eguchi *et al.*, 1991; Yoshida *et al.*, 1999; Igarashi *et al.*, 2000).

#### **1.7.3.3 PAs in glycolysis.**

Polyamines involve in the activation of certain enzymes which are important for the metabolism. Adenosine Monophosphate (AMP) deaminase is specifically activated by polyamines (Parsons, 2004). This enzyme produces increased concentration of ammonium ions by AMP deaminase reaction in adenylate degradation. This ammonium ion in turn activates phosphofructokinase (PFK) and pyruvate kinase (PK), which are key enzymes in glycolysis (Saavedra *et al.*, 2005). Spermidine protects AMP deaminase from inhibition by fatty acid. The increased ammonium level is responsible for enhancement of phosphofructokinase (PFK) activity, and glycolytic flux (Seo *et al.*, 2011).

#### **1.7.3.4 PAs in oxidative defense mechanism**

Oxygen radicals found to be toxic to human body and cells undergo stress and death under oxidative stress condition (Groppa *et al.*, 2008; Kumar *et al.*, 2012). PAs can stabilize the membranes and prevents cell collapse due to osmotic shocks. Spermine functions as a scavenger of hydroxyl radical under oxidative stress. Spermidine also scavenges hydroxyl radical and maintains the appropriate reduction state of the biological membrane for protecting it from thiols, which are responsible for pore formation. They protect the phospholipids containing acidic vesicles and inhibit peroxidation by reactive hydrogen peroxide radicals (Parchment *et al.*, 1989; Nilsson and Gritli-Linde 2000; Seiler, 2000).

#### **1.7.3.5 PAs in signal transduction**

Polyamines are potent  $\alpha$ -amino-3-hydroxy-5-methyl-4-isoxazolepropionic acid (AMPA) and kainate receptor blockers; especially cytoplasmic spermine, spermidine and philanthotoxin

are weakly permeable open-channel blockers. The regulation of cellular polyamines is a central convergence point for the multiple signaling pathways. Normal epithelial cell proliferation in the intestinal mucosa depends on the supply of polyamines to the dividing cells. PAs have been demonstrated to effect directly the conformation of the estrogen responsive element in DNA (Thomas *et al.*, 1997; Lewis *et al.*, 2000). They are also involved in regulatory synthesis of transcription factors or modulate their binding activity via phosphorylation (Wang *et al.*, 1993, 1999, 2001; Pfeffer *et al.*, 2000).

#### **1.7.3.6 PAs in mitochondria metabolism**

The submitochondrial particles and F1-ATPase have been studied thoroughly to understand the effect of polyamines on them. Spermine stimulates the reaction P1-ATP exchange and succinate dependent ATP synthesis, catalyzed by submitochondrial particles. In addition, spermine and spermidine are able to inhibit the degradation of ATP, the reaction catalyzed by submitochondrial particles and F1-ATPase (Igarashi *et al.*, 1989). The cells deficient in polyamine contents show lower ATP content as compare to normal cells. These results suggested the possible role of spermine to keep the concentration of ATP at high level in the cell system (Igarashi *et al.*, 1989).

#### **1.7.3.7 PAs in central nervous system**

Elevated levels of polyamines during the regeneration of neurons signify their role during the development and differentiation of central nervous system. Their essence is well documented in neuronal cell division, differentiation, axonogenesis, synaptogenesis and synaptic plasticity. Spermidine can promote the regeneration of optic nerves and CNS axons after injuries (Cai *et al.*, 2002). Different pathological stimuli in the brain such as physical, chemical, thermal and metabolic stress induce and enhance the ODC activity (Kauppinen RA *et al.*, 1995; Johnson, 1998; Bernstein *et al.*, 1995, 1999; Seiler, 2000). The ODC activity of the brain starts declining from few weeks or months to 70 fold lower during the adult age as compared to the day of birth (Suorsa *et al.*, 1992).

### 1.7.3.8 PAs in angiogenesis and cancer

The polyamines are essential for the growth and differentiation of eukaryotic cells, and accordingly elevated polyamine levels are indispensable for neoplastic transformation, proliferation, and survival. They are essential for cancer cell proliferation during tumorigenesis. PAs also involved in the regulation of non-malignant cells essential for angiogenesis-dependent tumor progression. They regulate early events of angiogenic processes involving micro-vessel sprouting and endothelial cell migration. PAs level and polyamine biosynthesis are highly elevated in the cancer cells or tissues. Cells treated with chemical carcinogens and tumor promoters show highly activated ODC (Hölttä *et al.*, 1988; Pegg, 1988; Sistonen *et al.*, 1989; Auvinen *et al.*, 1992).

### 1.7.4 PAs in plant

PAs play important role in plant growth and development. In addition, they are also involved in plant stress tolerance (Young *et al.*, 1983, 1984), senescence, modulation of enzyme activity, and also stabilize the nucleic acids and cell membranes (Tiburcio *et al.*, 1989, 1990; Evans *et al.*, 1989; Zheliaskova *et al.*, 2000). Polyamine biosynthesis is also helpful in the maintenance of photosynthetic activity during senescence responses induced by osmotic stress (Borrell *et al.*, 1995). They also provide protection to cells and cell compartments from oxidative damage (Drolet *et al.*, 1986; Balasundaram *et al.*, 1993). Many plants form toxic alkaloids from polyamines (Guggisberg *et al.*, 1983; Burtin *et al.*, 1997), as in tobacco plant putrescine gets metabolized to pyrrolidine ring of nicotine which is its major alkaloid (Tiburcio *et al.*, 1985). Putrescine enhances xylogenesis of xylem cells in *Helianthus* tuber (Phillips *et al.*, 1988; Bienz *et al.*, 2002).

### 1.7.5 PAs in animal cell cycle

Several studies have indicated the critical role played by polyamines during cell proliferation (Pegg, 1986; Piacenza *et al.*, 2001), including differentiation, and cell growth (Hobbs *et al.*, 2000). Cells in the G<sub>0</sub> phase are usually dormant. These quiescent cells require signal in the form of hormones or growth factors to enter the G<sub>1</sub> state and initiate the process of cell division. In mammalian cells, they promote cell cycle from G<sub>1</sub>-S transition and S to M



transition to keep rolling the cell cycle and preventing cell arrests (Figure 1.4) (Hsu *et al.*, 2008).

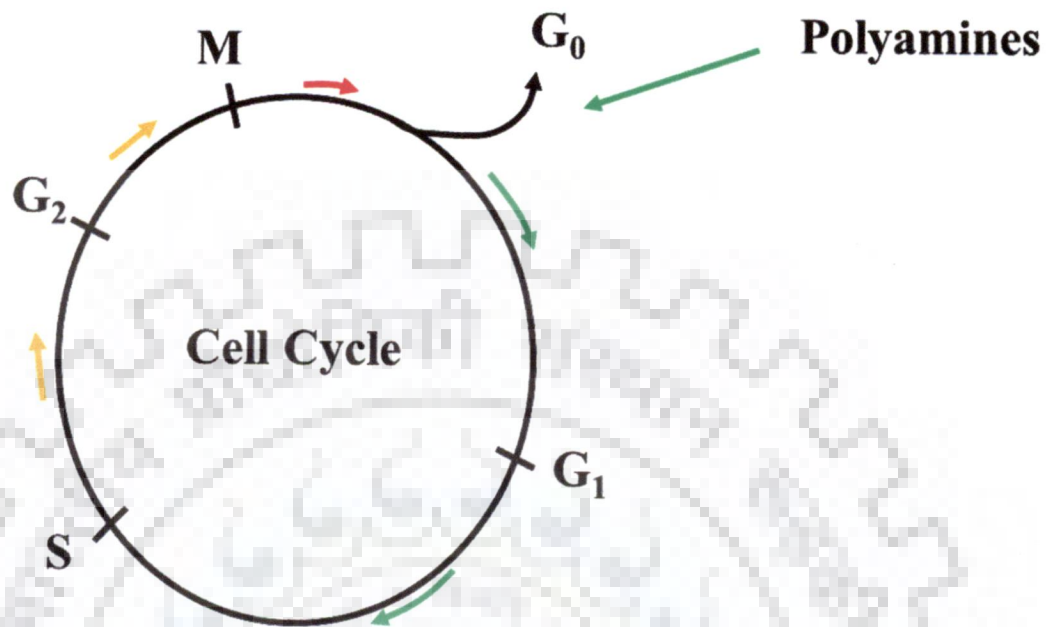


**Figure 1.4: Schematic representation of various phases of the cell cycle and the mediators of cell cycle progression.** Progression of cell cycle depends upon different polyamines at different stages of growth. Arrow indicates PAs concentration in the direction of cell cycle progression. The abundance of different polyamines are indicated by different colors. Presence of all PAs are indicated by green, and presence of spermidine and putrescine are indicated by orange, and absence of PAs are indicated in red (Ravanko *et al.*, 2000; Field *et al.*, 2004).

Embryos from the mutant larvae, developing in polyamine deficient medium failed to develop unless supplemented with polyamines. Cell cycle progression in polyamine depleted cells found to be halted in early growth phase (Thomas *et al.*, 1997, 2001) Polyamines involve in intensifying the signaling processes for the production of hormones/growth factors. Putrescine level increase from S to G<sub>2</sub> stage only. Spermidine constantly increases throughout the entire cycle in contrast to spermine which increases only from G<sub>1</sub> to S phase (Figure 1.4) (Celano *et al.*, 1989).



### 1.7.6 PAs in bacteria

PAs are essential for normal growth of bacterial cell. This fact has been proved by studying the requirement of polyamines by auxotrophic *E. coli* strains (Haffner *et al.*, 1979). Exogenous polyamines bind to membranes and stabilize spheroplasts and protoplasts in *E. coli* (Tabor *et al.*, 1973), also help in protection of the halophilic bacteria from osmotic shock (Tabor *et al.*, 1985). The *E. coli* and *S. typhimurium* outer membrane contains four times more PAs than cytoplasmic membrane (Koski *et al.*, 1991).

### 1.7.7 PAs in protozoa

Polyamine putrescine and spermine are found to be essential for all parasitic protozoa studied till date. *Giardia*, *Trachomonas* (North *et al.*, 1986), *Entamoeba*, *Leishmania sp.* (Vannier-Santos *et al.*, 2008; North *et al.*, 1987), *Trypanosoma*, *acanthamoeba*, *Eimeria*, *Naegleria* and *Plasmodium sp.* (Haldar, 1992; Haider *et al.*, 2005) reported to be able to produce spermine but in small quantity.

Putrescine is most common PA found in *Leishmania*, *Trypanosoma* and other protists while trace amounts of spermine have also been detected (Baláña-Fouce *et al.*, 1991). PAs uptake is a regulatory stage for cell cycle more specifically putrescine is the main regulatory polyamine (Gonzalez *et al.*, 1992), which helps in elucidating its importance in growth and proliferation of parasites. Interestingly, addition of putrescine to ODC-deficient *L. donovani* mutants restores parasite growth more rapidly and to a greater extent than higher PAs (Jiang *et al.*, 1999).

Furthermore, this diamine leads to higher concentrations of trypanothione. In *E. histolytica*, polyamines have been studied in context to both hypusination and trypanothione synthesis (McKerrow *et al.*, 1993; Que *et al.*, 1997). Polyamine concentration reported to be present in parasitic protozoa has been given in the Table 1.2 (North *et al.*, 1986; Bacchi *et al.*, 2002).

Name of protozoan parasite	Concentration of polyamine in nmol/mg			
	Putrescine	Spermidine	Spermine	Putrescine /Spermine
<i>Entamoeba histolytica</i>	92	2.6	0.03	35.5
<i>Giardia lamblia</i>	10	9.6	0.8	1.0
<i>Leishmania donovani</i> (promastigotes)	35	37.1	0	0.9
<i>Leishmania donovani</i> (amastigotes)	2	18.8	3.5	0.1
<i>Plasmodium falciparum</i> <sup>d</sup>	9	33.0	8.0	0.3
<i>Tetrahymena thermophila</i> <sup>c</sup>	10	3.0	0	3.1
<i>Trichomonas vaginalis</i>	38	3.5	1.3	10.9
<i>Trichomitus batrachorum</i>	114	17.6	15	6.5
<i>Trypanosoma cruzi</i>	+	+	+	
<i>Trypanosoma brucei</i>	4	24.5	0	0.17
<i>Trypanosoma rhodesiense</i>	4	21.0	1.2	0.18

**Table 1.3: Polyamine concentration reported to be present in parasitic protozoa. In this table:** <sup>c</sup> is for concentration in milimolar; <sup>d</sup> is for concentration in pmol/10<sup>6</sup> parasitized erythrocyte (Bacchi *et al.*, 2002; Sharma *et al.*, 1989; Hamana *et al.*, 1995; Rathaur *et al.*, 1988; Gordon *et al.*, 1989).

#### 1.7.7.1 PAs in *Entamoeba histolytica*

In *E. histolytica*, most prominent polyamine is putrescine which is present in detectable amount as compared to others (Bakker-Grunwald *et al.*, 1995). This assertion was supported by presence of experimentally characterize ornithine decarboxylase enzyme (Arteaga-Nieto *et al.*, 2002). Other enzymes responsible for higher polyamine synthesis have not been reported in the genome sequence of *E. histolytica*.

## 1.8 Polyamine biosynthetic pathway.

Polyamine biosynthesis takes place in most of the living organisms from precursor amino acids, arginine and methionine (Davis *et al.*, 1992; Marton *et al.*, 1995, 1999). Significant research has been done to establish the fact that synthesis and inter-conversion of polyamines are strictly regulated. The initial steps committed to polyamine biosynthesis are formation of putrescine through decarboxylation of ornithine. Polyamine biosynthesis regulation is mainly reckoned by key enzymes, ornithine decarboxylase (ODC, EC 4.1.1.17). The activities of the enzymes fluctuate rapidly in response to various positive or negative stimuli. The half-life of ODC enzyme activity is between 10 to 20 minutes (Seely *et al.*, 1982; Isomaa *et al.*, 1983). Putrescine further converted to spermidine in a spermidine synthase (SDE) catalyzed reaction. This enzyme transfers an aminopropyl group donated by decarboxylated S-adenosylmethionine to putrescine. Spermine is formed by addition of the second aminopropyl moiety to spermidine, this reaction is catalyzed by a different aminopropyl transferase namely, spermine synthase (SME) (Figure 1.5) (Tiburcio *et al.*, 1990).

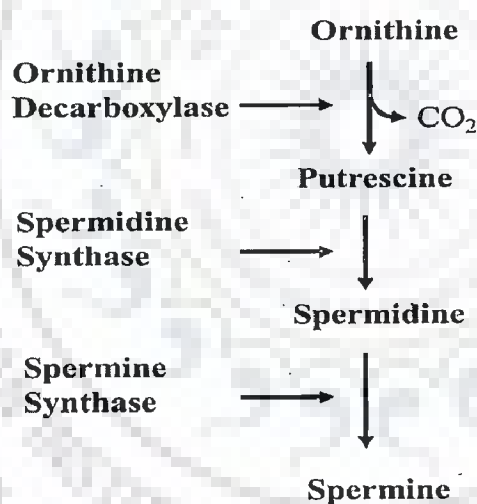


**Figure 1.5: Biosynthetic pathway of polyamines putrescine and higher polyamines. 1) Ornithine decarboxylase; 2) Spermidine synthase; 3) Spermine synthase (Wallace *et al.*, 2003).**

Two constitutively expressed and stable enzymes spermidine synthase and spermine synthases play considerably minor role in regulation of intracellular polyamine levels. They

both are regulated mainly by the availability of their substrate and decarboxylated S-adenosylmethionine.

## 1.9 Ornithine Decarboxylase (ODC)

### 1.9.1 ODC as regulatory enzyme of PA biosynthetic pathway

The enzyme ornithine decarboxylase is pyridoxal 5' phosphate (PLP) dependent enzyme. Function of ODC is conversion of L-ornithine to diamine putrescine, first step of polyamine biosynthesis. The process of polyamine biosynthesis gets regulated by ODC enzyme. Inhibition of this enzyme would lead to arrest of cell growth and subsequent death. Failed regulation of cell processes can be attributed to increased ODC activity which may lead to malignant transformation and uncontrolled growth.

### 1.9.2 ODC as PLP dependent enzyme

The secondary structure profiles together with biochemical information allowed Grishin *et al.*, 1995 to classify all PLP dependent enzymes into seven fold types (Figure 1.6). Their analysis grouped the eukaryotic ODCs and alanine racemas to same fold type.

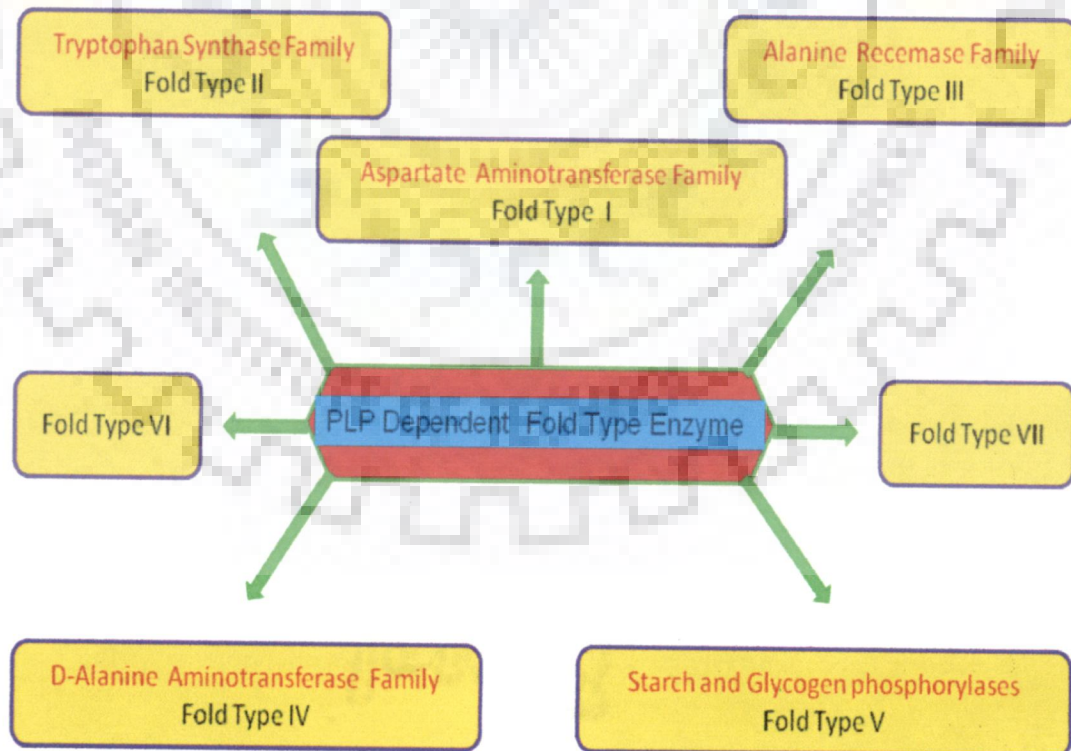


**Figure 1.6: Classification of the Pyridoxal 5' phosphate dependent enzyme on the basis of sequences, secondary structure, biochemical information and hydrophobicity profile (Grishin *et al.*, 1995).**

The presence of ornithine decarboxylase in both Fold type I and III derive us in a direction of evolutionary relationship (Table 1.4).

Fold type I	
<b>Prokaryotic ornithine decarboxylase (ODC)</b>	EC 4.1.1.17
Prokaryotic lysine decarboxylase (LDC)	EC 4.1.1.18
<i>E. coli</i> bio-degradative arginine decarboxylase	EC 4.1.1.19
Glutamate decarboxylase (GAD)	EC 4.1.1.15
Histidine decarboxylase (HDC)	EC 4.1.1.22
Aromatic-L-amino-acid decarboxylase	EC 4.1.1.28
Glycine decarboxylase	EC 1.4.4.2
Fold type III	
Eukaryotic ornithine decarboxylase (ODC)	EC 4.1.1.17
Prokaryotic diaminopimelic acid decarboxylase- (DAPDC)	EC 4.1.1.20
Bacterial and plant biosynthetic arginine- decarboxylase	EC 4.1.1.19 EC 5.1.1.1
Alanine racemase (ALR)	

**Table 1.4: Pyridoxal 5' phosphate dependent enzymes fold types.** Show PLP dependent enzymes of fold-type I and III from eukaryotic and prokaryotic organisms (Grishin *et al.*, 1995).

These decarboxylases share certain traits which are conserved in both fold I and III type. In all PLP dependent ODCs, Lys residue is found in the  $\alpha$ -helix of the active site

domains. Lys forms a Schiff base with PLP in both fold type I and fold type III (Grishin *et al.*, 1995; Choi *et al.*, 2006).

### 1.9.3 Fold type III ODC available

Over 100 crystal structures of PLP-dependent enzymes (with substrate, inhibitors, or mutants), have been solved till date. Fold type III (Decarboxylase) PLP dependent enzymes are given here (Table 1.5).

Enzyme	Species	Function	Year	PDB
<b>Fold Type III</b>				
Ornithine Decarboxylase				
	Mouse	Decarboxylation	1999	7ODC
	<i>T. brucei</i>	Decarboxylation	1999	1QU4
	Human	Decarboxylation	2007	2000

**Table 1.5: Fold type III ODC which have been crystallized. (Data retrieved from NCBI).**

The enzyme ornithine decarboxylase has been reported to be categorized in both Fold type I and Fold type III, depending upon the existence in either prokaryotic or eukaryotic organisms.

### 1.9.4 Decarboxylase subfamily.

The amino acid decarboxylases (AADCs) which were placed into two different fold types were further subdivided into four different groups by Sandmeier *et al.*, in 1994. They grouped different PLP dependent decarboxylases into four groups which seemed to be evolutionarily unrelated to one another (Figure 1.7). AADCs found in animals are responsible for biosynthesis of biogenic amines and polyamines.

Bacterial AADCs fulfill similar biosynthetic functions as animal AADCs. In addition they also regulate the pH of cell and its environment in the process of decarboxylation of amino acids by inducible bio-degradative enzymes.



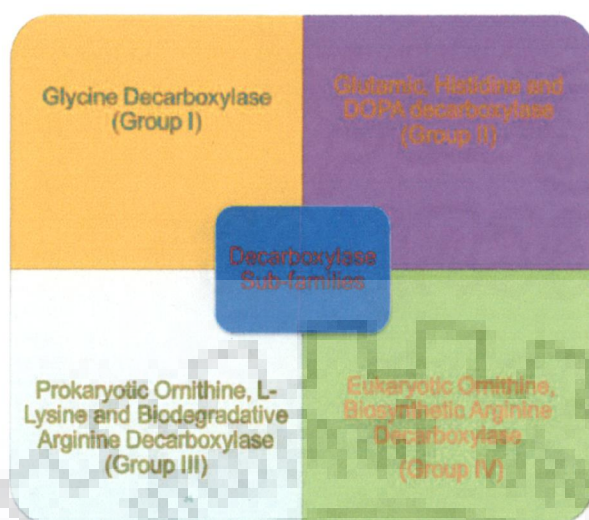


**Figure 1.7: Classification of decarboxylases into subfamilies on the basis of sequence similarity (Sandmeier *et al.*, 1994).**

It is important to consider the fold type and the group classification because Group I, II and III are related to fold type I and group IV is related to fold type III decarboxylase and some have characteristic features similar to both fold type (Sandmeier *et al.*, 1994; Gibrat *et al.*, 1996).

### 1.10 Characteristic features of ODCs

ODCs sequence has been reported from large number of eukaryotic organisms. Structural properties of ODCs are similar to alanine racemase family. The two third of the sequence or about 300 residues considered to play structural role and belongs to N-terminal domain. Sequence shows arrangement of  $\alpha$ -helix,  $\beta$ -sheet alternate to one another at the N-terminal, and large number of sheets at the C-terminal (Figure 1.8) (Tobias *et al.*, 1993; Osterman *et al.*, 1995, 1995; Kern *et al.*, 1999, Almrud *et al.*, 2000).

There are notable differences in the secondary structure arrangements which separate II and III fold types. Fold type III have one  $\beta$ -strand followed by one  $\alpha$ -helix at the N-terminus but in fold type II two  $\beta$ -strands followed by one  $\alpha$ -helix. In fold III family Schiff base lysine immediately followed by a hydrophobic  $\beta$ -strand rather than a loop structure which is prominent in fold type II enzymes. Fold type III enzymes noticed to have various

conserved motifs in which one invariant residue has critical role in activity or stability.  $\beta$ -sheets are mainly hydrophobic and parallel to one another (Alexander *et al.*, 1994; Sandmeier *et al.*, 1994).

In case of *T. brucei*, conserved residues Lys69, Asp134, Arg154, His197, Asp233, and Gln274 are present mainly at the C-terminus of each strand or loop. These residues arrange themselves in a close conformation and compact active site forms at the center. Gly276, Gly358 and Asp364 are conserved in addition to Lys69 and Cys360 at the active site pocket. The C-terminal region shows low sequence similarity due to insertions or variations and considered as a site for proteolysis and degradation (Figure 1.8) (Kern *et al.*, 1999; Jackson *et al.*, 2000; Osterman *et al.*, 1995).

### 1.11 Reaction mechanism of ODC

Ornithine decarboxylase catalyzes the decarboxylation by a basic general mechanism which includes four essential steps namely transimination, decarboxylation,  $\alpha$ -protonation, and second transimination (Toney, 2005). First step is a Schiff base formation between PLP and Lys69 (internal aldimine) at the active site. This step is followed by enzymatic substitution of amino acid substrate (external aldimine), now lysine form Schiff base with ornithine and release enzymatic lysine. Decarboxylation takes place which results in the formation  $\text{CO}_2$  and a spectrally detectable quinoid intermediate (Figure 1.9) (Grishin *et al.*, 1999; Poulin *et al.*, 1992; Jackson *et al.*, 2000).

This intermediate decays in two steps: first step involve the co-operative shift of protons from  $\text{C}_\alpha$  to  $\text{C4}'$  of PLP. Second step is protonation of  $\text{C}_\alpha$  carbon to form Schiff base with putrescine (intermediate). This intermediate is attacked by lysine and releases putrescine product. This finally results in the formation of PLP bound ornithine decarboxylase enzyme (Toney, 2005; Jansonius, 1998).

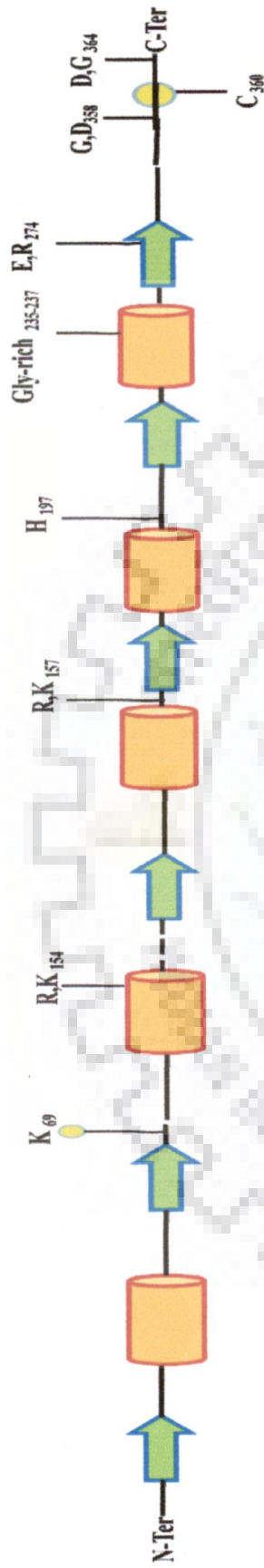


**Figure 1.8: Secondary structure elements and consensus sequence of PLP binding fold type III decarboxylase.** Strands are shown as arrows, helices as cylinders and loops as lines, dashed lines denoted the regions in the sequence that are not conserved (numbered as in mouse ODC). Schiff base is marked by circle (Grishin *et al.*, 1999).

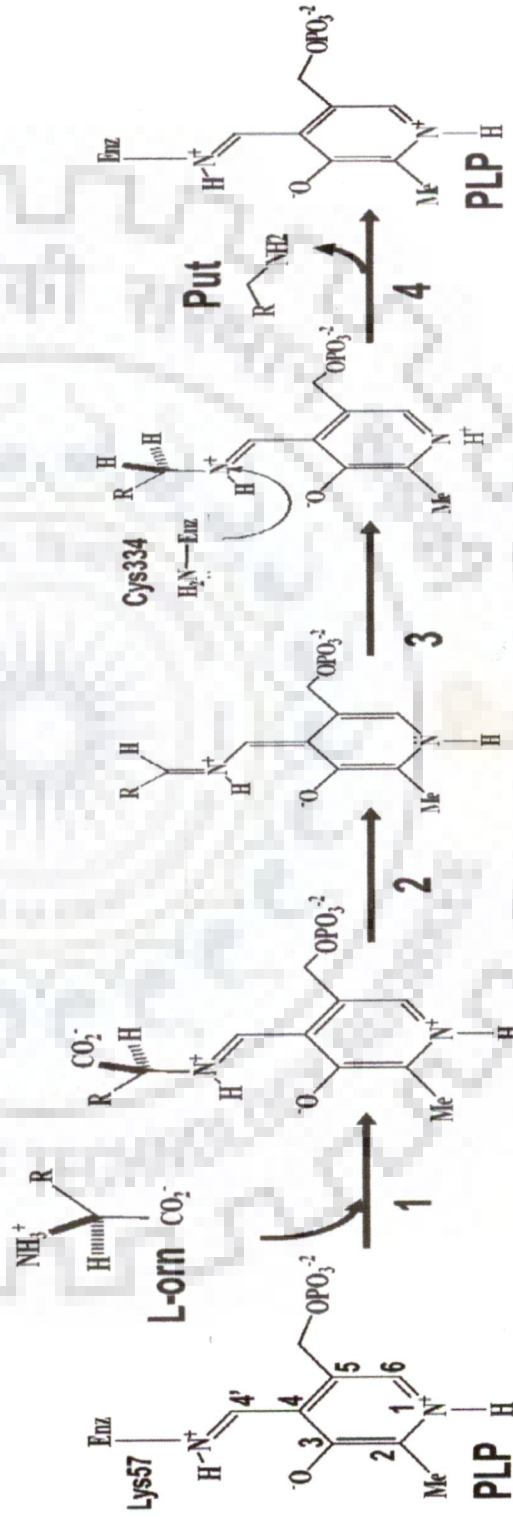


**Figure 1.9: Reaction mechanism of ornithine decarboxylase.** Four steps:- 1) Transamination; 2) Decarboxylation; 3)  $\alpha$ -Protonation and 4) Second transamination. PLP is Pyridoxyl 5' phosphate; L-orn is substrate L-ornithine and Put is the product putrescine (Toney, 2005; Poulin *et al.*, 1992).

## 1.12 Regulation mechanisms of ODC

Several mechanisms contribute to modulation of ODC activity, four basic regulations are at the transcription level (Abrahamsen *et al.*, 1991, 1992; Katz *et al.*, 1987), post-translational modification (Lu *et al.*, 1991), regulation by products of polyamine biosynthesis in negative feedback control and proteasome mediated ubiquitin-independent degradation which gets induced due to antizyme (AZ) binding (Murakami *et al.*, 1996; Kanamoto *et al.*, 1986; Hayashi *et al.*, 1995; Li and Coffino, 1992; Canellakis *et al.*, 1979, 1993). All the above mechanisms are interlinked, as binding of AZ result in increased polyamine levels which in turn promotes the fidelity of the AZ-mRNA translational frame shifting, responsible for formation of increased concentrations of AZ (Matsufuji *et al.*, 1995). This Az selectively binds to the inactive ODC monomer (Li and Coffino, 1992; Mitchell *et al.*, 1990), and finally the ODC:AZ heterodimer targets itself for degradation by the 26S proteasome (Coffino, 1998; Murakami *et al.*, 1996).

### 1.12.1 Antizyme mediated ODC regulation.

Putrescine which is the end product of ODC found to be involved in the induction of synthesis of a protein known as antizyme. This protein with an apparent molecular weight of 26,500 Da was infused with an ability to modulate ODC activity as noncompetitive inhibitor. Distal products of ODC as spermidine and spermine, also induces the production of this protein named as ODC-antizyme (Heller *et al.*, 1976). Ornithine decarboxylase-antizyme is a negative regulator of polyamine at cellular level (Fong *et al.*, 1976; Heller *et al.*, 1976). It acts by destabilizing the first enzyme of polyamine biosynthetic pathway namely ODC and inhibits the uptake of polyamine (Mitchell *et al.*, 1994; Suzuki *et al.*, 1994). This antizyme binding to ODC inactivate the enzyme and target it for degradation by 26S proteasome (Figure 1.10) (Hayashi *et al.*, 1985; Murakami *et al.*, 1992; Li *et al.*, 1994).

Recently, many antizyme forms have been known to exist, many isoform of mammalian antizyme, antizyme 1 (Hayashi *et al.*, 1997) 2 and 3 (Ivanov *et al.*, 1998, 2000) have been characterized. AZ binding induces the conformational modification in the structure and



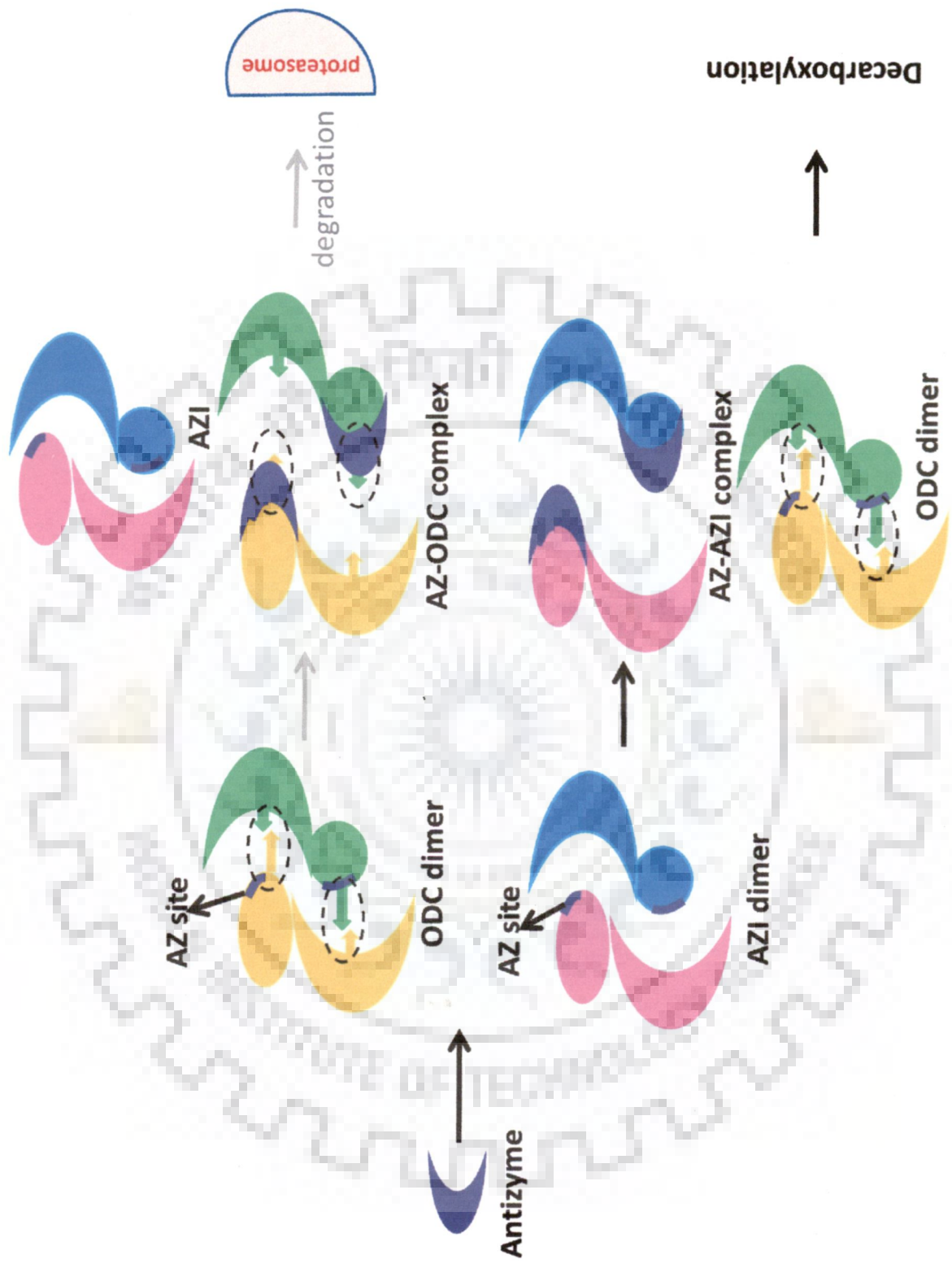
expose the C-terminus of monomeric ODC and consequently 26S proteasome mediated degradation of enzyme occurs (Coffino, 1998, 2000). Mechanism of ODC-AZ mediated proteolysis process is unknown. But some results revealed the outcome of ODC-AZ interactions result in the inactivation and dramatically accelerated degradation of ODC. AZ dependent degradation requires the previously characterized carboxyl-terminal destabilization segment of ODC (Figure 1.10).

AZ binding locus of human ODC was inspected to be at the N-terminus residue 117-140. AZ binding locus composed mainly of positively charged residues which render it as electropositive patch at the interface of dimer. These residues are partially buried in the dimeric structure and unable to bind antizyme and consequent degradation (Figure 1.10) (Almrud *et al.*, 2000).

### 1.12.2 Antizyme inhibitor (AZI) mediated ODC Regulation

Antizyme inhibitor is ortholog of ODC which have lost the ability to decarboxylate L-ornithine to putrescine. Instead AZI shows great affinity towards the antizyme as compared to ODC and protect the ODC enzyme from antizyme mediated degradation, result in the up-regulation of ODC activity. AZ binding region of human ODC and AZI are found to be almost identical except five residues from 117-140 (Li *et al.*, 1992). These residues are K125, V126, C133, N135, and K140 whereas residues K125 and K140 play critical role during the antizyme binding (Figure 1.10) (Liu *et al.*, 2011).

**Figure 1.10: Mechanism of regulation of ODC mediated by Antizyme (AZ) and Antizyme inhibitor (AZI).** AZ binds to recognition site (purple color) of either ODC or AZI result in the formation of heterodimer complex of AZ-ODC and AZ-AZI. In addition, it also causes dissociation of dimers to monomer. The AZ-ODC complex undergoes degradation mediated by 26S proteasome (gray arrows). AZ-AZI complex formation allows the escape of ODC to undergo degradation and active enzyme catalyzes decarboxylation reaction (black arrows).





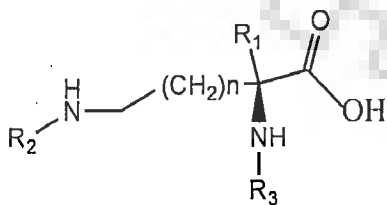
### 1.13 Inhibition mechanism of ODC

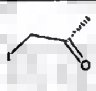
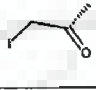
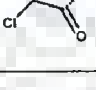
Ornithine decarboxylase is an important drug target due to its important role in polyamine biosynthesis. An elegant approach is to design a specific, irreversible and potent inhibitor, possessing the reactive groups binding to active site and results in the inactivation of enzyme. Many inhibitors have been designed against ODCs of pathogens to overcome the virulent effect. Inhibitors mainly belong to active site binding components which are substrate, product, analogues and derivatives of both. Recently, cofactor-substrate or cofactor-product analogues are also coming in application. Fluorine and methylene based inhibitors are more prevalent for the structure based drug designing (Robertson, 2005; Silverman *et al.*, 1996; Karukurichi *et al.*, 2007; Mayhoub *et al.*, 2011).

#### 1.13.1 Substrate analogues and derivatives

The substrate analogue  $\alpha$ -difluoromethylornithine (DFMO) (eflornithine) has been shown to block the proliferation process of *G. lamblia* but no effect on *E. invadens*, *E. histolytica*, *T. cruzi*, *Leishmania donovani* and *Schistosoma mansoni* (Gillin *et al.*, 1984; Calvo-Mendez *et al.*, 1993; Kaur *et al.*, 1986; Coons *et al.*, 1990; Hesse *et al.*, 2001).

DFMO has been successfully used as a chemotherapeutic agent to eradicate the pathogenic protist *T. brucei* (McCann *et al.*, 1981; Bitonti *et al.*, 1985). Some other substrate analogues have been studied viz.  $\alpha$ -monofluoromethyl-3,4-dehydroornithine;  $\alpha$ -monofluoromethyl-3,4-dehydro-ornithine methyl ester;  $\alpha$ -monofluoromethyl-3,4-dehydro-ornithine ethyl ester (Table 1.6).



Compound	n	R1	R2	R3	$K_d(\mu\text{M})^a$	$K_d(\mu\text{M})^b$	$K_d(\mu\text{M})^c$
Ornithine	1	H	H	H	250	0.80	1.41
1	1	H	H	NH <sub>2</sub>	0.5	0.46	5.59
2	1	CH <sub>2</sub> F	H	H	75	1.55	0.50
3	1	CH <sub>2</sub> F <sub>2</sub>	H	H	39	1.56	0.89
4	1	H		H	nd	2.16	1.30
5	3	H		H	nd	3.33	5.59
6	1	H		H	2500	4.47	4.40

**Table 1.6: Chemical structures of substrate analogues with different side chains.** The basic structure given above the table and different side chains are presented with the  $K_d$  values (Bey *et al.*, 1978).  $K_d$  values from: <sup>a</sup> Experimental data (Regunathan and Reis, 2000; Brooks and Phillips, 1997; Rodriguez Paez *et al.*, 1997; Abdel-Monem *et al.*, 1975; Sjoerdsma and Schechter, 1984) and from docking simulations at <sup>b</sup> PLP and at <sup>c</sup> Cys 360 from monomer B.

### 1.13.1.1 Inhibition mechanism of substrate analogues

Out of the several inhibitors of ODC the most widely used is DFMO, it was introduced and used efficiently since more than two decades. DFMO covalently interacts with Cys360 of ODC and binds irreversibly to the active site (Seiler, 2003). DFMO has been proved as an efficient therapeutic agent acts in dose dependent manner on cancerous cells (Vlastos *et al.*, 2005; Karukurichi *et al.*, 2007). DFMO is a well-known drug to eradicate African sleeping sickness caused due to *trypanosome brucei* infection. But it is a weakly bound and reversibly removed from the site by increased concentration of substrate ornithine.

Substrate analogues have special characteristics of replacing substrate from the active site of the enzyme. These compounds undergo decarboxylation and result in the formation of

intermediate carbanionic species. First is conjugated imine production by elimination of leaving group. Next is the internal cysteine, attacking the alkylic ( $\beta$ ) position result in tautomeric imine formation and release of fluoride via an extended conjugation mechanism. Both imines alkylate a nucleophilic residue at or near the active site to covalently bind the inhibitor to enzyme (Figure 1.11) (Casero *et al.*, 2005; Silverman *et al.*, 1996; Karukurichi *et al.*, 2007).

ODC enzyme catalyzes decarboxylation of the  $\alpha$ -methyl moiety of its substrate analogue. The irreversible inhibition takes place when DFMO undergoes decarboxylation which results in expulsion of fluoride as opposed to  $\alpha$ -protonation. Next step involves the attack of Cys at the  $\beta$ -position result in the release of fluoride. Reformation of internal aldimine leads to covalent modification of Cys which in turn inactivates the enzyme (Figure 1.11). DFMO might get displaced *in vivo* by endogenous substrate of ODC. In human plasma the concentration of ornithine seems to be high. Cells develop resistance due to inefficient uptake of DFMO or fast clearance from the site of action. The up regulation of ODC expression and presence of transporter for polyamines in the cell are further drawbacks which displace DFMO as efficient therapeutic agent (Casero *et al.*, 2005; Marton *et al.*, 1995).

### 1.13.2 Product analogues

The enzyme ODC is regulated by inactivation in the presence of polyamines (Seely *et al.*, 1983). *In vitro* studies revealed that putrescine is a strong inhibitor of ODC from lower eukaryotes such as fungi (Calvo-Mendez *et al.*, 1987). However, *Neurospora* ODC gets less suppressed by putrescine and remains unaffected in the presence of spermidine and spermine (DiGangi *et al.*, 1987). The anti-proliferative effect of product (spermidine) analogue 2, 4-diamino-2-butanone (DAB) is mainly reported for mitochondrial destruction (Stevens, 1977). DAB causes the inactivation of ODC *in vivo* by acting as an irreversible competitive inhibitor (Stevens *et al.*, 1978; Chapman *et al.*, 1978; Alhonen-Hongisto *et al.*, 1979; Sertich *et al.*, 1987). Putrescine analogues can have less adverse effect on cell growth, as cells get recovered after three days of incubation. Some other product analogues viz. 5-Hexyne-1,4-diamine, *trans*-hex-2-en-5-yne-1,4-diamine, and (2*R*,5*R*)- $\delta$ -methyl- $\alpha$ -acetylenic putrescine have been applied as inhibitor. ODC studied from *Entamoeba* species reported to be inhibited

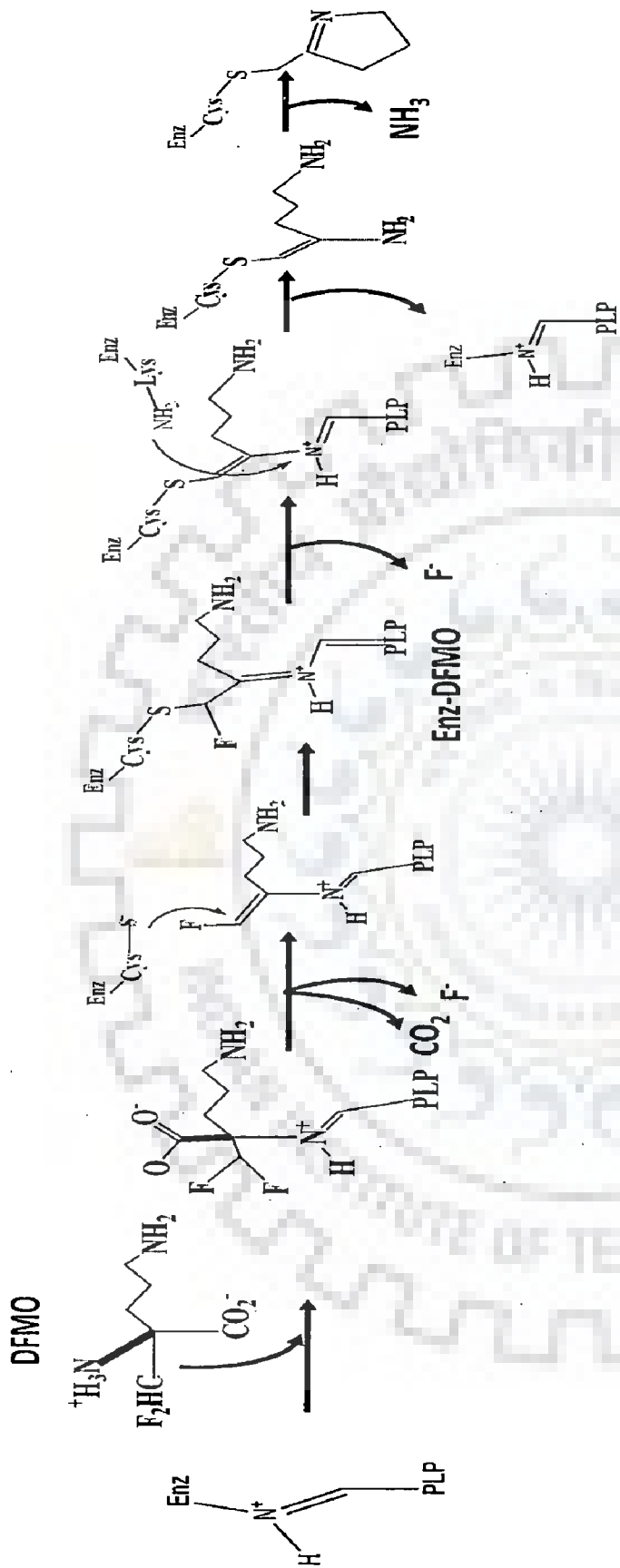


**Figure 1.11: Reaction mechanism of inhibition of Ornithine Decarboxylase Enzyme in the presence of DFMO (*T.brucei*)** (Grishin NV et al., 1999; Poulin R et al., 1992).

by 3 polyamines analogues in decreasing order of effectiveness as putrescine > spermidine > spermine respectively (Calvo-Mendez *et al.*, 1993; Persson *et al.*, 1985).

### 1.13.2.1 Inhibitor mechanism of product analogue

Product analogues are capable of replacing putrescine at the active site, the proton abstraction implicit in reverse reaction lead to propargylic anion formation yield an allene on protonation. This allene conjugated to pyridoxalimine and functions as reactive Michael acceptor which could alkylate a nucleophilic residue in the active site.

### 1.13.3 Cofactor-substrate analogues

Cofactor-substrate analogues are the compounds having PLP with a substrate amino acid attached to it (Christen *et al.*, 2001). These compounds mimic the structure which forms at transition state during enzymatic reaction (Eliot *et al.*, 2004; Christen *et al.*, 2001). They bind with high affinity to apoprotein and enzyme cannot transform it and thus gets inhibited very efficiently (Raso *et al.*, 1975; Heller *et al.*, 1975). These compounds have high degree of specificity as phosphopyridoxal-ornithine inhibits ODC without affecting *S*-adenosylmethionine decarboxylase (Heller *et al.*, 1975). Other such compound is *N*-(4'-pyridoxal)-ornithine (BOC)-OMe.HCl (POB) having the same properties of inhibition as substrate analogue attached to PLP and act as a transition state of decarboxylation reaction.

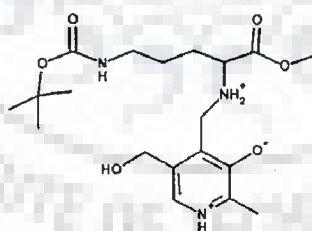


**Figure 1.12: Structure of cofactor-substrate analogue. *N*-(4'-pyridoxal)-ornithine (BOC)-OMe.HCl (POB) (Wu *et al.*, 2009).**

**1.13.3.1 Inhibition mechanism of cofactor-substrate analogues-** Several membrane permeable pyridoxyl derivatives as pyridoxyl-amines (Zhang *et al.*, 1992, 1991) and pyridoxyl-methionine analogues (Ogier *et al.*, 1993) have also been investigated. Phosphopyridoxyl-ornithine analogue binds very efficiently to newly synthesized apo ODC

with high affinity and affects the ODC induced cell proliferation (Eliot *et al.*, 2004; Christen *et al.*, 2001). Phosphopyridoxal-ornithine has one drawback that due to its negative charge it is impermeable to the cell membrane and cannot be used for *in vivo* therapy.

However, (*N*-(4'pyridoxal)-ornithine (BOC)-OMe.HCl (POB) compound can be taken up efficiently by cells and inhibits the proliferation of tumor or transformed cell better than DFMO and DAB. The compound POB contains an additional hydrophobic BOC group and the  $\epsilon$ -amino group of ornithine has no negative net charge (Figure 1.12). These characteristics allow the efficient penetration through the membrane as compared to other cofactor-substrate analogues (Wu *et al.*, 2009).

#### 1.14 Structure of ODC

The visual aspect of enzyme ornithine decarboxylase monomer belongs to english alphabet L shaped structure. Each monomer can be subdivided into two domains  $\beta/\alpha$ -barrel, and  $\beta$ -sheet domain connected by loops. One helix bridges between the two domains. The sheet domain is subdivided into two domains S1 and S2. L shaped monomers rapidly form dimer by interacting with other monomer in head to tail manner (Grishin *et al.*, 1999; Kern *et al.*, 1999; Almrud *et al.*, 2000). Monomers come together by forming some weak bonds, salt bridges and interface electrostatic interactions. Enzyme functions actively in homodimeric state and exist in cells by maintaining equilibrium between monomeric and dimeric forms (Figure 1.13) (Grishin *et al.*, 1999).

The dimer interface constitutes two active sites, each between  $\beta/\alpha$ -barrel of one monomer and  $\beta$ -sheet domain of other monomer. Substrate and Co-factor interact with residues of both the subunits at the interface and actively catalyze the conversion of substrate to product putrescine.



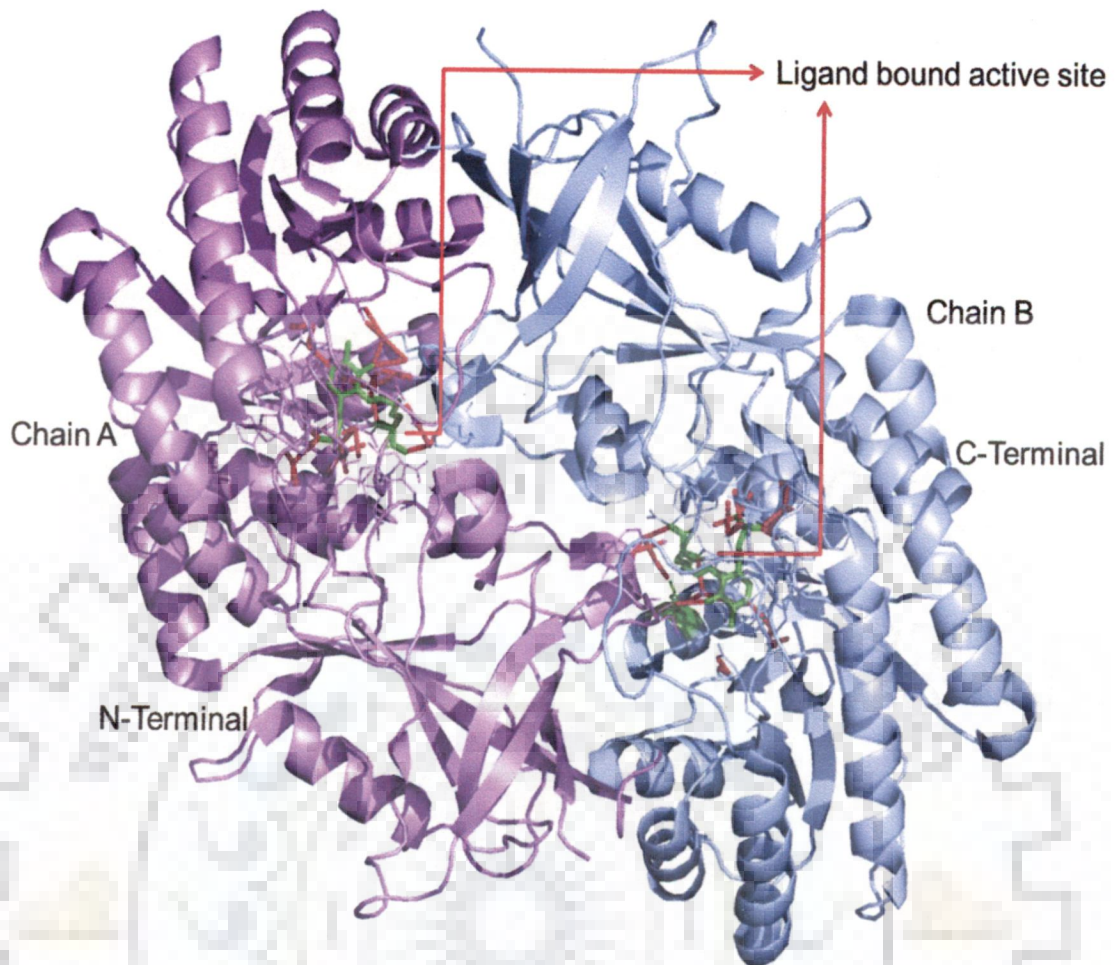


**Figure 1.13: Cartoon diagram of human ODC.** Showing dimer with chain A, chain B are in purple and blue color respectively. Structure starts with N-terminus of Chain A and ends with C-terminus of Chain B. Two active sites at the interface, the ligands shown in green and contacts are marked in red dots (PDB ID-1D7K, Almrud *et al.*, 2000).

The ODC enzyme interacts with PLP and forms a Schiff base with Lys69 in the active site. Substrate ornithine forms Schiff base at one end with PLP and interacts with Asp332, and Tyr389 of one monomer and Asp361, Phe397, Tyr323 and Cys360 of other monomer (Figure 1.14) (Kern *et al.*, 1999; Osterman *et al.*, 1995-1997; Coleman *et al.*, 1993; Tobias and Kahana, 1993; Tsirka and Coffino, 1992).

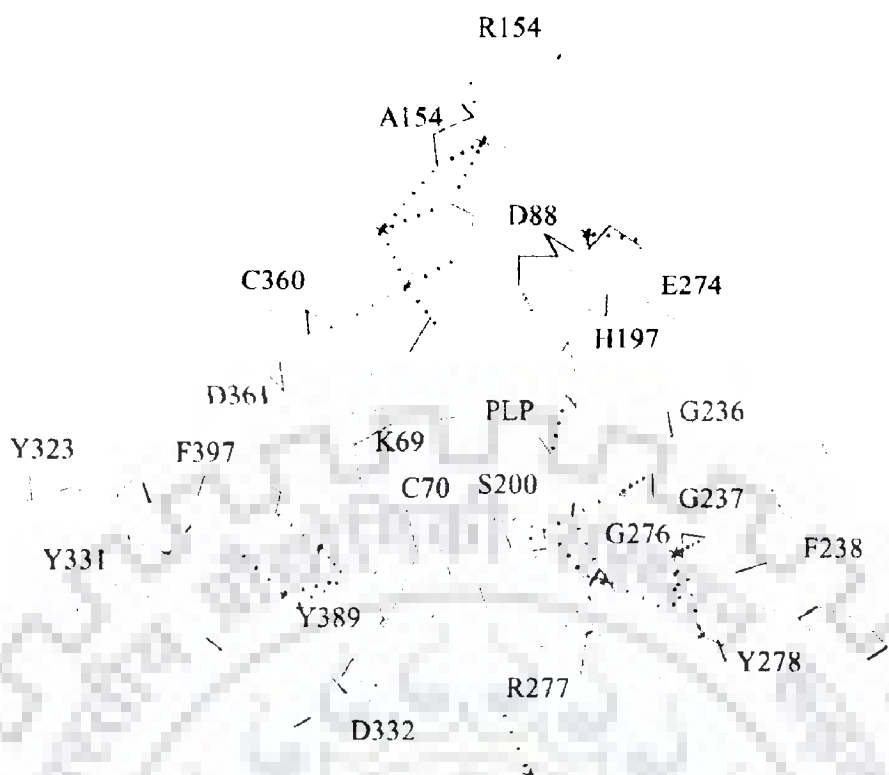


**Figure 1.14: Active site of human ODC.** Showing PLP in yellow color and surrounding residues in gray color, water molecule are indicated by green color interaction between enzyme and cofactor and water molecules have been represented by green color dashed lines. (Almrid *et al.*, 2000).

### 1.14.1 Crystal structures of ODC available

Crystal structure of many eukaryotic and prokaryotic ODCs are available in RCSB/PDB database (Table 1.7). Although basic crystallographic symmetry varied from species to species but overall structure obtained was dimeric in all structures. In prokaryotic ODC, the basic functional unit was dimer even if the structure obtained varied from tetrameric to dodecameric.

Organism	PDB-ID	Oligomeric state/ resolution	Year	Space group
<i>Trypanosoma brucei</i> (Tb)	1QU4	Dimer /2.9Å	1999	P2 <sub>1</sub>
<i>Homo sapien</i> (Hs)	1D7K	Dimer/2.1Å	2000	P2 <sub>1</sub> 2 <sub>1</sub> 2 <sub>1</sub>
<i>Mus musculus</i> (Mm)	7ODC	Dimer/1.6 Å	1999	P2 <sub>1</sub> 2 <sub>1</sub> 2
<i>Vibrio vulnificus</i> (Vv)	2PLJ	Dimer/1.7 Å	2007	P2 <sub>1</sub> 2 <sub>1</sub> 2 <sub>1</sub>
<i>Lactobacillus</i> 30a (L30a)	1ORD	Dodecamer/ Dimer/3.1 Å	1995	P6

**Table 1.7: Enzyme ODC structure data from eukaryotic and prokaryotic organisms.** Show the oligomeric state of ODCs from different groups of decarboxylases, with their PDB-ID and the space group. Data obtained from RCSB PDB (<http://www.rcsb.org>).

Crystal structure obtained as in above table were grown either native or with substrate, product, inhibitor or certain drugs which were thought to be having detrimental inhibitory effect on the ODC activity. These studies revealed the relative difference in the structural geometry of the crystal. The effect of certain type of inhibitors have been postulated and detected.

These finding established the fact that old or new therapeutic and inhibitory agents which are available for ODC and their physiological impacts (Table 1.7, 1.8) (Grishin *et al.*, 1999; Almrud, 2000; Yarlett, 1992; Jeongmi, 2007).

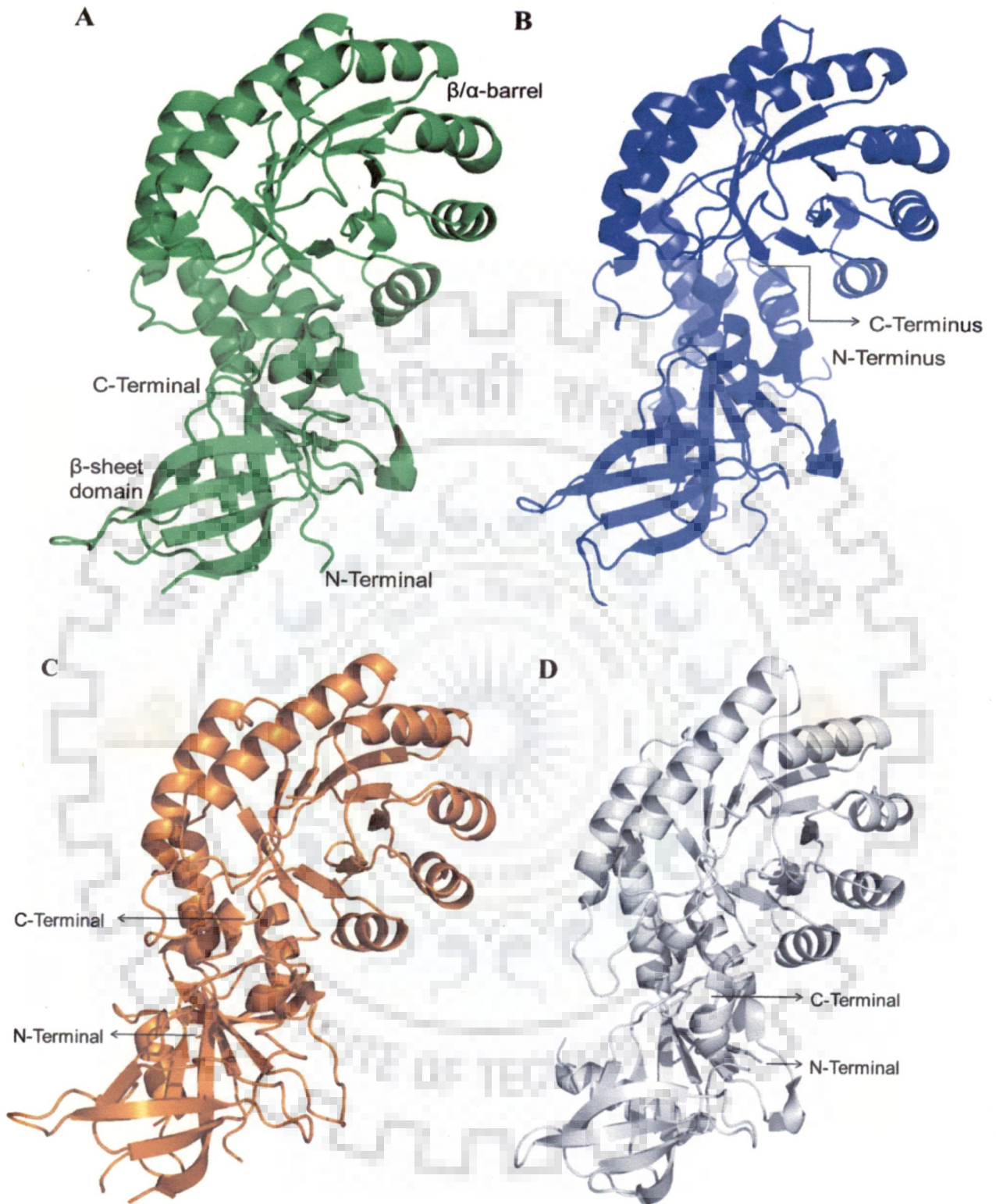
Organism	Year	Inhibitor of ODC
<i>E. coli</i>	1982	DL- $\alpha$ -monofluoromethyl putrescine (DFMO)
<i>C. albicans</i>	1990	1,4 diamino-2-butanone (DAB)
<i>Pneumocystis carinii</i>	1994	DL- $\alpha$ -monofluoromethyl putrescine (DFMO)
<i>Plasmodium falciparum</i>	2000	DL- $\alpha$ -monofluoromethyl putrescine (DFMO)
<i>N. glutinosa</i>	2001	5,5'-dithiobis-(2-nitrobenzoic acid) (DTNB)

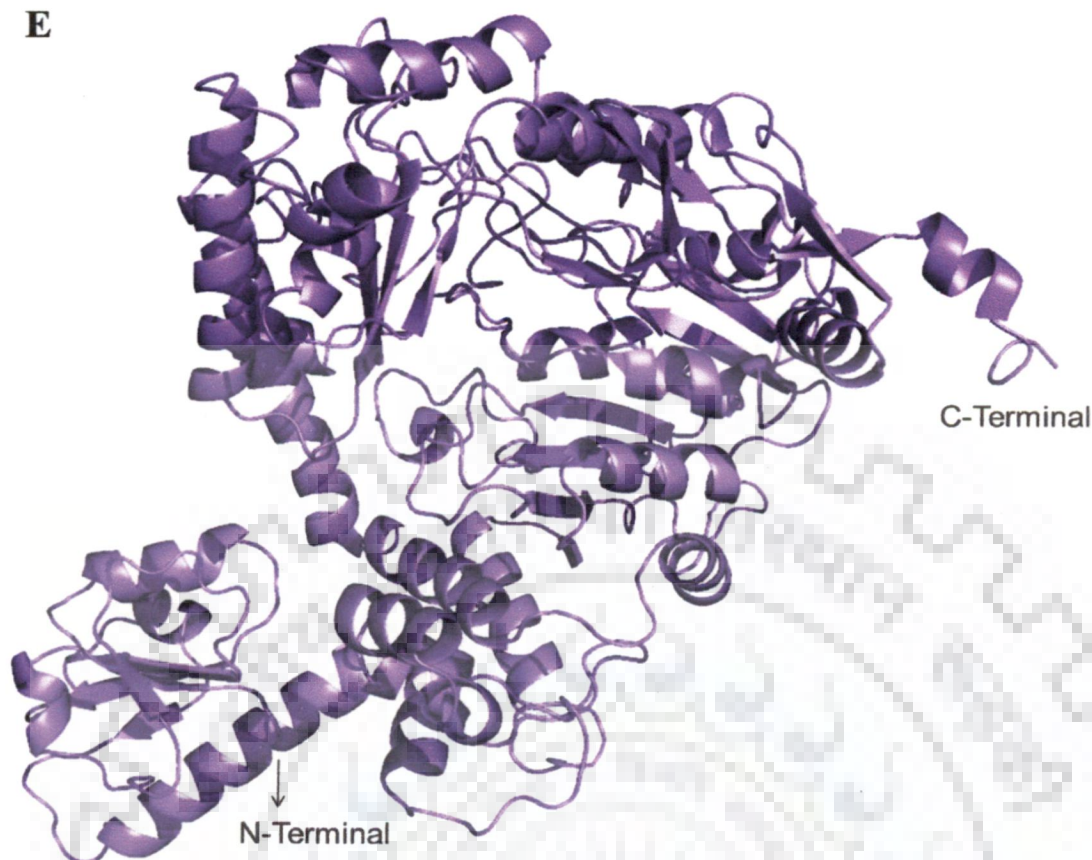
**Table 1.8: Enzyme ODCs identified and characterized for studying the effect of inhibitors.**

#### 1.14.2 Basic structure of ODC from fold type I and III family

Structure of the ODC from different protozoa appears to have same basic fold type and overall symmetry of *Tb*ODC, *Mm*ODC, *Hs*ODC and *Vv*ODC is almost similar but different from fold type I as of *lactobacillus* (Figure 1.15) (Grishin *et al.*, 1999; Almrud *et al.*, 2000; Yarlett, 1992; Lee *et al.*, 2007; Momany *et al.*, 1995). All eukaryotic ODCs are actively functional in dimeric state, where two active sites comprise the interface.





**E**

**Figure 1.15: Structure of ODCs from different fold type comprised of common secondary structure and fold pattern of  $\alpha/\beta$ -barrel and  $\beta$ -sheet domain. A) Structure of *T.brucei* ODC B) human ODC, C) mouse ODC D) *Vibrio vulnificus* ODC and E) *Lactobacillus* (30a) ODC.**

Structures (monomers) given in figure 1.14 belong to different fold type but overall symmetry does not vary from species to species. Monomer structures share the pattern of amino acid arrangements except (E) *Lactobacillus* (Gopal, 1997). Secondary structures of molecules are identical and having barrel and sheet domains in all the ODCs followed same special properties as alanine racemas family. ODC-L30a is representative of Fold type I family of large bacterial PLP-dependent decarboxylases. This ODC exists as a dodecamer composed of dimers with 1,460 amino acid residues per asymmetric unit (Hackert *et al.*, 1994). It is structurally similar to PLP binding domain of aspartate aminotransferase (AAT). In addition it has secondary structure folds similar to decarboxylase.



### 1.15 Mutational studies of ODC

Mutation of any specific site of the enzyme, allows one to study the role of the residue and effect of such mutation on the activity. Many mutational studies have been carried out to characterize the active site, binding affinity of inhibitors and other structural properties of the enzyme. The site directed mutagenesis helped in determining the functions of some of the very highly conserved regions invariant in all known eukaryotic ODCs. The residues of the conserved region studied so far including 357-361 which is evidently very near the active site of the enzyme, Cys360 substrate binding site, Lys69 cofactor PLP binding site and the region surrounding it probably forms a part of the active site (Osterman *et al.*, 1999; Tsirka *et al.*, 1999; Jackson *et al.*, 2000; Tobias *et al.*, 1993).

Name	PDB-ID	Resolution	Year
<i>T. brucei</i> ODC K69 mutant with DFMO	2TOD	2.0 Å	1999
Mutant <i>Tb</i> ODC	1SZR	2.15Å	2004
<i>Tb</i> ODC complex with D-ornithine and G418	1NJJ	2.45Å	2003
<i>Tb</i> ODC complex with putrescine	1F3T	2.0Å	2000
Human and <i>Leishmania</i> ODC complex with 3-aminooxy-1-aminopropane	2ON3	3.0 Å	2007
Human and <i>Leishmania</i> ODC complex with 3-aminooxy-1-aminopropane	2OO0	1.9Å	2007
<i>Vf</i> ODC complex with putrescine	2PLJ	1.7Å	2007
<i>Vf</i> ODC complex with cadaverine	2PLK	2.14Å	2007
<i>L30a</i> ODC dodecamer	1ORD	3.0Å	1995
<i>Lactobacillus30a</i> ODC Gly121Tyr mutant	1C4K	2.7Å	2000

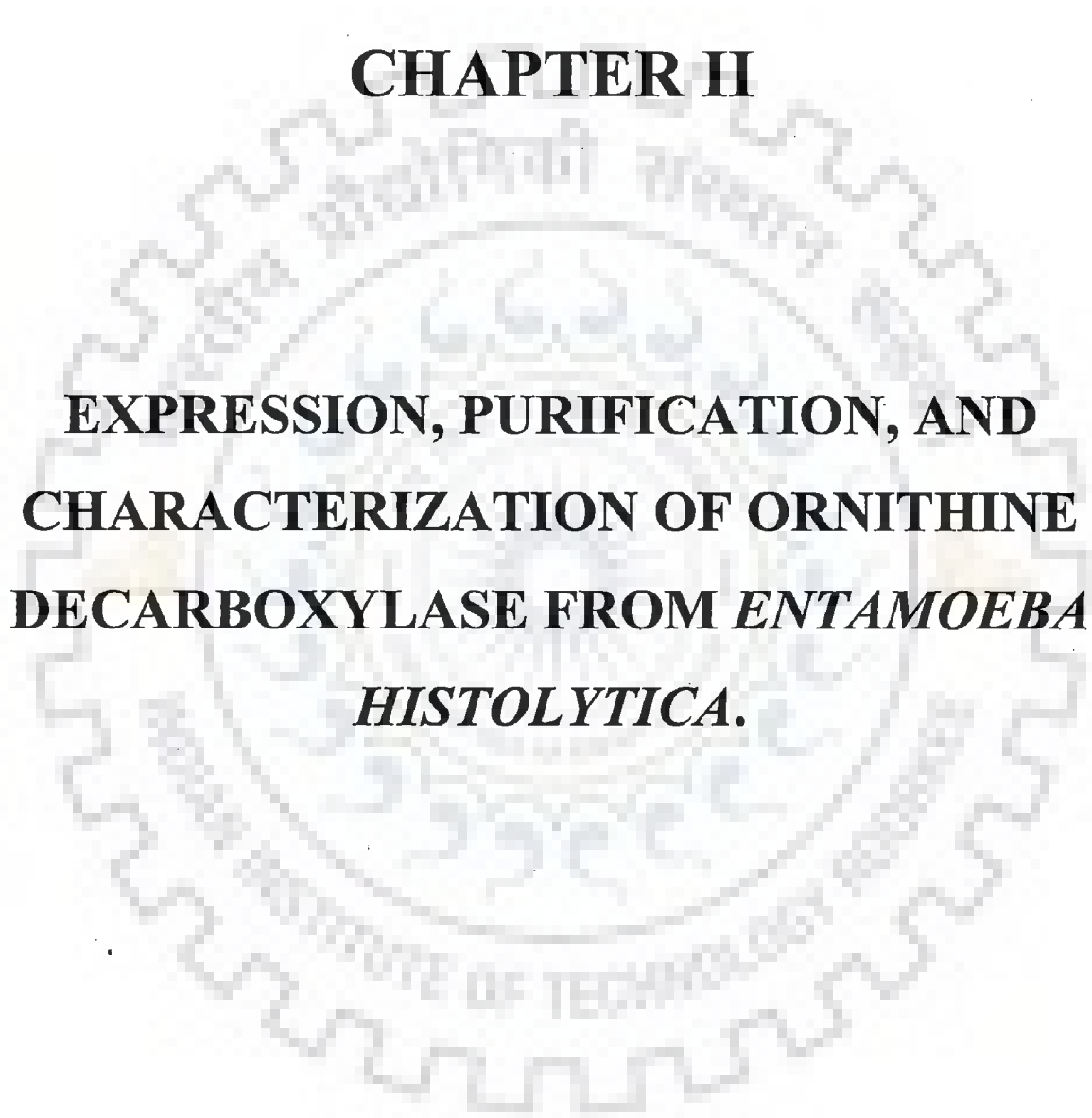
**Table 1.9: Structure data of mutants and complexes of ODCs with substrate/inhibitors.**

Residues 232-238 glycine rich sequences are found to form a part of the cofactor PLP binding region. Gly387 is essential for the formation of stable homodimers (Tobias *et al.*, 1993). The reported mutations of residues Lys115 to Arg, Lys169 to arginine or alanine and His197 to alanine all abolish catalytic activity (Table 1.9) (Jackson *et al.*, 2003). The binding element for the antizyme involved in the polyamine-mediated degradation of ODC, has been localized between residues 117 and 140 (Liu *et al.*, 2011). Various residues at the carboxy-terminus of ODC are required for rapid intracellular turnover of the ODC protein (Lu *et al.*, 1991).



## **CHAPTER II**

# **EXPRESSION, PURIFICATION, AND CHARACTERIZATION OF ORNITHINE DECARBOXYLASE FROM *ENTAMOEBIA HISTOLYTICA*.**



## 2.1 Abstract

This chapter mainly deals with the expression, purification, catalytic activity and characterization of recombinant ornithine decarboxylase from *E. histolytica*. Biophysical and biochemical characterization in addition to oligomeric state determination of purified protein was done using various methods.

*Entamoeba histolytica* is responsible for causing amoebiasis. Polyamine biosynthesis pathway enzymes are potential drug targets in parasitic protozoan diseases. The first and rate-limiting step of this pathway is catalyzed by ornithine decarboxylase (ODC). ODC functions as an obligate dimer. However, partially purified ODC from *E. histolytica* (*Eh*ODC) is reported to exist in a pentameric state. The recombinant *Eh*ODC enzyme was over-expressed in *Escherichia coli* and purified. Pure protein was used for estimation of activity by colorimetric product determination assay. Furthermore, the secondary structure content of enzyme was determined using Circular Dichroism spectroscopy. The percentages of  $\alpha$ -helices,  $\beta$ -sheets and random coils in *Eh*ODC were estimated to be 39 %, 25 % and 36 % respectively. Moreover, the oligomeric state of *Eh*ODC was re-investigated. Size-exclusion chromatography, crosslinking and mass spectrophotometry analysis revealed that *Eh*ODC enzyme exists in dimeric form.

## 2.2 Introduction

Amoebiasis is an infectious disease caused by single-celled parasitic protozoan *E. histolytica*. The parasite mainly affects primates and humans, and is transmitted by ingestion of water and food contaminated with feces containing cysts of *E. histolytica*. The enzymes of polyamine biosynthesis pathway are potential drug targets in parasitic protozoan diseases. The first and rate-limiting step of this pathway is catalyzed by ornithine decarboxylase (ODC). The enzyme ODC has been investigated and characterized from *T. brucei*, human, and mouse which revealed that the monomeric subunits interacts in head to tail manner and forms two catalytic active sites at the dimer interface (Grishin *et al.*, 1999; Kern *et al.*, 1999; Almrud *et al.*, 2000). Dimer formation is not only important for its catalytic function but also for its protection against antizyme-dependent endoproteolysis.

The pyridoxal 5' phosphate (PLP) binding residue Lys69 forms a Schiff base with it and indirectly helps in forming enzyme substrate complex. The enzyme ODC from *Leishmania mexicana* (*LmODC*) showed absolute requirement of PLP, but activity restoration after removing PLP revealed that the removal does not cause denaturation of enzyme (Sanchez *et al.*, 1995). In contrast ODC from *T. vaginalis* (*TvODC*) gets irreversibly inactivated in the absence of PLP (North *et al.*, 1986). PLP not only provides a reactive site but also participates in bringing up some conformational changes which may be required for correct assembly and full enzymatic activity.

ODC from other parasitic sources revealed different physiological properties but same biochemical outcomes. A number of enzymes possess flexibility in substrate specificity and active site conformation (Akey *et al.*, 2011). Broad distribution of ODC categorizes it into two major forms, monomeric and dimeric. As in case of *TvODC*, the one enzyme subunit was found to be of molecular weight 55 kDa (Yarlett *et al.*, 1993). *LmODC* reported to be consisting of three or four subunits of 50-70 kDa (Sanchez *et al.*, 1995). The molecular weight of one subunit of ODC from *T. brucei*, mouse and *Glycine max* was equivalent to 45, 53 and 55 kDa respectively. The molecular weight of one subunit of *N. glutinosa* ODC (*NgODC*) was 92 kDa. Secondary structure of *NgODC* was predicted by CD spectra and other bioinformatics analyses showed 9  $\alpha$ -helices and 16  $\beta$ -sheets, the overall percent secondary structures were reported to be 29 %  $\alpha$ -helix, 35.3 % turn and 35.6 % random coils (Lee *et al.*, 2001).

Analysis of mouse ODC (*mODC*) in the presence of monomeric and dimeric buffers constituting different salt concentrations showed great changes in physiological and biochemical properties. The *mODC* was investigated to check the heterodimer formation and its degradation pattern. Crosslinking experiments were performed for determining the homo or heterodimer formation and revealed that 50 % subunits were in heterodimeric form (Rosenberg-Hasson *et al.*, 1991). A wide variety of cellular responses gets regulated by transient protein-protein interactions. Interestingly, ODC protein-protein interaction significantly mediates the regulation of its catalytic activity. Inter-protein linkage studies have offered us small molecular model of interface and other useful features of enzyme which are potentially significant in enzyme activity and would aid in structure based drug designing (Bhattacharya *et al.*, 2011). Chemical crosslinking studies of ODCs provided clear

view of interactions and facilitated the topological analysis of protein (Fadouloglou *et al.*, 2008; Wine *et al.*, 2007; Back *et al.*, 2003). Protein ODC is under investigations since last few decades for determining the oligomeric states and physiological and biochemical properties. It has been reported that ODC from various sources exists mostly in the form of homodimers, although higher order oligomers have also been reported (Sanchez *et al.*, 1995; Yarlett *et al.*, 1993; Rosenberg-Hasson *et al.*, 1991).

High resolution mass spectroscopy is a powerful tool for elucidation of size and solubility of biomolecules. The broad applicability of soft ionization techniques, such as matrix assisted laser desorption ionization (MALDI) is choice of platform for characterizing the structural and functional states of protein. Most of the ODC enzymes from different species of eukaryotes exhibit several modified forms including phosphorylated and transamidated forms (Atmar *et al.*, 1981; Russell *et al.*, 1981; Tomar *et al.*, 2011). Previous studies have suggested the existence of equilibrium between active and cryptic forms of ornithine decarboxylase under different physiological conditions (Canellakis *et al.*, 1979). Moreover multiple forms of ODC have been observed using size exclusion chromatography under different investigatory experiments (Kitani *et al.*, 1984; Mitchell *et al.*, 1978). Physiological significance of these forms has been analyzed to study the structural and functional relations.

Substrate and other ionic molecules exhibit detrimental effect on the structure and activity of the ODC (Kitani *et al.*, 1984; Lapointe *et al.*, 1983). Noticeably, salt greatly affects the aggregation state of the protein. Increasing the ionic strength resulted in the increase of  $K_m$  value for L-ornithine and causes subunit dissociation of the rat liver ODC. Similarly, ODC from *phycomyces* gets inhibited and the equilibrium between the monomeric and dimeric form also gets disrupted by salt (Mitchell *et al.*, 1978; Lapointe *et al.*, 1983). Increased urea concentration has several remarkable impacts on the protein. It can either induce solubility or results in denaturation of protein (Wetlaufer *et al.*, 1964). Urea molecule tends to denature the structured protein by disrupting the hydrophobic interactions (Frieden C, 1979; Meyer *et al.*, 1977).

Despite of being a potent therapeutic target in *E. histolytica*, we do not know much about the biophysical and biochemical properties of *Eh*ODC. Earlier reports suggest that the



*Eh*ODC exist only as a homopentamer, however we observed the existence of active dimer and inactive monomer form of the enzyme under various physiological conditions.

## 2.3 Materials and Methods

### 2.3.1 Reagents

The *E. coli* expression vector pET 30a (Novagen) containing full-length gene of *Eh*ODC having N-terminal Histidine tag (6x His) followed by enterokinase cleavage site was used for over-expression of the enzyme (Jhingran *et al.*, 2008). For protein purification 5 ml HisTrap HP and HiLoad 16/60 Superdex 200 gel filtration columns were obtained from GE Healthcare. Imidazole (low absorbance at 280) was obtained from Acros. AKTA Prime plus system from GE Healthcare was used for protein purification. Putrescine, 4-aminoantypyrine, diamine oxidase, horseradish peroxidase and L, D-ornithine were procured from Sigma Aldrich. Amicon ultra protein concentrators were purchased from Millipore. All other chemicals were of analytical grade and obtained from commercial sources.

### 2.3.2 Methodology

#### 2.3.2.1 Expression and Solubility of *Eh*ODC

The *E. coli* expression vector pET 30a (Novagen) containing full-length gene of *Eh*ODC having N-terminal Histidine tag (6x His) followed by enterokinase cleavage site was used for over-expression of the enzyme.

The expression and purification of *Eh*ODC enzyme was done by following the published procedure with minor modifications given below (Jhingran *et al.*, 2008). The plasmid pET30a having the full-length *Eh*ODC gene insert (pET30a-*Eh*ODC) was transformed into freshly prepared *E. coli* BL21 (DE3) competent cells and plated on Luria-Bertani (LB) agar plate containing kanamycin (50 µg/ml). Plates were incubated overnight at 37 °C and colonies were obtained. Single colony was picked and cells were seeded in 5 ml LB broth containing 50 µg/ml of kanamycin and culture was grown overnight at 37 °C with agitation. Overnight culture was used for inoculation of 1 liter LB broth. Culture was induced with 1 mM isopropyl β-D-thiogalactoside (IPTG) when optical density ( $A_{600}$ ) reached 0.6.

After induction, culture was moved to different temperatures (37 °C, 25 °C, and 18 °C) and was grown for 4, 6, and 14 hours respectively.

Cells were harvested by centrifugation at 5,000 rpm at 4 °C for 10 min and cell pellets were stored at -80 °C until further processing. Expression and solubility of the protein was confirmed by analysis of lysed cell supernatant and pellet on 12 % sodium dodecyl sulfate-polyacrylamide gel electrophoresis (SDS-PAGE).

### 2.3.2.2 Purification of *Eh*ODC

The Histidine-tagged *Eh*ODC was purified using two-step procedure that employed metal ion affinity chromatography followed by gel filtration chromatography. All purification steps were performed at low temperature (4 °C – 6 °C). Briefly, frozen cell pellets from a 1 liter culture were thawed on ice and re-suspended in buffer A [50 mM Tris-HCl (pH 7.5), 40 mM imidazole, 250 mM NaCl and 5 % glycerol (v/v)] containing lysozyme (0.7 mg/ml) and 0.2 mM phenylmethanesulfonylfluoride (PMSF). Cells were disrupted by sonication on ice with a pulse of 20 sec on and 1 min off for 10 times. The obtained cell lysate was clarified by centrifugation at 18,000 g for 45 min at 4 °C and supernatant was applied on HisTrap HP column (5 ml) pre-equilibrated with buffer A. Unbound proteins were removed by washing the column with ~40 ml of buffer A. Bound protein fractions were eluted using a linear gradient of 40 mM to 1 M imidazole of 60 ml at a flow rate of 1 ml/min. Eluted fractions were examined on 12 % SDS-PAGE and fractions containing pure protein were pooled together.

Enterokinase was added to pure protein (~0.02 units/mg protein) for His tag cleavage and incubated for ~12 hours at 4 °C and simultaneously dialyzed against buffer A without imidazole. To remove uncleaved tagged protein and the cleaved His tag, the sample was reloaded onto HisTrap HP column and the flow-through containing untagged *Eh*ODC was collected and concentrated using a 10 kDa cutoff Amicon Ultra-15 concentrator (Millipore, Bedford, Massachusetts, USA). For removal of enterokinase, the concentrated sample was loaded onto HiLoad 16/60 prep grade Superdex 200 size-exclusion chromatography column pre-equilibrated with buffer B [50 mM Tris-HCl (pH 7.5), 250 mM NaCl, 0.2 mM dithiothreitol (DTT) and 5 % glycerol (v/v)]. Fractions of the major peak containing pure protein were pooled and concentrated. Homogeneity of the concentrated enzyme preparation

was analysed by 12 % SDS-PAGE. The yield and concentration of purified *Eh*ODC was measured using the Bio-Rad protein-assay kit with bovine serum albumin (BSA) as a standard.

### 2.3.2.3 *Eh*ODC enzyme assay

Ornithine decarboxylation activity of *Eh*ODC was spectrophotometrically determined by the method developed by Badolo *et al.*, 1999. This method is based on the reaction between diamine oxidase (DAO) and putrescine, the product of the ODC-catalyzed reaction. For *Eh*ODC enzyme assay, the purified protein was buffer exchanged with 20 mM sodium phosphate buffer (pH 7.5) and concentrated to final concentration of 0.3 mg/ml. The reaction mixture of 180  $\mu$ l containing 20 mM sodium phosphate buffer (pH 7.5), 0.1 mM EDTA, 0.1 mM PLP, 0.2 mM DTT, and 1 mM of L-ornithine was prepared to which 20  $\mu$ l of protein solution was added to make up the final volume of 200  $\mu$ l. The reaction mixture was incubated at 37 °C for 5 hours.

Further, 100  $\mu$ l of the above *Eh*ODC reaction mixture was added to 900  $\mu$ l of diamine oxidase (DAO) reaction mixture composed of 50 mM Tris-HCl (pH 9.8) containing 100  $\mu$ g/ml phenol, 100  $\mu$ g/ml 4-aminoantipyrine (4-AAP), 0.02 U of DAO, and 7 U of horseradish peroxidase (HRP). The reaction was incubated at 25 °C for 60 min and then terminated by heating the solution at 90 °C for 4 min. The concentration of putrescine formed by ornithine decarboxylation catalysis was determined by measuring the absorbance at 492 nm for the colored complex formed as a result of the reaction of H<sub>2</sub>O<sub>2</sub> with 4-AAP and phenol catalyzed by HRP (Singh *et al.*, 2011). For negative controls, purified protein or substrate L-ornithine was substituted with buffer in the reaction mixtures. Effect of stereoisomer of substrate was observed by incubation of L and D-ornithine at 37 °C. Mechanism of reaction catalyzed and the formation of colored product has been given in figure 2.1.

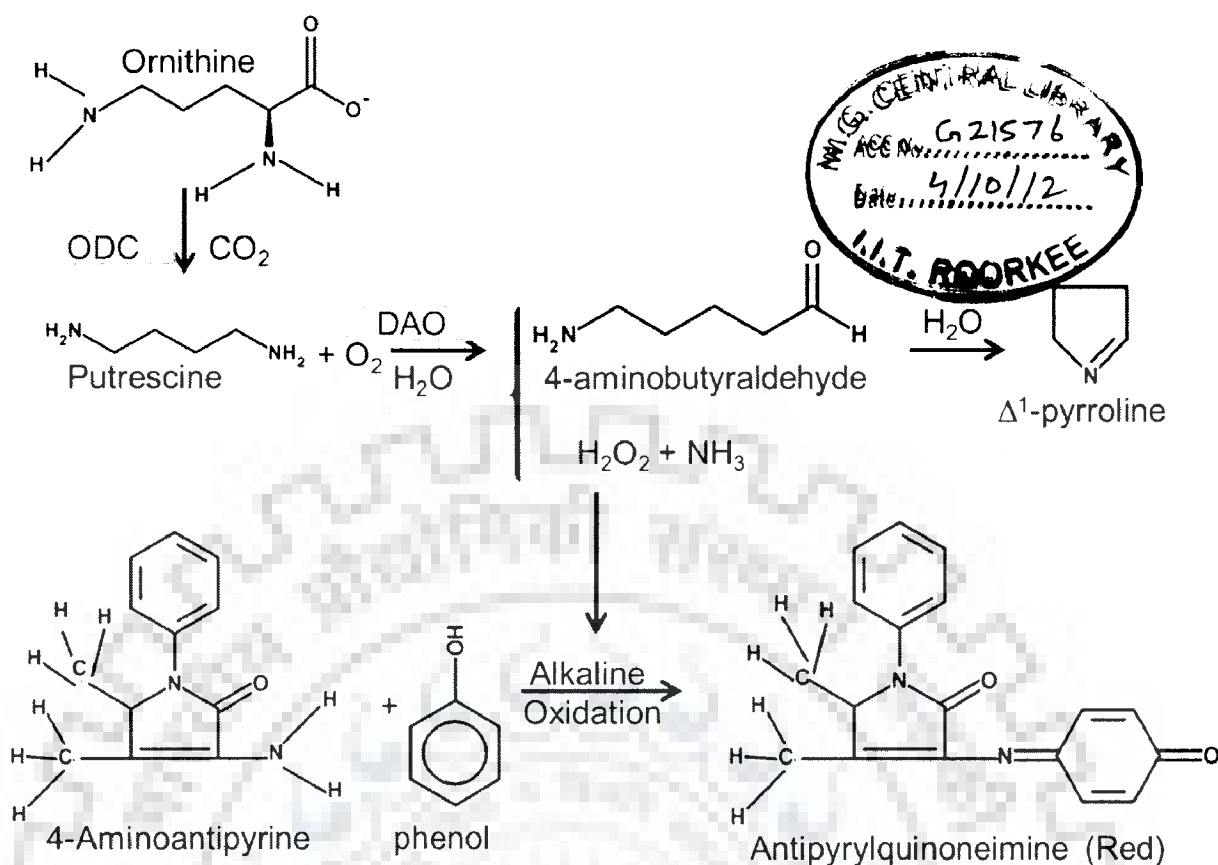


**Figure 2.1:** Schematic representation of enzymatic decarboxylation of substrate L-ornithine to product putrescine and colorimetric assay used to determine the product formation (Courtesy Badolo *et al.*, 1999).

### 2.3.3 Secondary Structure Analysis

Various enzymes from different families possess the property of decarboxylation of ornithine, lysine, arginine etc. Most of the ODCs characterized till date possess catalytic activity and exhibit the property of dimerization. The enzyme shows characteristically different morphology and oligomeric state in the presence of denaturing agents and salts (Kitani *et al.*, 1984; Mitchell *et al.*, 1988). Protein association and dissociation behavior can be studied by MALDI-TOF which also helps in determining its oligomerization state.

ODC enzymes are obligate homodimer and two active sites are present at the dimer interface. This property of dimerization of *Eh*ODC was analyzed by using various biophysical and biochemical techniques. The *Entamoeba* ODC has been reported as a multi-

subunit enzyme that possesses the property of decarboxylation of only L-ornithine (Arteaga-Nieto *et al.*, 1996; Jhingran *et al.*, 2008). *EhODC* thought to be a pentameric enzyme in which active site present at the subunits interface. Our goal was to identify the oligomeric state of the enzyme.

### **2.3.3.1 Far-UV Circular Dichroism spectrum**

For estimation of secondary structure elements, purified *EhODC* was subjected to circular dichroism (CD) analysis using Chirascan Circular Dichroism Spectrometer (Applied Photophysics Ltd., Surrey KT22 7PB, United Kingdom). CD spectra were collected using a 1 mm quartz cell under constant nitrogen purge between 190 to 260 nm in 0.5 nm wavelength steps and an average time of 3.0 sec at 25 °C. The protein solution was buffer exchanged with 20 mM potassium phosphate buffer (pH 7.5) at 4 °C. Protein samples at concentration 0.35 mg/ml were analyzed and three scans were collected, averaged and the baseline corresponding to the above buffer was subtracted to obtain the final values. The obtained data were analyzed using the software K2d (<http://www.embl.de/~andrade/k2d.html>) (Andrade MA *et al.*, 1993).

### **2.3.4 Characterization of oligomeric state of *EhODC***

#### **2.3.4.1 Chemical crosslinking**

To obtain preliminary information on the oligomeric association of *EhODC*, glutaraldehyde crosslinking experiment was performed using the method described by Fadouloglou VE *et al.*, 2008. Purified protein solution was exchanged with 20 mM sodium phosphate buffer (pH 7.5) for cross-linking studies. Experiment was carried out using 24 well crystallization plate (Hampton research) and a siliconized coverslip in a manner similar to a hanging drop crystallization method. For cross-linking *EhODC*, 40 µl of 12.5 % glutaraldehyde solution (v/v) acidified with 1 µl 5 N HCl was added in the well of crystallization plate. Then, 15 µl of protein solution (1 mg/ml) was loaded onto the coverslip, which was inverted on the reservoir well and sealed with vacuum grease (Hampton Research). The entire setup was incubated at 37 °C for 10 min and then the sample was mixed with an equal volume of 2 X SDS-PAGE loading buffer and boiled for 4 min on a dry bath. Cross-linked oligomers were analysed on 12 % SDS-PAGE followed by Coomassie Blue R-250 staining.

One entirely different protocol to determine the oligomeric state was followed in which a chemical crosslinker was dimethyl suberimidate dihydrochloride (DMS) (Davies GE *et al.*, 1970). Purified protein was crosslinked in the presence of DMS concentration varied from 0.8 to 2 mg/ml in a reaction mix of 100  $\mu$ l and phosphate buffer pH 7.5 incubated at 37 °C for three hours. The reaction was terminated by adding reducing dye and analyzing on 12 % SDS-PAGE.

#### **2.3.4.2 Molecular mass and oligomeric state determination**

The molecular mass of recombinant *Eh*ODC was determined by running purified protein on 12 % SDS-PAGE with standard molecular weight protein marker (Bio-Rad). To analyze the oligomerization state, 500  $\mu$ l of purified and concentrated (~10 mg/ml) protein was applied onto a HiLoad 16/60 Superdex 200 gel filtration column pre-equilibrated with buffer B using 500  $\mu$ l sample loop at a flow rate of 0.5 ml/min on ÄKTA purifier chromatographic system (GE Healthcare) and protein elution profile was monitored by measuring the absorbance at 280 nm. The size-exclusion column was calibrated with blue dextran (2000 kDa), and Gel Filtration HMW Calibration kit containing ferritin (440 kDa), aldolase (158 kDa), conalbumin (75 kDa) and ovalbumin (43 kDa) (GE Healthcare) for determination of the void volume, construction of the standard curve and estimation of the molecular weight of purified protein.

The oligomerization state of *Eh*ODC was also analyzed by matrix-assisted laser desorption/ionization time of flight mass spectrometry (MALDI/TOF MS). The purified protein sample was dialyzed against 50 mM Tris buffer (pH 7.5) containing low concentration of NaCl (25 mM) and 0.2 mM DTT to avoid any instrumental interference and was concentrated to ~2 mg/ml using 10 kDa cutoff Amicon ultra 15 (Millipore). The MALDI/TOF MS analysis was carried out at Proteomics Facility, TCGA (New Delhi, India) using Ultraflex mass spectrometer (Bruker Daltonics, Germany). The protein ionization spectra were analyzed on FLEX-PC2 mass spectrometer and data was acquired across the range of about 0 to 250 amu.



#### **2.3.4.3 Effect of Urea and NaCl on *Eh*ODC oligomerization**

To study the effect of urea and NaCl on oligomeric state of protein, purified and concentrated *Eh*ODC was pre-incubated with variable concentration (2 M or 4 M) of above chemical agents separately at 4 °C for 4 hours. The protein was further loaded onto Hi-load 16/60 superdex 200 gel filtration column equilibrated with buffer B containing the same concentration of urea or NaCl and elution profiles were analyzed and compared with the standard molecular weight marker and native *Eh*ODC protein.

### **2.5 Results and Discussion**

The completion of genome sequence project of *E. histolytica* headed by the Institute of Genome Research (TIGR, Rockville, USA.) opened up the possibilities of new therapeutic targets as well as detailed mechanisms of various biosynthetic pathways (Loftus *et al.*, 2005). The polyamine biosynthesis in *E. histolytica* is an essential pathway required for the existence of the pathogen (Thomas *et al.*, 2001; Oredsson, 2003). In present study, the sequence of *Eh*ODC, the first and rate-limiting enzyme of polyamine biosynthetic pathway, has been retrieved from NCBI database with accession number AAX35675. The protein consists of 413 amino acids with predicted molecular weight of 46.43 kDa. In *E. histolytica*, the gene encoding ODC is of 1,242 bps, thus it implies that there is no intron present in the gene. The enzyme has been previously characterized by Jhingran *et al.*, 2008. Single copy gene (ORF) was found to be located on 1.9-Mb chromosome.

#### **2.5.1 Plasmid isolation and verification for *Eh*ODC insert**

Plasmid pET30a with insert of *Eh*ODC enzyme of size 1,242 bps was isolated and checked on the 1% agarose gel to confirm the plasmid. Plasmid was digested with *Bam*HI and *Xho*I enzymes to confirm the insert size of 1,242 bps (Figure 2.2). Sequencing of *E. histolytica* ornithine decarboxylase was done to confirm the insert and the derived amino acid sequence of *Eh*ODC has been given in the figure 2.3.

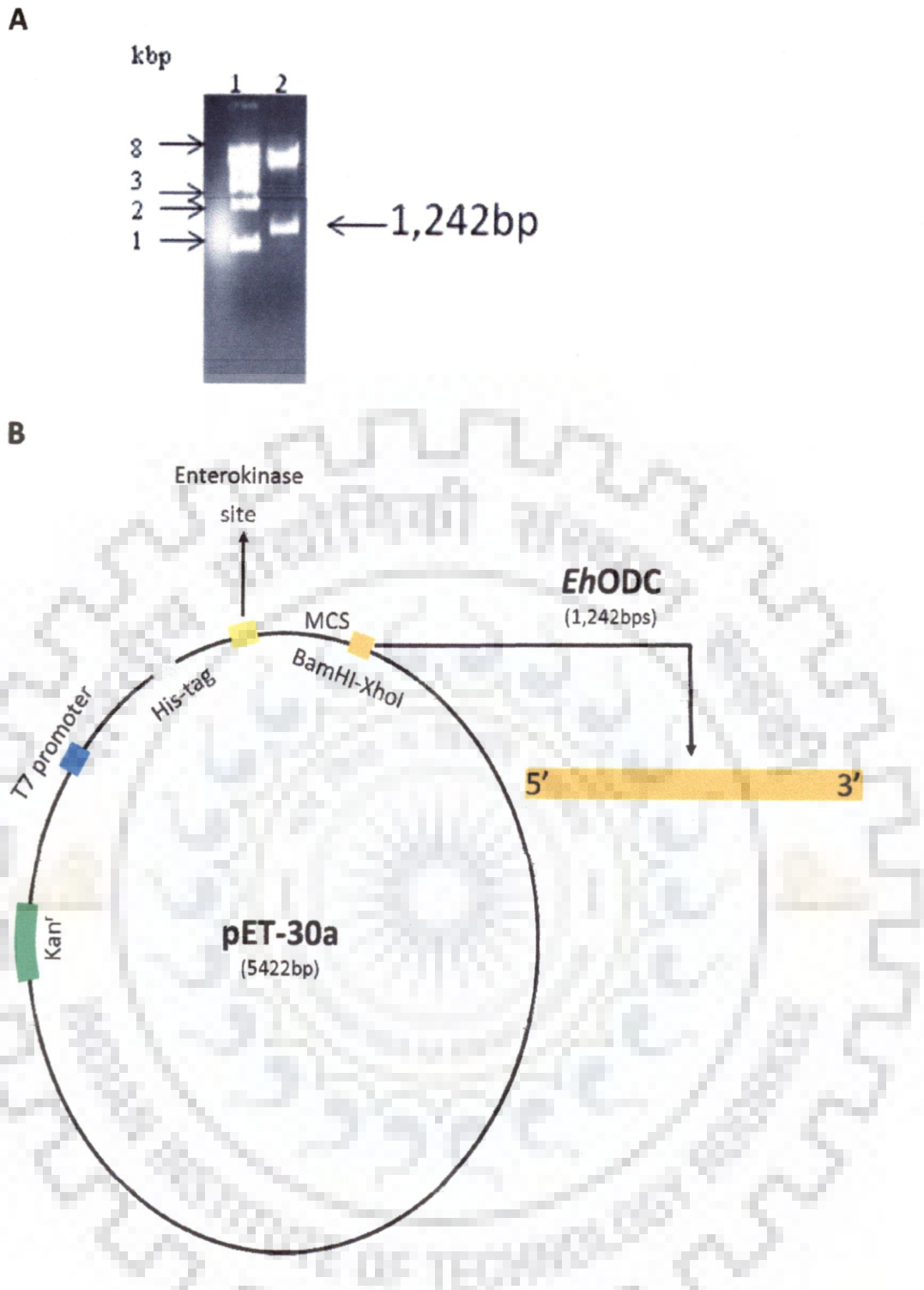


**Figure 2.2: Plasmid pET30a-*EhODC*.** A) Gel showing cloned plasmid digested with restriction enzymes *Bam*HI and *Xho*I releasing an insert of 1,242 bps. Lane 1: DNA ladder; Lane 2: RE digested plasmid. B) Schematic representation of the vector map pET30a-with *EhODC* insert. The colored tag represents the specific antibiotic resistance gene, restriction sites, insert gene and promoter region (Jhingran *et al.*, 2008).

## 2.5.2 Nucleotide along with the amino acid code of *Eh*ODC

atgaaacaaacatctctagaagtaaagaattcgctcttaatcttatcagccaatttgaa  
M K Q T S L E V K E F A L N L I S Q F E  
ccagaaaaccaaccacttgggtttttggatttttgatactgaagggtgttgaaaaagcagtt  
P E N Q P L G F W I F D T E G V E K A V  
gaaagatggaaaaagaatatgccaacagttagaccttgctttgctgttaaatgtaatcct  
E R W K K N M P T V R P C F A V K C N P  
gaacctcatttagttaagcttttaggtgaattaggatgtgggttttgattgtgcttcattg  
E P H L V K L L G E L G C G F D C A S L  
aatgaaataaaagaagatttagaccttggatttaatcctgaagacattacatattcacia  
N E I K E V L D L G F N P E D I T Y S Q  
actttcaaaccatataatcaattaattgaagcaagtcatttaggaattaatcatacaatt  
T F K P Y N Q L I E A S H L G I N H T I  
gtagattcaattgatgaagttcaaaaaattgcaaaaatatgcacaaaaatgggtataatg  
V D S I D E V Q K I A K Y A P K M G I M  
ataagaattatggaaaatgatacatcagcaggtcatgtatttggagagaaatttggactt  
I R I M E N D T S A G H V F G E K F G L  
catgatgatgaggttgaaatagttttaaaagaaattaaagacaaaggattaaatttagat  
H D D E V E I V L K E I K D K G L N L D  
ggagtccattttcatgttgggaagtgattctcataatagtgaagttttactaaagcatta  
G V H F H V G S D S H N S E V F T K A L  
actaaagcaagaacactgttacatttagcagaacaatttggaatgaaaccatatttaatt  
T K A R N T V T L A E Q F G M K P Y L I  
gatattggaggaggatttagtcaagttgctccatttgaagaatttgcagcaacaattgaa  
D I G G G F S Q V A P F E E F A A T I E  
aaaacaataaaagaatttagagtttccagaaagaacaagatttatttgcagaacctggaaga  
K T I K E L E F P E R T R F I A E P G R  
tatatggcatctaattgcatttcatcttgttagttctttacatggtaaaagagtaagaata  
Y M A S N A F H L V S S L H G K R V R I  
cagaatggaaagaacaaattgaatatacttcaggtgatgggtttacatggaagttttgga  
Q N G K K Q I E Y T S G D G L H G S F G  
tgttgtatttggtttgaaaaacaaaaaagttgtgaatgtattacacaaaaagttaatgaa  
C C I W F E K Q K S C E C I T Q K V N E  
aatactaaaatgtatgaaagtattatattatggaccttcttgtaatggaagtataaagta  
N T K M Y E S I I Y G P S C N G S D K V  
gcaactcaagaactaccagaaatggagccagggaaagattggttattatatttcccaatatg  
A T Q E L P E M E P G K D W L L F P N M  
ggtgcttatacaattttctatggcaactaactttaatggatttgaagaagaatcatgtc  
G A Y T I S M A T N F N G F E E R N H V  
atttatactttaccattaaagtcaacaaaaattattcaaattccctaagtcaattgaatgt  
I Y T L P L K S T K I I Q I P K S I E C  
aactcagttccatcattaaatgggtattccacactatgcttaa  
N S V P S L N G I P H Y A -

Figure 2.3: Nucleotide and derived amino acid sequence of *Eh*ODC.

### 2.5.3 Strategy used for *Eh*ODC protein expression

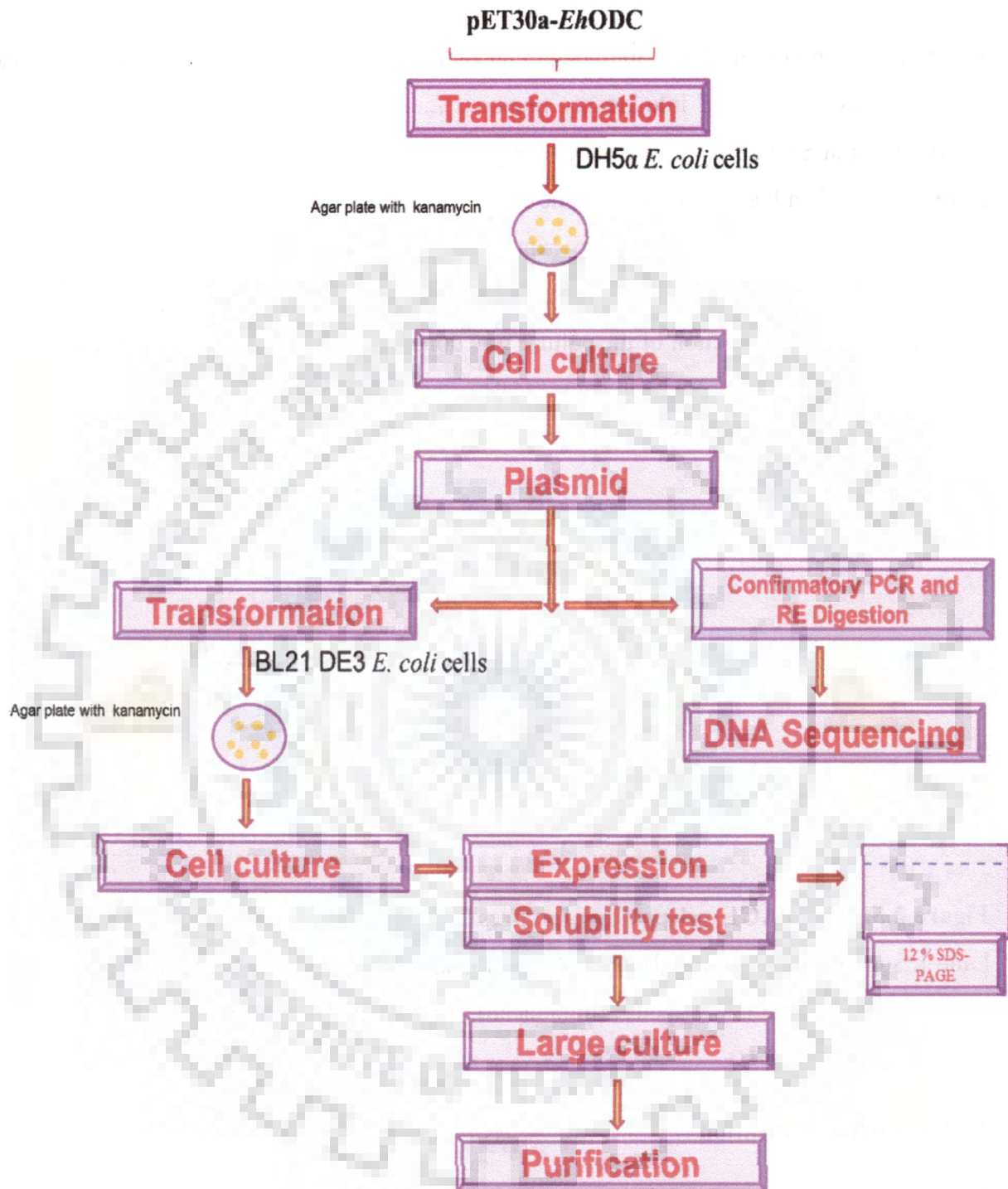


**Figure 2.4:** Schematic representation of the strategy used for obtaining pure recombinant *Eh*ODC protein.



#### 2.5.4 Expression and solubility of *Eh*ODC

In this study, the plasmid pET30a containing the full-length *Eh*ODC gene insert (pET30a-*Eh*ODC) was transformed into freshly prepared *E. coli* BL21 (DE3) competent cells and plated on Luria-Bertani (LB) agar plate containing kanamycin (50 µg/ml). The strategies that were developed and used to overcome the hurdles encountered during the protein purification are discussed here (Figure 2.4). The expression and solubility of *Eh*ODC construct was checked by growing *E. coli* containing expression vector at various temperatures (37 °C, 25 °C and 18 °C). The induction of the culture was done with 1 mM IPTG when optical density at ( $A_{600}$ ) reached to 0.6. Recombinant *Eh*ODC protein was showing high expression and solubility at 18 °C (Figure 2.5).

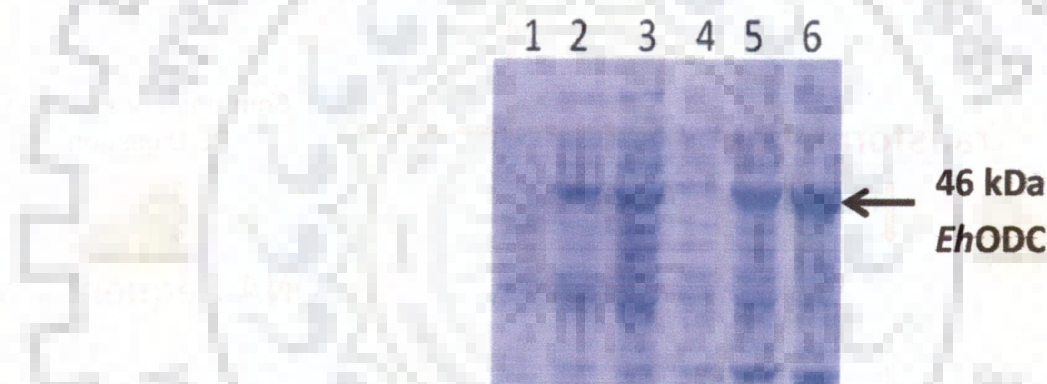


**Figure 2.5:** SDS-PAGE gel profile of expression of *Eh*ODC at different temperatures. Lane 1: supernatant (uninduced); Lane 2: supernatant (induced at 37 °C); Lane 3: supernatant (induced at 18 °C); Lane 4: pellet (uninduced); Lane 5: pellet (induced at 37 °C); Lane 6: pellet (induced at 18 °C).

#### 2.5.5 *Eh*ODC purification

The recombinant *Eh*ODC protein was purified to homogeneity using two step procedure consisting  $Ni^{2+}$  affinity chromatography and size exclusion chromatography. The crude containing over-expressed *Eh*ODC from *E. coli* having N-terminal His-tag was loaded onto HisTrap  $Ni^{2+}$  column and eluted using a linear gradient of imidazole.

The N-terminal His-tag from eluted protein sample was removed using enterokinase and sample was re-loaded onto HisTrap Ni<sup>2+</sup> column. Then, the flow-through containing *Eh*ODC without His-tag was collected, concentrated and loaded onto HiLoad 16/60 superdex 200 gel-filtration column for further purification. Homogeneity of pure protein sample was estimated on 12 % SDS-PAGE, which exhibited a single band of ~46 kDa corresponding to the molecular weight of *Eh*ODC protein (Figure 2.6, 2.7). The yield of the purified protein was estimated to be ~3.0 mg/L of culture and protein was concentrated to ~6 mg/ml.

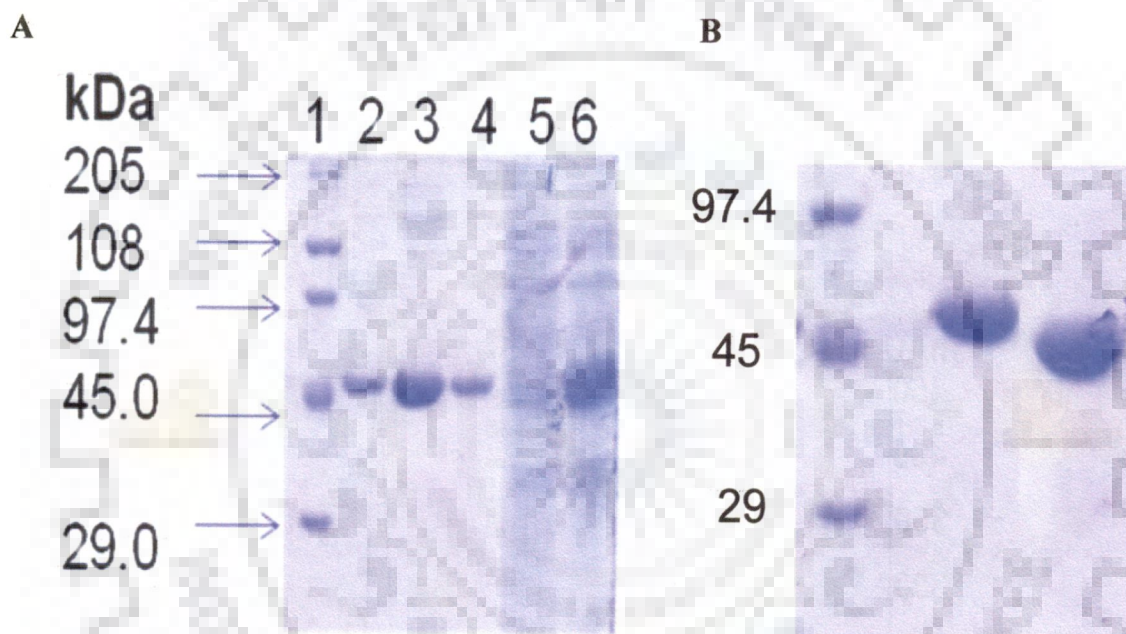


**Figure 2.6: Purification of *Eh*ODC. A) Affinity purification of *Eh*ODC showing purified protein in 12 % SDS-PAGE. Lane 1: molecular weight marker (kDa); Lane 2-4: *Eh*ODC full length purified protein; Lane 5: Flow-through; Lane 6: Supernatant showing soluble fractions of *E. coli* lysate. B) 12 % SDS-PAGE gel showing purified *Eh*ODC His tag cleaved protein. Lane 1: Molecular weight marker; Lane 2: Purified *Eh*ODC-His tagged protein; Lane 3: Purified His tag cleaved protein with molecular weight ~46 kDa.**



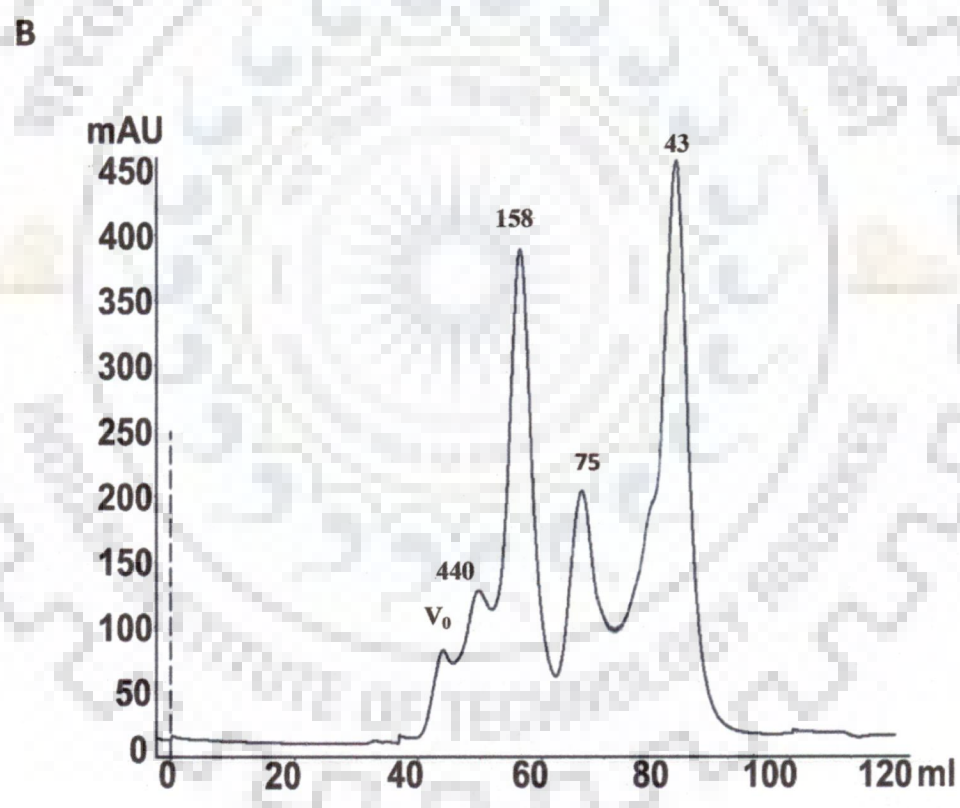
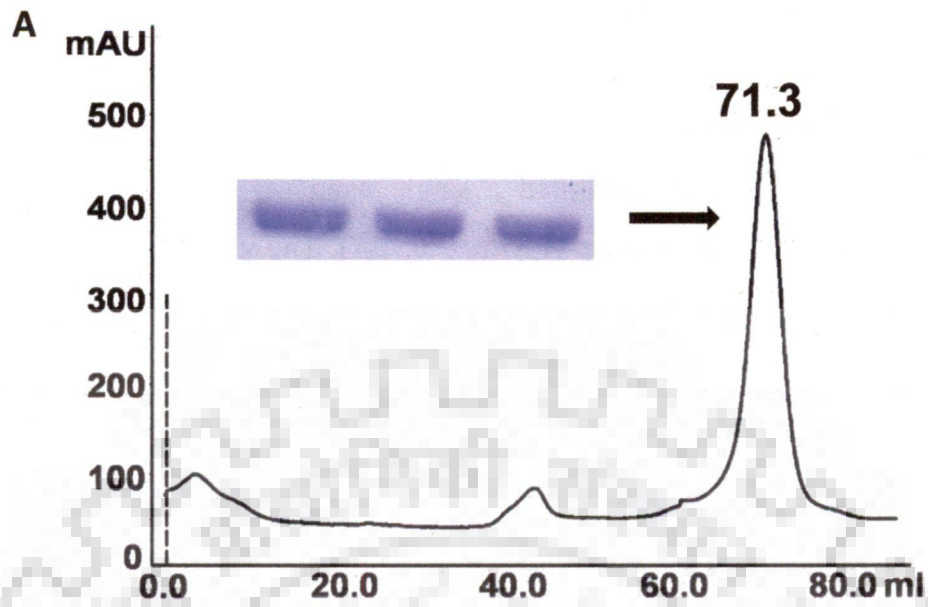


**Figure 2.7: A) Size-exclusion chromatography profile.** Elution profile of *Eh*ODC and 12 % SDS-PAGE (insert) analysis of major peak fractions. **B) The elution profile of standard molecular weight markers through HiLoad 16/60 Superdex 200 column.** The column void volume ( $V_0$ ) and molecular weight (kDa) of standard proteins are indicated.

### 2.5.6 *Eh*ODC enzyme activity

The enzymatic activity of purified protein was demonstrated using the simple and rapid colorimetric ODC activity assay (Badolo *et al.*, 1999). The decarboxylation activity of purified enzyme was assayed in 200  $\mu$ l reaction containing 20 mM sodium phosphate buffer (pH 7.5), 0.1 mM EDTA, 0.1 mM PLP and 1-10 mM of L-ornithine. The reaction was assayed in terms of the formation of product, putrescine by its oxidation using DAO enzyme which releases  $H_2O_2$  that forms a colored complex antipyrylquinoneimine as described in materials and methods. His-tagged and untagged protein showed no difference in the enzymatic activity. Furthermore, the purified *Eh*ODC actively catalyzed the conversion of L-ornithine to putrescine, while it showed no activity when D-ornithine was used as a substrate in enzyme reaction. This reveals that *Eh*ODC enzyme is stereospecific in binding to L-ornithine substrate suggesting that substrate based stereospecific inhibitors may be designed for *Eh*ODC (Figure 2.8).

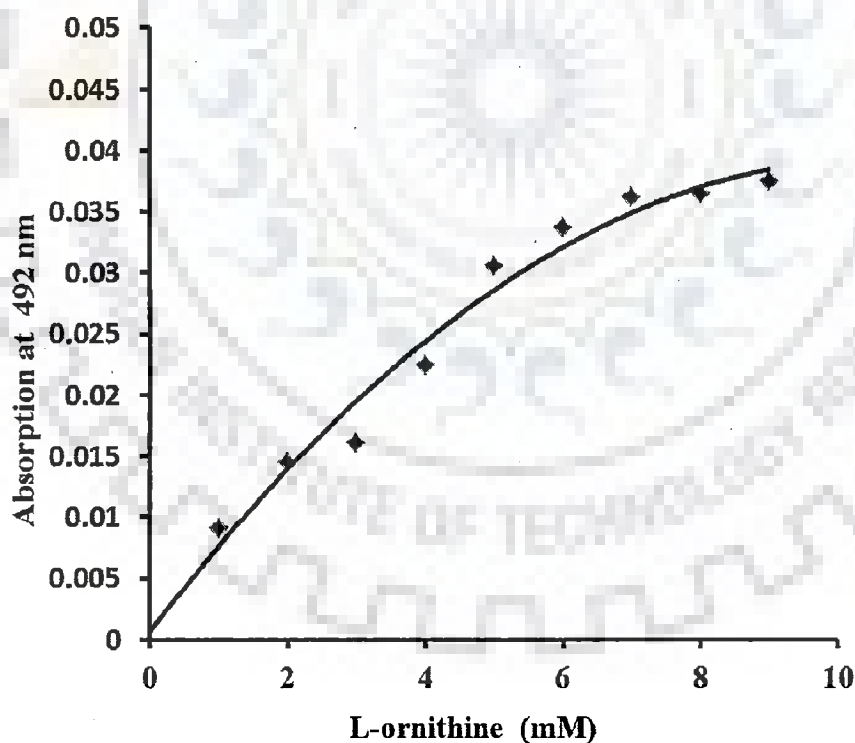


**Figure 2.8: The formation of antipyrylquinoneimine measured at 492 nm with different concentration of substrate L-ornithine.**

### 2.5.7 Secondary structure analysis of *Eh*ODC

An effort was made to elucidate the secondary structure of *Eh*ODC by using Far-UV circular dichroism (CD). CD spectrum analysis of *Eh*ODC exhibits two negative peaks at 211 and 219 nm and a positive peak in the range of 192-203 nm, as expected for a protein with  $\alpha/\beta$  content, indicating that purified protein has a well-defined structure (Figure 2.9). The deconvolution of CD data with K2d program indicates a secondary structural content of 39 %  $\alpha$ -helix, 25 %  $\beta$ -sheet, and 36 % random coil (<http://www.embl.de/~andrade/k2d.html>) (Andrade MA, 1993). For comparative secondary structure analysis, the server SOPMA was used for the prediction of secondary structural elements in *Eh*ODC sequence (Geourjon *et al.*, 1995). K2d results were found to be in agreement with the result of SOPMA showing 33 %  $\alpha$ -helix and 25 %  $\beta$ -sheet content (Table 2.1). These estimations are in accordance with the available crystal structures of ODCs and also with the molecular model for *Eh*ODC, which was generated by homology modeling in the present study. These results reveal that *Eh*ODC contains an  $\alpha/\beta$  tertiary structure and has the overall folding pattern similar to the other ODCs from mammals, plants and protozoa.

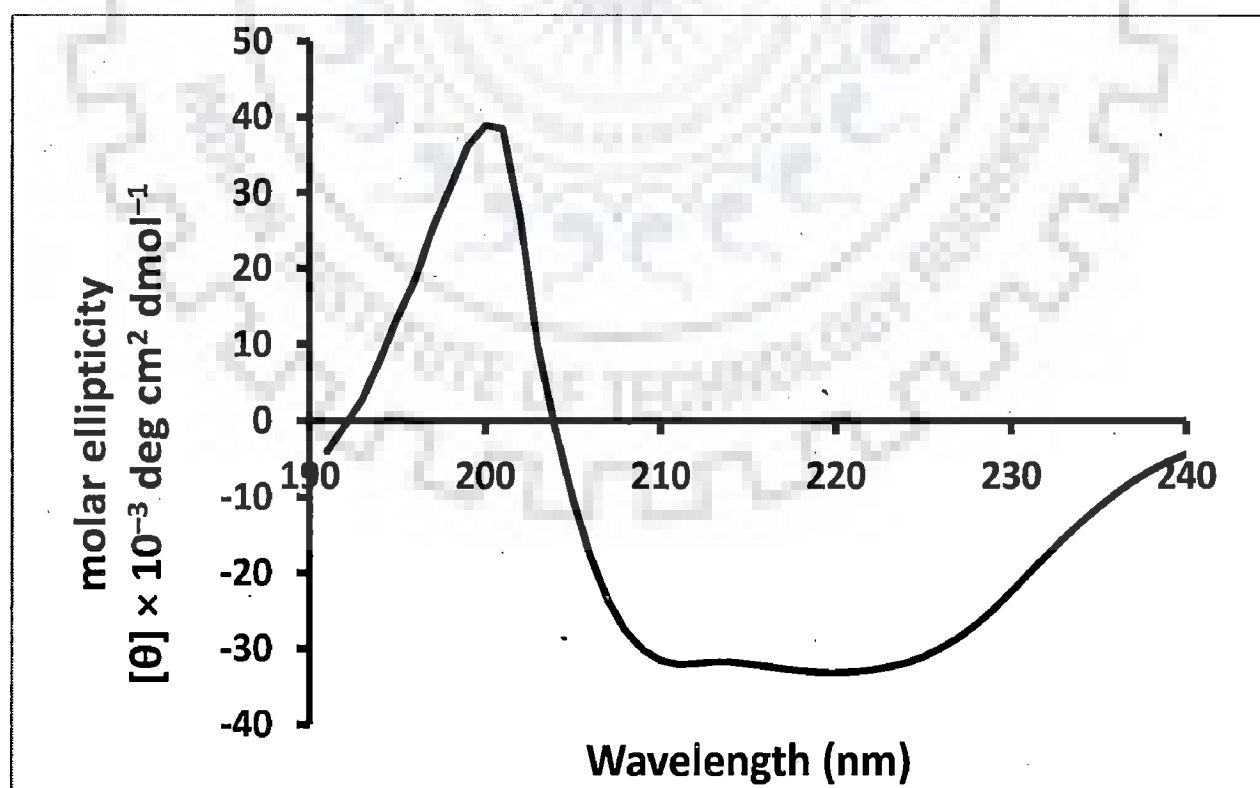


**Figure 2.9: Circular Dichroism spectroscopy of *Eh*ODC.** A Far-UV CD spectrum of 0.35 mg/ml *Eh*ODC protein. Data were analyzed using online K2d server for determining the secondary structure contents.

	$\alpha$ -Helix	$\beta$ -Sheet	Random coils
CD analysis	39%	25%	36%
SOPMA	33%	25%	41%

Table 2.1 Showing the comparative secondary structure content obtained by CD data analysis and SOPMA server.

### 2.5.8 Characterization of oligomeric state of *Eh*ODC

ODC purified from *E. histolytica* has previously been reported to exist in a pentameric state (Arteaga-Nieto *et al.*, 1999). Three dimensional crystal structure studies of ODCs from different sources have shown that the enzyme exists as a homodimer and association of monomeric subunits directs the formation of two equivalent catalytic pockets at the dimer interface. Therefore, we were interested in characterizing the functional oligomeric form of *Eh*ODC. To accomplish this, we purified recombinant *Eh*ODC enzyme and first confirmed that the purified protein is enzymatically active and then searched for oligomeric state.

### 2.5.9 Biochemical and biophysical methods

#### 2.5.9.1 Crosslinking analysis

##### 2.5.9.1.1 Glutaraldehyde crosslinking

Cross-linking agent, glutaraldehyde is used for obtaining crude information about the quaternary structure of protein (Fadoulglou *et al.*, 2008). Previously, the crosslinking experiment has been performed to reveal the dimeric form of mouse ODC (Rosenberg-Hasson *et al.*, 1991; Tobias *et al.*, 1993). Therefore, *Eh*ODC was cross-linked using glutaraldehyde in a closed setup similar to protein hanging drop crystallization method. After incubation for 10 min, the protein sample was analyzed using SDS-PAGE. The cross-linked

sample showed two bands of ~90 kDa and ~46 kDa corresponding to the molecular weight of *Eh*ODC dimer and monomer (Figure 2.10) indicating the possibility of *Eh*ODC dimerization.

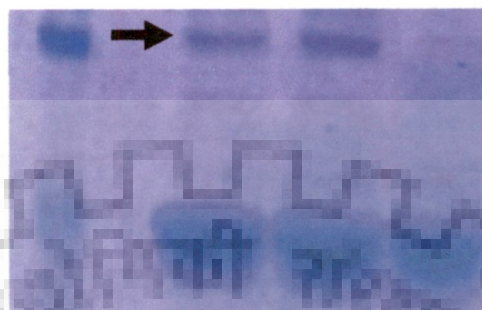


**Figure 2.10: Gel showing chemical crosslinking in the presence of glutaraldehyde analyzed by 12 % SDS-PAGE.** Lane 1: Molecular weight marker; Lane 2-3: Protein treated with glutaraldehyde showing two sharp bands corresponds to molecular weight of ~90 kDa and ~46 kDa respectively; Lane 4: Untreated purified protein. Arrow pointing to a sharp band represents the dimer of ~90 kDa.

#### 2.5.9.1.2 Dimethyl suberimidate dihydrochloride (DMS) crosslinking

Crosslinking of *Eh*ODC was also done in the presence of DMS. The purified *Eh*ODC protein (1 mg/ml) was incubated with different concentrations of DMS for 3 hours at 37 °C.

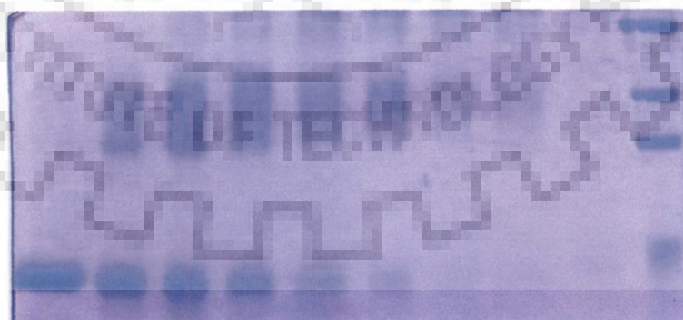


**Figure 2.11: Crosslinking in the presence of dimethyl suberimidate dihydrochloride (DMS).** Lane 1: Untreated protein; Lane 2-8: Concentration of DMS (0.8 to 2 mg/ml); Lane 9: Molecular weight marker.

The protein sample analyzed by 12 % SDS-PAGE revealed that the protein was crosslinked to dimer of molecular weight ~90 kDa. The concentration of DMS from 0.8-1 mg/ml showing the dimer formation but as the concentration increased to 2 mg/ml the protein was showing aggregation (Figure 2.11). These result also provided a clear indication that *Eh*ODC exist in dimeric form in the solution but as the concentration of crosslinking agent increases it led to aggregation.

#### 2.5.9.2 Gel filtration and MALDI-TOF analysis of *Eh*ODC.

To further analyze *Eh*ODC oligomerization, the molecular weight of purified protein was estimated by applying the sample onto a HiLoad 16/60 prep grade Superdex 200 gel-filtration column using ÄKTA purifier. Purified protein showed a major peak with the elution volume 71.3 ml (Figure 2.7 A). Using a standard curve based on molecular weight markers, the molecular weight of major elution peak was calculated and was estimated to be approximately ~90 kDa, which corresponds to the molecular weight of *Eh*ODC dimer (Figure 2.7 A, B). This suggests that *Eh*ODC exists in dimeric form.

Furthermore, MALDI/TOF MS analysis of the purified protein was carried out to verify and confirm the dimerization of protein. MS data showed two narrow peaks having average intensity of 44558.430 m/z and 90667.295 m/z and these correspond to the monomeric and dimeric state of the protein respectively (Figure 2.12). Thus, it was established that *Eh*ODC enzyme exists in dimeric state.



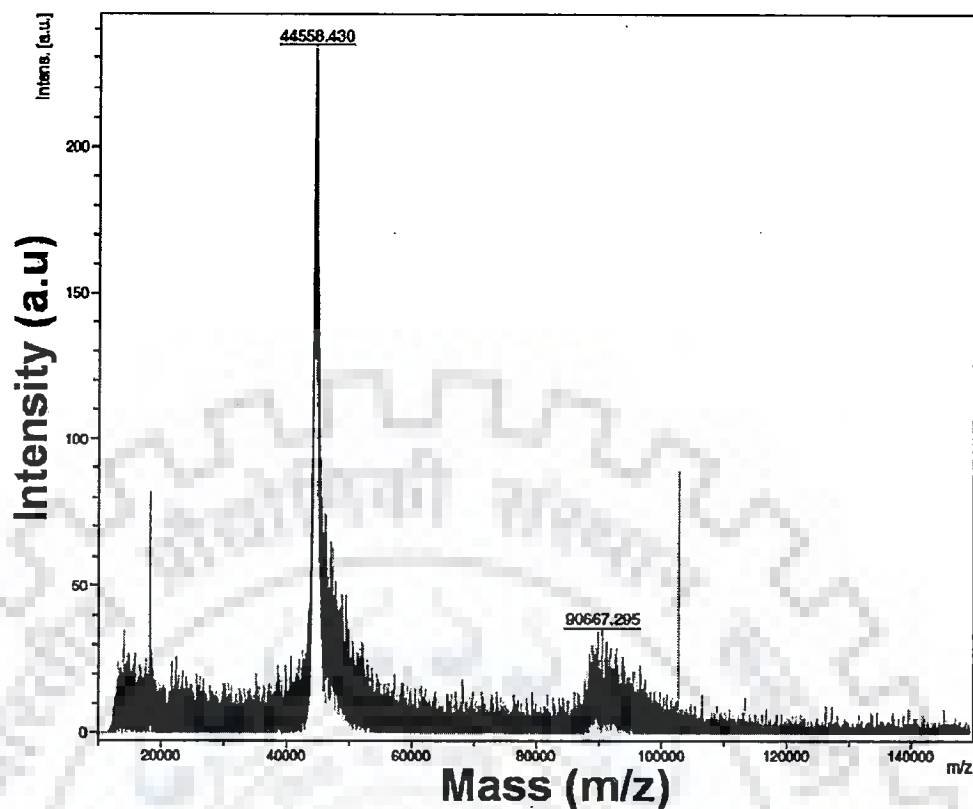


**Figure 2.12:** MALDI-TOF MS analysis of *Eh*ODC showing two peaks corresponding to ~44558.430 Da and ~90667.295 Da.

### 2.5.9.3 Effect of urea and NaCl on oligomeric state of *Eh*ODC

The study of effect of chaotropic agents on oligomeric state is critical to evaluate the stability of quaternary structure of proteins. The behaviour of ODC in presence of such agents differs from species to species and dissociation of oligomeric state is dependent on the concentration of chaotropic agents (Solano *et al.*, 1985; Tsirka *et al.*, 1993). In *T. brucei*, ODC dissociates into monomers in presence of high concentration of salt and urea (Osterman *et al.*, 1994). This provoked us to examine the effect of different concentrations of NaCl and urea on oligomeric state of *Eh*ODC.

Incubation of protein sample with 2 M and 4 M of NaCl resulted in partial dissociation of dimeric enzyme to monomeric state (Figure 2.13 A, B). Two peaks were observed in gel filtration chromatogram: one at 71 ml elution volume followed by a smaller peak at 81 ml elution volume which corresponding to the molecular mass of the dimeric and

monomeric forms of *Eh*ODC respectively (Figure 2.13 A). With increased concentration of NaCl from 2 M to 4 M, the small peak corresponding to monomer becomes more distinct demonstrating that higher concentration of NaCl partially disrupts the dimerization. This also suggests the role of inter-molecular salt-bridges and weak polar interactions in *Eh*ODC dimerization. Similar results were observed when the protein was treated with 2 M and 4 M urea (Figure 2.13 C, D). Destabilization of *Eh*ODC dimers in higher urea concentration points to the presence of inter-molecular hydrophobic interactions at the dimer interface.

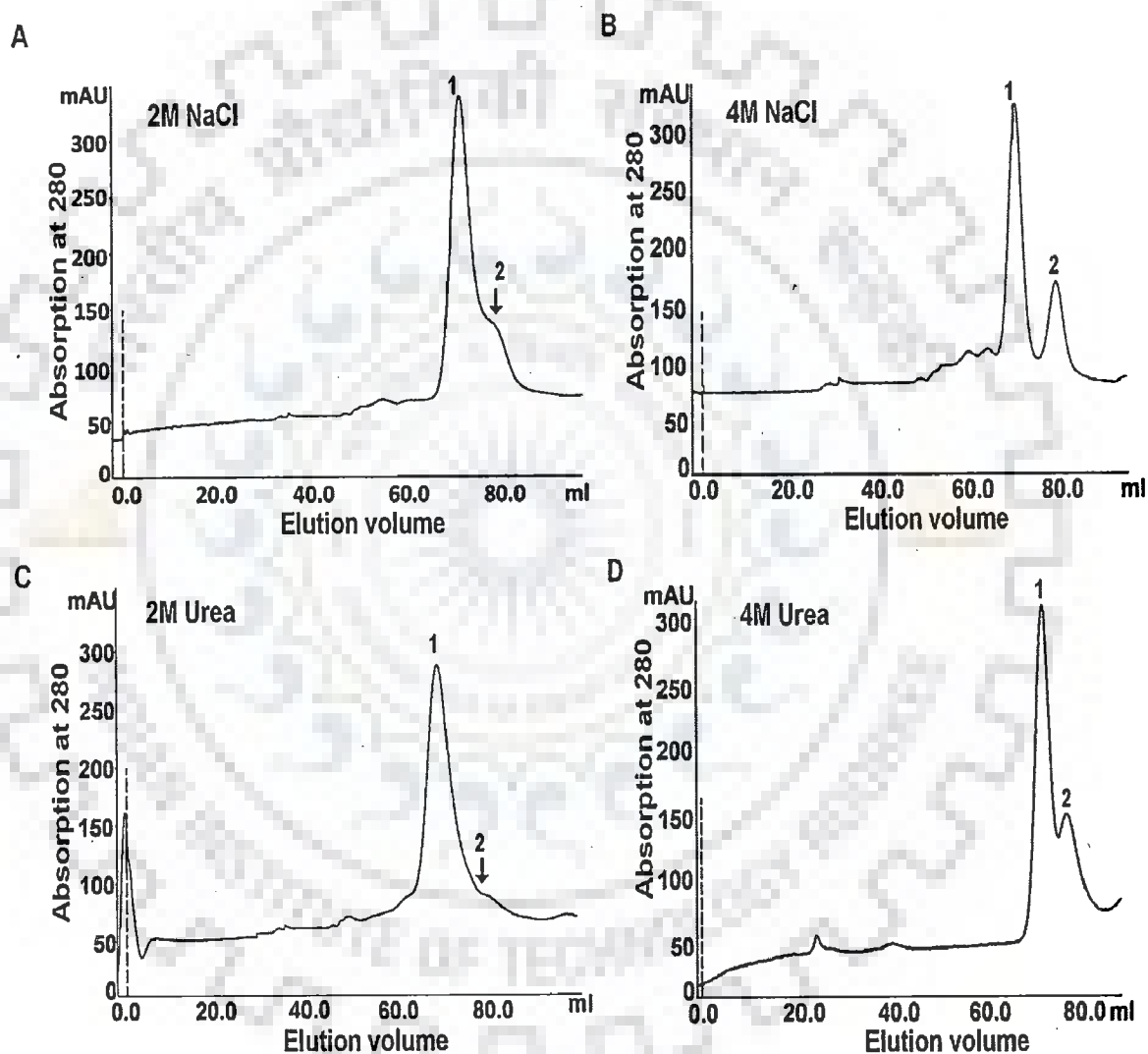


**Figure 2.13: Effect of chaotropic agents on oligomeric property of *Eh*ODC. (A) & (B):** Gel-filtration chromatogram showing the elution profile of *Eh*ODC protein treated with 2 M and 4 M NaCl respectively; (C) & (D): Gel filtration chromatogram showing the profile of protein treated with 2 M and 4 M urea respectively.

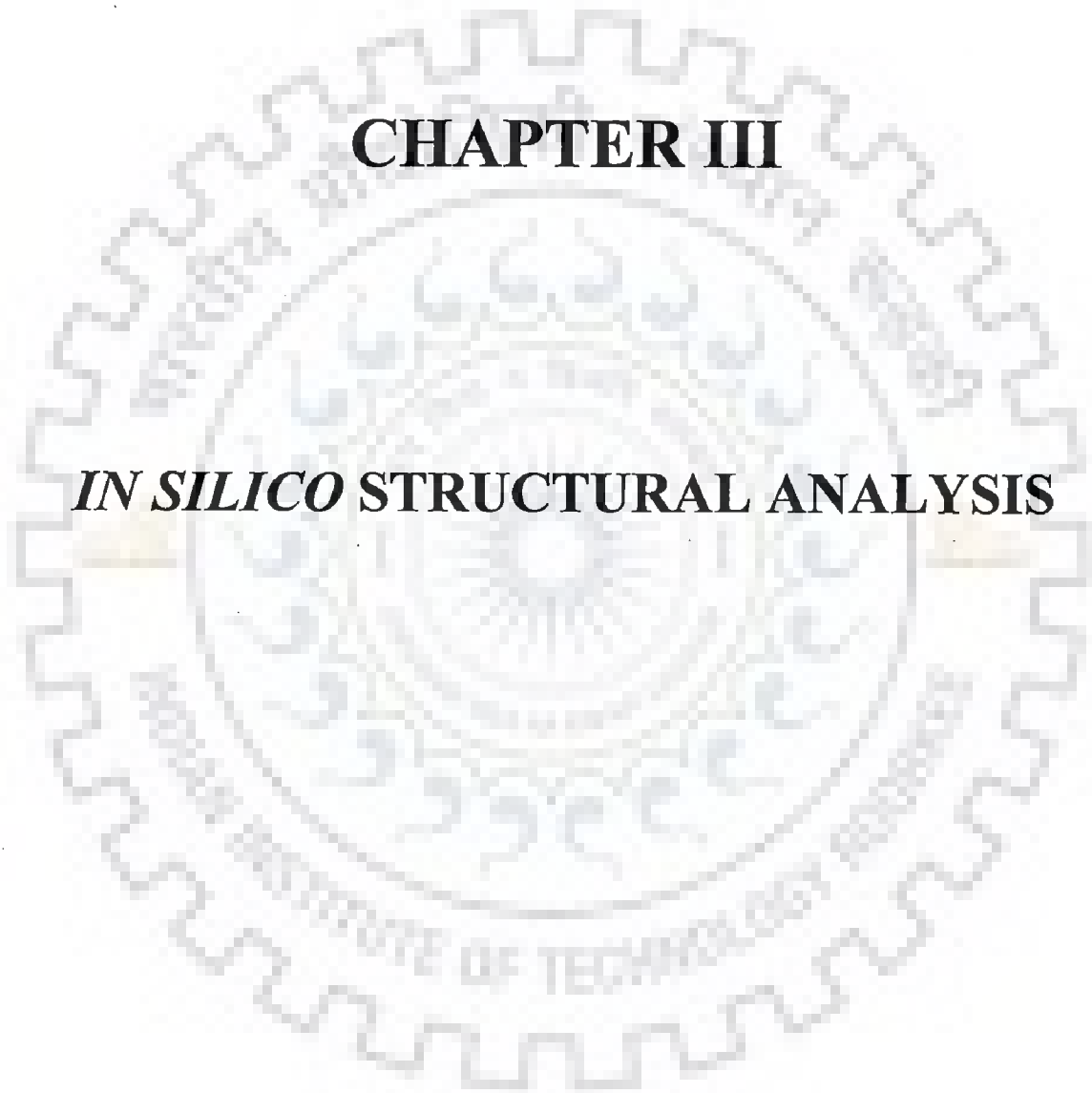
## 2.6 Conclusion

In this chapter we evidently demonstrated that ODC enzyme from *E. histolytica*, which has been previously reported to exist in homopentameric state exist as dimer. For studying the oligomeric state of the protein under different physiological conditions firstly we expressed and purified it to homogeneity. Further, the purified protein was analyzed for the active decarboxylation of substrate L-ornithine by colorimetric product detection assay and was found to be active. Purified protein was used for determining the secondary structure content by circular dichroism and it was also compared with other well characterized ornithine decarboxylase enzyme from different sources. Secondary structure analysis revealed the presence of  $\alpha$ -helix,  $\beta$ -sheets and random coils which were estimated to be 39 %, 25 % and 36 % respectively. In addition to this, the crude information for the oligomeric state of the *Eh*ODC protein was determined by crosslinking analysis in the presence of crosslinking agents. These experiments indicated the presence of dimeric form of protein in the presence of glutaraldehyde while in the presence of DMS, the protein was aggregating and unable to demonstrate the clear oligomeric state. The purified sample was further characterized by gel filtration chromatography, and MALDI-TOF mass spectra which confirmed the existence of *Eh*ODC in dimeric state of ~90 kDa.

These studies further encouraged us to analyze the behavior and protein-protein interaction properties under different physiological conditions of chaotropic agents. The chaotropic agents such as urea and salt demonstrate considerable protein dissociation and disruption of intermolecular interaction with increase in concentration from 2 M to 4 M. These results suggest that the *Eh*ODC protein exist in dimeric form in the solution which is in equilibrium with the monomer.

# CHAPTER III

## *IN SILICO* STRUCTURAL ANALYSIS



### 3.1 Abstract

This chapter describes the primary sequence analysis, secondary structure predictions and homology modeling of *Eh*ODC. The homology modeling and sequence analysis have been used to get insight into the structural geometry of enzyme. Sequence analysis revealed that *Eh*ODC has sequence similarity of 33 % with *Datura stramonium*, 36 % with human, and 32 % with *Trypanosoma brucei* ODC. In addition to this, computational model of *Eh*ODC dimer was generated. The homodimer contains two separate active sites at the dimer interface with Lys57 and Cys334 residues of opposite monomers contributing to each active site. Molecular dynamic simulations were performed and the dimeric structure was found to be stable with RMSD value ~0.327 nm.

The *Eh*ODC gene is a 1,242 nucleotide bases long stretch of DNA, encode for a monomeric protein of 413 amino acid residues. Primary sequence comparison with other ODCs helped in predicting that only 380 residues play structural and functional role in *Eh*ODC. The monomer of ODC consists of two domains, a primarily conserved N-terminal domain and a variable C-terminal domain with little sequence homology.

### 3.2 Introduction

Structural biology deals with an interesting phenomenon where protein with similar tertiary fold may exhibit diverse functionality (Tatusov *et al.*, 1997, 2001; Apic *et al.*, 2001; Qian *et al.*, 2001). The global architecture of enzyme is essential for determining the role of each residue of the active site and reaction mechanism. In the absence of crystal structure, 3D model can be generated and bioinformatics studies can be performed to investigate the role of active site residues and stability of the enzyme (Murzin *et al.*, 1995; Wilson *et al.*, 2000; Sali *et al.*, 1993). Molecular dynamics simulations help to derive the collective fluctuation and determination of domain motions which help in analyzing the function of enzyme. Motion predicted by dynamics studies suggests the possible conformations for the enzyme (Karplus *et al.*, 1996).

Polyamine biosynthetic pathway has gained attention due to the important role of polyamine in cell growth. Investigations have been done using polyamine as a potent drug

target in cancer treatment (Palavan-Unsal *et al.*, 2006). The enzyme ornithine decarboxylase has been reported to be present in various protozoa including *Leishmania*, *Giardia* and *Plasmodium* and is a validated drug target in *Trypanosoma brucei* for treatment of African sleeping sickness (Bacchi *et al.*, 1980; Gillin *et al.*, 1984; Balana-Fouce *et al.*, 1991; Bitonti *et al.*, 1989; Müller *et al.*, 2000; Birkholtz *et al.*, 2011). ODC catalyzes the decarboxylation of ornithine to putrescine, which is the first and rate-limiting step in polyamine biosynthesis (Figure 3.1) (Jackson LK *et al.*, 2003).

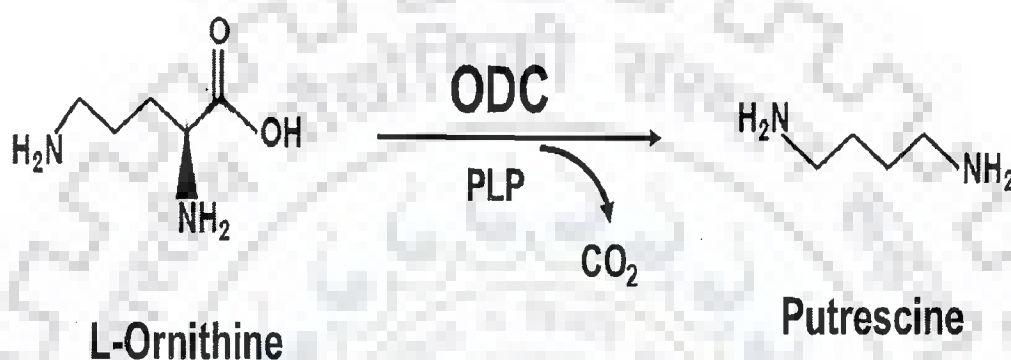


**Figure 3.1:** The enzymatic reaction catalyzed by ornithine decarboxylase. The pyridoxal phosphate (PLP)-dependent ODC catalyzes decarboxylation of ornithine and produces putrescine.

The enzyme belongs to fold type III group IV decarboxylase of a B<sub>6</sub>-dependent family, having characteristics of alanine racemas family. Under this classification, three crystal structures are available till date including human, mouse and *Trypanosome brucei* ODC (Almrud *et al.*, 2000; Kern *et al.*, 1999; Grishin *et al.*, 1999). Crystal structures revealed that the enzymes exist as dimer forming two active sites at the interface. Each monomer of ODC has been found to consist of two domains: N-terminal barrel and C-terminal sheet domain. Interestingly, the active site residues involve Lys69 of one monomer and Cys360 of opposite monomer at the active site pocket. There are many more residues present at the active site, interacting directly or indirectly through water molecules and contribute for active catalysis of substrate.



Active site pocket present at the interface involves residues from barrel of one monomer and sheet domain of other. The subunit association is driven by many small energetic contributions distributed throughout the interface. The mutational studies and kinetic analysis of interfacial hydrogen bonds and salt bridges in protein-protein interfaces suggested that residues involved in the inter-subunit association might influence the energetics of association of the two subunits. Furthermore, the interactions may be influenced by amino acid residues that directly participate in the active site structure and present throughout the subunit interface (Myers *et al.*, 2001; Freire, 1999; Lockless *et al.*, 2000).

ODCs have been reported to possess disordered regions responsible for its short half-life as reported in mouse, human, and other ODCs. Mouse ODC (mODC) consist of 3 short disordered regions: residues 158-168 connecting H7 to B8 which corresponds to protease-sensitive loop, residue 30-35 connecting H1 to B3 and residues 298-311 connecting B12 to B13, third loop found to be located near the active site (Osterman *et al.*, 1995). In addition to this, C-terminal domain of mouse ODC has been identified as an intrinsic signal for degradation by antizyme mediated 26S proteasome dependent proteolysis (Rosenberg-Hasson *et al.*, 1991). Interestingly, an element required for constitutive degradation lies within the 37 amino acids at C-terminus. This region is rich in amino acids proline (P), glutamate (E), serine (S) and threonine (T) PEST which might be a signal sequence for proteasome mediated degradation (Almrud *et al.*, 2000). The phenomenon of antizyme dependent degradation was not observed in *Tb*ODC. Interestingly, the mODC was found to be stable when its C-terminus was replaced by C-terminus of *Tb*ODC (Li *et al.*, 1992; Hua *et al.*, 1995). Sequence comparison and secondary structure prediction help in determining the residues playing critical role at the active site pocket.

*In silico* analysis helped in determining the polar, hydrophobic and other electrostatic interactions which might be involved in dimer formation under physiological conditions and verification of biochemical properties of enzyme.

### **3.3 Hardware and software**

Amino acid sequences of representative organisms were retrieved from National Center for Biotechnology Information (NCBI). Multiple sequence alignment and phylogenetic analysis

were performed using online servers ESPript 2.2, MULTALIN, and CLUSTALW. Homology model was generated by SWISS-MODEL, PHYRE, Geno3D, and MODELLER 9v8 (<http://salilab.org>). Models were evaluated by PROCHECK, PROSA, and VERIFY-3D using online SAVES server. Salt bridges in the dimer model were determined by using ESBRI server (<http://bioinformatica.isa.cnr.it/ESBRI/input.html>). Molecular dynamic simulations were done using GROMACS. Analysis of interactions and visualization of molecular structure was done using PyMol.

### **3.4 Methods**

#### **3.4.1 Sequence analysis**

The ODC sequence of *E. histolytica* was retrieved from NCBI database. Blast and PSI-blast search were performed using AAX35675.1 as query against the non-redundant protein sequence database to identify and analyze orthologous sequences. The homologous sequences were retrieved from the NCBI database, multiple sequence alignment was generated using ClustalW and compared for phylogenetic analysis (Thompson *et al.*, 1994).

#### **3.4.2 Secondary structure prediction**

The secondary structures of *Eh*ODC were predicted using PSIPred and ESPript program (<http://bioinf.cs.ucl.ac.uk/psipred/>; <http://esprpt.ibcp.fr/ESPript/ESPript/>) (Gouet *et al.*, 2003; Jones, 1999). The intrinsic disordered regions in the protein were analyzed by online server DisEMBL (<http://dis.embl.de/>) (Linding *et al.*, 2003). Salt bridge interaction in the *Eh*ODC dimer structure model was estimated by ESBRI server (Sarakatsannis *et al.*, 2005).

#### **3.4.3 Molecular modeling**

Three-dimensional (3D) homology model of *Eh*ODC homodimer was generated by comparative modeling using MODELLER 9v8 (Sali *et al.*, 1993). To obtain an effectual model, five sequential steps were performed: template selection from Protein Data Bank (PDB), sequence-template alignment, model building, refinement of the obtained model and validation. Template search was done using NCBI BLAST search tool for PDB database (Altschul *et al.*, 1990). BLASTP algorithm was run with BLOSUM62 as a scoring matrix.

Crystal structure of human ODC (PDB ID: 2O00) which has 34 % sequence identity with *Eh*ODC was selected as a template for structure modeling (Almud *et al.*, 2000). The graphically enhanced alignment with secondary structures was obtained using ESPript 2.2 server (Gouet *et al.*, 1999).

MULTALIN server was used to align the query sequence with the template sequence (Corpet, 1988). Some manual corrections were done in the alignment file for missing residues in the template sequence. The cofactor, PLP was incorporated into the modeled structure of *Eh*ODC from the template structure and five preliminary models were generated using MODELLER 9v8. All models were selected on the basis of lowest DOPE scores and assessed sterio-chemically by PROCHECK (Luthy *et al.*, 1992).

Energy minimizations of the best chosen models were performed using Swiss-PDB Viewer4.01 (<http://www.expasy.org/spdbv/>). Loop refinement module of the MODELLER was used for the refinement of the disorganized residues in loops and refinement process was considered for structure validation. Each refined model was verified using ERRAT plot which gives the measure of structural errors in each model at residue level in the protein (<http://nihserver.mbi.ucla.edu/SAVES/>). The refined model was further validated by ProSA energy plot and VERIFY-3D of the SAVES server (Luthy *et al.*, 1992; Wiederstein *et al.*, 2007). All the graphical visualization and image production were performed using PyMOL (DeLano, 2002).

#### **3.4.4 Molecular dynamics simulation**

Molecular dynamics (MD) simulation of dimeric model of *Eh*ODC was performed using GROMACS (v 4.5.4) package (Hess *et al.*, 2008). GROMOS96 43a1 force field and 47324 SPC water molecules for solvation of protein were used for simulation. The molecule was solvated in a cubic box at a distance of 1.0 nm between the proteins and the box edge. Electrostatic interactions were calculated using the Particle-mesh Ewald method. Van der Waal and coulomb interactions were truncated at 1 nm. Molecule was neutralized by adding 24 Na<sup>+</sup> counter ions to the surface and was allowed to undergo 1000 energy minimization steps. All bond lengths including hydrogen atoms were constrained by the LINCS algorithm. To maintain the system at isothermal and isobaric conditions of 300 K and 1 bar, a V- rescale

and Parrinello-Rahman barostat coupling was applied for 100 ps. Following to the equilibration, MD simulation was initiated for 1 ns and then extended to 8 ns, with all trajectories sampled at every 1.0 ps.

### 3.5 Results and discussion

#### 3.5.1 Sequence analysis and phylogeny

In present study, the sequence of *Eh*ODC has been retrieved from NCBI database with accession number AAX35675. The protein consists of 413 amino acids with predicted molecular weight of 46.43 kDa (Figure 3.2). In *E. histolytica*, the gene encoding ODC is of 1,242 bps, thus it implies that there is no intron present in the gene.

```

      10      20      30      40      50      60
MKQTSLEVK E FALNLI SQFE PENQPLGFWI FDTEGVEKAV ERWKKNMPTV RPCFAVKCNP
      70      80      90     100     110     120
EPHLVKLLGE LGC GFDCASL NEIKEVLDLG FNPEDITYSQ TFKPYNQLIE ASHLGINHTI
     130     140     150     160     170     180
VDSIDEVQKI AKYAPKMGIM IRIMENDTSA GHVFGEKFG L HDDEVEIVLK EIKDKGLNLD
     190     200     210     220     230     240
GVH FHVGS DS HNSEVFTKAL TKARNTVTILA EQFGMKPYLI DIGGGFSQVA PFE EFAATIE
     250     260     270     280     290     300
KTIKELEFPE RTRFIAEPGR YMASNAFHLV SSLHGKRVRI QNGKKQIEYT SGDGLHGSFG
     310     320     330     340     350     360
CCIWF EKQKS CECITQKVNE NTKMYESI IY GPSCNGSDKV ATQELPEMEP GKDWLLFPNM
     370     380     390     400     410
GAYTISMATN FNGFEERNHV IYTLPLKSTK IIQIPKSIEC NSVPSLNGIP HYA

```

**Figure 3.2: Amino acid sequence of *Eh*ODC encoded for 413 residues with number of residues labeled.**

The enzyme has been previously characterized by Jhingran *et al.*, 2008. The amino acid sequence alignment of *Eh*ODC with representative ODCs from different sources revealed that the active site residues along with dimer interface residues responsible for dimerization are highly conserved (Figure 3.3).

*Eh*ODC showed overall 36 to 39 % identity with plants, 15 to 25 % with bacteria, 35 to 38 % with fungi and 32 to 38 % with animals. Interestingly, *E. histolytica*, being a

protozoan was expected to show high sequence identity, but surprisingly it shows same range of identity with other protozoa including *T. brucei*, *D. dasциulates* and *P. falciparum*, etc. i.e. 32 to 35 %. Further sequence analysis revealed that the substrate binding motif having a consensus sequence WGPTCDGL(I)D is highly conserved in human, mouse and *T. brucei* where (C) Cys of this sequence plays a critical role in catalysis. However, in *Eh*ODC, though C is conserved, but the sequence exists as 330 YGPSCNGSD 338 (Figure 3.3).



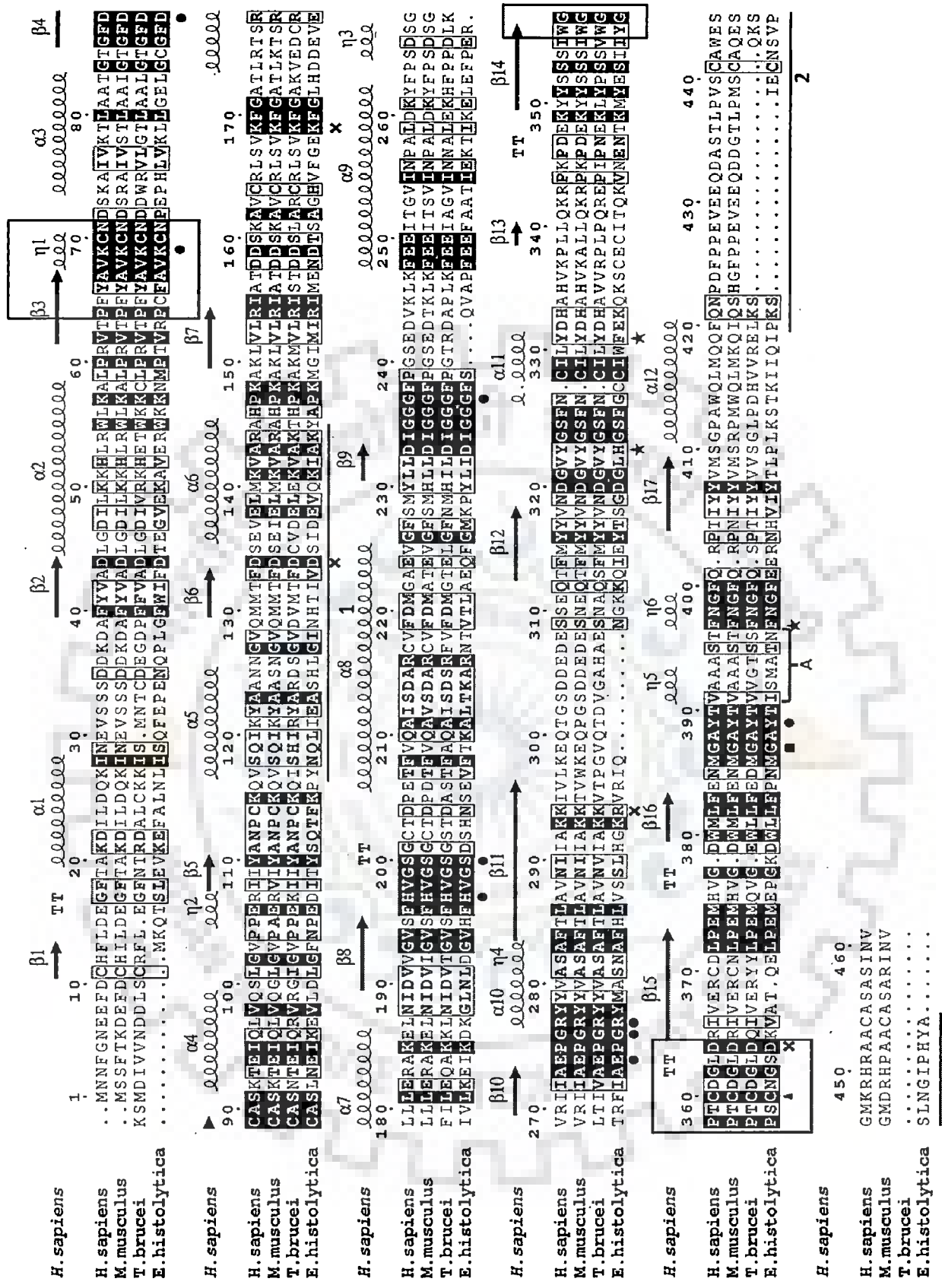




**Figure 3.3: Multiple sequence alignment of *Eh*ODC (AAX35675) with other ODC sequences.** The conserved residues are highlighted with black background color. The secondary structure elements and numbering of amino acid sequence of human ODC are presented above the aligned sequences. The signatory motifs PxxAVKC(N) (PLP binding motif) and WGPTCDGL(I)D (substrate binding motif) are highlighted in boxes where “x” signifies any amino acid and amino acids in brackets depict the option at a given position. Underlined sequence denotes the amino acids showing similarity with (1) Antizyme binding region (2) PEST like region. The circles under the amino acid indicate the residues interacting with cofactor PLP whereas triangles denote the substrate L-ornithine binding residues in the active site pocket. The residues denoted with cross mark are involved in the formation of salt bridges in between two monomers. The residues indicated with stars are present at the interface and form a stack of aromatic rings. Residue important for dimer formation and present away from the interface is denoted with a square. The motif A represents the interface residues of two monomers present very closer to each other. Alignments are obtained using ESPript.

From phylogenetic tree, the ODC from plants, fungi and bacteria make different clusters on the basis of sequence homology whereas the protozoan ODCs do not cluster together instead are distributed throughout showing resemblance with bacteria, fungi and plants (Figure 3.4). However, *Eh*ODC shows maximum homology with plant ODCs and the evolutionary origin of *Eh*ODC or protozoan ODCs on the basis of phylogenetic analysis is not conclusive. Nevertheless, sequence analysis shows conservation of dimer interface residues which specify the possibility of *Eh*ODC enzyme dimerization similar to other ODCs.

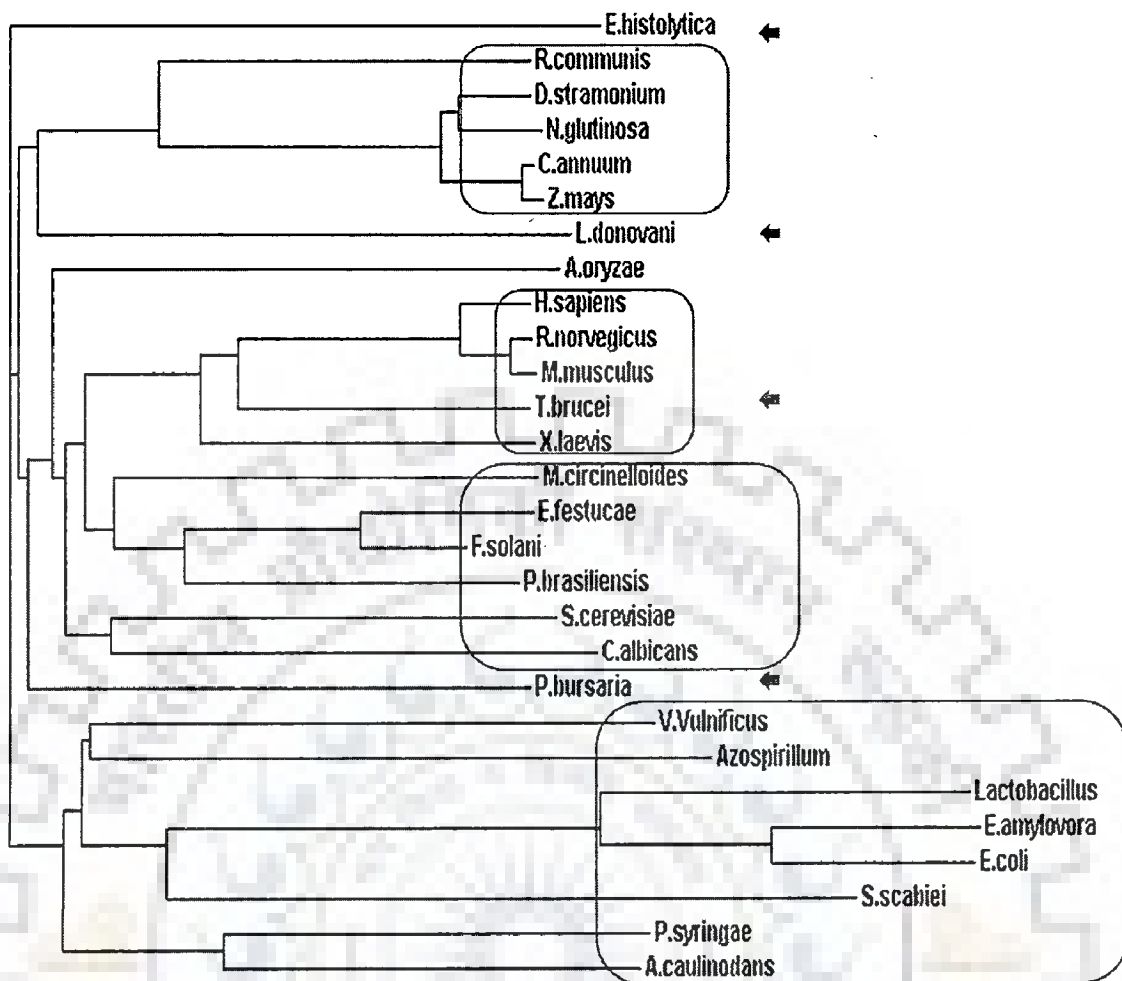


**Figure 3.4: Phylogeny of ornithine decarboxylase from various sources.** The amino acid sequences of ODC were taken from plants *R. communis* (XP\_002510610.1), *N. glutinosa* (AAG45222.1), *C. annuum* (AAL83709.1), *Z. mays* (AAM92262.1), *D. stramonium* (P50134.1); animals *X. laevis* (NP\_001079692.1), *R. norvegicus* (NP\_036747.1), *M. musculus* (P00860.2), *H. sapiens* (P11926.2); fungi *A. oryzae* (XP\_001825149.2) *M. circinelloides* (CAB61758.1), *E. festuca* (ABM55741.1), *P. brasiliensis* (AAF34583.1), *S. cerevisiae* (EDN60096.1) *F. solani* (ABC47117.1), *C. albicans* (AAC49877.1); protozoa *P. bursaria* (NP\_048554.1), *T. brucei* (P07805.2), *L. donovani* (P27116.1), *E. histolytica* (AAX35675) and bacteria *V. vulnificus* (YP\_004188159.1), *A. caulinodans* (YP\_001523249.1), *P. syringae* (AAO58018.1), *E. amylovora* (YP\_003539917.1), *S. scabiei* (YP\_003491041.1), *Azospirillum* (BAI72082.1), *E. coli* (BAE77028.1), *Lactobacillus* (P43099.2). Different clusters representing a particular group are highlighted in boxes whereas the representatives of protozoa ODC are highlighted by arrow marks.

The regulation of ODC activity is partially modulated by antizyme-induced, ubiquitin-independent degradation by the 26S proteasome, which is the characteristic of mammalian ODC (Li *et al.*, 1992; Hayashi *et al.*, 1985; Kanamoto *et al.*, 1986; Murakami *et al.*, 1996). Antizyme binds to the inactive ODC monomer forming a hetero-dimer complex which promotes proteolysis degradation (Li *et al.*, 1992; Mitchell *et al.*, 1988).

In human ODC, the antizyme binding locus consists of 30 residues at N-terminal ranging from 115Lys to 144Arg residues. The same locus is also highly conserved in mouse. However, this locus in *Eh*ODC which corresponds to 105Tyr to 132Lys having 23 % identity is not conserved. In this locus, three residues 121Lys, 141Lys and 144Arg (in human ODC) are highly conserved and responsible for antizyme binding (Kern *et al.*, 1999). However, in *Eh*ODC, 121Lys and 144Arg are substituted by 109Ile and 132Lys respectively. Thus, it may be possible that these differences in sequence makes *Eh*ODC insensitive or poorly sensitive to antizyme binding as antizyme dependent ODC degradation has not been reported in *E. histolytica* till date. The antizyme binding locus in *Eh*ODC begins at the N-terminal of  $\alpha 5$  followed  $\beta 7$  and reaches mid-way of  $\alpha 6$  superimposing the putative antizyme binding element with *Hs*ODC, *Mm*ODC (PDB-ID 1d7k residues 115-144) calculated root mean square deviation (RMSD) of 0.294 Å and 0.224 Å respectively but with the *Tb*ODC it was 3.292 Å.

### 3.5.2 Secondary structure analysis

In chapter II section 2.5.7 the secondary structure content of recombinant *Eh*ODC was determined experimentally by Circular Dichroism spectroscopy. To further support the experimental results, we analyzed the sequence of *Eh*ODC by bioinformatics tools such as ESPript, PSIPred. The secondary structure content of *Eh*ODC was predicted to be 39 %  $\alpha$ -helix, 25 %  $\beta$  sheets and 36 % random coils (Table 2.1). The secondary structures content obtained by bioinformatics analysis of the sequence was also equivalent to the experimental results (Figure 3.3, 3.5, 2.9).

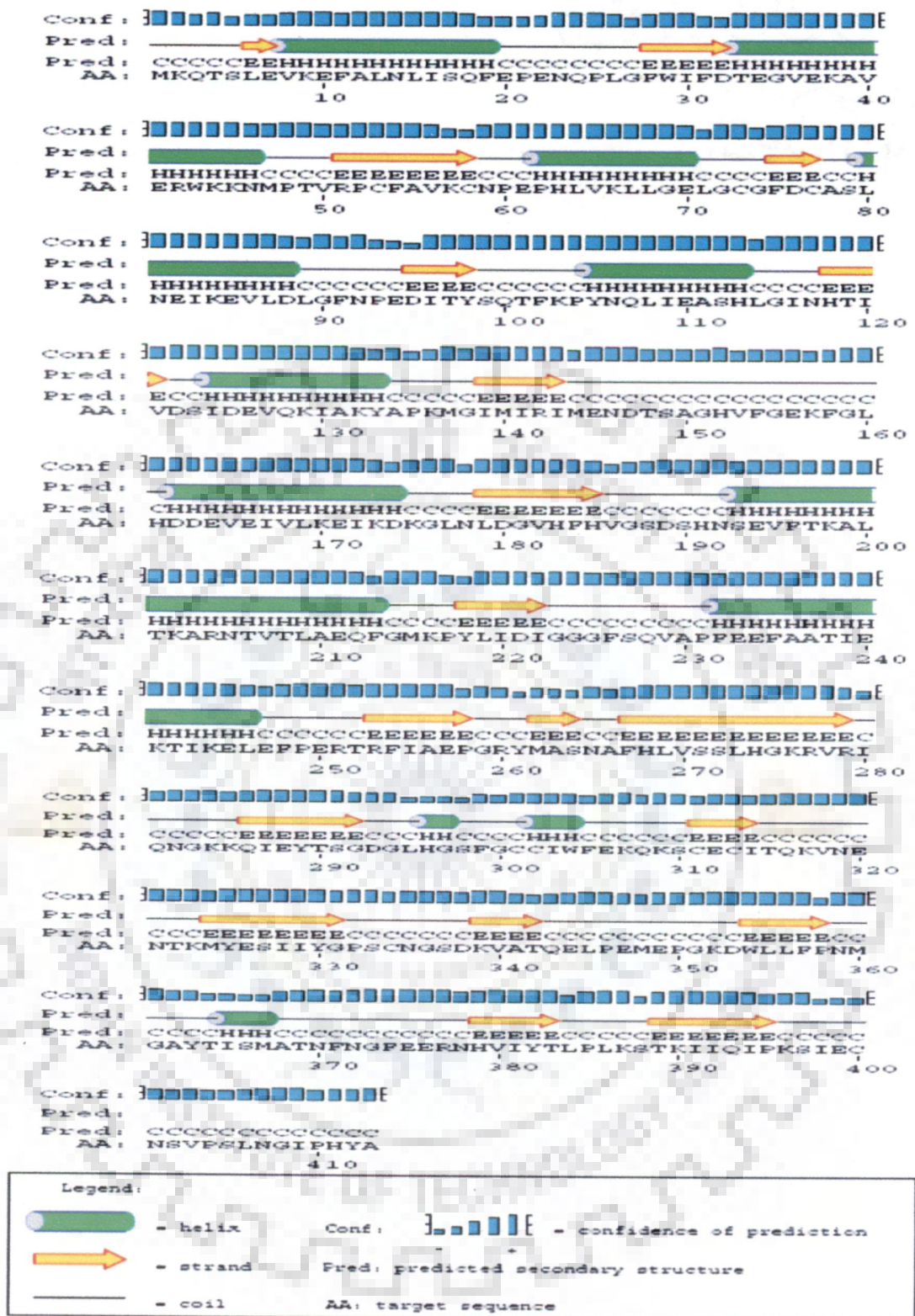


Figure 3.5: Secondary structure prediction from the primary sequence of *EhODC* by using PSIPred server.

The *Eh*ODC secondary structure predicted by primary sequence using PSIPred server has been given in figure 3.5.

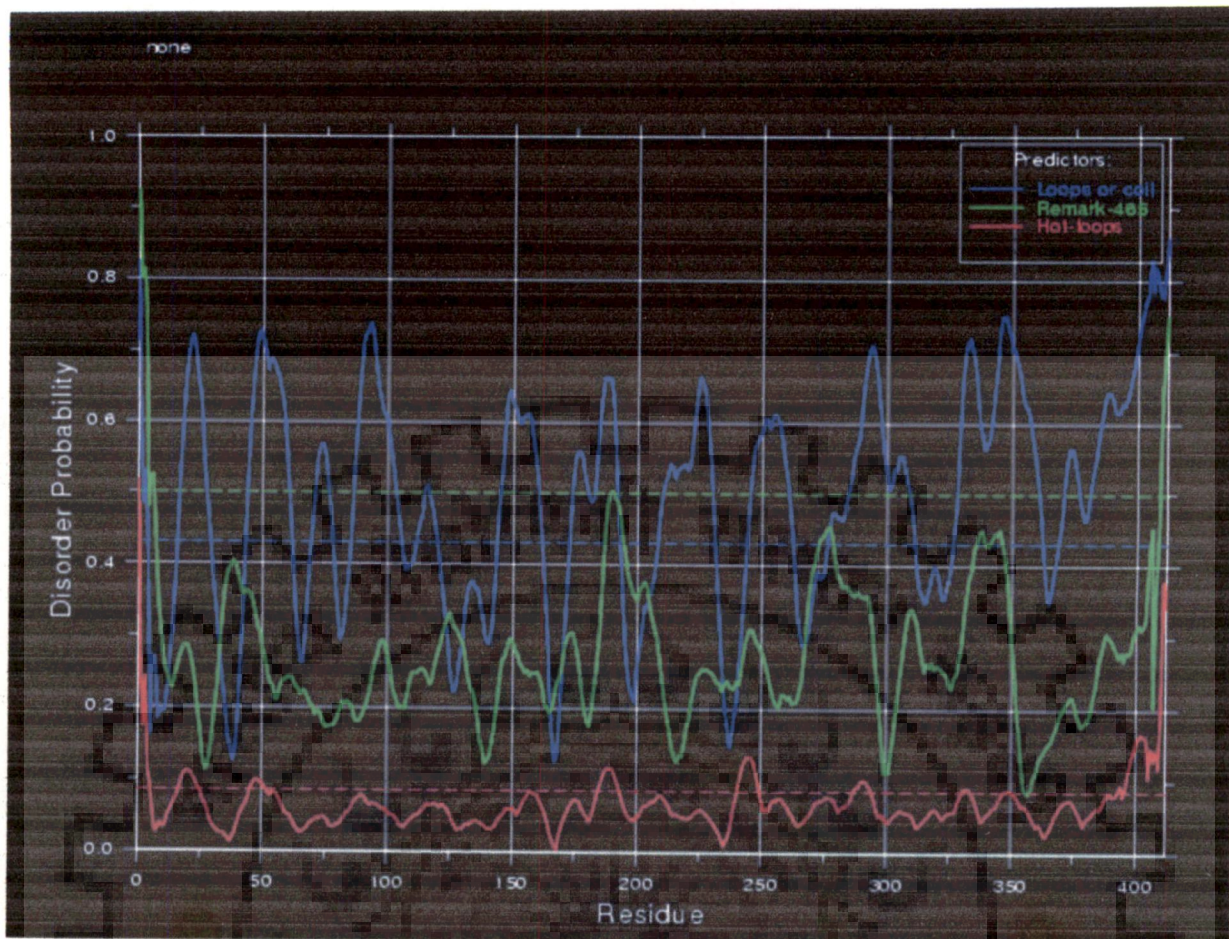
### 3.5.3 Prediction of the disordered regions

Many proteins have been found to be disordered under physiological conditions. They contain no or very less ordered structure content which increase with organism complexity (Wang *et al.*, 2011; Shur *et al.*, 2011). Disordered regions are found in significantly higher percentage in homodimer as compare to heterodimer (Shur *et al.*, 2011). The intrinsically disordered region has great impact on protein expression, solubility, purification and crystallization. Deletion or truncation of this region may increase solubility and probability of crystallization of protein. Therefore we found structurally disordered regions in *Eh*ODC by using online DisEMBL program (Linding *et al.*, 2003). Two stretches which were found disordered at the C-terminal included 242-250 and 397-413 (Figure 3.6). Deletion of the longest disordered stretch from the protein sequence improved the expression, solubility and crystallization properties of *Eh*ODC.

### 3.5.4 Disordered regions in *Eh*ODC sequence

In human ODC many disordered regions are present in the sequence. Comparison of the conserved primary sequence *Eh*ODC with mouse and human ODC provide clue to identify the potential bonding site of antizyme and PEST rich basal degradation element.





mkqtslevke falnlisqfe penqplgfwi fdtegvkav erwknmptv rpcfavkcnp ephlvkllge lgcgfdcasl  
 neikevldlg fnpeditysq tfkpynqlie ashlginhti vsidevqki akyapkmgim irimendtsa ghvfgekfgl  
 hddeveivlk eikdkglnd gvfhvgsds hnsevtkal tkarntvta eqfgmkpyli digggfsqva pfeefaatie  
 k**TIKELEFPE** rtrfiaepgr ymasnafhlv sslhgkrvri qngkkqieyt sgdglhgsfg ceiwfekqks  
 cecitqkvne ntkmyesiyy gpcngsdkv atqelpemep gkdwllfpm gaytismatn fngfeernhv iytlplkstk  
 iiqipk**SIEC NSVPSLNGIP HYA**

**Figure 3.6: Prediction of structurally disordered regions of EhODC.** The disordered regions are depicted in red and folded regions are depicted in green. Two regions found to be disordered has been denoted in red color and ranging from 242-**TIKELEFPE**-250, to 397-**SIEC NSVPSLNGIP HYA**-413. Predictions were done using DisEMBL 1.5 (dis.embl.de/).

Addition to this, in mouse ODC two basal degradation elements (376 to 424 and 422 to 461) at C-terminal are reported which are rich in proline (P), glutamic acid (E), serine (S) and threonine (T) called PEST sequence (Almrud *et al.*, 2000). In this region, Cys441 (in



both mouse and human ODC) is identified to be a critical residue that promotes polyamine-dependent proteolysis (Li *et al.*, 1992; Ghoda *et al.*, 1992). Similar pattern of sequence arrangement is also observed in *Eh*ODC where it ranges from 395 to 413, and conserved Cys400 corresponds to Cys441 in mouse ODC.

### 3.5.5 Generation and stability of 3D model of *Eh*ODC

The molecular structure and subunit interactions in *Eh*ODC were investigated by constructing a dimeric model of the enzyme using homology modeling approach. The sequence homology search for *Eh*ODC gave the hits of 29 sequences against PDB database. The crystal structure of human ODC was the first hit with 34 % sequence identity (PDB ID: 2O00) followed by *Tb*ODC (33 %, PDB ID: 1QU4). For comparative homology modeling, it could be significant to select a template for ODC from protozoan source i.e. *Tb*ODC. However, too much variations in the sequences of ODC within protozoa (Figure 3.4) and higher sequence identity of *Eh*ODC with plant and mammalian ODC, give an indication of caution required in the interpretation of template selection. Here, we have selected human ODC as template for a reliable model generation considering two major facts: Firstly, the N-terminal loop region consisting of approximately eight amino acids is missing in all crystal structures of ODC except human ODC. Secondly, multiple sequence alignment analysis showed a sequence in the C-terminal region of *Eh*ODC sequence that has similarity with PEST like sequence in human ODC (Figure 3.3).

The model for *Eh*ODC along with its cofactor PLP was generated from PDB 2O00 as a template using MODELLER 9v8 and model with lowest DOPE score was considered for further loop refinement using MODELLER loop refinement tool. The model was subjected to energy minimization where PROCHECK, ERRAT plot and ProSA energy plot were used for validation and quality assessment of the model.

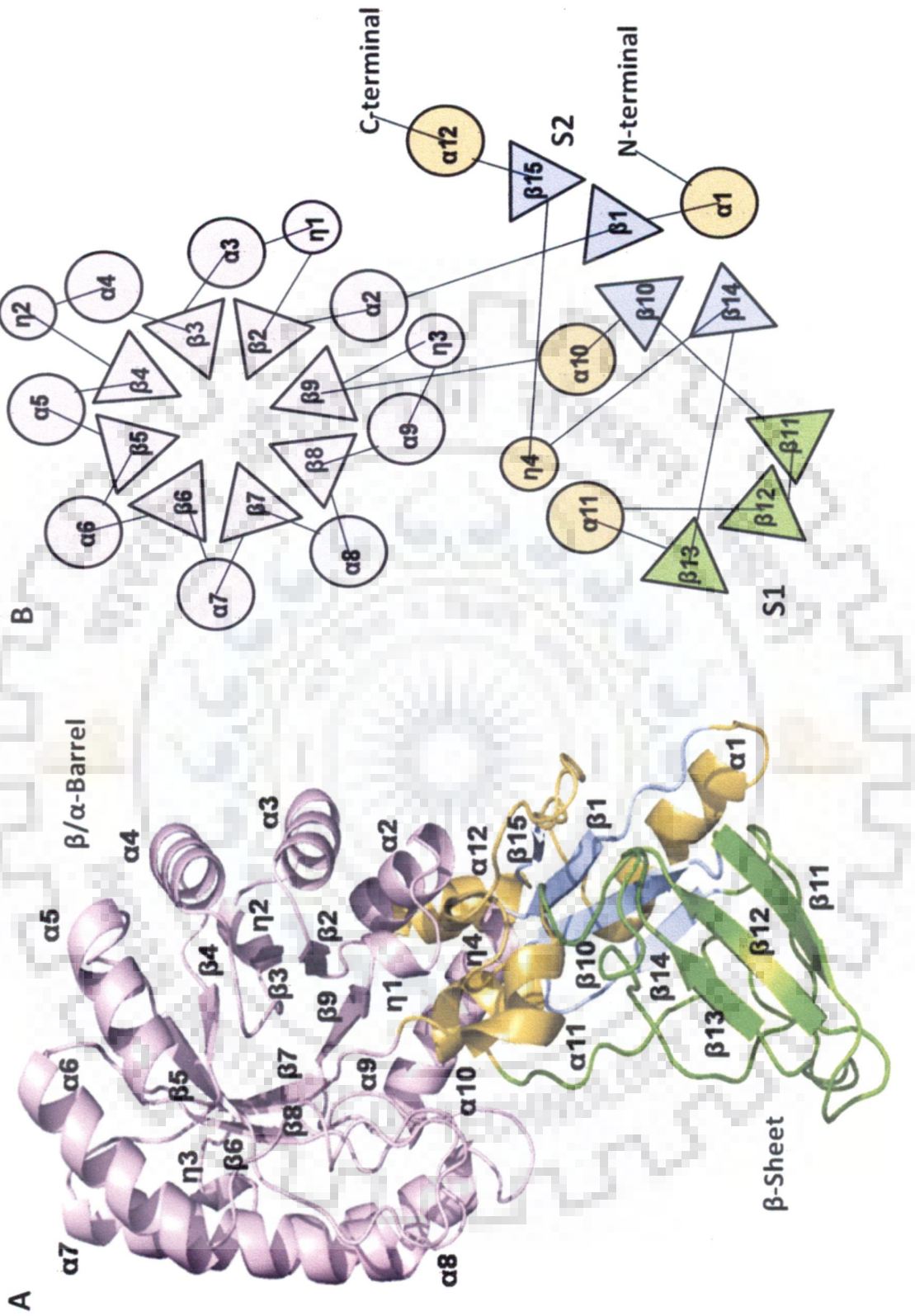
The final *Eh*ODC dimeric model along with the cofactor was showing the root-mean-square deviations (RMSD) of  $\sim 0.744$  Å with the template structure. Ramachandran plot of the model generated by PROCHECK showed 90.3 % residues in the core region, 7.8 % in allowed region, 0.6 % in generously allowed region and 0.3 % in disallowed region. The

generated models have been submitted to Protein Model database (PMDB) with PMDB id: PM0077698 (monomer) and PM0077699 (dimer).

### 3.5.6 Structure analysis of *Eh*ODC monomeric subunit

Structure of *Eh*ODC monomer subunit consists of two major domains i.e.  $\beta/\alpha$ -barrel and  $\beta$ -sheet domain which is a distinct characteristic of ODC structure (Figure 3.7). In human ODC, N-terminal starts with a  $\beta$  strand while in *Eh*ODC, it starts with an  $\alpha$ -helix. The N-terminal emerges from  $\beta$ -sheet domain and enters the barrel through a coil connecting both the domains. The barrel contains eight parallel strands each followed by a helix in the order  $\alpha_2\beta_2$ ,  $\eta_1\alpha_3\beta_3$ ,  $\alpha_4\eta_2\beta_4$ ,  $\alpha_5\beta_5$ ,  $\alpha_6\beta_6$ ,  $\alpha_7\beta_7$ ,  $\alpha_8\beta_8$  and  $\alpha_9\eta_3\beta_9$ . One important feature observed in *Eh*ODC is the presence of turns in a pattern at the N-terminal barrel secondary structures. Such pattern has been observed in ODC like antizyme inhibitor proteins that have structures similar to ODC, but do not possess decarboxylation activity (Albeck *et al.*, 2008). The sheet domain is subdivided into two clusters of sheets S1 and S2 as observed in all ODC structures. These sheets S1 and S2 remain perpendicular to each other having four helices with one turn ( $\alpha_1$ ,  $\alpha_{10}$ ,  $\alpha_{11}$ ,  $\alpha_{12}$  and  $\eta_4$ ) around it. Sheet S1 includes three parallel  $\beta$  strands ( $\downarrow\beta_{11}$ ,  $\uparrow\beta_{12}$  and  $\uparrow\beta_{13}$ ) which extends into S2 containing four parallel  $\beta$ -strands ( $\downarrow\beta_{10}$ ,  $\uparrow\beta_{14}$ ,  $\uparrow\beta_{15}$  and  $\uparrow\beta_1$ ) (Figure 3.7).

**Figure 3.7: 3D structure of *Eh*ODC monomer.** (A) Cartoon diagram of *Eh*ODC model generated using MODELLER 9v8. (B) Topological arrangement of secondary structures in *Eh*ODC monomer. Monomer of *Eh*ODC consists of two domains,  $\beta/\alpha$ -barrel shown in purple and sheet domain having sheet S1 in green, sheet S2 in blue and helices and turns in orange. The helices are presented by circles, strands are represented by triangles and the loops connecting these structures are represented as connecting lines.



### 3.5.7 Structure analysis of dimeric *Eh*ODC

In the dimeric structure of enzyme, two active site pockets rest at the dimer interface involving the interactions of residues from both the subunits.  $\beta/\alpha$ -barrel domain is the main site for cofactor PLP binding whereas residues from the sheet domain of other subunit interacts with the substrate L-ornithine to form the complete catalytic pocket for enzymatic activity. The subunits associate in a head to tail manner (Figure 3.8).

The dimeric structure is stabilized by various polar interactions present between the two subunits at the dimer interface as shown in figure 3.8. However, four major salt bridges K157-D338' and D122-R277', D338-K157' and R277-D122' are observed and these have been reported to play a vital role in the dimer formation of human, mouse, and *T. brucei* ODCs (<http://bioinformatica.isa.cnr.it/ESBRI/CGI/esequi.cgi>) (Sarakatsannis *et al.*, 2005; Kern *et al.*, 1999). These interface residues are partially hydrophilic and are highly conserved in human, mouse and *Eh*ODC.

Furthermore, the most prominent feature observed near C-terminal domain is presence of a stack of aromatic rings i.e. F371'/H296'/F305 and F305'/ H296/ F371 which is anticipated to function as an amino acid zipper (Figure 3.8). Distal amino acid residues of the zipper participate in active site pocket formation. Further, the structural analysis revealed that the close packing of dimers shields the putative N-terminal antizyme binding loop (residues 105Tyr-132Lys) as well as the C-terminal PEST like sequence because these are concealed in between the two subunits of the dimer. Thus, it is expected that the dimerization of *Eh*ODC may be responsible for protecting *Eh*ODC enzyme from proteolysis degradation.



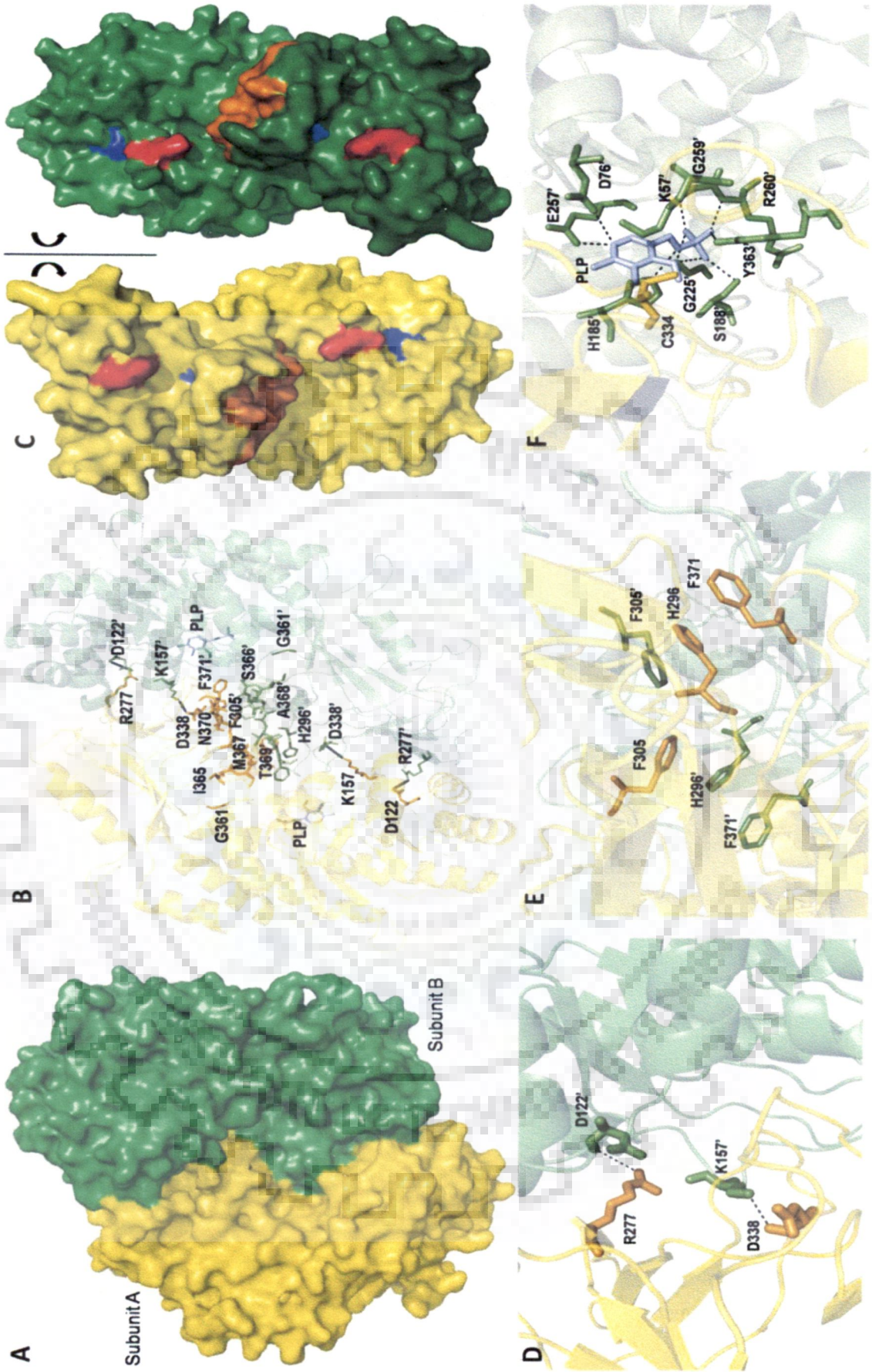




**Figure 3.8: Schematic representation of dimer interface and active site of *Eh*ODC.** (A) Subunits of the dimer are arranged in head to tail manner where subunit A and B are shown in yellow and green colors respectively. (B) The residues critically important for dimer formation are presented in sticks and overall dimeric structure is presented in cartoon. Residues from opposite monomer are marked by apostrophe (') sign. (C) Surface view of monomeric chains highlighting the residues at the dimer interface in different colors. The monomers have been separated and rotated to 90° giving clear view of interface residues. Red and blue color indicates residues involved in salt bridge formation and orange color depicts hydrophobic interactions. (D) Closer view of residues at the interface forming salt bridge. (E) Aromatic residues at the interface arranged as a stack of ring structures forming amino acids zipper. (F) Residues at the active site interacting with cofactor PLP from each monomer are presented in sticks. Residues from subunit A and B are shown in yellow and green colors respectively.

### 3.5.8 Stability of the dimeric model of *Eh*ODC

The molecular model of *Eh*ODC dimer that was generated using the crystal structure of human ODC dimer as a template was MD simulated for 8 ns in equilibration with water molecules. Evaluation of the dimer stability was made by monitoring the RMSD of C $\alpha$  of dimer which was computed against the starting structure.

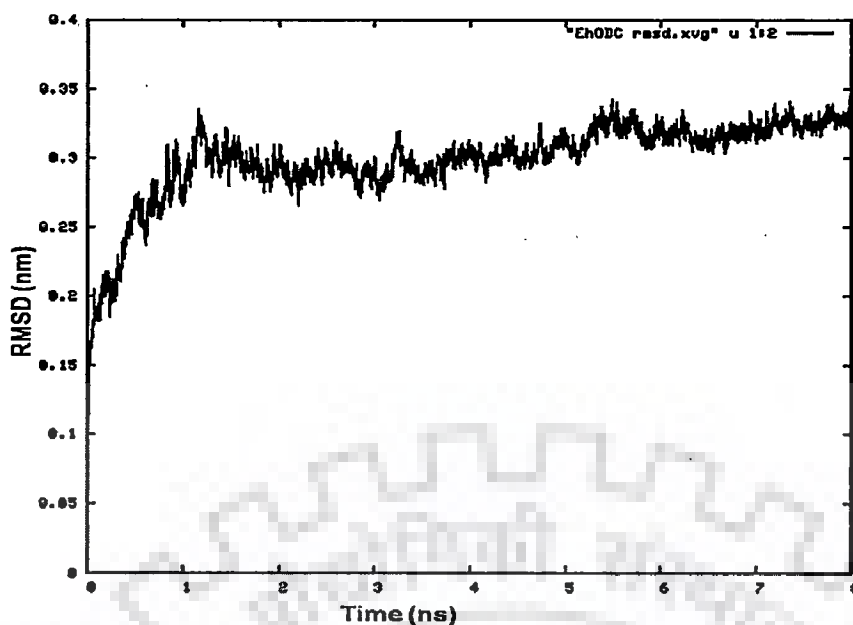


**Figure 3.9: Molecular dynamics simulation profile.** RMSD of dimeric protein after molecular dynamics simulation for 8 ns relative to pre-MD dimeric structure.

Analysis of MD trajectory of *Eh*ODC homodimer revealed that RMSD value increases to 0.327 nm in about 1.2 ns and this plateau value is stable till the end of the simulation indicating a stable conformation of the dimer (Figure 3.9).

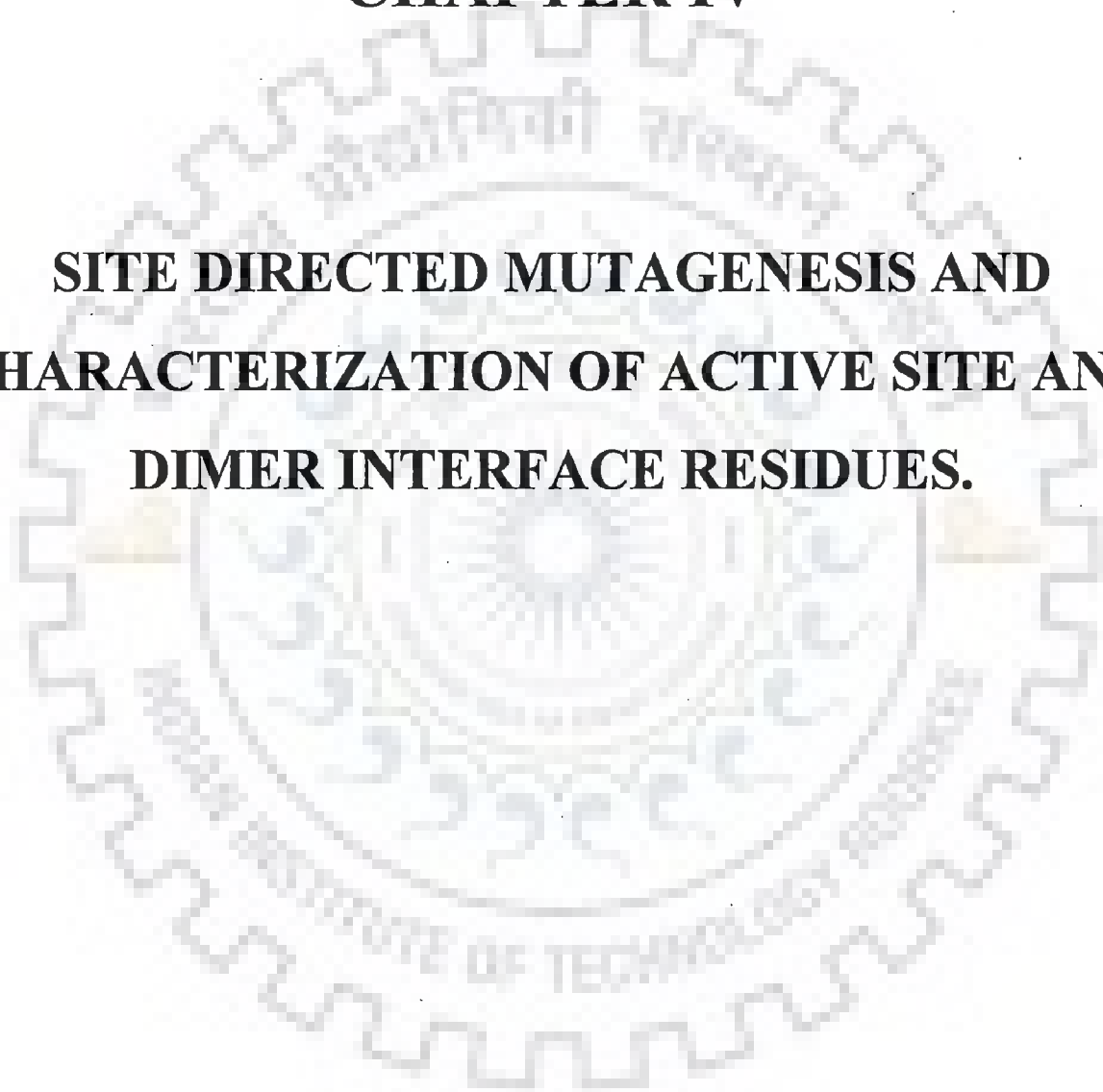
### 3.6 Conclusion

In this chapter we continued to analyze the sequence of *Eh*ODC to determine the consensus sequences and amino acid residues important for the enzymatic activity and dimer formation. To analyze the conserved residues, we compared ODC enzyme sequence from wide range of phyla which demonstrated the conservation of sequence of *Eh*ODC at the active site and dimer interface. Further to support the secondary structure data of circular dichroism spectra different serves were used and revealed that the secondary structure contents were comparable to other ODCs. 3D model was generated and analyzed for the stability by using molecular dynamics simulations. These studies also demonstrate that the sequence of *Eh*ODC is well conserved and the dimer is the stable state of *Eh*ODC protein. Further analysis was done to identify the conservation of active site residues responsible for active catalysis and dimer formation. It has already been well documented in the literature that dimer of ODC interact in head to tail manner and form two active site at the dimer interface.

This analysis revealed that, residue K57 and C334 are conserved in *Eh*ODC and responsible for cofactor and substrate binding in other ODCs. The residue K69 form Schiff base with cofactor and C360 residue of opposite monomer interact with the substrate at the active site. However, residues G361 and K157 of *Eh*ODC are corresponding to G387 and K169 of other ODCs which involve in dimer formation and salt bridge interaction at the interface. Furthermore, it was analyzed by salt bridge determination server that four major salt bridges K157-D338' and D122-R277', D338-K157' and R277-D122' present at the interface and play pivotal role in dimer formation. More interestingly, the C-terminal region of *Eh*ODC was found to be showing similarity to the C-terminal of human ODC which is reported to be PEST rich sequence responsible for 26S proteasome mediated degradation of ODC enzyme. In addition to this, DisEMBL server revealed the presence of disordered sequence at the C-terminal region of the *Eh*ODC amino acid sequence which corresponds to the C-terminal PEST sequence of human ODC.

## **CHAPTER IV**

# **SITE DIRECTED MUTAGENESIS AND CHARACTERIZATION OF ACTIVE SITE AND DIMER INTERFACE RESIDUES.**



## 4.1 Abstract

This chapter describes the site directed mutagenesis, activity and characterization of mutant *EhODC* enzymes containing substitution at the active site and dimer interface. Based on the sequence analysis and computational 3D model of *EhODC*, the residues which were identified to play critical role in the activity and dimer stability of the enzyme were mutated. These mutants were further characterized biochemically and compared with the wild type *EhODC*.

To gain insight into the functional role, the interface residues critical for dimerization and active site formation were identified and mutated. Mutation of the active site residues Lys57Ala or Cys334Ala completely abolished enzyme activity. Interestingly, partial restoration of the enzyme activity was observed when inactive Lys57Ala and Cys334Ala mutants were mixed confirming that the dimer is the active form. Furthermore, Gly361Tyr and Lys157Ala mutations at the dimer interface were found to abolish the enzyme activity and destabilize the dimer.

The following mutations were inserted at specific sites K57A, C334A, G361D, G361Y, K157A and G361Y-K157A using complimentary site specific primers. Expression, purification of each mutant enzyme was done following the same protocols given in chapter II that were used for wild type full length *EhODC*. Enzymatic activity of each mutant was compared with wild type. Characteristic properties of mutants were analyzed by various biophysical and biochemical methods. These studies revealed the role played by the residues in either activity or stability or both in cofactor and substrate binding or subunit interactions.

## 4.2 Introduction

Site directed mutagenesis is a molecular biology technique in which a mutation is created at a specific site to know its impact on gene functioning (Carpenter *et al.*, 2010). It is a powerful research technique to study protein function, identify active sites and designing novel protein in drug discovery. Single mutation in the protein sequence might show distinct physiological and biochemical properties. Functional role of conserved regions present in the protein sequence can be investigated using site-directed mutagenesis (Carpenter *et al.*, 2010; Ren *et*



*al.*, 2011). Various studies have shown that the substitution of critical residues of an enzyme with alanine results in loss of enzyme function (Rose *et al.*, 2011).

Mutation with amino acid having same characteristic properties may not disrupt the function. In contrast to this, bulky or large group at the place of simplest amino group may cause structural disruption and instability in the protein. Mutagenesis has opened the door for studying the catalytic reaction kinetics. Role of residues can be determined by comparing the efficiency and catalytic properties of the mutant and wild type enzymes (Szczepanowska *et al.*, 2012; Zhou *et al.*, 2012).

Ornithine decarboxylase of mouse and *T. brucei* has been investigated using mutagenesis of single residue that greatly reduces the catalytic activity. The role of residues at the active site and subunit interface discloses various structural properties of protein (Osterman *et al.*, 1995; Tsirka *et al.*, 1993; Lu *et al.*, 1991). ODC function as a dimer where two active sites form at the interface, each active site contains residue K69 of one subunit and residue C360' of other subunit. Mixing of purified mutant ODC with other mutants and wild type, result in exchange of subunit and heterodimer formation. This hetero-dimer formation may facilitate antizyme binding and rapid enzyme turnover (Tobias *et al.*, 1993; Osterman *et al.*, 1994; Lu *et al.*, 1991). Kinetic analysis of ODC from many parasites including *T. brucei*, *L. donovani* identified K69 as PLP attachment site and C360 as covalent adduct forming residue with L-ornithine (Tobias *et al.*, 1993; Osterman *et al.*, 1994). Alanine scanning mutagenesis of the ODC of *T. brucei* at dimer interface was targeted to determine the energetic contribution of these residues for subunit association. Out of 23 mutants, none was found to decrease the stability greater than 1kcal/mol. These data suggested the distribution of energetically interacting residues across the interface (Clackson, 1995, 1998; Myers *et al.*, 2001).

In mammalian ODC 19 conserved residues were mutated. Among all these mutations only G387 was found to play important role in dimer formation (Tobias *et al.*, 1993). The inability of mutants to associate with each other and form active dimer is solely responsible for catalytic inactiveness (Pilzi *et al.*, 1990; Ghoda *et al.*, 1989). Salt bridges in the molecular structure are proven to be involved in stabilizing interactions, regardless of whether they are buried or exposed. Strong electrostatic interactions of the salt bridging with side-chains or

charges in the protein surrounding are due to the absence of solvent masking. Spatial geometry is a major factor for determining the stability of salt bridges which in turn provide favorable positioning and stabilizes the structure anywhere in the protein interior (Sarakatsannis *et al.*, 2005). In human ODC, the K169 which is involved in the salt bridge formation with D364' of other subunit at a distance of 2.9 Å. Salt bridge ties two monomers properly so that C360' and D361' complement a functional site (Almud *et al.*, 2000).

In the previous chapter III, we identified the conserved active site and interface residues important for catalysis and stability of the dimer. In present study we created mutants of *EhODC* substituted at these particular sites and characterized each mutant to insight into the functioning of *EhODC* enzyme.

### **4.3 Materials and Methods**

#### **4.3.1 Reagents**

The *E. coli* expression vector pET 30a (Novagen) containing full-length gene of *EhODC* having N-terminal Histidine tag (6x His) followed by enterokinase cleavage site was used as template-for mutant gene amplification (Jhingran *et al.*, 2008). Oligonucleotides for site directed mutagenesis were ordered from Imperial Life Sciences (India). Restriction endonuclease *DpnI* and Phusion DNA polymerase were acquired from New England BioLab Inc.

#### **4.3.2 Methodology**

##### **4.3.2.1 Site directed mutagenesis**

The pET30a-*EhODC* plasmid containing *EhODC* gene was mutated using the QuikChange XL mutagenesis kit by following the instructions of manufacturer (Stratagene, La Jolla, CA). Mutations were introduced into the synthetic mutagenic oligonucleotide primers and were used for construction of mutant plasmids. Mutations and respective mutagenic primers are listed in table 4.1. The pET30a-*EhODC* plasmid was used as a template in the primer extension reaction for constructing the mutants. The reaction mixture used for PCR amplification contained 10 µl of 5X HF Phusion buffer supplied with the enzyme, 300 µM of dNTP mix , 6.25 pmol of each primer, 10 ng of template DNA, 2.5 U of Phusion polymerase

and water was added to make up the final volume of 50  $\mu$ l. PCR reaction was performed by subjecting the samples to 20 cycles of 30 s denaturation at 95 °C, 1 min at annealing temperature (as given in Table 4.1) and 6 min 50 s elongation at 72 °C, and finally reaction was completed by doing extension for 15 min at 72 °C. PCR products were analyzed on 1 % agarose gel electrophoresis. The parent methylated template plasmids were digested with *DpnI* restriction enzyme at 37 °C for 1 h. Digested product was directly used to transform XL-1 Blue competent cells. Transformed cells were plated on LB agar plate containing 50  $\mu$ g/ml of kanamycin and plates were incubated at 37 °C for ~16 h. The presence of the mutations in the constructed plasmids were confirmed by DNA sequencing using T7 promoter or terminator universal primers at genomic and proteomic facility of TCGA (New Delhi, India).

Mutant	Nucleotide sequence	(T <sub>m</sub> )
Lys57Ala (S)	CTTGCTTTGCTGTT <u>G</u> CATGTAATCCTGAACCTCA	53 °C
Lys57Ala (An)	TGAGG TTCAGGATTACAT <u>G</u> CAACAGCAAAGCAAG	
Cys334Ala (S)	GTATTATTTATGGACCTTCT <u>G</u> CTAATGGAAGTGATAAAG	57 °C
Cys334Ala (An)	CTTTATCACTTCCATTAG <u>C</u> AGAAGGTCCATAAATAATAC	
Gly361Asp(S)	GGTATTATTTCCCAATATGGATGCTTATAACAATTC	51 °C
Gly361Asp (An)	GAAATTGTATAAGCATCCATATTGGGAAATAATAACC	
Gly361 Tyr(S)	GGTATTATTTCCCAATATG <u>T</u> ATGCTTATAACAATTC	50°C
Gly361Tyr (An)	GAAATTGTATAAGCAT <u>A</u> CATATTGGGAAATAATAACC	
Lys157Ala (S)	ATGTATTTGGAGAG <u>G</u> CATTTGGACTTCATGATGA	58 °C
Lys157Ala (An)	TCATCATGAAGTCCAAAT <u>G</u> CCTCTCCAAATACAT	

**Table 4.1: Sequences of mutagenic primers and annealing temperatures used for PCR amplification of mutant plasmids. Mutated nucleotides are underlined. S: sense and An: antisense.**

#### **4.3.2.2 Purification, activity and size exclusion chromatography of mutants *Eh*ODC protein**

All the mutants obtained by site directed mutagenesis were purified using the standard protocol for wild *Eh*ODC purification as mentioned previously in chapter II. The activity of each mutant was done according to the colorimetric assay and analysis on gel filtration column using same buffer composition as for wild type *Eh*ODC.

#### **4.4 Results and discussion**

The critical residues responsible for dimerization and catalytic activity of *Eh*ODC were identified on the basis of multiple sequence alignment of *Eh*ODC with human mouse and *T. brucei* ODC (Figure 3.3). The sequence alignment of *Eh*ODC showed that many conserved domains are present which play important role in active site formation in other ODC. The K57 was found to be present in the conserved domain AVKCN and critical for cofactor PLP binding to the active site during catalysis. Similarly C334 was found to be present in the conserved domain corresponding to the C360 of human ODC which is responsible for substrate binding at the active site pocket.

In addition to this, residues which were found to be responsible for dimer formation in human and mouse ODC were also found to be conserved in the *Eh*ODC sequence. The residue G387 of mouse which is responsible for dimer formation was conserved in *Eh*ODC and sequenced as G361. K169 of mouse and human ODC involved in salt bridge interactions with opposite monomer were also identical and corresponding to the residue K157 of *Eh*ODC.

##### **4.4.1 Site directed mutagenesis**

The pET30a-*Eh*ODC plasmid was used as a template in the primer extension reaction for constructing the mutants. Oligonucleotide site directed mutagenesis primers were designed on the basis of nucleotide sequence of *Eh*ODC (Table 4.1, Figure 4.1, 4.2).

atgaaacaaacatctctagaagtaaagaattcgctcttaatcttatcagccaatttgaa  
M K Q T S L E V K E F A L N L I S Q F E  
ccagaaaaccaaccacttggtttttggatttttgatactgaagggttgaaaaagcagtt  
P E N Q P L G F W I F D T E G V E K A V  
gaaagatggaaaaagaatatgccaacagtttagaccttgcttttgctgtttaaattgtaattcct  
E R W K K N M P T V R P C F A V K C N P  
gaacctcatttagttaagcttttaggtgaattaggatgtgggttttgattgtgcttcattg  
E P H L V K L L G E L G C G F D C A S L  
aatgaaataaaagaagtatttagaccttggtttaaattcctgaagacattacatattcacia  
N E I K E V L D L G F N P E D I T Y S Q  
actttcaaaccatataatcaattaattgaagcaagtcatttaggaattaatcatacaatt  
T F K P Y N Q L I E A S H L G I N H T I  
gtagattcaattgatgaagttcaaaaaattgcaaaaatgacacaaaaatgggtataatg  
V D S I D E V Q K I A K Y A P K M G I M  
ataagaattatggaaaatgatacatcagcaggtcatgtatttgagagaaatttgactt  
I R I M E N D T S A G H V F G E K F G L  
catgatgatgaggttgaaatagttttaaagaaattaaagacaaaggattaaatttagat  
H D D E V E I V L K E I K D K G L N L D  
ggagtccattttcatggttggaagtgattctcataatagtgaagttttactaaagcatta  
G V H F H V G S D S H N S E V F T K A L  
actaaagcaagaacactggttacatttagcagaacaatttggaatgaaaccatattttaatt  
T K A R N T V T L A E Q F G M K P Y L I  
gatattggaggaggatttagtcaagttgctccatttgagaatttgacagcaacaattgaa  
D I G G G F S Q V A P F E E F A A T I E  
aaaacaataaaagaatttagagtttccagaagaacaagatttattgcagaacctggaaga  
K T I K E L E F P E R T R F I A E P G R  
tatatggcatctaattgcatttcatcttggttagttctttacatggtaaaagagtaagaata  
Y M A S N A F H L V S S L H G K R V R I  
cagaatggaaagaacaaattgaaataacttcaggtgatggtttacatggaagttttgga  
Q N G K K Q I E Y T S G D G L H G S F G  
tggtgtattttggtttgaaaaacaaaaagttgtgaaatgtattacacaaaaagttaatgaa  
C C I W F E K Q K S C E C I T Q K V N E  
aataactaaaatgtatgaaagtattatttatggaccttcttgtaatggaagtgataaagta  
N T K M Y E S I I Y G P S C N G S D K V  
gcaactcaagaactaccagaaatggagccagggaaagattggttattatttcccaatag  
A T Q E L P E M E P G K D W L L F P N M  
ggtgcttatacaattttctatggcaactaactttaatggatttgaagaaagaatcatgtc  
G A Y T I S M A T N F N G F E E R N H V  
atttatactttaccattaaagtcaacaaaaattattcaaattccctaagtcaattgaaatg  
I Y T L P L K S T K I I Q I P K S I E C  
aactcagttccatcattaaatgggtattccacactatgcttaa  
N S V P S L N G I P H Y A -

**Figure 4.1:** Amino acid sequence with nucleotide codons. Residues in red font are showing the corresponding mutation site in the *EhODC* protein sequence.



#### 4.4.2 Plasmid map for mutant *EhODC*

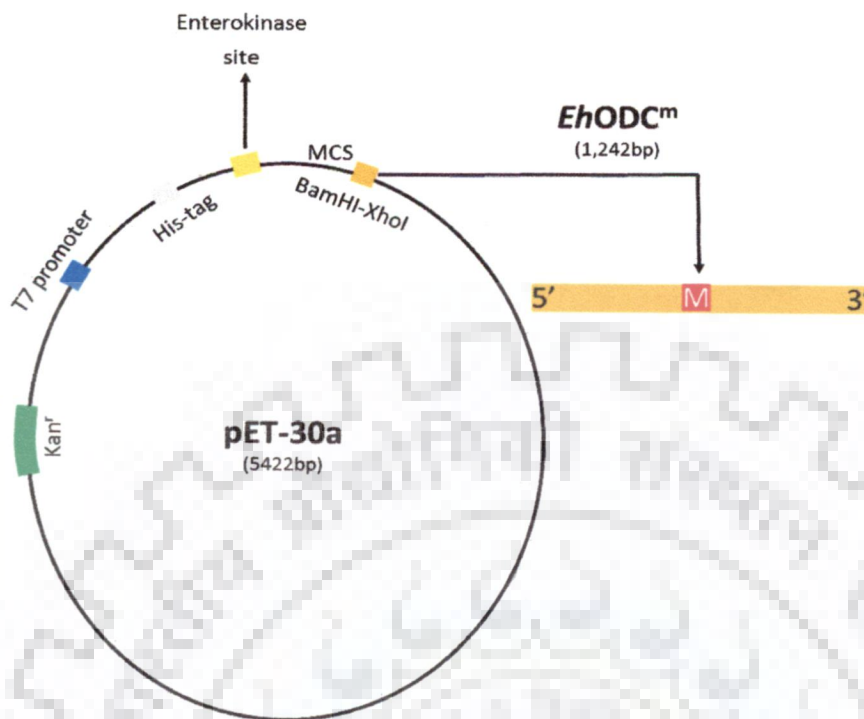


**Figure 4.2:** Schematic representation of the map of vector pET30a-with *EhODC*. The colored tag represents the specific restriction sites, insert gene and promoter region. The insert gene of *EhODC* with mutated site *EhODC<sup>m</sup>* in the sequence has been represented with red color.

#### 4.4.3 Analysis of mutated plasmid

The amplified PCR products were analyzed on 1 % agarose gel.

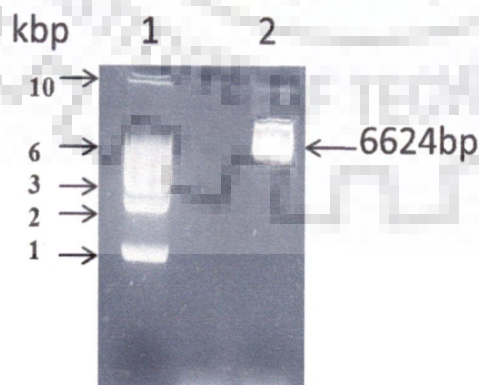


**Figure 4.3:** PCR product containing amplified mutant plasmid. Lane 1: DNA ladder (1kb); Lane 2: PCR product containing mutant *EhODC*.

The presence of the mutations in the constructed plasmids were confirmed by DNA sequencing using T7 promoter or terminator universal primers at genomic and proteomic facility of TCGA (New Delhi, India) (Figure 4.1, 4.2, 4.3).

#### 4.4.4 Strategy used for site directed mutagenesis of *Eh*ODC

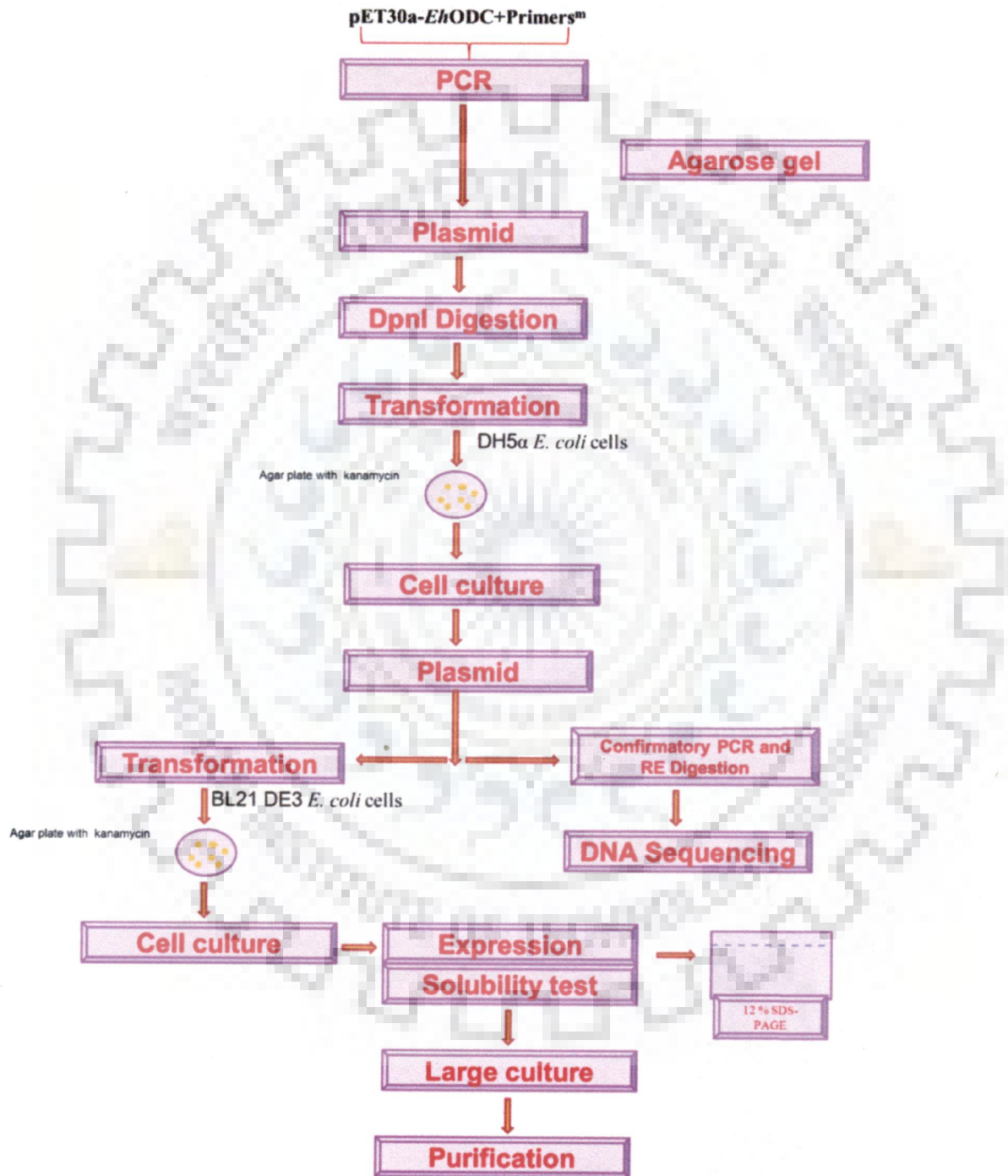
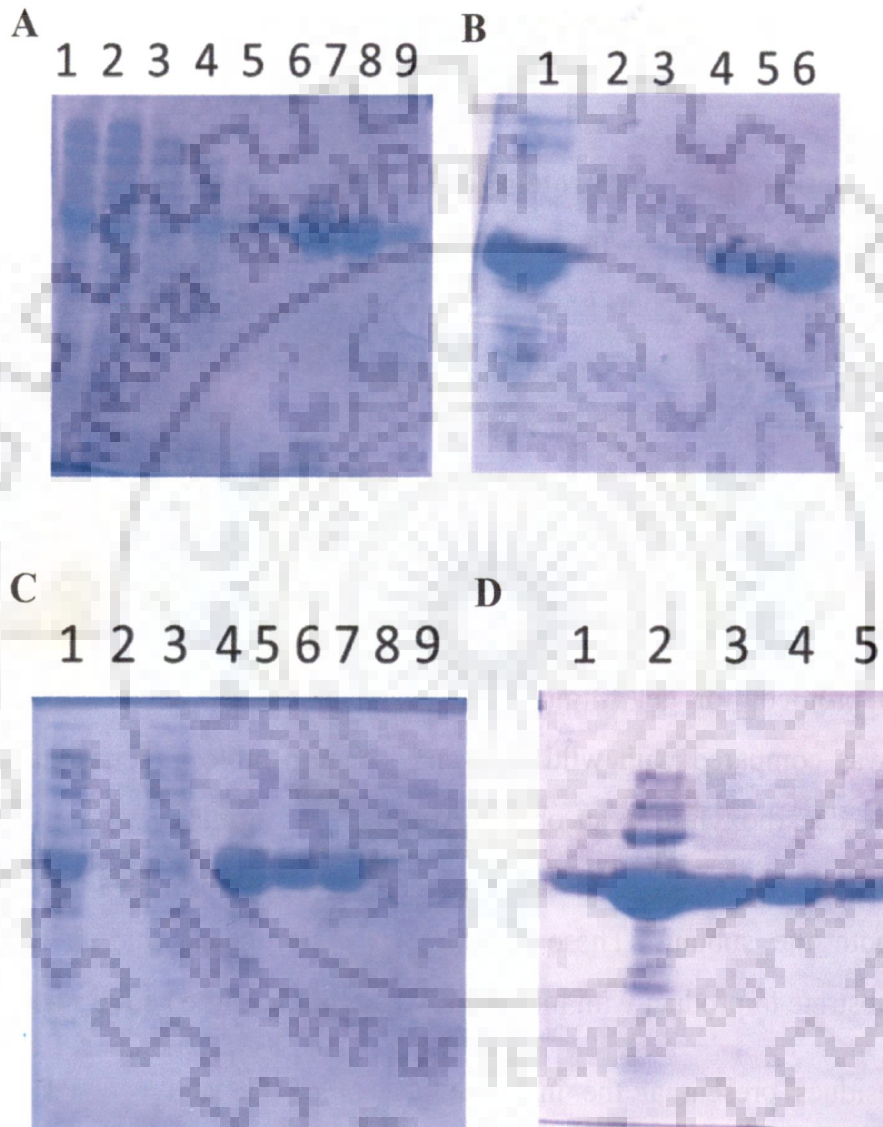


Figure 4.4: Schematic representation of strategy used for creating mutant *Eh*ODC.

#### 4.4.5 Purification, activity and size exclusion chromatography of *Eh*ODC mutants

All the mutants obtained by site directed mutagenesis were purified using affinity chromatography. Strategy used for cloning and purification of mutant *Eh*ODCs has been represented in figure 4.4. Purification profiles of mutants involving substitutions at active site and dimer interface residues are given in figure 4.5





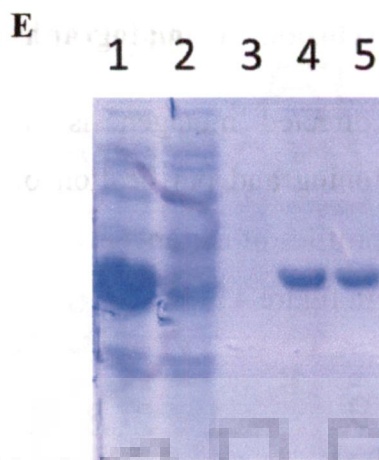


**Figure 4.5: Purification of mutant proteins of *Eh*ODC.** **A) Mutant K57A:** Lane 1: Pellet; Lane 2: Supernatant; Lane 3: Flow-through; Lane 4: Washing; Lane 5-9: Purified fractions. **B) Mutant C334A:** Lane 1: Pellet; Lane 2: Supernatant; Lane 3: Flow-through; Lane 4-6: Purified fractions. **C) Mutant K157A:** Lane 1: Pellet; Lane 2: Supernatant; Lane 3: Flow-through; Lane 4: Washing; Lane 5-9: Purified fractions. **D) Mutant G334D:** Lane 1: Pellet; Lane 2: Supernatant; Lane 3: Flow-through; Lane 4-5: Purified fractions. **E) Mutant G334Y:** Lane 1: Pellet; Lane 2: Supernatant; Lane 3: Flow-through; Lane 4-5: Purified fractions.

Standard protocol for gel filtration was carried out using superdex 200. Elution chromatogram was compared with wild type and standard molecular weight marker. The enzyme ornithine decarboxylase is an obligate homodimer forming two active sites at the dimer interface. Each active site form a pocket to PLP and substrate and specific residues interact from both the subunit. These residues play significant role in catalyzing the conversion of substrate to product with intermediate formation at the active site.

Some residues present at the interface also share the active site known for the stabilization of dimer by forming weak/strong inter-subunit interactions. These residues have been identified in many ODCs and sequence alignment revealed the conservation of such residues in *Eh*ODC. Mutation at these sites has unfolded the actual function of these residues and their importance in catalysis. In this study the stability and functional aspects of some residues have been investigated to further elucidate the efficacy and impact of such mutation on *Eh*ODC catalytic efficiency.

#### 4.4.6 Characterization of active site mutant *Eh*ODC

Molecular model of the *Eh*ODC dimer evidently showed that the conserved catalytic residues from both monomeric subunits form two equivalent active sites at the dimer interface (Figure 3.3, 3.8). Consequently, it can be hypothesized that the dimeric state of *Eh*ODC enzyme is the active form. Therefore, 3D structure based site-directed mutagenesis approach was used to examine the functional role of *Eh*ODC dimerization. Conserved residues of the catalytic pocket present at the dimer interface and also the conserved residues of the dimerization interface were mutated.

The conserved catalytic residues Lys57 and Cys334 present in the active site were selected for mutational studies, because the structure model as well as the sequence alignment of *Eh*ODC with human ODC revealed that Lys57 of one subunit (Lys69 in human) and Cys334 of other subunit (Cys360 in human) jointly play critical role in catalysis and substrate specificity in a single active site pocket (Figure 3.3, 3.8) (Lu *et al.*, 1991; Poulin *et al.*, 1992; Jackson *et al.*, 2000). The residue Lys57 plays crucial role in PLP binding by forming Schiff base to aldehyde group with its  $-NH_2$  group, thus serves as a proton donor during catalysis (Osterman *et al.*, 1999). The interaction of Lys57 with PLP governs its position and correct orientation at the active site. Gel filtration analysis indicates that K57A mutant exists in the dimeric form indicating that this mutation does not disrupt dimerization. However, when enzyme activity was examined, K57A mutation was found to abolish enzyme activity with ~2 % activity as compared to the wild type (Figure 4.6).

Moreover, Cys residue in the same active site from other subunit is involved in substrate binding and stabilizes the quinonoid intermediate by using its carbonyl group (Poulin *et al.*, 1992; Jackson *et al.*, 2003). This residue is crucial for decarboxylation of L-ornithine and release of decarboxylated product towards the interface to exit from active site. The C334A mutant was also found to be a dimer indicating that mutation does not affect dimerization. However, C334A was also found to be inactive with ~2 % enzymatic activity as compared to wild type (Figure 4.6).



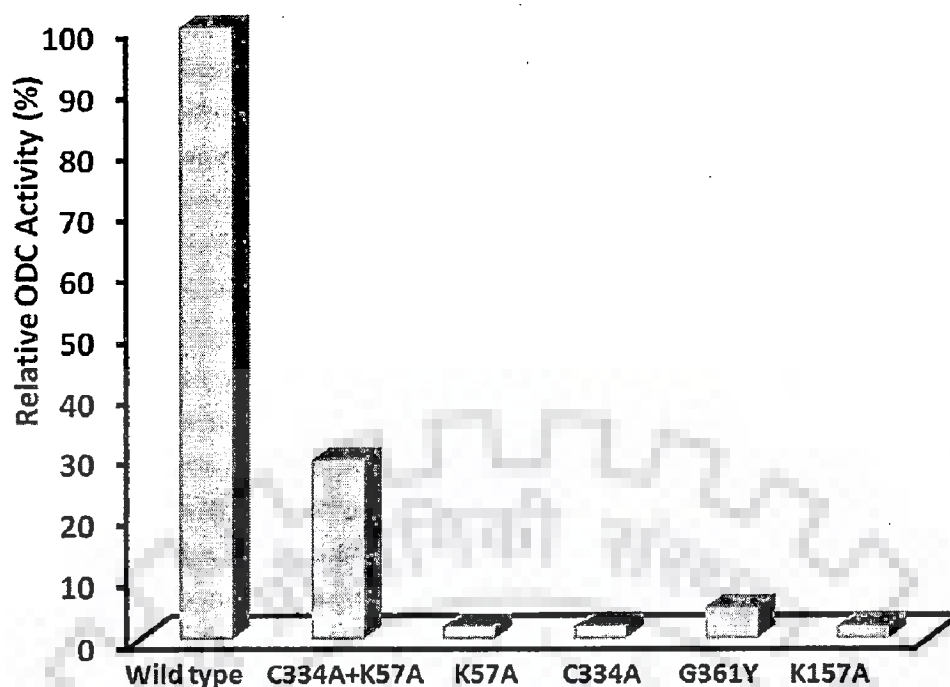


**Figure 4.6: Enzyme activity of wild type *Eh*ODC and its mutants.** Enzymatic activity of *Eh*ODC mutants relative to the activity of the wild-type enzyme. Cys334Ala, Lys57Ala Gly361Tyr and Lys157Ala are inactive. Cys334Ala and Lys57Ala mutants were mixed in 1:1 ratio and the mixture shows recovery of approximately 29 % of the wild-type enzyme activity. The plot represents the average of three measurements.

Interestingly, when the two mutant proteins K57A and C334A were mixed in equal concentration, the enzyme activity was partially regained having 29 % activity as compared to wild type (Figure 4.6). The recovery of enzyme activity on mixing these two mutants is only possible when the two mutants associate to form a heterodimer. The formation of heterodimer is anticipated to restore one of the two active sites at the dimer interface as depicted in figure 4.7. Three types of enzyme populations are expected in mutant mixture of i.e. homodimers of K57A, homodimers of C334A and heterodimers of K57A and C334A. Therefore, restoration of approximately one-third of the wild-type enzyme activity in the mixture of mutants is due to the dimerization of K57A and C334A which possesses a catalytically active site pocket at one end of the heterodimer. These mutagenesis results evidently demonstrate that dimeric state is the functional form of ODC enzyme in *E. histolytica* (Figure 4.7).

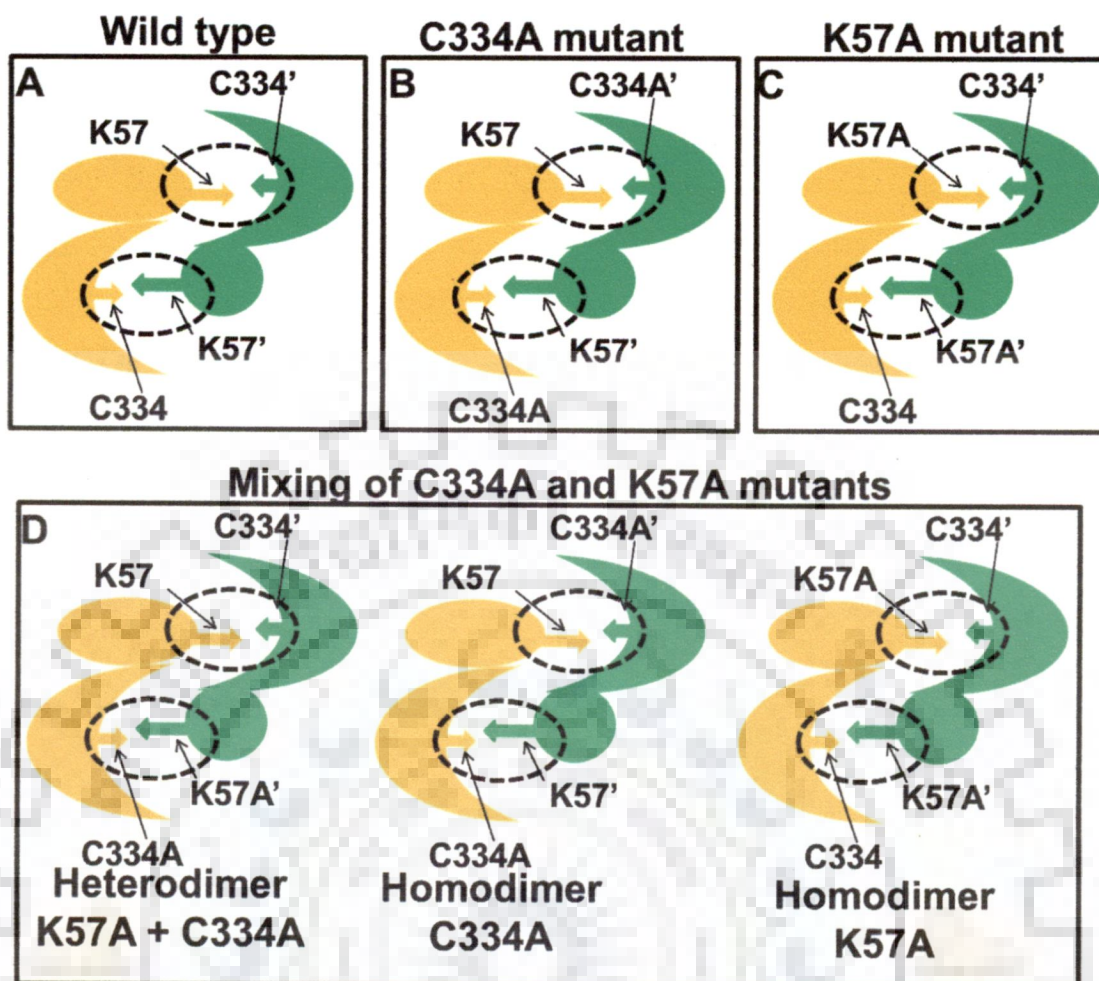


**Figure 4.7:** Schematic representation of homodimers and heterodimers in the mixture of *EhODC* Cys334Ala and Lys57Ala mutants. (A-C) Homodimer formation of wild-type and mutants of *EhODC* in individual solution. (D) Possible combinations of *EhODC* monomeric subunits in the mixture of Cys334Ala and Lys57Ala mutants forming heterodimer and homodimers.

#### 4.4.7 Characterization of interface mutant *EhODC*

In mouse, 19 conserved residues at the dimer interface were mutated to identify the key residues responsible for dimerization (Tobias *et al.*, 1993). It was noted that substitution of conserved Gly387 to any amino acid except alanine abolished the enzymatic activity. The same result is also observed in case of *Lactobacillus* and hamster, where the corresponding glycine was mutated to any bulky amino acid resulted in inactivation of the enzyme (Gopal, 1997; Pilz *et al.*, 1990). Crystal structure of mouse ODC revealed that this mutation could

position  $\beta/\alpha$ -barrel at a different angle to  $\beta$ -sheet so that in the mutant protein these domains have different orientations in the dimer compared to the wild type which makes the enzyme inactive (Kern *et al.*, 1999). In the present study, mutation at Gly361 was done by substitution of Gly361 to Asp as in mouse ODC. Results obtained with *Eh*ODC-Gly361asp mutant were not favoring the properties of mouse ODC which resulted in disruption of dimer. Elution chromatogram was compared with wild type showing a peak at ~71.4 ml which is of molecular weight (~90 kDa) equivalent to the dimer (Figure 4.8). This observation revealed that mutation of Gly361Asp unable disrupts the dimer to monomer.

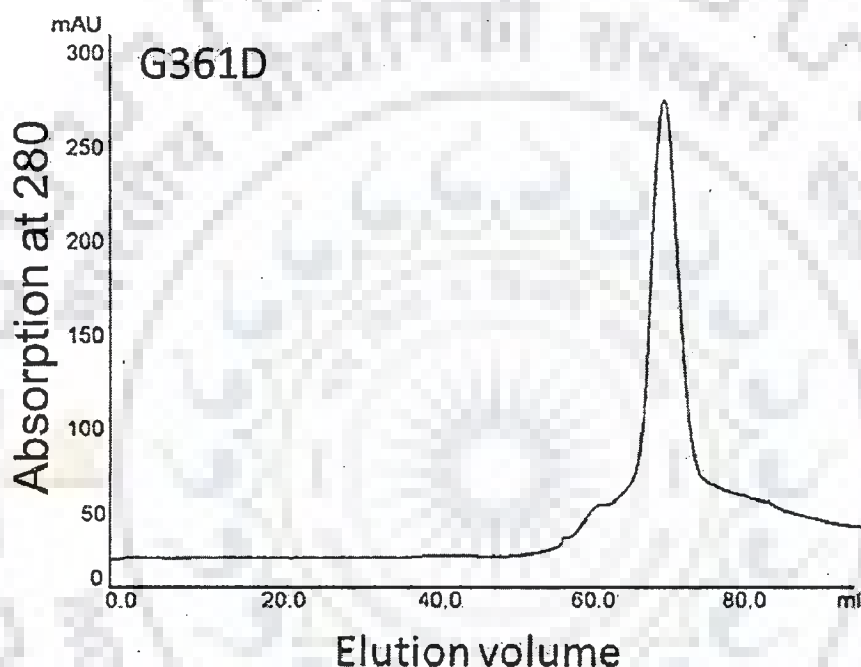


**Figure 4.8: Gel filtration analysis of interface residue mutants.** Gel-filtration chromatogram of Gly361Asp mutant showing monomer peak corresponding the wild type *Eh*ODC (~90 kDa).

Interestingly, when *Eh*ODC Gly361 (Gly387 in mouse) was mutated to bulky Tyr residue and its influence on dimerization was assessed by gel filtration analysis. The chromatogram showed partial destabilization of dimer with two distinct peaks corresponding to the molecular weight of monomer and dimer (Figure 4.9). The G221Try mutation was observed in case of *Lactobacillus* 30aODC. The examination of enzyme activity showed that the Gly361Tyr mutant is functionally inactive (Figure 4.6). These results suggest that Gly361 in

*Eh*ODC is not involved in direct interaction between the two subunits of dimer, however it plays an indirect role in the dimer stability through long range molecular interactions.

Additionally, in the structure model and sequence alignment analysis, Lys157 of *Eh*ODC is conserved and forms a salt bridge with Asp338' connecting the two monomeric subunits. At the same position in the crystal structure of human ODC, Lys169 of one subunit is involved in the salt bridge formation with Asp364' of other subunit near the active site (Grishin *et al.*, 1999, Kern *et al.*, 1999). Thus, Lys157 of *Eh*ODC plays a critical role in spatial arrangement of active site residues from both the subunits in a proper orientation along with its role in dimer formation. Mutation of Lys157 to Ala (K157A) leads to inactivation of enzyme (Figure 4.6). Moreover, partial disruption of the dimer as compared to the wild type protein was observed for K157A mutant, because a peak corresponding to the monomeric state of *Eh*ODC along with the dimer peak was observed in the gel filtration chromatogram (Figure 4.9). These results suggest that Lys157 plays a direct role in dimerization that eventually leads to the active site formation.

Furthermore, a double mutant of *Eh*ODC having two mutations i.e. G361Y and K157A was expressed in *E. coli*. The protein was over-expressed using high IPTG concentration of ~2 M for induction. This double mutant was found to be unstable and susceptible to protease degradation during purification. Therefore, it could not be purified for further analysis. The instability of the double mutant G361Y and K157A could be due the dimer disruption making the protein insoluble as well as proteolytically unstable.

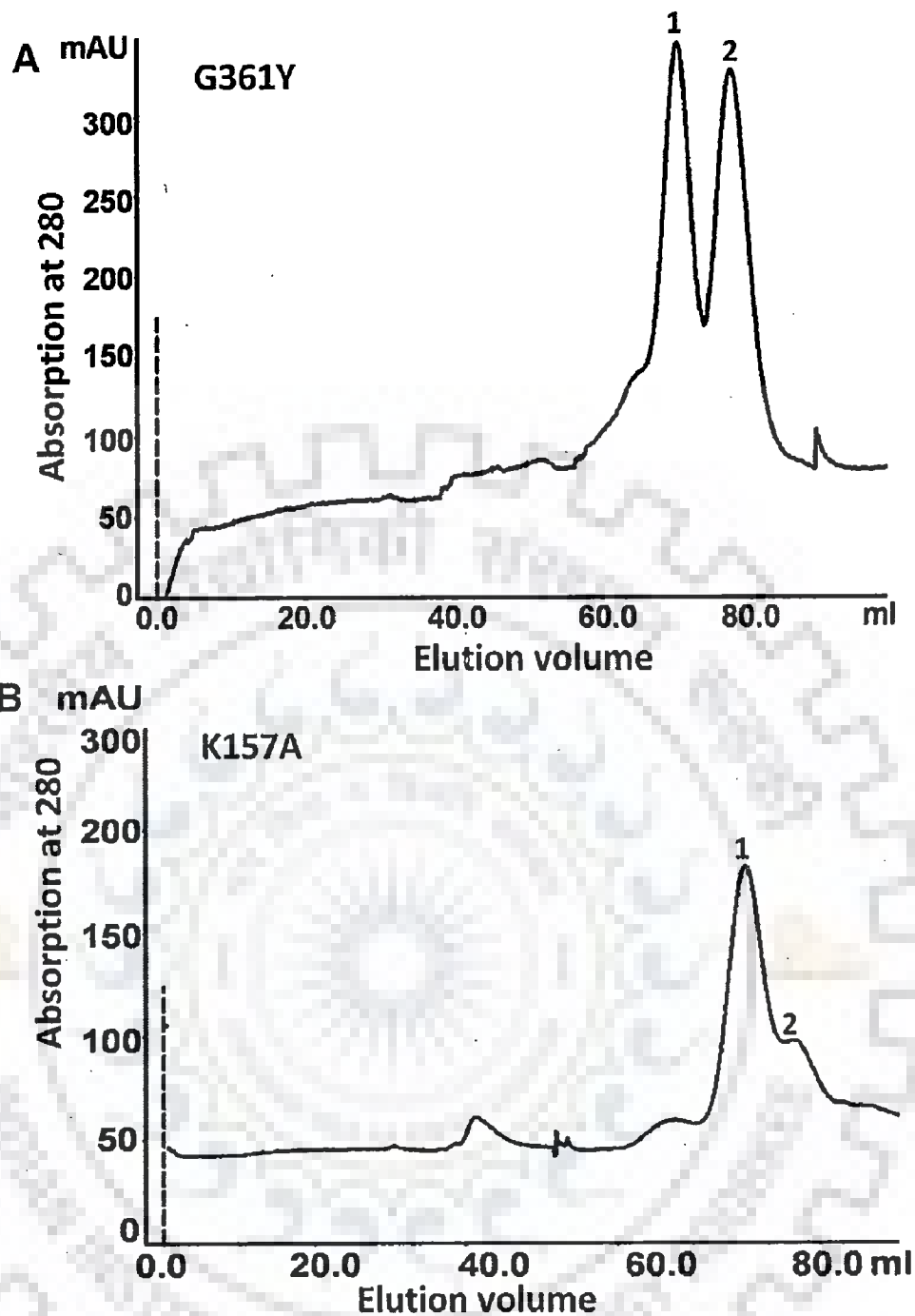


**Figure 4.9: Gel filtration analysis of interface residue mutants.** A) Gel-filtration chromatogram of Gly361Tyr mutant showing partial dissociation of dimers into monomers; B) Gel-filtration chromatogram of Lys157Ala mutant showing partial dimeric disruption.

#### 4.5 Conclusion

In this study, the role of dimerization with respect to functionality was investigated by comparative structure modeling and mutational studies. Molecular structure reveals a sharp complementary arrangement of interface and active site residues to support the proper spatial

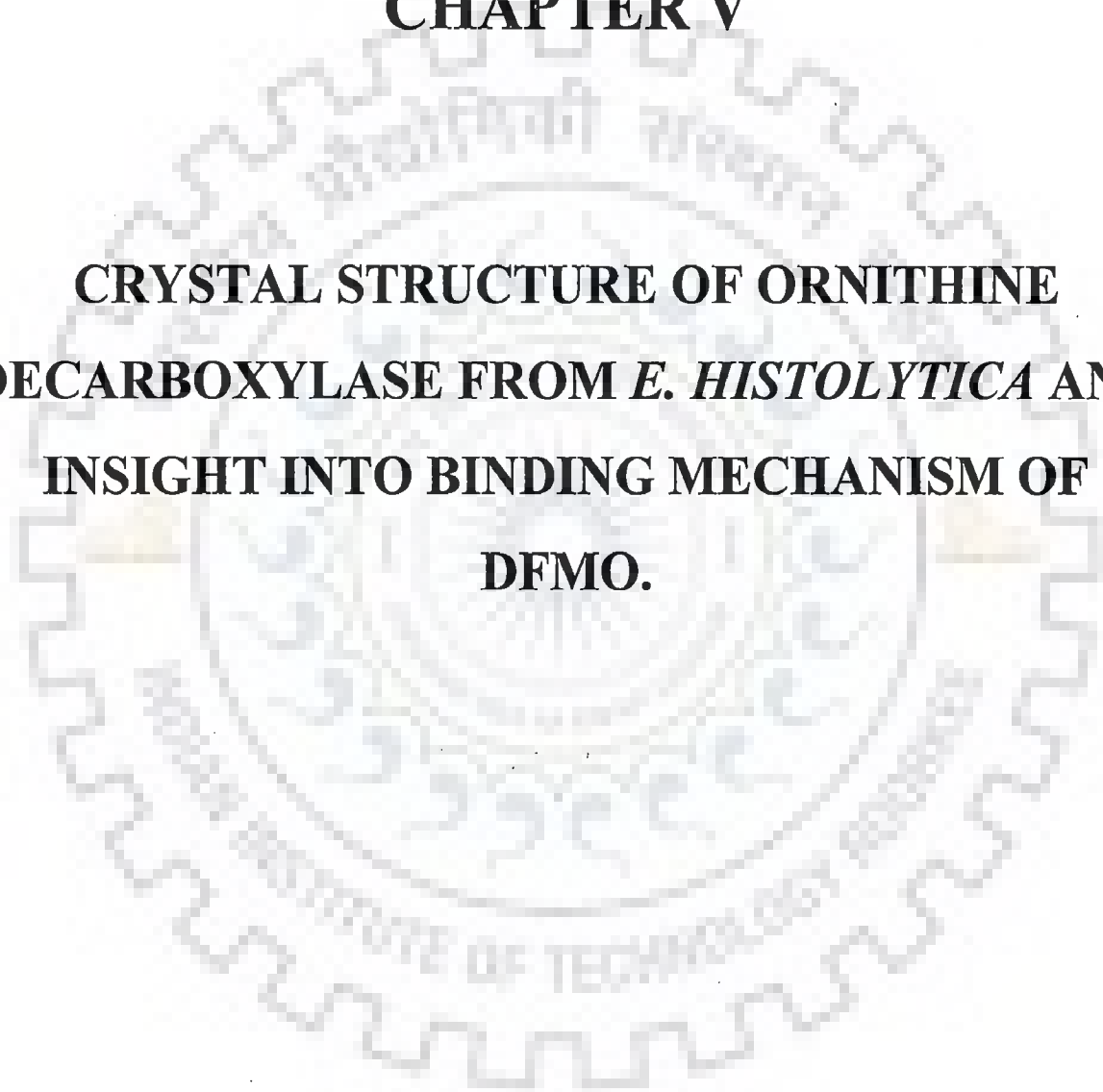


arrangement. Thus, it contributes both the subunits in generation of two equivalent active sites. The partial recovery of the enzyme activity on mixing the two mutants, C334A and K57A which were individually inactive, shows that dimer is the active form of *EhODC*. Additionally, a single substitution at G361Y resulted in partial destabilization of the dimer and renders the enzyme inactive. Further, K157A mutation expected to disrupt a salt bridge K157-D338' between two subunits didn't completely disrupt the dimer but inactivates the enzyme. These results signify that various long and short range forces play a crucial role in the dimerization and the geometry of the dimer interface is ideal for enzyme activity.



## **CHAPTER V**

# **CRYSTAL STRUCTURE OF ORNITHINE DECARBOXYLASE FROM *E. HISTOLYTICA* AND INSIGHT INTO BINDING MECHANISM OF DFMO.**



## 5.1 Abstract

In this chapter, crystal structure of DFMO resistant ornithine decarboxylase (at resolution 2.8Å) from *E. histolytica* is described. The flexible 15 residues from the C-terminal of the *Eh*ODC were truncated to decrease the conformational heterogeneity and to facilitate crystallization. Purified C-terminal truncated protein was found to be as active as full-length wild type *Eh*ODC.

The ODC of *E. histolytica* has attracted attention as it is reported to be the only enzyme of polyamine biosynthetic pathway present in this protozoan. The ODC enzyme of polyamine biosynthetic pathway is validated target for several protozoan diseases. In addition to this, *Eh*ODC has been reported to be insensitive to  $\alpha$ -Difluoromethylornithine (DFMO), a potent and specific irreversible inhibitor of ODC.

Therefore, realizing the importance of structure based drug design. We determined the crystal structure of *Eh*ODC at resolution 2.8 Å. Structure was solved by molecular replacement method. The enzyme forms orthorhombic crystal exhibiting  $P2_12_12_1$  symmetry with unit cell parameters  $a = 76.66$  Å,  $b = 119.28$  Å,  $c = 179.28$  Å. Interestingly, structure analysis of *Eh*ODC revealed that the active site has amino acid substitutions in the substrate binding pocket, making it unable to interact with DFMO. However, these substitutions still allow the binding of substrate and the enzyme is active. Furthermore, substitutions were not only limited to bring resistance, but sequence analysis showed similar substitutions in antizyme inhibitor (AZI), a paralogue of ODC.

Structure, sequence and phylogenetic studies of *Eh*ODC revealed the structural basis for molecular evolutionary adaptation that make it DFMO resistant as well as indicates its evolutionary relationship with AZI, the inactive ODC paralogue.

## 5.2 Introduction

Polyamine biosynthetic pathway is essential for growth and proliferation of cell. This pathway is tightly regulated at first rate limiting step which results in the formation of diamine putrescine. The reaction is catalyzed by the enzyme ornithine decarboxylase (ODC).

Regulation of ODC not only confined to transcriptional level but also to translational and post translational levels. In addition to this, C-terminal domain of ODC possesses an intrinsic signal responsible for its rapid intracellular degradation (Rosenberg-Hasson *et al.*, 1991; Ghoda *et al.*, 1989). Deletion of this domain provides stability to the ODC (Rosenberg-Hasson *et al.*, 1991). Similar stability was observed in mouse due to the truncation of 37 C-terminal amino acids (Ghoda *et al.*, 1989). Sequence analysis of human ODC suggested the presence of basal degradation element that is required for antizyme-mediated proteolysis at the C-terminus. These elements have been proposed to be solvent accessible rather than to be buried in the core of the homodimeric protein (Almud *et al.*, 2000).

Antizyme is the most critical regulatory protein of polyamine synthesis which acts as a non-competitive inhibitor of ODC and results in its sequestration (Fong *et al.*, 1976; Heller *et al.*, 1976; Coffino, 2001; Murakami *et al.*, 1986). It has been detected in wide variety of organisms from higher eukaryotes such as rat, human to protists and eubacteria (Kyriakidis *et al.*, 1978, 1983; Pantazaki *et al.*, 1999; Ivanov *et al.*, 1998, 2000; Tosaka *et al.*, 2000). The antizyme is 26kDa protein containing 227 amino acids (in mouse). It is a down-regulator of ODC that interacts with the monomeric form of ODC and results in the formation of AZ:ODC heterodimer (Murakami *et al.*, 1992; Takeuchi *et al.*, 2007). The carboxy-terminal 121-227 is responsible for binding to ODC and 69-112 residues mediate the destabilization process in 26S proteasome mediated proteolysis (Chattopadhyay *et al.*, 2001; Ichiba *et al.*, 1994).

Sequence and structure-function studies revealed the arise of a new homologue of ODC which lost its ability of decarboxylation due to mutation of critical residues in active site (Murakami *et al.*, 1996, 2009; Mangold, 2006; Kahana, 2009). These homologues hold the ability to regulate various life processes in addition to protect ODC degradation due to antizyme (Mangold *et al.*, 2008). The homologues of ODC are designated as antizyme inhibitors (AZI) due to their unique property of binding to antizyme (Murakami *et al.*, 1996, 2009). However, binding of AZI to antizyme is stronger as compared to ODC which results in sequestration of antizyme and elevated level of ODC (Fujita *et al.*, 1982; Nilsson *et al.*, 2000; Cohavi *et al.*, 2009; Keren-Paz *et al.*, 2006).

Binding of ODC and AZI to the antizyme is mostly reported at N-terminal region from 117 to 140 residues. This sequence is highly conserved in both antizyme and ODC except residues 125, 126, 133, 135 and 140 (numbering according to human ODC). The AZIs have lost the decarboxylation activity due to some significant changes in the sequence, especially at the active site. Inability of cofactor (PLP) binding and decarboxylation of ornithine can be attributed to substitution of cofactor and substrate binding residues. X-ray structures of large number of eukaryotic and prokaryotic ODC (Lee *et al.*, 2007) have been solved. Crystal structures of ODC available till date are from *Trypanosome brucei*, *Homo sapiens*, *Lactobacillus 30a*, *Mus musculus*, and *Vibrio vulnificus* (Almud *et al.*, 2000; Kern *et al.*, 1999; Wang *et al.*, 1995; Grishin *et al.*, 1999; Dufe *et al.*, 2007). These eukaryotic organisms share a common fold structure and have overall structural similarity to alanine racemas family (Grishin *et al.*, 1995).

The crystal structure of *Tb*ODC was determined at 2.5 Å in space group P2<sub>1</sub> (a = 67.8 Å, b = 88.5 Å, c = 150.4 Å, β = 90.03°). The final model contained 4 monomers in asymmetric unit. In general, this enzyme is an obligate homodimer and monomer is composed of β/α-barrel domain and β-sheet domain. Two identical active sites are formed at the interface between N-terminal domain of one and C-terminal domain of other subunit (Grishin *et al.*, 1999). In addition, many other residues present surrounding to the active site pocket play role in active catalysis by directly or indirectly interacting with substrate or product.

Many conserved domain in the sequence contain residues important for interaction with cofactor and substrate. Importantly, D88, A111, R154, H197, S200, G235-F238, E274, G276-Y278, Y323, Y331 and Y389 residues interact with PLP in human ODC. The δ-amino group of both substrate and product (e.g. D-ornithine, DFMO, and putrescine) interacts with D361 of one monomer and D332' of other monomer. These two residues are present at the active site pocket and interact directly with substrate (Grishin *et al.*, 1999; Osterman *et al.*, 1995, 1997, 1999; Brooks *et al.*, 1997; Swanson *et al.*, 1998). In the present studies, we analyzed the structural changes and critical substitutions in the active site pocket of *Eh*ODC which render it insensitive towards DFMO and allow us to characterize it as a bridge between the functional ODC and nonfunctional antizyme inhibitor.



## 5.3 Materials and methods

### 5.3.1 Reagents

Restriction enzymes *NdeI*, *XhoI*, T4-DNA ligase and phusion polymerase were purchased from NEB. Primers were ordered from Integrated DNA Technology. HisTrap HP Ni Sepharose column and Hiload 16/60 Superdex 200 pg size exclusion column were obtained from GE healthcare. For crystallization, Crystal screens were obtained from Hampton Research (Hampton Research Inc. Aliso Viejo, CA). The plasmid pET30 (a) containing full length of *EhODC* was taken as template for sub-cloning (Jhingran *et al.*, 2008). Docking studies were performed using Glide and AutoDock 4.0 (<http://autodock.scrip.t.edu/>).

### 5.3.2 Methodology

#### 5.3.2.1 Cloning of C-terminal truncated *EhODC*

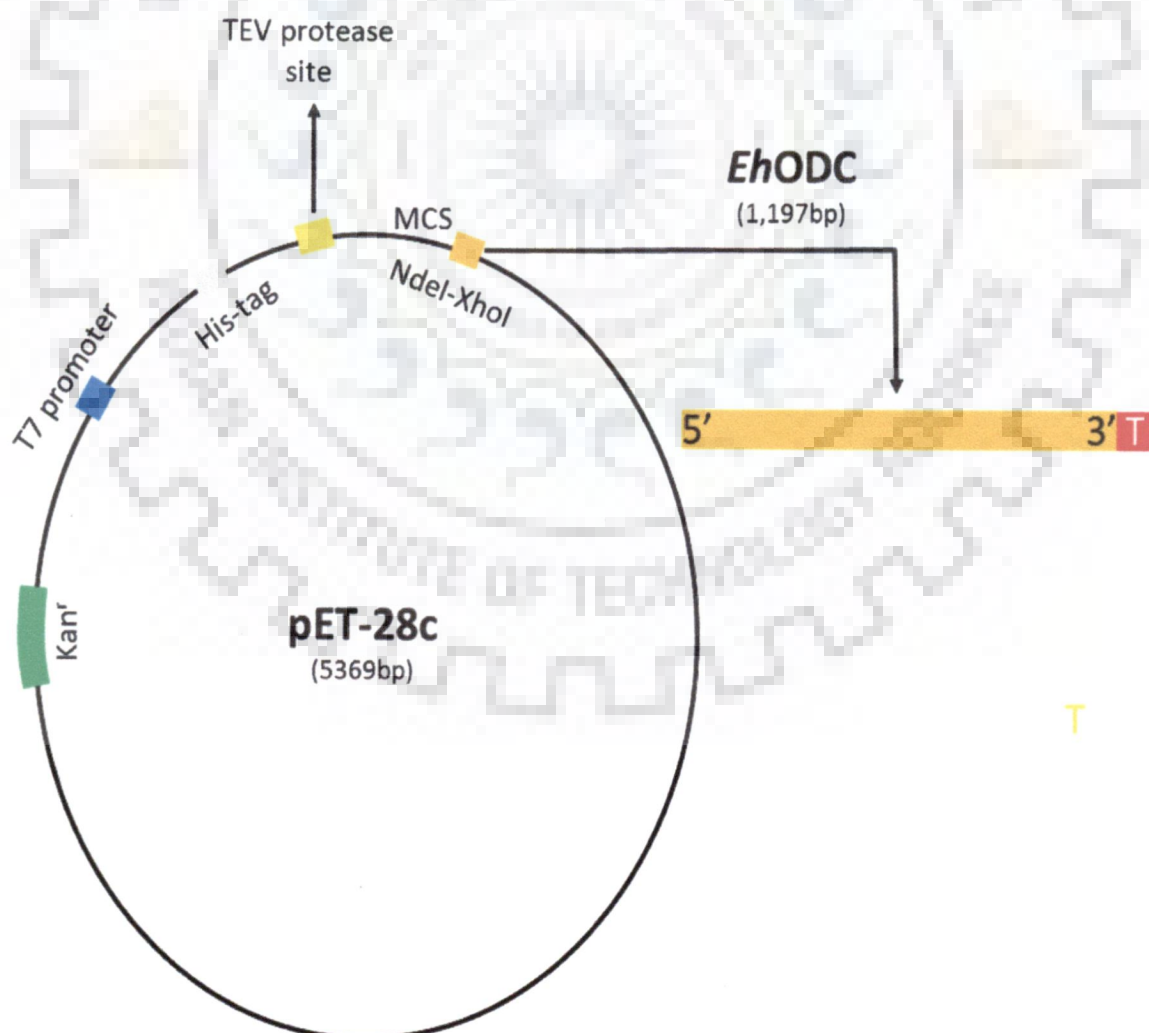
A common practice that facilitates crystallization is to truncate the flexible N and/or C terminus of the polypeptide to decrease the conformational heterogeneity. The amino acid sequence of *EhODC* was examined to identify flexible disordered terminus using bioinformatics tools DisEMBL (Linding *et al.*, 2003) and globplot (Linding and Russell, 2003). These programs predicted that a fragment of approximately 13-17 residues at the C-terminus of *EhODC* was flexible. Based on these observations, C-terminal truncation having 15 residues deleted from the *EhODC* sequence was designed. The  $15\Delta cEhODC$  construct was obtained by Polymerase Chain Reaction (PCR) using forward primer 5'-ATATCCATATGAAACAAACATCTCTAGAAG-3' and reverse primer 5'-GAACCTCGAGTCATTCAATTGACTTAGGGATTTGAAT-3' with *NdeI* and *XhoI* restriction enzyme sites respectively.

The full length *EhODC* cloned into pET 30(a) was taken as template (Jhingran *et al.*, 2008; Preeti *et al.*, 2012). The PCR reaction was set up for 50  $\mu$ l volume contained 10  $\mu$ l of 5X HF Phusion buffer supplied with the enzyme, 300  $\mu$ M of dNTP mix, 6.25 pmol of each primer, 10 ng of template DNA, 1ul of 2.5 U/ $\mu$ l Phusion polymerase and water. PCR reaction

was performed with initial denaturation at 95 °C for 30 s, followed by 30 PCR cycles of denaturation at 95 °C for 30 s, annealing at 51 °C for 60 sec, extension at 72 °C for 1 min 15 sec and a final extension at 72 °C for 15 min. Amplified product was digested with *NdeI* and *XhoI*, and ligated into *NdeI-XhoI* backbone fragment of pET 28(c) expression vector. The gene was cloned with His<sub>6</sub>-tag preceding the N-terminal and included a tobacco etch virus (TEV) protease cleavage site to allow the removal of tag from recombinant protein (Figure 5.1).

Ligated product was transformed into freshly prepared *E. coli* BL21 (DE3) competent cells. Kanamycin resistant transformants were selected and were grown in LB broth supplemented with 50 µg/ml kanamycin. The plasmid was isolated and right construct was confirmed by DNA sequencing from TCGA, New Delhi (Figure 5.2).

### 5.3.2.2 Plasmid map of 15Δ*Eh*ODC construct



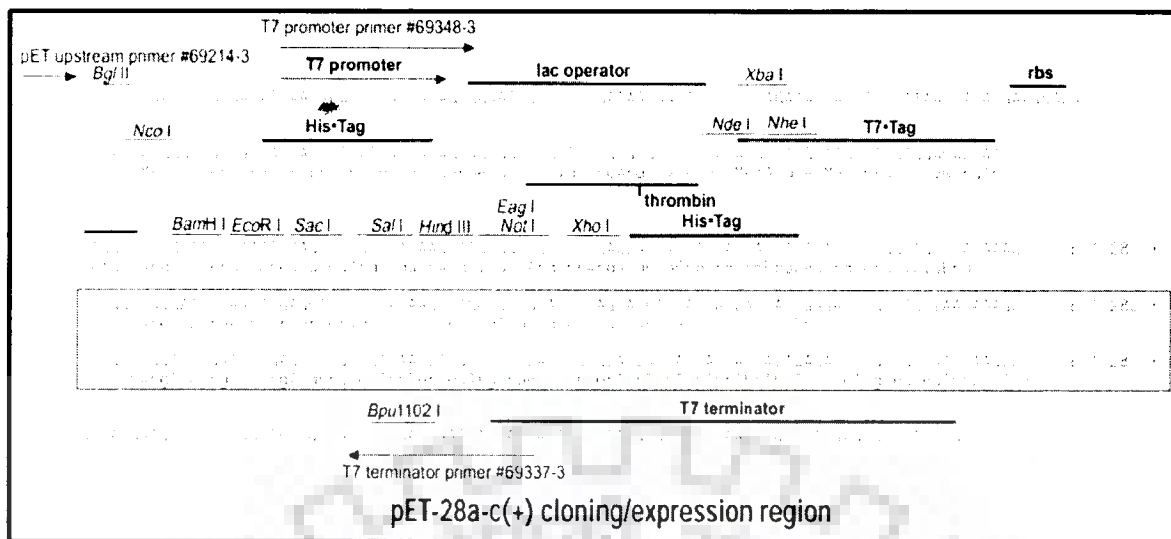


**Figure 5.1: Schematic diagram of the cloned 15ΔcEhODC construct map.** pET28c expression vector with TEV protease cleavage site and 15ΔcEhODC of 1,197 bps was inserted in between *NdeI-XhoI* fragment red zone with T indicate the C-terminal region that has been deleted from the sequence.

### 5.3.2.3 Strategy used for cloning and purification.

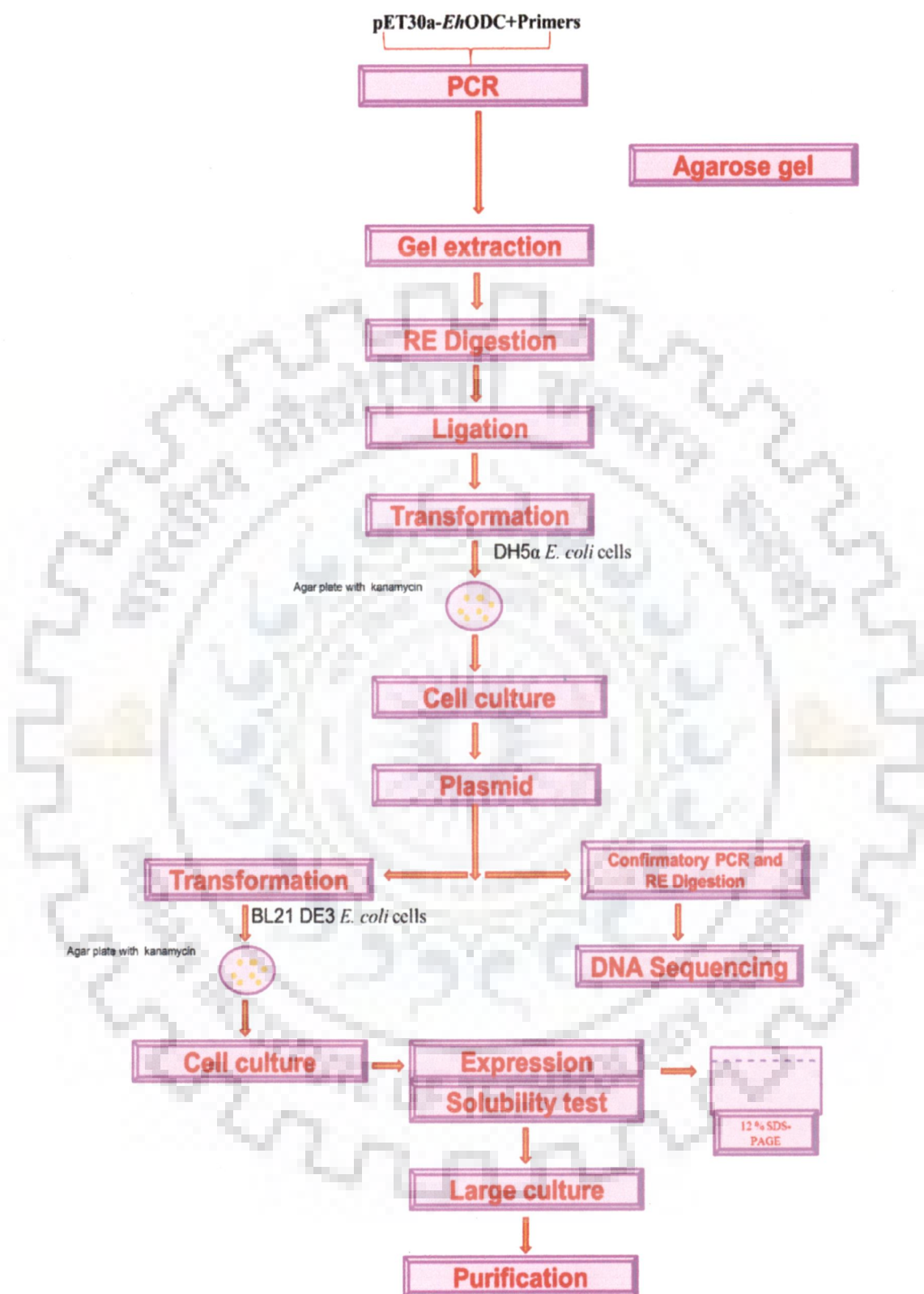


Figure 5.2: Schematic representation of the strategy used for the cloning of 15Δ*EhODC* from full-length *EhODC* construct.

#### **5.3.2.4 Expression and purification**

The recombinant 15 $\Delta$ *cEh*ODC transformed in *E. coli* BL21 (DE3) was induced with 0.5 mM isopropyl  $\beta$ -D-thiogalactoside (IPTG) at optical density (OD<sub>600</sub>) of 0.6 and further continued to grow for 14 hours at 18 °C with agitation. Bacterial culture was then harvested by centrifugation at 5000 rpm at 4 °C and pellets were stored at -20 °C until further use.

The over-expression and purification of 15 $\Delta$ *cEh*ODC was done following the standard protocol of wild type *Eh*ODC protein with little modification in tag cleavage steps. His-tag was cleaved using TEV protease with protein to TEV ratio 1:20 (v/v) at 4 °C and tag-cleaved protein was again reloaded onto HisTrap HP affinity column to get purified cleaved protein in flow-through. The cleaved protein was further loaded onto Hiload 16/60 Superdex 200 size exclusion column equilibrated with 30 mM HEPES-Na buffer (pH 7.5) containing 300 mM NaCl, 1 mM EDTA, 10% (v/v) glycerol and 1mM DTT. The different eluents were analyzed on 12% SDS-PAGE. The fractions containing purified recombinant 15 $\Delta$ *cEh*ODC were further concentrated to 5 mg/ml using a 10 kDa cutoff Amicon Ultra-15 concentrator 165 (Millipore, Bedford, Massachusetts, USA).

#### **5.3.2.5 Enzymatic activity of 15 $\Delta$ *cEh*ODC**

Decarboxylation activity of purified 15 $\Delta$ *cEh*ODC was determined spectrophotometrically as reported by Badolo *et al.*, 1999, using the same protocol as for full-length *Eh*ODC.

#### **5.3.2.6 Gel filtration analysis**

The average molecular weight of 15 $\Delta$ *cEh*ODC was determined using size exclusion chromatography and compared with previously characterized full length *Eh*ODC (Preeti *et al.* 2012). In brief, the purified protein (5 mg/ml) was injected onto Hiload Superdex 200 16/60 gel filtration chromatography column using AKTA purification system (GE Healthcare). The protein was allowed to pass through the column at a rate of 0.5 ml/min. Further, elution volume of the protein was compared with the standard molecular weight markers (GE healthcare) loaded onto the same column.



### 5.3.2.7 Crystallization

Crystallization conditions of 15 $\Delta$ *cEh*ODC were obtained using Hampton crystallization screens (Hampton Research Inc. Aliso Viejo, CA). The homogeneously purified protein solution was concentrated to 12.5 mg/ml in 30 mM HEPES-NaOH buffer (pH 7.5) containing 1 mM EDTA, 0.2 M NaCl, 1mM DTT and 10 % (v/v) glycerol. The crystals were grown at 20 °C by sitting drop vapor diffusion method using 2  $\mu$ l of protein solution mixed with 1  $\mu$ l of reservoir solution containing 20 % PEG 3350 in 0.2 M LiCl solution maintained at pH 6.8 as provided in Hampton PEG ION screen. Diamond shaped single crystal appeared in four months after crystallization. Prior to data collection, crystals were cryo-protected by directly transferring it to mother liquor containing 3 % (v/v) ethylene glycol. Crystal was flash-frozen under cryogenic conditions at 100 K using liquid nitrogen stream to prevent radiation decay during data collection.

### 5.3.2.8 Data collection and structure determination

All diffraction data of 15 $\Delta$ *cEh*ODC crystal were collected as consecutive series of 1° rotation images using rotating anode X-ray source (Bruker Microstar) assembled with MAR345 detector plate installed at home station, IIC, IIT Roorkee, India. The data were indexed, integrated and scaled using HKL2000 program. A summary of data processing has been described in Table 5.1.

The structure of 15 $\Delta$ *cEh*ODC was solved by molecular replacement method. Patterson searches were computed using Molrep program of CCP4-6.0 suite (Vagin *et al.*, 1997). Model was generated using previously reported crystal structure of human ODC (PDB accession number 2ON3) (Dufe *et al.*, 2007). The crystal contained two copies of 15 $\Delta$ *cEh*ODC dimer in the asymmetric unit. Non-crystallographic symmetry restraints were applied throughout the refinement stages using four 15 $\Delta$ *cEh*ODC molecules in asymmetric unit. Further, refinement was performed using CNS v.1.2, REFMAC 5.2, and Phenix v 1.7.2-869 refinement tools/software (Brünger *et al.*, 1998, 2007; Adams *et al.*, 2010; Vagin *et al.*, 1997, 2004). Rounds of model building were carried out using program Coot v 0.6.2 and iterative cycles of computational refinement interspersed with visual inspection and manual adjustments, values of R / R<sub>free</sub> reached to 0.35 / 0.395 (Emsley *et al.*, 2004). Further,

Crystallography and NMR system (CNS) refinement involving typical protocol of simulated annealing, minimization, grouped B-factor refinement reduced the R / R<sub>free</sub> value to 0.30/0.325. Later, the refinement strategy was shifted to omit map and simulated annealing with slowcool protocol, thus further reduced the R / R<sub>free</sub> value to 0.25/0.299. The quality of the model was evaluated by PROCHECK. The structure has been deposited in Protein Data Bank with accession code 4AIB.

### 5.3.2.9 Sequence analysis, model generation and docking

The sequence of *Eh*ODC along with the ODCs and antizyme inhibitor from other representatives were retrieved from NCBI database. Multiple sequence alignment and phylogenetic tree of these sequences were obtained by using ClustalW applying default settings. In crystal structure, as different loops were missing at different positions of all subunits, the complete model for active site analysis was generated using MODELLER 9.10 and crystal structure of 15Δ*AcEh*ODC as a template (Sali *et al.*, 1993). Multalin program was used for sequence alignments and manual corrections were done for gap regions in the structure sequence (Corpet, 1988). Evaluation of the stereochemical properties of obtained model was performed using PROCHECK (Luthy *et al.*, 1992).

The docking studies of substrate, cofactor and substrate based inhibitor were performed using GLIDE v 5.5 software (Grid-based ligand docking with energetics) by Schrödinger running on Red Hat enterprise Linux 5 operation system installed on HPxw8400 workstation (Cross *et al.*, 2009). Maestro's protein preparation wizard was used for adding hydrogen, assigning bond orders and overall structure minimization to RMSD (Root Mean Square Deviation) of 0.30 Å using OPLS2005 force-field. All ligands were generated with cofactor PLP using chemdraw and energy minimization of the ligand was done using chemdraw Ultra 8.0. Ligand preparation module of Maestro was then used for ligand preparation. GLIDE receptor grid generated to the centroid of the selected amino acids of active site residues and docking of the ligand was done using extra precision mode (Friesner *et al.*, 2004). Best pose was selected by evaluation of Glide score rank, glide energy and visually inspecting the molecule by PyMol (DeLano, 2002).

## 5.4 Result and Discussion

### 5.4.1 Sequence analysis and cloning of 15 $\Delta$ *Eh*ODC

The *Eh*ODC protein belongs to fold type III group IV decarboxylase of a B6-dependent family, having characteristics of eukaryotic ornithine decarboxylases. Under this classification, three crystal structures are available till date including human, mouse and *T. brucei* ODC (Almud *et al.*, 2000; Kern *et al.*, 1999; Grishin *et al.*, 1999; Dufe *et al.*, 2007). From previous studies, it was reported that deletion of C-terminal of functional ODC resulted in increased stability of the protein without affecting the activity (Rosenberg-Hasson *et al.*, 1991; Ghoda *et al.*, 1989). In mouse, as C-terminal contains a PEST like sequence responsible for ubiquitin independent 26S proteasome mediated degradation process and deletion of 37 residues from C-terminal increased the stability of ODC (Fujita *et al.*, 1982; Kitani *et al.*, 1989; Nilsson *et al.*, 2000; Cohavi *et al.*, 2009; Keren-Paz *et al.*, 2006). However, in *T. brucei*, no such phenomenon has been observed (Hua *et al.*, 1995).

In *Eh*ODC, the C-terminal sequence shows similarity with mouse ODC having a similar kind of PEST sequence though such kind of degradation is not reported till date. With our repeated trials, we didn't find any crystals with expression of full length *Eh*ODC. However, we increased the stability of the protein with deletion of 15 residues from C-terminal. The primers for PCR amplification for 15 $\Delta$ *Eh*ODC were designed on the basis of sequence alignment of full length *Eh*ODC with *T. brucei* ODC and mouse ODC. The gene was cloned into pET28(c) expression vector and expressed with N-terminal His tag (Figure 5.1, 5.3). Further, His tag was cleaved by TEV protease and used for enzyme assay, and crystallization study.

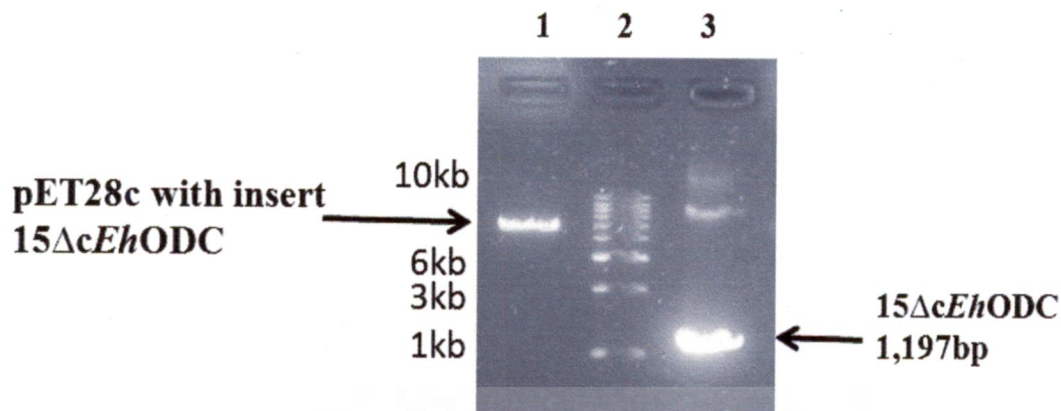


**Figure 5.3: Agarose gel profile of 15ΔcEhODC:** Lane 1: Cloned plasmid containing the 15ΔcEhODC with insert size 1,197 bps; Lane 2: 1 kb DNA ladder; Lane 3: Cloned plasmid RE digested with *NdeI* and *XhoI* enzymes.

#### 5.4.2 Expression and purification of 15ΔcEhODC

The overexpression of 15ΔcEhODC was done with 0.5 mM IPTG at 18 °C for 14 hours (Figure 5.4). The over-expression and purification of 15ΔcEhODC was done following the standard protocol of wild type *EhODC* protein with little modification in tag cleavage steps as mentioned in material and method section above (Figure 5.4).

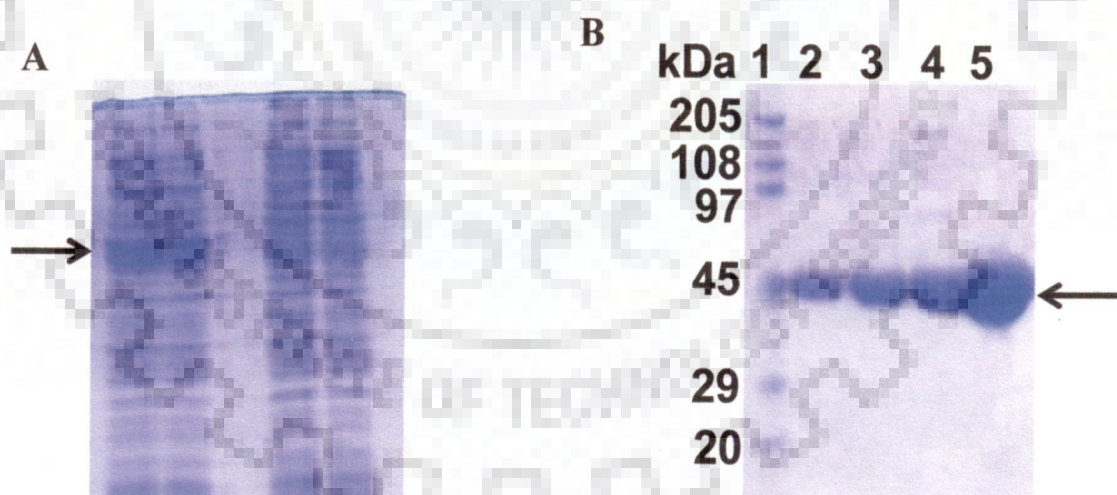


**Figure 5.4: 12% SDS-PAGE gel showing the expression and purification of 15ΔcEhODC.** A) Lane 1: Induced pellet; Lane 2: Induced supernatant; Lane 3: Uninduced pellet; Lane 4: Uninduced supernatant arrow indicating the overexpressed 15ΔcEhODC. B)



Lane 1: Molecular weight marker; Lane 2-5: Purified fractions. Arrow points to the protein of molecular weight ~44 kDa.

### 5.4.3 Oligomeric state analysis in solution

To determine the oligomeric state, 15 $\Delta$ *cEh*ODC was loaded on to Hiload Superdex 200 16/60 gel filtration chromatography column and was loaded onto 12 % SDS-PAGE revealed a sharp band corresponds to molecular weight of 43.7 kDa (Figure 5.5). Comparing the results of both the experiments, we found the protein exist in dimeric form in the solution having a molecular weight of ~87 kDa (Figure 5.4, 5.5).

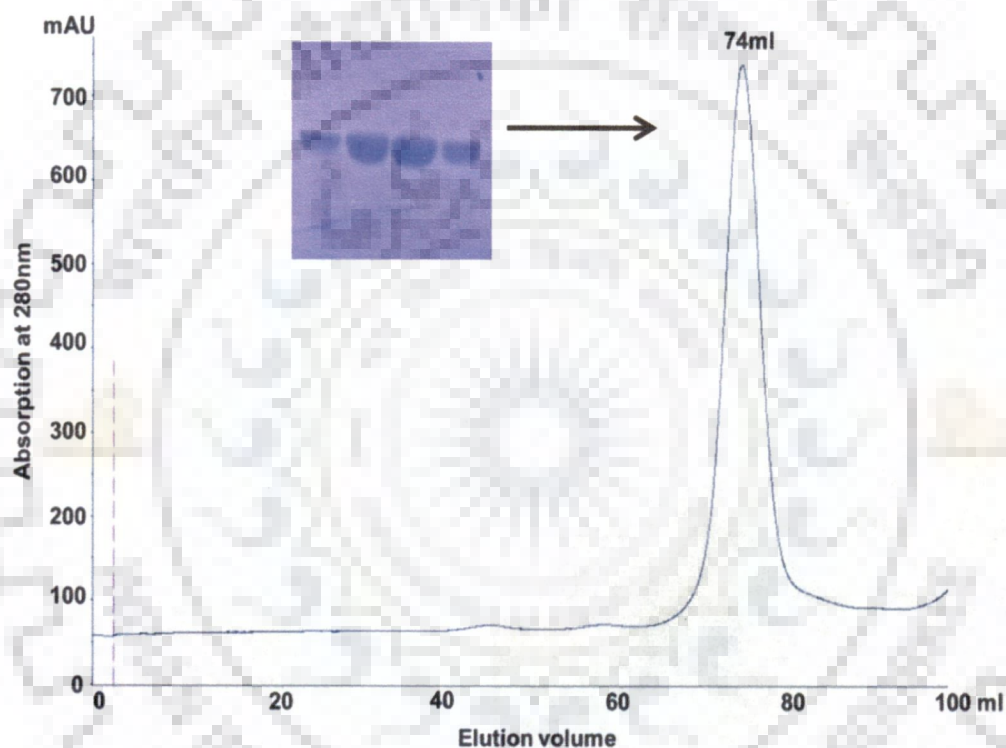


**Figure 5.5: The gel filtration chromatogram elution profile of the 15 $\Delta$ *cEh*ODC protein.** The elution volume of 15 $\Delta$ *cEh*ODC protein was compared with the standard molecular weight markers. The protein was eluted at a volume of 74 ml corresponding to molecule weight of ~87 kDa. Insert shows the purified protein in 12 % SDS-PAGE after gel filtration chromatography.



#### 5.4.4 Activity of 15 $\Delta$ *Eh*ODC

The enzyme assay of 15 $\Delta$ *Eh*ODC was performed spectrophotometrically as reported by Badolo *et al.*, 1999. We didn't report any change in activity of 15 $\Delta$ *Eh*ODC with respect to full length *Eh*ODC.

#### 5.4.5 Crystal packing

Crystallization of 15 $\Delta$ *Eh*ODC was performed using sitting drop vapor diffusion method. Crystals of *Eh*ODC were obtained at 20 °C in Hampton PEG Ion screen 4 containing 20 % (v/v) PEG 3350, 0.2 M LiCl maintained at pH 6.8 (Figure 5.6). The crystal belonged to orthorhombic unit cell exhibiting P2<sub>1</sub>2<sub>1</sub>2<sub>1</sub> symmetry with unit cell parameters  $a = 76.66$ ,  $b = 119.28$ ,  $c = 179.28$  Å and  $\alpha = \beta = \gamma = 90^\circ$  (Figure 5.6, 5.7). The crystal was diffracted up to 2.8 Å and its Mathew coefficient is 2.2. The crystal has the solvent content of 46.69 % with four numbers of molecules per asymmetric unit. Quality of the model obtained was assessed by PROCHECK. Model was found to contain 88.7 % residues in allowed region and 0.4 % in residues in disallowed region of Ramachandran Plot (Table 5.1).

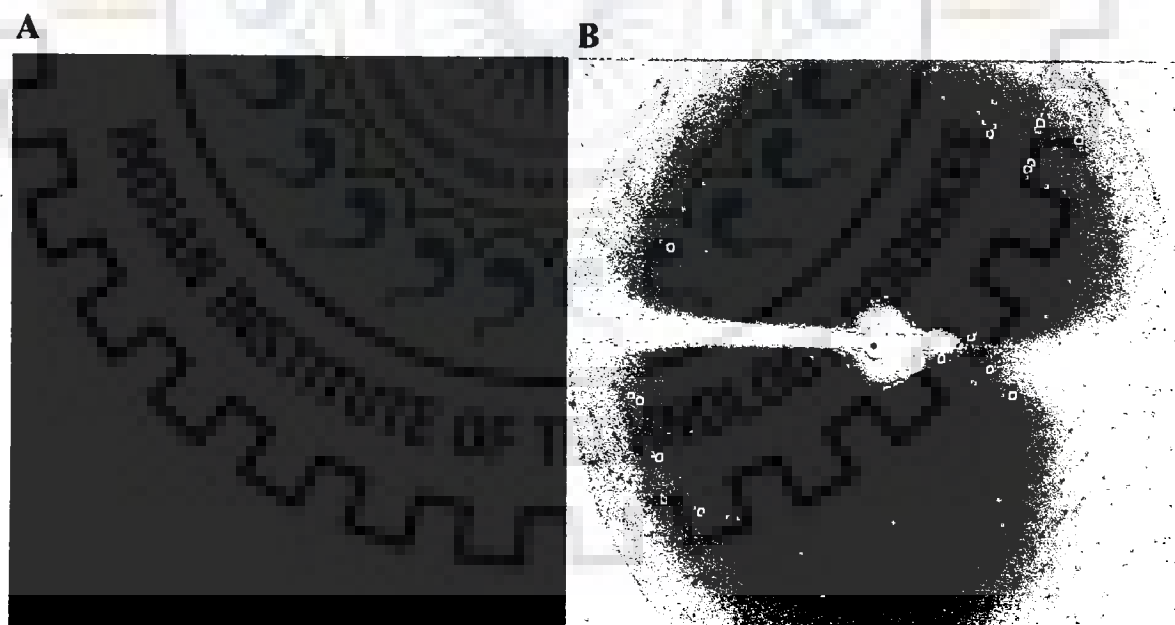


**Figure 5.6: Crystals of 15 $\Delta$ *Eh*ODC along with the diffraction pattern. A) Diamond shaped crystals in 20% (v/v) PEG 3350, 0.2 M LiCl maintained at pH 6.8. B) Diffraction pattern of 15 $\Delta$ *Eh*ODC crystal at 2.8 Å.**

Monomers in asymmetric unit are arranged as two separate dimers (subunits A, B and subunits C, D) facing each other at convex surfaces (Figure 5.7). The arrangement and interaction between two monomers was found to be different from their symmetry mates within the unit cell. Dimer of chain A and chain B was arranged in head to tail manner at origin O of orthorhombic unit cell.  $\beta/\alpha$ -barrel of A and  $\beta$ -sheet of B chain were arranged at origin and their counterpart in x direction (Figure 5.7). Each monomer makes side to side as well as back to back contacts and forming a cavity at the center. In a dimer, one subunit arranged above other forming a curved structure. The  $\beta$ -sheet of C and  $\beta/\alpha$ -barrel of D make back to back contact with dimer of B and A chains at the curved surface. Dimer of AB is situated along with axis x by making an angle of  $30^\circ$  approximately, rotation angle of other dimer CD is  $180^\circ$  with a screw distance of  $19.1 \text{ \AA}$  which is equivalent to one quarter of edge a of unit cell.

The crystallized structure of  $15\Delta cEhODC$  is of a tetramer (Figure 5.7). The asymmetric unit contains two dimers comprising of chain A, B, C, D. Although in all chains, the loops at the dimer interface are disordered, clear electron density was not observed. The total area of the molecule of *EhODC* containing four molecules was estimated to be  $61227.6 \text{ \AA}^2$ . Each dimer interacts with its symmetry mate to form dimer-dimer interfaces as A-B dimer interacts with C-D dimer. Interface area evaluated by PISA web server was averaged to  $1373.4 \text{ \AA}^2$  which was  $1599.8 \text{ \AA}^2$  and  $1147.0 \text{ \AA}^2$  between B, A and D, C respectively. Each monomer interacts with other counterpart monomer, making extensive contact area of  $18487.5 \text{ \AA}^2$ . Buried surface area of each assembly of dimer A, B and C, D that shields a combined area of protein from solvent was averaged to  $5490.0 \text{ \AA}^2$ . Crystal packing provides additional contacts between molecules.

<i>Data collection</i>	
Space group	P2 <sub>1</sub> 2 <sub>1</sub> 2 <sub>1</sub>
<i>Unit cell parameters</i>	
<i>a</i> (Å), <i>b</i> (Å), <i>c</i> (Å)	76.66, 119.28, 179.28
Resolution (Å)	99.5-2.87 (2.92-2.87) <sup>a</sup>
Number of reflections	35570
Completeness (%)	92.1(59.0) <sup>a</sup>
Mean redundancy	3.4 (2.1) <sup>a</sup>
<i>I</i> / $\sigma$	4.82 (2.0) <sup>a</sup>
<i>R</i> <sub>merge</sub> (%)	0.150 (0.670) <sup>a</sup>
<i>Refinement strategy</i>	
Resolution (Å)	99.5-2.87 (2.92-2.87) <sup>a</sup>
<i>Number of non-H atoms in asymmetric unit</i>	
Protein	10484
Water molecules	101
<i>R</i> -factor (%)	25.3
<i>R</i> <sub>free</sub> value (%)	29.9
Average <i>B</i> -factor (Å <sup>2</sup> )	54.4
<i>Rms deviations</i>	
bond lengths (Å)	0.005
bond angles (°)	0.831
Ramachandran plot	
Residues in favored region (%)	88.7
Residues in allowed region (%)	10
Residues in generously allowed region (%)	0.9
Residues in outlier region (%)	0.4

**Table 5.1: Statistical representation of data collection and structure refinement parameters along with quality of the model accessed by Ramachandran plot. <sup>a</sup> value in parentheses are for the highest resolution shell.**

Crystal packing and 3D structure determined using molecular replacement method has been presented below

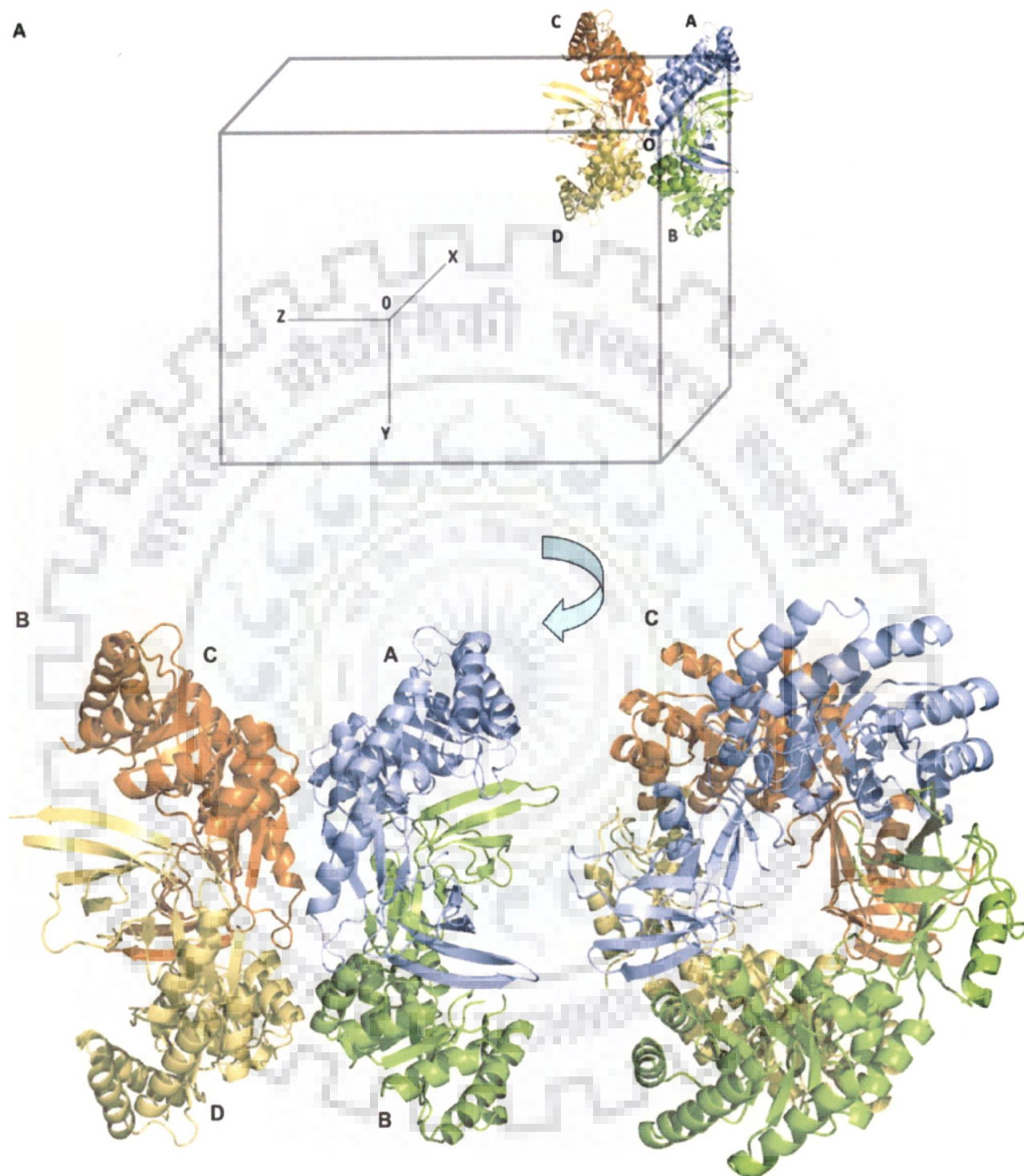


**Figure 5.7: Schematic representation of crystal packing and overall structure of the model obtained after molecular replacement. A)** Crystal packing of *Eh*ODC in an orthorhombic unit cell; O is the origin of the unit cell with four chains arranged on a, b and c

axis in x, y and z direction; **B**) Cartoon diagram of tetrameric model of *Eh*ODC showing AB-CD, dimer-dimer interface; **C**) Tetrameric model rotated to 90° to insight into the center of the molecule.

#### 5.4.6 Overall structure and folding

Each monomer consists of  $\beta/\alpha$  barrel and  $\beta$  sheet domains which are arranged identical to previously known ODC structure. However, the tetramer arrangement displays a number of unusual features. Residues from barrel involved in contact formation are located at the surface or in proximity to sheet domain of opposite monomer and resulted in homodimer formation. Residues of A chain barrel are in helix  $\alpha 5$ ,  $\alpha 7$ ,  $\alpha 8$ ,  $\alpha 9$  which appear to be at interface and form extensive contacts with sheet domain S2 of B chain.

All four chains in asymmetric unit showed similar structures and involved same interaction. The analysis of dimer-dimer interactions exhibited large intermolecular distances of  $\sim 4.0$  Å, N-terminal of the monomer starts with the helix  $\alpha 1$  (L6-Q18) facing other dimer of asymmetric unit. Helix  $\alpha 1$  is connected to sheet  $\beta 1$  (G27-F31) through a loop and enters to the barrel which is an arrangement of 8 helices following 8 parallel sheets. Helix  $\alpha 2$  (T33-N46),  $\alpha 3$  (P62-L71),  $\alpha 4$  (L80-L89),  $\alpha 5$  (Y105-L114),  $\alpha 6$  (I124-Y133),  $\alpha 7$  (D163-K175),  $\alpha 8$  (E194-F213),  $\alpha 9$  (F232-L246), follow the sheet  $\beta 2$  (R51-A55),  $\beta 3$  (G74-C77),  $\beta 4$  (I96-Y98),  $\beta 5$  (H118-V121),  $\beta 6$  (G138-R142),  $\beta 7$  (V182-F184),  $\beta 8$  (L219-D221) and  $\beta 9$  (R253-A256) following a helix-turn connecting the sheet domain. Sheet domain comprised of eight randomly arranged sheets which can be further divided into S1 and S2 sheets perpendicular to one another. Sheet S1 consisted of four sheets  $\beta 10$  (F267-S271),  $\beta 15$  (L355-F357),  $\beta 16$  (I381-T383) in addition to  $\beta 1$ , which are roughly perpendicular to S2 containing  $\beta 11$  (H274-Q281),  $\beta 12$  (K284-S291),  $\beta 13$  (Y325-Y330) and  $\beta 14$  (A341-L345) (Figure 5.8).

Residues Glu110 and His113 of chain B are at a distance of 4.1Å and 3.3Å from Lys84 and Asp88 of chain D respectively, similarly Asp88 of chain A forms direct interaction with residue Leu386 of chain C and vice versa. The structure of *Eh*ODC has several disordered regions. These include the first four residues at the N-terminal, 13 residues of C-terminal in all chains. Chain A containing disordered regions (146-156), (297-308), (331-337) and (366-378); Chain B (146-159), (187-192), (228-229), (292-308), (336-337), and (336-378); chain



C (146-162), (187-192), (228-229), (331-337), (366-378) showing density for K and S at the C-terminal which is absent in other chains. Chain D similar to chain C having disordered regions in same loops except region (293-304).

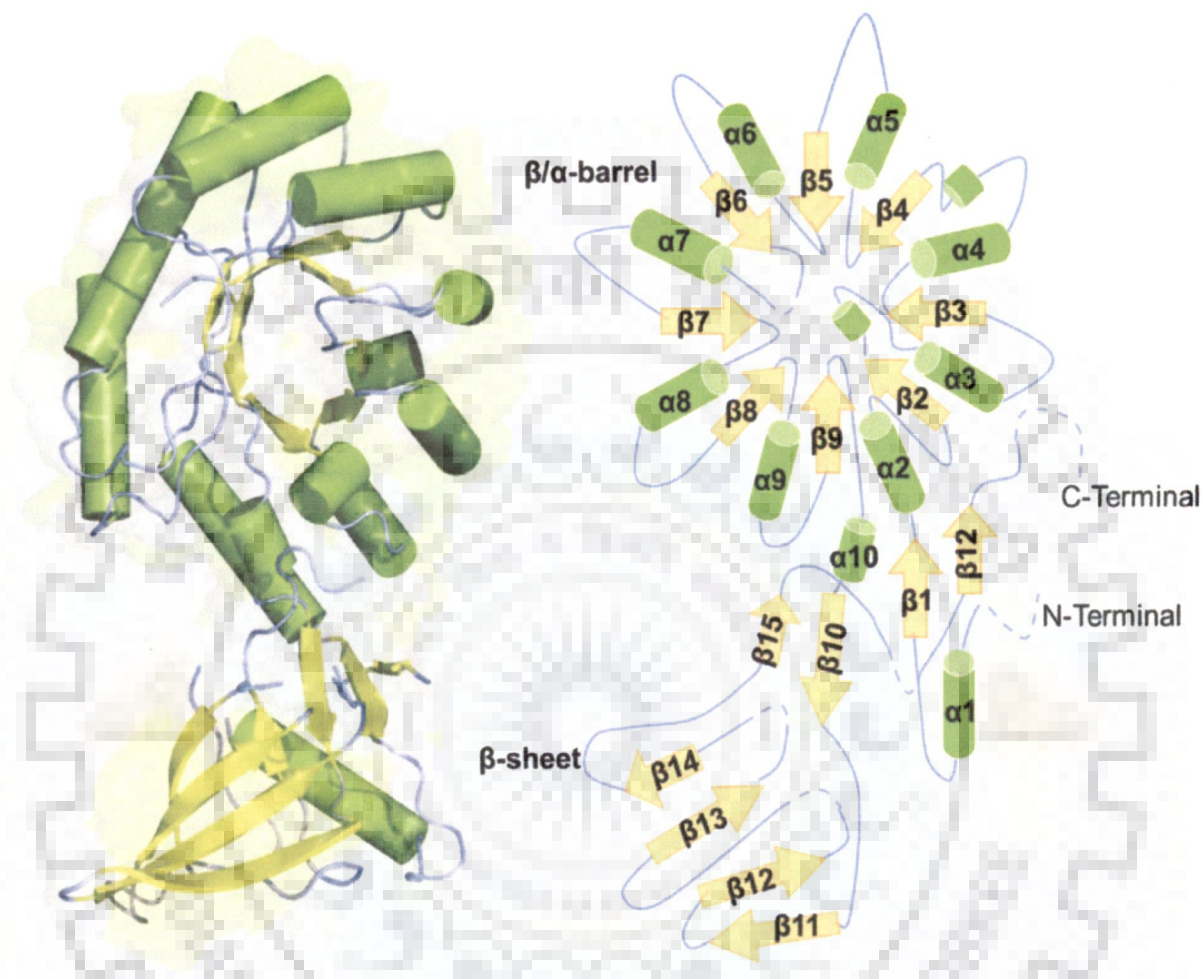


**Figure 5.8: Crystal structure of *EhODC* monomeric subunit.** A) Cartoon diagram of the monomer showing arrangement of barrel and sheet domain. B) Topology diagram of monomer of *EhODC* where helices are represented with cylinder and sheets with the arrows connected with loops, dashed line indicates the sequence missing in the structure.

#### 5.4.7 Active site of *EhODC*

Electron density corresponding to cofactor and substrate was not identified in the putative sites. All the residues involved in PLP binding are absolutely conserved in *EhODC*. Electron density was clear and distinct for almost all cofactor binding residues in all chains but

substrate binding residues were only observed in B and D chains. In active site, A111 (No. according to human ODC) was found to be existed at the active site. Residue A111 is also conserved in *T. brucei* and mouse ODC where it interacts through water and Arg154 which in turn interacts with PLP and maintains the integrity of active site. In *Eh*ODC A111 is substituted with S99 and in AZI same residue is substituted with T1/S.



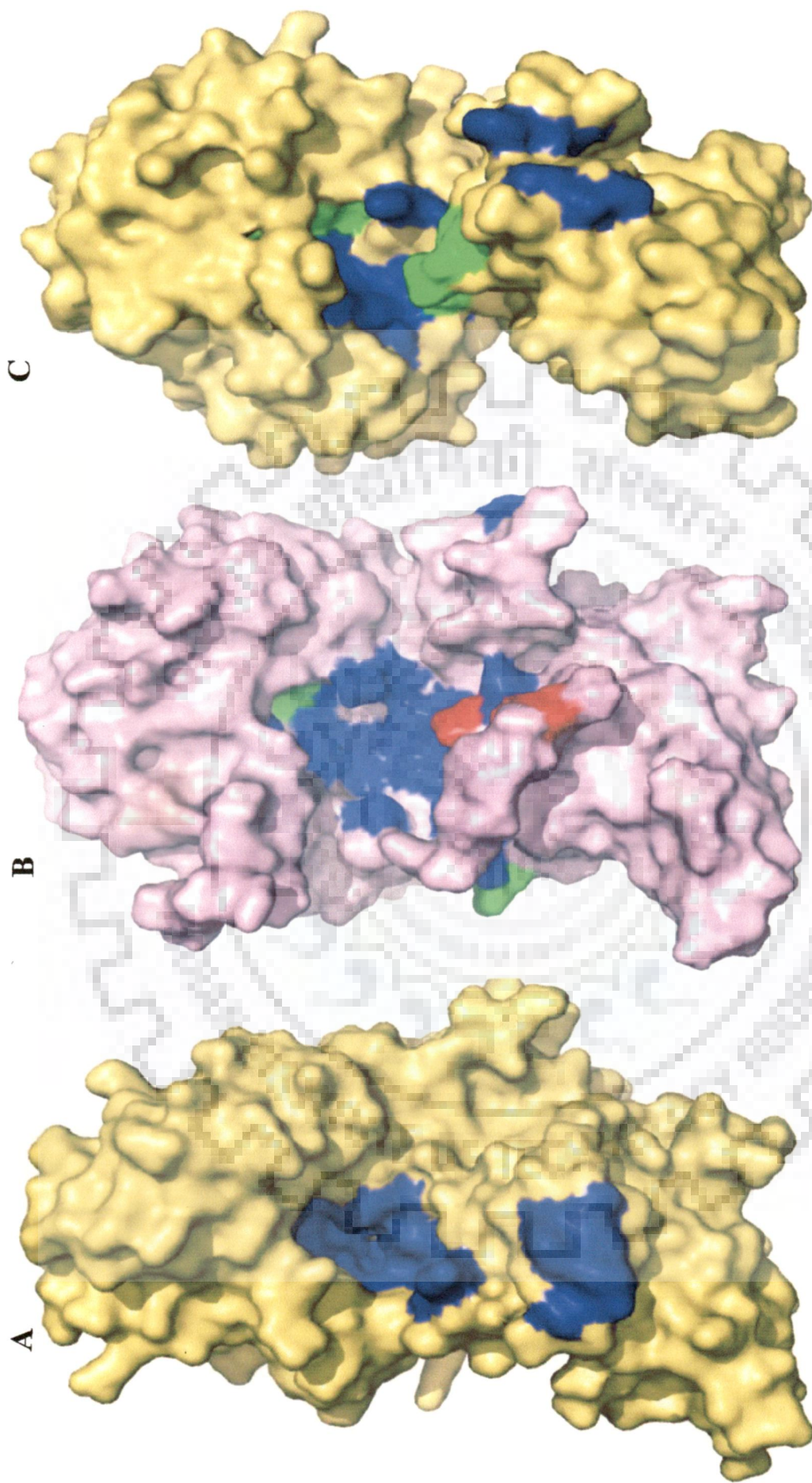


**Figure 5.9: Surface view diagram of active sites of functional ODC, nonfunctional antizyme inhibitor and *EhoDC*. A)** Monomer of human ODC with active site colored in blue. **B)** Monomer of *EhoDC* showing active site residues identical to human ODC colored blue, identical to AZI colored green and unique to *EhoDC* colored red. **C)** Monomer of AZI showing residues identical to human ODC in blue and those are mutated colored green



In AZI, some mutations of conserved residues important for PLP binding resulted in incapability to bind PLP. Residues found to be mutated in active mouse ODC and mouse AZI are as follows D88/A88, A111/T111, R154/H154, R277/S274 Y331/S329, D332/E330 and Y389/D387. However, the PLP and substrate binding residues of *Eh*ODC are conserved except four residues which show similarity to AZI residues. These four residues of *Eh*ODC/ODC/DrAZI are S99/A111/S111, binds to PLP and F305/Y331/F329, E306/D332/E330 (mAZI) and N335/D361/D361 binds to substrate respectively (Figure 5.9, Table 5.3). These observations signify that *Eh*ODC is evolutionarily developing in the direction of AZI. Thus, it is safe to hypothesize that ODC from *E. histolytica* is the bridge between the antizyme inhibitor and active form of ODC having decarboxylation capability.

### 5.5 Active site pattern revealing insensitivity towards DFMO

Earlier reports have indicated that *Eh*ODC is resistant to DFMO, an irreversible inhibitor of *Tb*ODC (Arteaga-Nieto *et al.*, 2002). Investigations of this interesting property draw our attention towards the active site of *Eh*ODC. The generated crystal structure was lacking some loops at the active site in different chains. Thus, it was necessary to generate a complete dimeric model to insight into difference in the binding of DFMO and L-ornithine at the active site. Homology model was generated using MODELLER 9.10 with *Eh*ODC crystal structure as template. Docking of cofactor-substrate and DFMO was performed using the Glide docking version 5.5. Docking of L-ornithine and DFMO was revealing the spatial position of substrate binding residues. Role of each residue for the substrate interaction was analyzed in detail to insight into the mechanistic function in *Eh*ODC.

Sequence analysis of *Eh*ODC revealed many substitutions of amino acid residues important for the decarboxylation of the substrate (Figure 5.10, 5.11, Table 5.3). It has been reported that substrate binding residues are present mainly at the C-terminal region. During earlier studies D-ornithine, L-ornithine and DFMO were used for substrate binding and reaction mechanism determination. Cys360 was found to play very important role by directly attaching to the substrate through a covalent bond (Poulin *et al.*, 1992). Cys360 is highly conserved in all functional ODC including *Eh*ODC (Cys334). The amino acid Asp361 (no according to human ODC) has been identified as an essential substrate binding determinant. Substitution of residue

Asp361 to Glu or Ala results in 2000 fold increase in  $K_m$  and significantly affects the binding of substrate to the active site. Function of Asp361 has been investigated in details and  $\beta$ -carboxylate group of this residue is reported to interact with substrate directly via forming salt bridge with either of the two amino group of substrate (Osterman *et al.*, 1995, 1999). However, in *Eh*ODC Asn335 was found to be uniquely substituted. Interestingly, it is uncharged polar residue having an amino group in contrast to Asp which is charged and have  $\beta$ -carboxyl group.

One more important acidic residue Asp364 (no according to human ODC) at the active site to provide a proton to carbanion formed after decarboxylation reaction. Mutation of Asp364 to Ala has most profound effect on catalysis which decreases  $K_{cat}/K_m$  by greater than 105 fold (Osterman *et al.*, 1995). Asp338 residue in *Eh*ODC that corresponds to conserved Asp364 at the active site and play essential role in ODC catalysis. The residue participates in catalytic function by interacting with substrate/analogues by either making direct or indirect contact through water. Furthermore, Tyr323 residue plays essential role in catalysis by making contact with substrate through water. The reactive hydroxyl (OH) moiety of Tyr323 makes hydrogen bond with water molecule and interacts with the amino group of substrate (Lu *et al.*, 1991; Grishin *et al.*, 1999; Tsirka *et al.*, 1993). In *Eh*ODC, residue Tyr323 a hydrophilic residue was found to be mutated with His296 a positively charged amino acid. Furthermore, Asp332 was found to be important for interacting with the substrate by making hydrogen bond with water (Grishin *et al.*, 1999). In *Eh*ODC, Asp332 found to be substituted by Glu306 which is conserved in antizyme inhibitor. It has been reported that poor identity around Asp332 or no Asp residue in surrounding region may have adverse effect on substrate binding capacity of ODC. Mutation of Asp332 to Glu may interfere with binding of substrate due to one extra methyl moiety which may not allow the proper orientation of side chain at the active site (Figure 5.10, Table 5.2).

Ligand attached with PLP	GLIDE score	GLIDE energy
L-ornithine	-5.550	-52.068
DFMO	-6.463	-49.789

**Table 5.2: Comparative glide score and energy for L-ornithine and DFMO for determining the binding efficiency of the ligand to dimer of *Eh*ODC.**





Property of substrate binding residues of *Eh*ODC and insensitivity towards DFMO were studied in details. Insight into the structure and property of active site of *Eh*ODC bring out one more important characteristic of residues which were found to be similar to AZI and may not allow the interaction with DFMO. In general, residue D332 (of human ODC) found to be present in active ODC that is substituted with E331 in AZI which interacts with substrate through water molecule. E331 has an extra methyl group and DFMO is already accompanied with two fluorine moieties result in steric hindrance. However, it has been reported that *Eh*ODC actively decarboxylate the ornithine, in contrast it is insensitive towards DFMO (Figure 5.10). This may be the result of inefficient accommodation of DFMO in the active site which can be speculated from the Table 5.2 showing the glide score and binding energy of both DFMO and substrate L-ornithine.

### 5.6 Sequence comparison with other ODC and AZI

The detailed sequence analysis of *Eh*ODC opened up a new phase for studying the structure function and evolutionary relationship with different ODC homologues. Recently, the sequence analysis of several functional and non-functional ODCs revealed that several orthologs of ODCs including putative antizyme inhibitors apparently arise independently through evolution (Ivanov *et al.*, 2010). However, from sequence analysis, we identified critical residues of functional *Eh*ODC which may represent the status of the protein as evolutionary bridge between functional and nonfunctional ODC.

Antizyme inhibitor is a homolog of ODC which has lost decarboxylation activity due to mutation of critical residues in active site (Murakami *et al.*, 1996, 2009; Kahana, 2009; Ivanov *et al.*, 2010; Hascilowicz *et al.*, 2002). However, they are important in mammals as they are responsible for antizyme down regulations, thus regulate the ODC activity in cell system (Ivanov *et al.*, 2007). Presently we have identified 27 residues from sequence alignment of ODCs from different sources responsible for formation of active site pocket and salt bridges in dimerization (Table 5.3). Out of 27 residues, 16 residues (as mentioned in table 5.3) contribute to active site interacting with cofactor PLP, 5 residues for substrate binding, 3 residues for salt bridges, 3 interface residues and 1 for dimerization.



E. histolytica ODC	K 5 7	D 7 6	S 9 9	R 1 4 2	C 1 1 5 9	G 1 5 9	H 1 8 5	C 1 1 8 5	S 1 8 5	C 1 1 8 5	G 1 2 2 2	G 1 2 2 2	C 1 1 2 2	F 1 2 2 2	E 1 2 2 2	G 1 2 2 2	R 1 2 2 2	Y 1 2 2 2	F 1 2 2 2	H 1 2 2 2	I/S 1 2 2 2	B 1 2 2 2	R 1 2 2 2	S 3 3 3 3	N 3 3 3 3	D 3 3 3 3	G 3 3 3 3	Y 3 3 3 3	F 3 3 3 3	N 3 3 3 3	% Identity		
Homo sapiens Azi	A	I	H																														27.8
Nomascus leucogeny Azi	A	I	H																														27.8
Macaca Mulata Azi	A	I	H																														27.8
Mus musculata Azi	A	T	H																														27.8
Rattus norvegicus Azi	A	T	H																														27.8
Monodelphis domestica Azi	A	I	H																														27.8
Xenopus laevis Azi	R	A	T	H	I																												26.3
Danio rerio Azi	S	V		Q	I																												24.2
Tetraodon nigroviridis Azi	R	I	Q	I																													25.6
Anolis crolinensis Azi	R	A	T	H	M																												28.3
Gallus gallus Azi	R	A	T	H																													27.8
Canis familiaris Azi		A	I	H																													27.8
Bos taurus Azi		A	I	H																													27.8
Loxodonta africana Azi		A	I	H																													28.5
Aedes aegypti ODC		A	A																														28.3
Plasmodium falciparum ODC		A	A																														39.5
Leishmania donovani ODC		A	A																														31.4
Datura stramonium ODC		A	A																														32.4
Solanum lycopersicum ODC		A	A																														32.9
Glycine max ODC		A	A																														32.68
Chlamydomonas reinhardtii ODC		A	A																														30
M.domestica ODC		A	A	S																													33
B. taurus ODC		A	A																														32.4
M.mulatta ODC		A	A																														32.2
H. sapiens ODC		A	A																														32.4
M. musculus ODC		A	A																														32.2
A.carolinensis ODC		A	A																														33
Trypanosoma brucei ODC		A	A																														30.2
X.laevis ODC		A	A																														33.6

**Table 5.3: Sequence analysis of ODC and antizyme inhibitor, comparing the active site residues of ODC/AZI from various organisms. Abbreviation denoted:-** C<sup>f</sup> for cofactor binding; B<sup>s</sup> salt bridge formation; S substrate binding residues; I<sup>f</sup> interface of dimer ; D<sup>i</sup> important for dimer formation. Species with the name of protein are shown on left side. **Colour indication:-** Violet columns signifies the mutation in AZI; Orange columns signifies the mutated residues in *E. histolytica* ODC which are similar to AZI; Gray shows the unique mutations in *Eh*ODC which is neither conserved in ODC nor in AZI; Blue indicate the mutation in *Eh*ODC which are rarely found in AZI and functional ODC; Olive color point out the mutations in *Eh*ODC which are similar to some ODC. Sequence analysis and numbering has been done according to *Eh*ODC. Residues which are not conserved have been shown by single letter codon and conserved “wild type” left blank. Δ indicates the deleted amino acid. % identity indicates the ODC sequence identity with the *Eh*ODC sequence (Ivanov *et al.*, 2010).

From various mutational studies, it is reported that Lys 57 (numbering is according to *Eh*ODC) is important as it forms Schiff base with PLP which is later displaced by L-ornithine which undergoes decarboxylation through nucleophilic attack via Cys334' (Osterman *et al.*, 1999; Myers *et al.*, 2001; Tsirka *et al.*, 1993). However, these residues are conserved in both functional ODCs and AZI except in few AZIs. Out of sixteen PLP binding residues, AZIs have major mutations in five positions. Thus, it may render low affinity of cofactor towards active site pocket. However, interestingly, *Eh*ODC has a mutation at 99 positions where Ala is substituted by Ser. The same substitution of Ala to Ser is also observed in few AZIs including AZI from *Danio rerio*, *Tetraodon nigroviridis* and *Anolis crolinensis* (Table 5.3) (Hascilowicz, 2002).

In Human ODC, four residues Tyr331, Asp332, Cys360 and Asp361 are reported to be key active site residues which interact with L-ornithine. In all functional ODCs these four residues are highly conserved and Cys360 plays a critical role in decarboxylation catalysis (Myers *et al.*, 2001; Tsirka *et al.*, 1993). However, *Eh*ODC is exception where Tyr and two Asp residues are substituted by His, Glu and Asn respectively.

The mutations of His296 and Asn335 are unique in case of *Eh*ODC as these two residues are substituted by Tyr and Asp respectively and conserved in both AZI and functional ODC. The mutation of Glu shows similarity with AZI as in maximum AZIs, out of four substrate binding



residues only Asp is substituted by Glu. In case of human and other functional ODCs, Tyr331 contributes to form an aromatic zipper responsible for complementary packing in two monomers (Grishin *et al.*, 1999; Kern *et al.*, 1999). In AZI this is mutated to Ser rendering a loose contact between monomers. But in *Eh*ODC, same residue is substituted by Phe performing same job in aromatic zipper. The mutation of Tyr to Phe is also reported in *Plasmodium falciparum*, *Leishmania donovani* and *Glycine max* ODCs (Table 5.3) (Jackson *et al.*, 2003; Ivanov *et al.*, 2010).

AZI genes have accumulated mutation in key active site residues which are important for ODC activity. In *Petromyzon marinus*, the ortholog of AZI as classified on the basis of conserved key amino acid residues is found to be functional ODC (Ivanov *et al.*, 2007). In contrast to this, *Aedes aegypti* ODC is found to be non-functional (Ivanov *et al.*, 2010). The mutation at active site, ranging from one residue to fourteen residues may cause the inactivation of the enzyme. In *T. nigroviridis*, 11 residues are altered in active site where as in mammals 4 residues are altered to make a functional ODC to a nonfunctional homolog. However, in *Drosophila melanogaster* ODC paralogs, though all 18 key residues of active site are conserved, but a single mutation of Asp332Tyr hinder dimer formation in addition to cofactor and substrate binding, thus cause to express the nonfunctional ODC (Table 5.3) (Ivanov *et al.*, 2010).

The evolutionary relationship of ODC and AZI can be evaluated by considering the root of phylogenetic tree which connects the branch of both homologs. Evidences indicated that both the homologs are from same subfamily and have evolved and diverged according to their function. In phylogenetic tree, the group of AZI and ODC make different clusters according to the sequence alignment. Interestingly *Eh*ODC is clustering to the ODC group just beneath the *Aedes aegypti* which is a nonfunctional ODC due to His197Asn and Asp332Arg substitution as given in table and sequence alignment. (Table 5.3, Figure 5.11, 5.12). If ODC of *Aedes aegypti* presents at the border line of functional ODCs and nonfunctional AZI then *Eh*ODC is also evolutionarily close to it. These evidences of sequence phylogeny and alignment profile of *Eh*ODC allow us to establish the fact that it can be considered as a bridge between active ODC and inactive AZI.



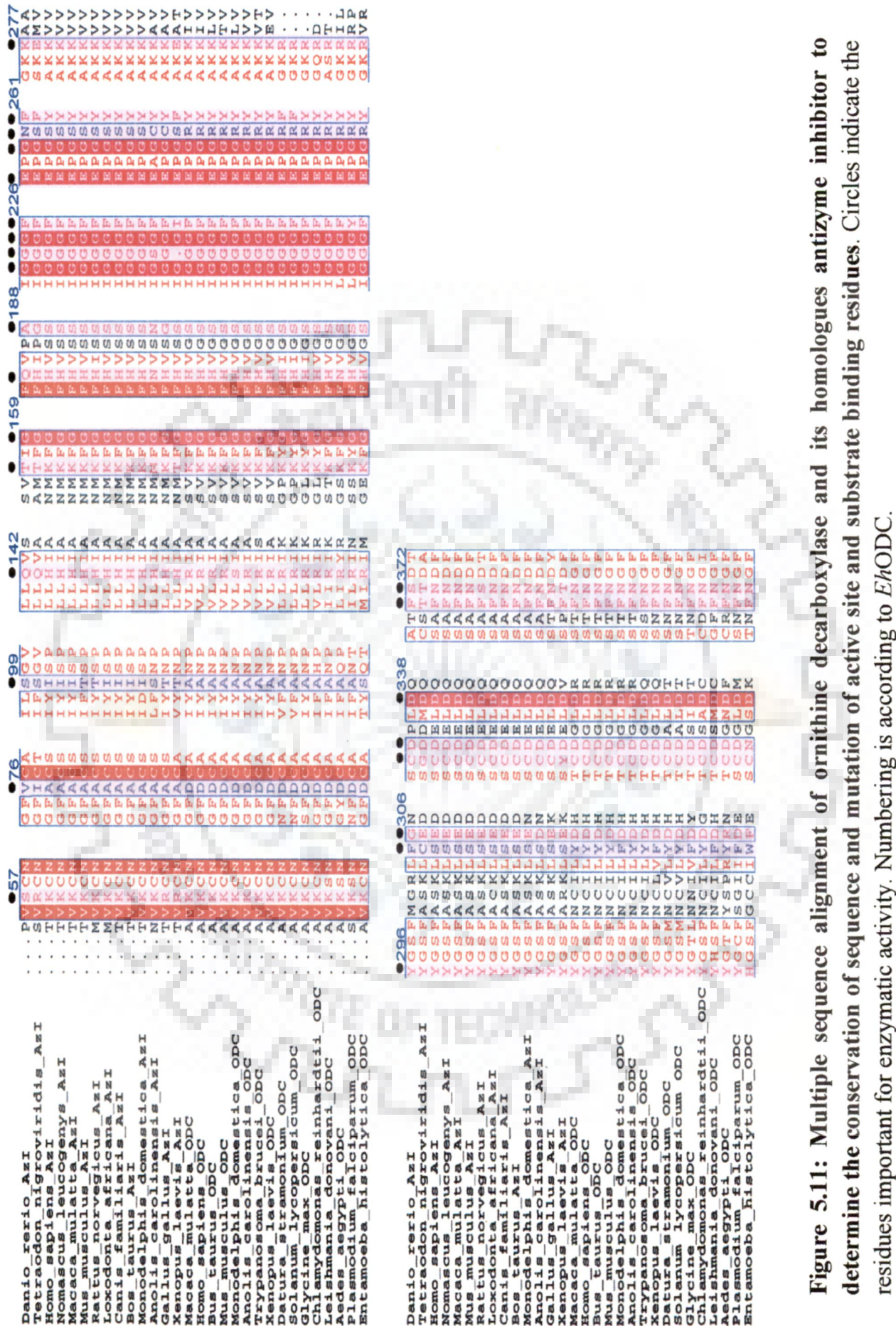
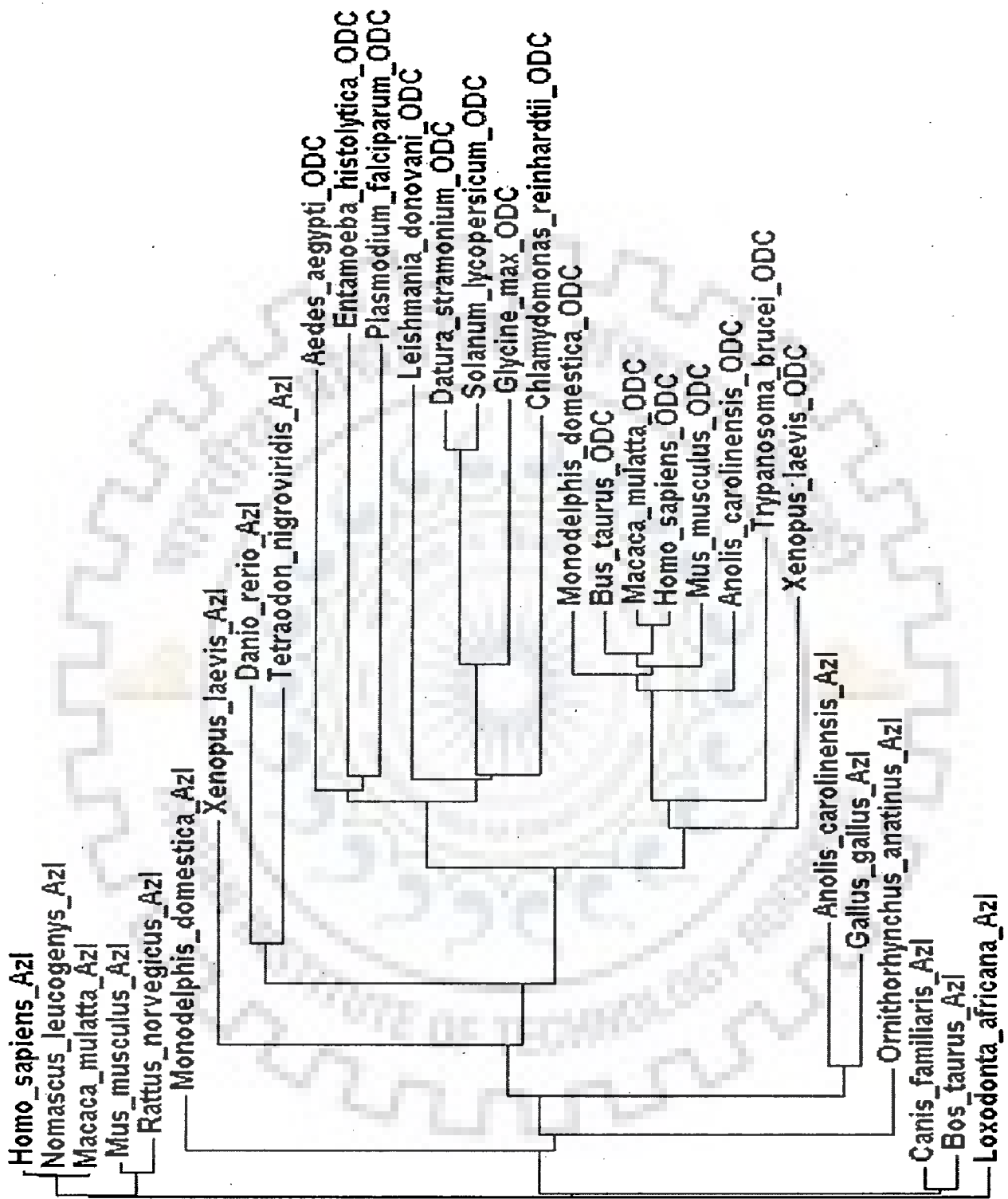


Figure 5.11: Multiple sequence alignment of ornithine decarboxylase and its homologues antizyme inhibitor to determine the conservation of sequence and mutation of active site and substrate binding residues. Circles indicate the residues important for enzymatic activity. Numbering is according to *Eh*ODC.



### Figure 5.12: Phylogenetic relationship of *Eh*ODC with antizyme Inhibitor and ODC:

Sequence of ODC and their evolutionary related homologous were retrieved from various sources. **Antizyme inhibitor** of *Homo sapiens* (BAA23593.1), *Nomascus leucogenys* (XP\_003256127.1), *Macaca mulatta* (XP\_002805501.1), *Mus musculus* (AAB87464.1), *Rattus norvegicus* (BAA23594.1), *Monodelphis domestica* (XP\_001369332.1), *Xenopus laevis* (NP\_001087584.1), *Danio rerio* (BAB84695.1), *Tetraodon nigroviridis* (ENSTNIT00000008148.1), *Anolis carolinensis* (XP\_003219500.1), *Gallus gallus* (NP\_001008729.1), *Ornithorhynchus anatinus* (XP\_001506230.1), *Canis familiaris* (XP\_849306.1), *Bos Taurus* (NP\_001076080.1), *Loxodonta africana* (XP\_003408472.1). **Ornithine decarboxylase sequence from** *Aedes aegypti* (EAT48998.1), *Entamoeba histolytica* (AAX35675.1), *Plasmodium falciparum* (AAF14518.1), *Leishmania donovani* (AAA29259.1), *Datura stramonium* (CAA61121.1), *Solanum lycopersicum* (NP\_001234616.1), *Glycine max* (CAD91349.1), *Chlamydomonas reinhardtii* (CAE46409.1), *Monodelphis domestica* (XP\_001371947.1), *Bos Taurus* (AAA92339.1), *Macaca mulatta* (NP\_001185615.1), *Homo sapiens* (NP\_002530.1), *Mus musculus* (NP\_038642.2), *Anolis carolinensis* (XP\_003215471.1), *Trypanosoma brucei* (AAA30219.1), *Xenopus laevis* (CAA39760.1).

### 5.7 Analysis of AZ binding sequence in *Eh*ODC

AZI lacks decarboxylase activity but possess higher affinity towards antizyme (Su *et al.*, 2009). The high binding efficiency of AZI towards AZ as compared to ODC has been studied in detail. Recent studies revealed that the residues K125 and K140 of AZI (human AZI) play significant role in binding to antizyme.

The differences in residues of ODC and AZI are responsible for the differential binding affinity towards the antizyme. The K125 and K140 of AZI introduce extra charge to the AZ binding site as compared to N125 and M140 which are neutral. In case of *Eh*ODC residue H present corresponds to K125/N125 of AZI/ODC which is having physiological properties similar to K in *Hs*AZI. In contrast to this, residue K140/M140 substituted by Q in *Eh*ODC which is neutral amino acid residue as in *Hs*ODC (Figure 5.13). The binding efficiency of ODC from *P. falciparum* can be considered as strongly towards antizyme due to the presence of K125/K140 interaction similar to AZI.



	117	140
<i>H. sapience</i> ODC	VSQIKYAANN	GVQMMTFDSEVELM
<i>H. sapience</i> AZI	VSQIKYAAK	VGVNILTCDNEIELK
<i>T. brucei</i> ODC	ISHIRYARD	SGVDVMTFDCVDELE
<i>P. bursaria</i> ODC	IDDLIFAKD	QGVDIATFDSSFELD
<i>L. donovani</i> ODC	LGDLREAQA	CGVTYVTVDNPLEME
<i>E. histolytica</i> ODC	YNQLIEASH	HLGINHTIVDSIDEVQ
<i>P. falciparum</i> ODC	INSLIYARKEN	INLCTFDNLDELK
	. : * . : * * :	

**Figure 5.13: Antizyme binding sequence of Human ODC (HsODC) is compared with EhODC. Residues 117-140 in HsODC, HsAZI and other ODC were considered for comparative analysis.** Antizyme binding region of *homo sapience*, *Trypanosome brucei*, *Paramecium bursaria*, *Leishmania donovani*, *Entamoeba histolytica* and *plasmodium falciparum* were aligned by ClustalW.

Interestingly the phylogeny analysis showed the close sequence similarity of *EhODC* with *P. falciparum*. Here we can consider the more affinity of *EhODC* towards antizyme as compared to active ODC which is one more evidence allow us to relate it as a bridge between AZI and ODC (Figure 5.12).

The antizyme has been reported to exist in wide range of organisms from higher eukaryotes to prokaryotes (Liu *et al.*, 2011; Palanimurugan *et al.*, 2004; Lioliou *et al.*, 2004). Different forms of AZs (AZ1, AZ2 and AZ3) have been reported possessing different roles in cell. Polyamines can induce a +1 translational frameshift on AZ mRNA and result in complete AZ protein synthesis (Miyazaki *et al.*, 1992; Hayashi *et al.*, 1985, 1997). Genome sequence analysis of *E. histolytica* using human AZ nucleotide as a query sequence in BLAST search was showing hypothetical sequence identity of 20-30% but sequence coverage was insufficient to predict anything. Without any confirmation about the presence of antizyme sequence in the genome, regulatory role of ODC as an AZI cannot be designated. It can be predicted here that

sequence of *Eh*ODC substitution towards AZI also resulted in the development of resistance towards DFMO a well-known drug against protozoan diseases.

## 5.8 Conclusion

In present chapter, we successfully determined the 3D structure of *Eh*ODC. The structure was found to be a tetramer composed of two dimers in one asymmetric unit. In contrast to these results, protein was found to be dimer in solution. Interestingly, the dimer in crystal showed extensive interactions with their symmetry mate within the unit cell. Based on sequence analysis, and investigation of evolutionary aspects we unveil many unique characteristics of *Eh*ODC. One important feature is, conservation of amino acids important for cofactor binding with other ODCs except S99. Second feature is substitution of all substrate binding residues except C334. Out of all substitution in *Eh*ODC some are unique to *Eh*ODC as H296 and N335 which are neither showing similarity to ODC nor to AZIs. One substitutions as E306 was identical to non-functional AZIs.

The extensive investigation revealed that even a single mutation at the active site may result in the formation of non-functional enzyme. Comparison of *Eh*ODC sequence with AZI and ODC revealed many residues which were identical to former but some residues important for activity were similar to ODC. More specifically the cofactor binding amino acids were conserved as ODC and substrate binding site was randomly mutated. The sequence analysis and evolutionary relationship of *Eh*ODC with AZI and ODC allow us to place it as an evolutionary bridge between AZI and ODC. This can be safely elaborated here as *Eh*ODC has evolved in the direction of AZI associated with function properties of ODC.

In addition to this, docking studies and structure analysis revealed inefficient binding of DFMO to substrate binding pocket. The DFMO is associated with two fluorine molecules which results in the inefficient accommodation due to substitution of Asp335 to Asn335 (numbering according to *Eh*ODC sequence) having NH<sub>2</sub> group instead of C=O group of Asp which is incapable of interacting with –NH group of DFMO. In addition another mutation of Asp332 to Glu332 which is having one methyl group long side chain and leave insufficient space for the substrate based inhibitor molecule.



- Abrahamsen MS, Li RS, Dietrich-Goetz W, Morris DR. Multiple DNA elements responsible for transcriptional regulation of the ornithine decarboxylase gene by protein kinase A. *J Biol Chem.* 1992, 267: 18866-18873.
- Adams PD, Afonine PV, Bunkóczi G, Chen VB, Davis IW, et al. PHENIX: a comprehensive Python-based system for macromolecular structure solution. *Acta Crystallogr D Biol Crystallogr.* 2010, 66: 213-221.
- Aguilar-Díaz H, Díaz-Gallardo M, Laclette JP, Carrero JC. In vitro induction of *Entamoeba histolytica* cyst-like structures from trophozoites. *PLoS Negl Trop Dis.* 2010, 4: e607.
- Alanimurugan R, Scheel H, Hofmann K, Dohmen RJ. Polyamines regulate their synthesis by inducing expression and blocking degradation of ODC antizyme. *EMBO J.* 2004, 23: 4857-4867.
- Albeck S, Dym O, Unger T, Snapir Z, Bercovich Z, et al. Crystallographic and biochemical studies revealing the structural basis for antizyme inhibitor function. *Protein Sci.* 2008, 17: 793-802.
- Alexander FW, Sandmeier E, Mehta PK, Christen P. Evolutionary relationships among pyridoxal-5'-phosphate-dependent enzymes. Regio-specific alpha, beta and gamma families. *Eur J Biochem.* 1994, 219: 953-960.
- Alhonen-Hongisto L, Pösö H, Jänne J. Inhibition of polyamine accumulation and cell proliferation by derivatives of diaminopropane in *Ehrlich ascites* cells grown in culture. *Biochim Biophys Acta.* 1979, 564: 473-487.
- Almud JJ, Oliveira MA, Kern AD, Grishin NV, Phillips MA, et al. Crystal structure of human ornithine decarboxylase at 2.1 Å resolution: structural insights to antizyme binding. *J Mol Biol.* 2000, 295: 7-16.
- Altschul SF, Gish W, Miller W, Myers EW, Lipman DJ. Basic local alignment search tool. *J Mol Biol.* 1990, 215: 403-410.
- Anderson IJ, Loftus BJ. *Entamoeba histolytica*: observations on metabolism based on the genome sequence. *Exp Parasitol.* 2005, 110: 173-177.

- Andrade MA, Chacón P, Merelo JJ, Morán F. Evaluation of secondary structure of proteins from UV circular dichroism using an unsupervised learning neural network. *Prot Eng*. 1993, 6: 383-390.
- Apic G, Gough J, Teichmann SA. Domain combinations in archaeal, eubacterial and eukaryotic proteomes. *J Mol Biol*. 2001, 310: 311-325.
- Argüello C, Valenzuela B, Rangel E. Structural organization of chromatin during the cell cycle of *Entamoeba histolytica* trophozoites. *Arch Med Res*. 1992, 23: 77-80.
- Ariyanayagam MR, Fairlamb AH. *Entamoeba histolytica* lacks trypanothione metabolism. *Mol Biochem Parasitol*. 1999, 103: 61-69.
- Arteaga-Nieto P, Lopez-Romero E, Teran-Figueroa Y, Cano-Canchola C, Luna Arias JP, et al. *Entamoeba histolytica*: purification and characterization of ornithine decarboxylase. *Exp Parasitol*. 2002, 101: 215-222.
- Arteaga-Nieto P, Villagómez-Castro JC, Calvo-Méndez C, López-Romero E. Partial purification and characterization of ornithine decarboxylase from *Entamoeba histolytica*. *Int J Parasitol*. 1996, 26: 253-260.
- Atmar VJ, Kuehn GD. Phosphorylation of ornithine decarboxylase by a polyamine-dependent protein kinase. *Proc Natl Acad Sci USA*. 1981, 78: 5518-5522.
- Auvinen M, Paasinen A, Andersson LC, Hölttä E. Ornithine decarboxylase activity is critical for cell transformation. *Nature*. 1992, 360: 355-358.
- Auvinen M, Laine A, Paasinen-Sohns A, Kangas A, Kangas L, et al. Human ornithine decarboxylase-overproducing NIH3T3 cells induce rapidly growing, highly vascularized tumors in nude mice. *Cancer Res*. 1997, 57: 3016-3025.
- Bacchi CJ, Nathan HC, Hutner SH, McCann PP, Sjoerdsma A. Polyamine metabolism: a potential therapeutic target in *trypanosomes*. *Science*. 1980, 210: 332-334.
- Bacchi CJ, Yarlett N. Polyamine metabolism as chemotherapeutic target in protozoan parasites. *Mini Rev Med Chem*. 2002, 2: 553-563.
- Bacchi CJ, Yarlett N. Polyamine metabolism in *Biochemistry and Molecular Biology of Parasites* edited by Marr JJ and Müller M academic press limited. London. 1995, 119-132.
- Back JW, de Jong L, Muijsers AO, de Koster CG. Chemical cross-linking and mass spectrometry for protein structural modeling. *J Mol Biol*. 2003, 331: 303-313.

- Badolo L, Berlaimont V, Helson-Cambier M, Hanocq M, Dubois J. Simple and rapid enzymatic assay of ornithine decarboxylase activity. *Talanta*. 1999, 48: 127-134.
- Bakker-Grunwald T, Martin JB, Klein G. Characterization of glycogen and amino acid pool of *Entamoeba histolytica* by <sup>13</sup>C-NMR spectroscopy. *J Eukaryot Microbiol*. 1995, 42: 346-349.
- Balaña-Fouce R, Escribano MI, Alunda JM. *Leishmania infantum*: polyamine biosynthesis and levels during the growth of promastigotes. *Int J Biochem*. 1991, 23: 1213-1217.
- Balasundaram D, Tabor CW, Tabor H. Spermidine or spermine is essential for the aerobic growth of *Saccharomyces cerevisiae*. *Proc Natl Acad Sci USA*. 1991, 88: 5872-5876.
- Balasundaram D, Tabor CW, Tabor H. Oxygen toxicity in a polyamine-depleted spe2 delta mutant of *Saccharomyces cerevisiae*. *Proc Natl Acad Sci USA*. 1993, 90: 4693-4697.
- Bansal D, Sehgal R, Chawla Y, Mahajan RC, Malla N. In vitro activity of antiamebic drugs against clinical isolates of *Entamoeba histolytica* and *Entamoeba dispar*. *Ann Clin Microbiol Antimicrob*. 2004, 3: 27.
- Beck WT, Bellantone RA, Canellakis ES. Puromycin stimulation of rat liver ornithine decarboxylase activity. *Nature*. 1973, 241: 275-277.
- Bendesky A, Menéndez D, Ostrosky-Wegman P. Is metronidazole carcinogenic? *Mutat Res*. 2002, 511: 133-144.
- Bernstein HG, Müller M. Increased immunostaining for L-ornithine decarboxylase occurs in neocortical neurons of Alzheimer's disease patients. *Neurosci Lett*. 1995, 186: 123-126.
- Bernstein HG, Müller M. The cellular localization of the L-ornithine decarboxylase/polyamine system in normal and diseased central nervous systems. *Prog Neurobiol*. 1999, 57: 485-505.
- Bey P, Danzin C, Van Dorsselaer V, Mamont P, Jung M, et al. Analogues of ornithine as inhibitors of ornithine decarboxylase. New deductions concerning the topography of the enzyme's active site. *J Med Chem*. 1978, 21: 50-55.

- Bhattacharya A, Prasad R, Sacks DL. Identification and partial characterization of a lipophosphoglycan from a pathogenic strain of *Entamoeba histolytica*. *Mol Biochem Parasitol*. 1992, 56: 161-168.
- Bhattacharya M, Das AK. Inverted repeats in the promoter as an autoregulatory sequence for TcrX in *Mycobacterium tuberculosis*. *Biochem Biophys Res Commun*. 2011, 415: 17-23.
- Bienz S, Detterbeck R, Ensich C, Guggisberg A, Häusermann U, et al. Putrescine, spermidine, spermine, and related polyamine alkaloids. *Alkaloids Chem Biol*. 2002, 58: 83-338.
- Birkholtz LM, Williams M, Niemand J, Louw AI, Persson L, et al. Polyamine homeostasis as a drug target in pathogenic protozoa: peculiarities and possibilities. *Biochem J*. 2011, 438: 229-244.
- Bitonti AJ, Dumont JA, Bush TL, Edwards ML, Stemerick DM, et al. Bis (benzyl)polyamine analogues inhibit the growth of chloroquine-resistant human malaria parasites (*Plasmodium falciparum*) in vitro and in combination with alpha-difluoromethylornithine cure murine malaria. *Proc Natl Acad Sci U S A* 1989, 86: 651-655.
- Borrell A, Culianez-Macia FA, Altabella T, Bestford RT, Flores D. et al. Arginine decarboxylase is localized in chloroplast. *Plant Physiol*. 1995, 109: 771-776.
- Brahe B, Harmfl P, Nicotera P, Orrenlus S. Spermine prevents endonuclease activation and apoptosis in thymocytes. *Exp Cell Res*. 1991, 195: 323-329.
- Brooks HB, Phillips MA. Characterization of the reaction mechanism for *Trypanosoma brucei* ornithine decarboxylase by multiwavelength stopped-flow spectroscopy. *Biochemistry*. 1997, 36: 15147-15155.
- Brüne B, Lapetina EG. Phosphorylation of nitric oxide synthase by protein kinase A. *Biochem Biophys Res Commun*. 1991, 181: 921-926.
- Brünger AT, Adams PD, Clore GM, DeLano WL, Gros P, et al. Crystallography & NMR system: A new software suite for macromolecular structure determination. *Acta Crystallogr D Biol Crystallogr*. 1998, 54: 905-921.
- Brunger AT. Version 1.2 of the Crystallography and NMR System, *Nature Protocols*. 2007, 2: 2728-2733.

- Burtin D, Michael AJ. Overexpression of arginine decarboxylase in transgenic plants. *Biochem J*. 1997, 325: 331-337.
- Cai D, Deng K, Mellado W, Lee J, Ratan RR, et al. Arginase I and polyamines act downstream from cyclic AMP in overcoming inhibition of axonal growth MAG and myelin in vitro. *Neuron*. 2002, 35: 711-719.
- Calvo-Méndez C, Villagómez-Castro JC, López-Romero E. Ornithine decarboxylase activity in *Entamoeba invadens*. *Int J Parasitol*. 1993, 23: 847-852.
- Canellakis ES, Viceps-Madore D, Kyriakidis DA, Heller JS. The regulation and function of ornithine decarboxylase and of the polyamines. *Curr Top Cell Regul*. 1979, 15: 155-202.
- Canellakis ES, Paterakis AA, Huang SC, Panagiotidis CA, Kyriakidis DA. Identification, cloning, and nucleotide sequencing of the ornithine decarboxylase antizyme gene of *Escherichia coli*. *Proc Natl Acad Sci USA*. 1993, 90: 7129-7133.
- Carpenter BM, Gancz H, Benoit SL, Evans S, Olsen CH, et al. Mutagenesis of conserved amino acids of *Helicobacter pylori* fur reveals residues important for function. *J Bacteriol*. 2010, 192: 5037-5052.
- Casero RA Jr, Frydman B, Stewart TM, Woster PM. Significance of targeting polyamine metabolism as an antineoplastic strategy: unique targets for polyamine analogues. *Proc West Pharmacol Soc*. 2005, 48: 24-30.
- Celano P, Baylin SB, Casero RA. Polyamines differentially modulate the transcription of growth-associated genes in human colon carcinoma cells. *J Biol Chem*. 1989, 264: 8922-8927.
- Chapman SK, Martin M, Hoover MS, Chiou CY. Ornithine decarboxylase activity and the growth of neuroblastoma cells. The effects of bromoacetylcholine, bromoacetate and 1,3-diaminopropane. *Biochem Pharmacol*. 1978, 27: 717-721.
- Chattopadhyay MK, Tabor CW, Tabor H. Polyamine deficiency leads to accumulation of reactive oxygen species in a spe2Delta mutant of *Saccharomyces cerevisiae*. *Yeast*. 2006, 23: 751-761.
- Chattopadhyay MK, Murakami Y, Matsufuji S. Antizyme regulates the degradation of ornithine decarboxylase in fission yeast *Schizosaccharomyces pombe*. Study in the spe2 knockout strains. *J Biol Chem*. 2001, 276: 21235-21241.



- Choi KH, Lai V, Foster CE, Morris AJ, Tolan DR, et al. New superfamily members identified for Schiff-base enzymes based on verification of catalytically essential residues. *Biochemistry* 2006, 45: 8546-8555.
- Christen P, Mehta PK. From cofactor to enzymes. The molecular evolution of pyridoxal-5'-phosphate-dependent enzymes. *Chem Rec.* 2001, 1: 436-447.
- Cirl C, Wieser A, Yadav M, Duerr S, Schubert S, et al. Subversion of Toll-like receptor signaling by a unique family of bacterial Toll/interleukin-1 receptor domain-containing proteins. *Nat Med.* 2008, 14: 399-406.
- Clackson T, Wells JA. A hot spot of binding energy in a hormone-receptor interface. *Science.* 1995, 267: 383-386.
- Clackson T. Redesigning small molecule-protein interfaces. *Curr Opin Struct Biol.* 1998, 8: 451-458.
- Clark CG, Alsmark UC, Tazreiter M, Saito-Nakano Y, Ali V, et al. Structure and content of the *Entamoeba histolytica* genome. *Adv Parasitol.* 2007, 65: 51-190.
- Coffino P. Polyamines in spermiogenesis: Not now, darling. *Proc Natl Acad Sci USA.* 2000, 97: 4421-4423.
- Coffino P. Antizyme, a mediator of ubiquitin-independent proteasomal degradation. *Biochimie.* 2001, 83: 319-323.
- Coffino P. Degradation of ornithine decarboxylase. Ubiquitin and the biology of the cell 1998: 411-427.
- Cohavi O, Tobi D, Schreiber G. Docking of antizyme to ornithine decarboxylase and antizyme inhibitor using experimental mutant and double mutant cycle data. *J Mol Biol.* 2009, 390: 503-515.
- Coleman CS, Stanley BA, Pegg AE. Effect of mutations at active site residues on the activity of ornithine decarboxylase and its inhibition by active site-directed irreversible inhibitors. *J Biol Chem.* 1993, 268: 24572-24579.
- Coleman CS, Stanley BA, Visanath R, Pegg AE. Rapid exchange of subunits of mammalian ornithine decarboxylase. *J Biol Chem.* 1994, 269: 3155-3158.
- Coons T, Hanson S, Bitonti AJ, McCann PP, Ullman B. Alpha-difluoromethylornithine resistance in *Leishmania donovani* is associated with increased ornithine decarboxylase activity. *Mol Biochem Parasitol.* 1990, 39: 77-89.

- Corley E, Wolosluk RA, Hertig CM. Regulation of the activation of chloroplast fructose-1, 6-bis phosphatase. Inhibition by spermidine and spermine. *Biochem Biophys Res Commun.* 1983, 115: 707-714.
- Corpet F. Multiple sequence alignment with hierarchical clustering. *Nucl Acids Res.* 1988, 16: 10881-10890.
- Coulombe B. DNA wrapping in transcription initiation by RNA polymerase II. *Biochem Cell Biol.* 1999, 77: 257-264.
- Cross JB, Thompson DC, Rai BK, Baber JC, Fan KY et al. Comparison of several molecular docking programs: pose prediction and virtual screening accuracy. *J Chem Inf Model.* 2009, 49: 1455-1474.
- Datta N, Schell MB, Roux SJ. Spermine stimulation of a nuclear NII kinase from pea plumules and its role in the phosphorylation of a nuclear polypeptide. *Plant Physiol.* 1987, 84: 1397-1401.
- Davies GE, Stark GR. Use of dimethyl suberimidate, a cross-linking reagent, in studying the subunit structure of oligomeric proteins. *Proc Natl Acad Sci USA.* 1970, 66: 651-656.
- Davis RH, Morris DR, Coffino P. Sequestered end products and enzyme regulation: the case of ornithine decarboxylase. *Microbiol Rev.* 1992, 56: 280-290.
- Deng AY, Gu L, Rapp JP, Szpirer C, Szpirer J. Chromosomal assignment of 11 loci in the rat by mouse-rat somatic hybrids and linkage. *Mamm Genome.* 1994, 5: 712-716.
- DeLano WL. The PyMol molecular graphics system. San Carlos, CA, USA: *DeLano Scientific.* 2002, <http://www.pymol.org>.
- DiGangi JJ, Seyfzadeh M, Davis RH. Ornithine decarboxylase from *Neurospora crassa*. Purification, characterization, and regulation by inactivation. *J Biol Chem.* 1987, 262: 7889-7893.
- Douki T, Bretonniere Y, Cadet J. Protection against radiation-induced degradation of DNA bases by polyamines. *Radiat Res.* 2000, 153: 29-35.
- Drolet G, Dumbroff EB, Legge RL, Thompson JE. Radical scavenging properties of polyamines. *Phytochem.* 1986, 25: 367-371.

- Dufe VT, Ingner D, Heby O, Khomutov AR, Persson L. A structural insight into the inhibition of human and *Leishmania donovani* ornithine decarboxylases by 1-amino-oxy-3-aminopropane. *Biochem J.* 2007, 405: 261-268.
- Emsley P, Cowtan K. Coot: model-building tools for molecular graphics. *Acta Crystallogr D Biol Crystallogr.* 2004, 60: 2126-2132.
- Eliot AC, Kirsch JF. Pyridoxal phosphate enzymes: mechanistic, structural, and evolutionary considerations. *Annu Rev Biochem.* 2004, 73: 383-415.
- Elnekave K, Siman-Tov R, Ankri S. Consumption of L-arginine mediated by *Entamoeba histolytica* L-arginase (*EhArg*) inhibits amoebicidal activity and nitric oxide production by activated macrophages. *Parasite Immunol.* 2003, 25: 597-608.
- Espinosa-Cantellano M, Martínez-Palomo A, Pathogenesis of intestinal amebiasis: from molecules to disease. *Clin Microbiol Rev.* 2000, 13: 318-331.
- Evans PT, Malmberg RL. Do polyamines have roles in plant development? *Annu. Rev. Plant Physiol.* 1989, 40: 235-269.
- Fadoulglou VE, Kokkinidis M, Glykos NM. Determination of protein oligomerization state: two approaches based on glutaraldehyde crosslinking. *Anal Biochem* 2008, 373: 404-406.
- Fahey RC, Newton GL, Arrick B, Overdank-Bogart T, Aley SB. *Entamoeba histolytica*: a eukaryote without glutathione metabolism. *Science.* 1984, 224: 70-72.
- Fairlamb AH, Cerami A. Metabolism and functions of trypanothione in the Kinetoplastida. *Annu Rev Microbiol.* 1992, 46: 695-729.
- Feuerstein BG, Pattabiraman N, Marton, LJ. Spermine-DNA interactions: a theoretical study. *Proc Natl Acad Sci* 1986, 83: 5948-5952.
- Feuerstein BG, Pattabiraman N, Marton LJ. Molecular dynamics of spermine-DNA interactions: sequence specificity and DNA bending for a simple ligand. *Nucleic Acids Res.* 1989 17: 6883-6892.
- Feuerstein BG, Pattabiraman N, Marton LJ. Molecular mechanics of the interaction of spermine with DNA: DNA bending as a result of ligand binding. *Nucleic Acids Res.* 1990, 18: 1271-1282.
- Feuerstein BG, Williams LD, Basu HS, Marton LJ. Implications and concepts of polyamine-nucleic acid interactions. *J Cell Biochem.* 1991, 46: 37-47.

- Field CJ, Schley PD. Evidence for potential mechanisms for the effect of conjugated linoleic acid on tumor metabolism and immune function: lessons from n-3 fatty acids. *Am J Clin Nutr.* 2004, 79: 1190S-1198S.
- Frieden C. Slow transitions and hysteretic behavior in enzymes. *Annu Rev Biochem.* 1979, 48: 471-489.
- Freire E. The propagation of binding interactions to remote sites in proteins: analysis of the binding of the monoclonal antibody D1.3 to lysozyme. *Proc Natl Acad Sci USA.* 1999, 96: 10118-10122.
- Friesner RA, Banks JL, Murphy RB, Halgren TA, Klicic JJ, Glide: a new approach for rapid, accurate docking and scoring. 1. Method and assessment of docking accuracy. *J Med Chem.* 2004, 47: 1739-1749.
- Fong WF, Heller JS, Canellakis ES. The appearance of an ornithine decarboxylase inhibitory protein upon the addition of putrescine to cell cultures. *Biochim Biophys Acta.* 1976, 428: 456-465.
- Fujita K, Murakami S, Hayashi S. A macromolecular inhibitor of the antizyme to ornithine decarboxylase. *Biochem J.* 1982, 204: 647-653.
- Gathiram V, Jackson TF. A longitudinal study of asymptomatic carriers of pathogenic zymodemes of *Entamoeba histolytica*. *S Afr Med J.* 1987; 72: 669-672.
- Geourjon C, Deléage G. SOPMA: significant improvements in protein secondary structure prediction by consensus prediction from multiple alignments. *Comput Appl Biosci.* 1995, 11: 681-684.
- Ghoda L, Van Daalen Wetters T, Macrae M., Ascherman, D., Coffino, P. Prevention of rapid intracellular degradation of ODC by a carboxyl-terminal truncation. *Science* 1989, 243: 1493-1495.
- Ghoda L, Sidney D, Macrae M, Coffino P. Structural elements of ornithine decarboxylase required for intracellular degradation and polyamine-dependent regulation. *Mol Cell Biol.* 1992, 12: 2178-2185.
- Gibrat JF, Madej T, Bryant SH. Surprising similarities in structure comparison. *Curr Opin Struct Biol.* 1996, 6: 377-385.

- Gillin FD, Reiner DS, McCann PP. Inhibition of growth of *Giardia lamblia* by difluoromethylornithine, a specific inhibitor of polyamine biosynthesis. *J Protozool.* 1984, 31: 161-163.
- Gopal R (1997). MA Thesis, University of Texas, Austin, Texas, USA.
- Gonzalez NS, Ceriani C, Algranati ID. Differential regulation of putrescine uptake in *Trypanosoma cruzi* and other trypanosomatids. *Biochem Biophys Res Commun.* 1992, 188: 120-128.
- Gordon R, Cornect M, Walters BM, Hall DE, Brosnan ME. Polyamine Synthesis by the Mermithid Nematode *Romanomermis culicivorax*. *J Nematol.* 1989, 21: 81-86.
- Gouet P, Courcelle E, Stuart DI, Métoz F. ESPript: analysis of multiple sequence alignments in PostScript. *Bioinformatics.* 1999, 15: 305-308.
- Grishin NV, Phillips MA, Goldsmith EJ. Modeling of the spatial structure of eukaryotic ornithine decarboxylases. *Protein Sci.* 1995, 4: 1291-1304.
- Grishin NV, Osterman AL, Brooks HB, Phillips MA, Goldsmith EJ. X-ray structure of ornithine decarboxylase from *Trypanosoma brucei*: the native structure and the structure in complex with alpha-difluoromethylornithine. *Biochemistry.* 1999, 38: 15174-15184.
- Groppa MD, Benavides MP. Polyamines and abiotic stress: recent advances. *Amino Acids.* 2008, 34: 35-45.
- Guggisberg A, Hesse M. In: The alkaloids: Chemistry and Pharmacology (Brossi A., ed.) *Academic Press, New York.* 1983, 22: 85-188.
- Hackert ML, Carroll DW, Davidson L, Kim SO, Momany C, et al. Sequence of ornithine decarboxylase from *Lactobacillus sp.* strain 30a. *J Bacteriol.* 1994, 176: 7391-7394.
- Hafner EW, Tabor CW, Tabor H. Mutants of *Escherichia coli* that do not contain 1,4-diaminobutane (putrescine) or spermidine. *J Biol Chem.* 1979, 254: 12419-12426.
- Ha HC, Sirisoma NS, Kuppusamy P, et al. The natural polyamine spermine functions directly as a free radical scavenger. *Proc Natl Acad Sci USA.* 1998, 95: 11140-11145.
- Ha HC, Yager JD, Woster PA, Casero RA Jr. Structural specificity of polyamines and polyamine analogues in the protection of DNA from strand breaks induced by reactive oxygen species. *Biochem Biophys Res Commun.* 1998, 244: 298-303.



- Hamana K, Hamana H, Shinozawa T. Alterations in polyamine levels of nematode, earthworm, leech and planarian during regeneration, temperature and osmotic stresses. *Comp Biochem Physiol B Biochem Mol Biol*. 1995, 111: 91-97.
- Hayashi SI, Kameji T, Fujita K, Murakami Y, Kanamoto R et al. Molecular mechanism for the regulation of hepatic ornithine decarboxylase. *Advan Enzyme Regul*. 1985, 23: 311-329.
- Hayashi T, Matsufuji S, Hayashi SI. Characterization of the human antizyme gene. *Gene* 1997, 203: 131-139.
- Hayashi SI, Murakami Y: Rapid and regulated degradation of ornithine decarboxylase. *Biochem J*. 1995, 306: 1-10.
- Haque R, Huston CD, Hughes M, Houpt E, Petri WA Jr. Amebiasis. *N Engl J Med*. 2003, 348: 1565-1573.
- Haque R, Ali IM, Sack RB Jr, et al. Amebiasis and mucosal IgA antibody against the *Entamoeba histolytica* adherence lectin in Bangladeshi children. *J Infect Dis*. 2001, 183: 1787-1793.
- Haque R, Mondal D, Kirkpatrick BD, Akther, S, Farr BM, et al. Epidemiologic and clinical characteristics of acute diarrhea with emphasis on *Entamoeba histolytica* infections in preschool children in an urban slum of Dhaka, Bangladesh. *Am J Trop Med Hyg*. 2003, 69: 398-405.
- Haider N, Eschbach ML, Dias Sde S, et al. The spermidine synthase of the malaria parasite *Plasmodium falciparum*: molecular and biochemical characterization of the polyamine synthesis enzyme. *Mol Biochem Parasitol*. 2005, 142: 224-236.
- Haldar K. Lipid transport in *Plasmodium*. *Infect Agents Dis*. 1992, 1: 254-262.
- Hascilowicz T, Murai N, Matsufuji S, Murakami Y. Regulation of ornithine decarboxylase by antizymes and antizyme inhibitor in zebrafish (*Danio rerio*). *Biochim Biophys Acta*. 2002, 1578: 21-28.
- Heffner JE, Ali R, Jeevanandam M. Urinary excretion of polyamines in the adult respiratory distress syndrome. *Exp Lung Res*. 1995, 21: 275-286.
- Heller JS, Canellakis ES, Bussolotti DL, Coward JK. Stable multisubstrate adducts as enzyme inhibitors. Potent inhibition of ornithine decarboxylase by N-(5'-phosphopyridoxyl)-ornithine. *Biochim Biophys Acta*. 1975, 403: 197-207.

- Heller JS, Fong WF, Canellakis ES. Induction of a protein inhibitor to ornithine decarboxylase by the end products of its reaction. *Proc Natl Acad Sci USA*. 1976, 73: 1858-1862.
- Heller JS, Canellakis ES, Bussolotti DL, Coward JK. Potent inhibition of ornithine decarboxylase by N-(5'-phosphopyridoxyl)-ornithine. *Biochim Biophys Acta*. 1975, 403: 197-207.
- Hesse M, Modolell M, La Flamme AC, Schito M, Fuentes JM. Differential regulation of nitric oxide synthase-2 and arginase-1 by type 1/type 2 cytokines in vivo: granulomatous pathology is shaped by the pattern of L-arginine metabolism. *J Immunol*. 2001, 167: 6533-6544.
- Hess B, Kutzner C, van der Spoel D et al. GROMACS 4: Algorithms for highly efficient, load-balanced and scalable molecular simulation. *J Chem Theory Comput*. 2008, 4: 435-447.
- Hobbs CA, Gilmour SK. High levels of intracellular polyamines promote histone acetyltransferase activity resulting in chromatin hyperacetylation. *J Cell Biochem*. 2000, 77: 345-360.
- Hölttä, E, Hovi T. Polyamine depletion results in impairment of polyribosome formation and protein synthesis before onset of DNA synthesis in mitogen-activated human lymphocytes. *Eur J Biochem*. 1985, 152: 229-237.
- Hölttä E, Pohjanpelto P, Control of ornithine decarboxylase in Chinese hamster ovary cells by polyamines. Translational inhibition of synthesis and acceleration of degradation of the enzyme by putrescine, spermidine, and spermine. *J Biol Chem*. 1986, 261: 9502-9508.
- Hölttä E, Sistonen L, Alitalo K. The mechanisms of ornithine decarboxylase deregulation in c-Ha-ras oncogene-transformed NIH 3T3 cells. *J Biol Chem*. 1988, 263: 4500-4507.
- Hougaard DM, Fujiwara K, Larsson LI. Immunocytochemical localization of polyamines in normal and neoplastic cells. Comparisons to the formaldehyde-fluorescamine and o-phthalaldehyde methods. *Histochem J*. 1987, 19: 643-650.

- Hsu PC, Hung HC, Liao YF, Liu CC, Tsay GJ, et al. Ornithine decarboxylase attenuates leukemic chemotherapy drugs-induced cell apoptosis and arrest in human promyelocytic HL-60 cells. *Leuk Res.* 2008, 32: 1530-1540.
- Hua SB, Li X, Coffino P, Wang CC. Rat antizyme inhibits the activity but does not promote the degradation of mouse ornithine decarboxylase in *Trypanosoma brucei*. *J Biol Chem.* 1995, 270: 10264-10271.
- Husain A, Sato D, Jeelani G, Mi-ichi F, Ali V, et al. Metabolome analysis revealed increase in S-methylcysteine and phosphatidylisopropanolamine synthesis upon L-cysteine deprivation in the anaerobic protozoan parasite *Entamoeba histolytica*. *J Biol Chem.* 2010, 285: 39160-39170.
- Ichiba T, Matsufuji S, Miyazaki Y, Murakami Y, Tanaka K. Functional regions of ornithine decarboxylase antizyme. *Biochem Biophys Res Commun.* 1994, 200: 1721-1727.
- Igarashi K, Kashiwagi K, Kobayashi H, Ohnishi R, Kakegawa T, et al. Effect of polyamines on mitochondrial F1-ATPase catalyzed reactions. *J Biochem.* 1989, 106: 294-298.
- Igarashi K, Kashiwagi K. Polyamines: mysterious modulators of cellular functions, *Biochem Biophys Res Commun.* 2000, 271: 559-564.
- Isomaa VV, Pajunen AEI, Bardin CW, Jänne OA. Ornithine decarboxylase in mouse kidney. *J Biol Chem.* 1983, 258: 13036-13041.
- Ivanov IP, Gesteland RF, Atkins JF. A second mammalian antizyme: conservation of programmed ribosomal frameshifting. *Genomics* 1998, 52: 119-129.
- Ivanov IP, Firth AE, Atkins JF. Recurrent emergence of catalytically inactive ornithine decarboxylase homologous forms that likely have regulatory function. *J Mol Evol.* 2010 70: 289-302.
- Ivanov IP, Matsufuji S, Murakami Y, Gesteland RF, Atkins JF. Conservation of polyamine regulation by translational frameshifting from yeast to mammals. *EMBO J.* 2000, 19: 1907-1917.
- Ivanov IP, Rohrwasser A, Terreros DA, Gesteland RF, Atkins JF. Discovery of spermatogenesis, stage specific, ornithine decarboxylase antizyme: antizyme 3. *Proc Natl Acad Sci USA* 2000, 97: 4808-4813.

- Ivanov IP, Atkins JF. Ribosomal frameshifting in decoding antizyme mRNAs from yeast and protists to humans: close to 300 cases reveal remarkable diversity despite underlying conservation. *Nucleic Acids Res.* 2007, 35: 1842-1858.
- Jackson LK, Brooks HB, Myers DP, Phillips MA. Ornithine decarboxylase promotes catalysis by binding the carboxylate in a buried pocket containing phenylalanine 397. *Biochemistry.* 2003, 42: 2933-2940.
- Jackson LK, Brooks HB, Osterman AL, Goldsmith EJ, Phillips MA. Altering the reaction specificity of eukaryotic ornithine decarboxylase. *Biochemistry.* 2000, 39: 11247-11257.
- Jansonius JN. Structure, evolution and action of vitamin B6-dependent enzymes. *Curr Opin Struct Biol.* 1998, 8: 759-769.
- Jhingran A, Padmanabhan PK, Singh S, Anamika K, Bakre AA et al. Characterization of *Entamoeba histolytica* ornithine decarboxylase- like enzyme. *PLoS Negl Trop Dis.* 2008, 2: e115. doi:10.1371/journal.pntd.0000115.
- Jiang Y, Roberts SC, Jardim A, Carter NS, Shih S, et al. Ornithine decarboxylase gene deletion mutants of *Leishmania donovani*. *J Biol Chem.* 1999, 274: 3781-3788.
- Johnson TD. Polyamines and cerebral ischemia. *Prog Drug Res.* 1998, 50: 193-258.
- Jones DT. Protein secondary structure prediction based on position-specific scoring matrices. *J Mol Biol.* 1999, 292: 195-202.
- Kahana C. Antizyme and antizyme inhibitor, a regulatory tango. *Cell Mol Life Sci.* 2009, 66: 2479-2488.
- Kanamoto R, Utsunomiya K, Kameji T, Hayashi S. Effects of putrescine on synthesis and degradation of ornithine decarboxylase in primary cultured hepatocytes. *Eur J Biochem.* 1986, 154: 539-544.
- Karplus M, Ichiye T. Comment on a "fluctuation and cross correlation analysis of protein motions observed in nanosecond molecular dynamics simulations". *J Mol Biol.* 1996, 263: 120-122.
- Karukurichi KR, de la Salud-Bea R, Jahng WJ, Berkowitz DB. Examination of the new alpha-(2'Z-fluoro) vinyl trigger with lysine decarboxylase: the absolute stereochemistry dictates the reaction course. *J Am Chem Soc.* 2007, 129: 258-259.

- Katz A, Kahana C. Isolation and characterization of the mouse ornithine decarboxylase gene. *J Biol Chem.* 1988, 263: 7604-7609.
- Kauppinen RA, Alhonen LI. Transgenic animals as models in the study of the neurobiological role of polyamines. *Prog Neurobiol* 1995, 47: 545-563.
- Kerppola TK. Transcriptional cooperativity: bending over backwards and doing the flip. *Structure.* 1998, 6: 549-554.
- Keren-Paz A, Bercovich Z, Porat Z, Erez O, Brenner O, et al. Overexpression of antizyme-inhibitor in NIH3T3 fibroblasts provides growth advantage through neutralization of antizyme functions. *Oncogene.* 2006, 25: 5163-5172.
- Kaur K, Emmett K, McCann PP, Sjoerdsma A, Ullman B. Effects of DL-alpha-difluoromethylornithine on *Leishmania donovani* promastigotes. *J Protozool.* 1986, 33: 518-521.
- Kern AD, Oliveira MA, Coffino P, Hackert ML. Structure of mammalian ornithine decarboxylase at 1.6 Å resolution: stereochemical implications of PLP-dependent amino acid decarboxylases. *Structure.* 1999, 7: 567-581.
- Khomutov RM, Dixon HB, Vdovina LV, et al. N-(5'-Phosphopyridoxyl) glutamic acid and N-(5'-phosphopyridoxyl)-2-oxopyrrolidine-5-carboxylic acid and their action on the apoenzyme of aspartate aminotransferase. *Biochem J.* 1971, 124: 99-106.
- Kilpeläinen P, Rybnikova E, Hietala O, Pelto-Huikko M. Expression of ODC and its regulatory protein antizyme in the adult rat brain. *J Neurosci Res.* 2000, 62: 675-685.
- Kitani T, Fujisawa H. Influence of salts on the activity and the subunit structure of ornithine decarboxylase from rat liver. *Biochim Biophys. Acta.* 1984, 784: 164-167.
- Kitani T, Fujisawa H. Purification and characterization of antizyme inhibitor of ornithine decarboxylase from rat liver. *Biochim Biophys Acta.* 1989, 991: 44-49.
- Koski P, Vaara M. Polyamines as constituents of the outer membranes of *Escherichia coli* and *Salmonella typhimurium*. *J Bacteriol.* 1991, 173: 3695-3699.
- Kumari V, Sharma R, Yadav VP, Gupta AK, Bhattacharya A, et al. Differential distribution of a SINE element in the *Entamoeba histolytica* and *Entamoeba dispar* genomes: role of the LINE-encoded endonuclease. *BMC Genomics.* 2011, 12: 267.



- Kumar AP, Mar PK, Zhao B, Montgomery RL, Kang DC, et al. Regulation of rat ornithine decarboxylase promoter activity by binding of transcription factor Sp1. *J Biol Chem.* 1995, 270: 4341-4348.
- Kumar A, Singh JD. An organoselenium-based highly sensitive and selective fluorescent "turn-on" probe for the Hg<sup>2+</sup> ion. *Inorg Chem.* 2012, 51: 772-774.
- Kusama-Eguchi K, Irisawa M, Watanabe S, Watanabe K, Igarashi K. Increase in fidelity of rat liver Ile-tRNA formation by both spermine and the aminoacyl-tRNA synthetase complex. *Arch Biochem Biophys.* 1991, 288: 495-499.
- Kuznetsov V, Radyukina NL, Shevyakova NI. Polyamines and stress: biological role, metabolism and regulation. *Russ J Plant Physiol.* 2006, 53: 583-604.
- Koski P, Vaara M. Polyamines as constituents of the outer membranes of *Escherichia coli* and *Salmonella typhimurium*. *J Bacteriol.* 1991, 173: 3695-3699.
- Kyriakidis DA, Heller JS, Canellakis ES. Modulation of ornithine decarboxylase activity in *Escherichia coli* by positive and negative effectors. *Proc Natl Acad Sci USA.* 1978, 75: 4699-4703.
- Kyriakidis DA, Heller JS, Canellakis ES: Purification of ornithine decarboxylase antizymes (*Escherichia coli*). *Meth Enzymol.* 1983, 94: 193-199.
- Kyriakidis DA: Effect of plant growth hormone and polyamines on ornithine decarboxylase activity during the germination of barley seeds. *Plant Physiol.* 1983, 57: 499-508.
- Laitinen J, Stenius K, Eloranta TO, Hölttä E. Polyamines may regulate S-phase progression but not the dynamic changes of chromatin during the cell cycle. *J Cell Biochem.* 1998, 68: 200-212.
- Lapointe DS, Cohen RJ. Ornithine decarboxylase in *Phycomyces*: *in vitro* and *in vivo* properties. *Arch Biochem Biophys.* 1983, 224: 515-525.
- Lee YS, Cho YD. Identification of essential active-site residues in ornithine decarboxylase of *Nicotiana glutinosa* decarboxylating both L-ornithine and L-lysine. *Biochem J.* 2001, 360: 657-665.
- Lee J, Michael AJ, Martynowski D, Goldsmith EJ, Phillips MA. Phylogenetic diversity and the structural basis of substrate specificity in the beta/alpha-barrel fold basic amino acid decarboxylases. *J Biol Chem.* 2007, 282: 27115-27125.

- Leippe M, Herbst R. Ancient weapons for attack and defense: the pore-forming polypeptides of pathogenic enteric and free-living amoeboid protozoa. *J Eukaryot Microbiol.* 2004, 51: 516-521.
- Leitner A, Reischl R, Walzthoeni T, Herzog F, Bohn S, et al. Expanding the chemical cross-linking toolbox by the use of multiple proteases and enrichment by size exclusion chromatography. *Mol Cell Proteomics.* 2012, 11: M111.014126.
- Leon-Avila G, Tovar J. Mitosomes of *Entamoeba histolytica* are abundant mitochondrion-related remnant organelles that lack a detectable organellar genome. *Microbiology.* 2004, 150: 1245-1250.
- Lewis JS, Thomas TJ, Shirahata A, Thomas T. Oligodeoxyribonucleotide harboring the estrogen response element in the presence of polyamines: ionic, structural, and DNA sequence specificity effects. *Biomacromolecules.* 2000, 1: 339-349.
- Li X, Coffino P. Regulated degradation of ornithine decarboxylase requires interaction with the polyamine-inducible protein antizyme. *Mol Cell Biol.* 1992, 12: 3556-3562.
- Lioliou EE, Kyriakidis DA. The role of bacterial antizyme: From an inhibitory protein to AtoC transcriptional regulator. *Microb Cell Fact.* 2004, 3: 8.
- Liu YC, Hsu DH, Huang CL, Liu YL, Liu GY, et al. Determinants of the differential antizyme-binding affinity of ornithine decarboxylase. *PLoS One.* 2011, 6: e26835.
- Linding R, Jensen LJ, Diella F, Bork P, Gibson TJ, et al. Protein disorder prediction: implications for structural proteomics. *Structure.* 2003, 11: 1453-1459.
- Linding R, Russell RB, Neduva V, Gibson TJ. GlobPlot: Exploring protein sequences for globularity and disorder. *Nucleic Acids Res.* 2003 Jul 1;31(13):3701-8.
- Lockless SW, Ranganathan R. Evolutionarily conserved pathways of energetic connectivity in protein families. *Science.* 1999, 286: 295-299.
- Loftus B, Anderson I, Davies R, Alsmark UC, Samuelson J, et al. The genome of the protist parasite *Entamoeba histolytica*. *Nature.* 2005, 433: 865-868.
- López-Vallejo F, Castillo R, Yépez-Mulia L, Medina-Franco JL, Benzotriazoles and indazoles are scaffolds with biological activity against *Entamoeba histolytica*. *J Biomol Screen.* 2011, 16: 862-868.

- Lorenzi HA, Puiu D, Miller JR, Brinkac LM, Amedeo P, et al. New assembly, reannotation and analysis of the *Entamoeba histolytica* genome reveal new genomic features and protein content information. *PLoS Negl Trop Dis*. 2010, 4: e716.
- Lu L, Stanley BA, Pegg AE. Identification of residues in ornithine decarboxylase essential for enzymic activity and for rapid protein turnover. *Biochem J*. 1991, 277: 671-675.
- Luthy R, Bowie JU, Eisenberg D. Assessment of protein models with three-dimensional profiles. *Nature*. 1992, 356: 83-85.
- Mackintosh CA, Pegg AE. Effect of spermine synthase deficiency on polyamine biosynthesis and content in mice and embryonic fibroblasts, and the sensitivity of fibroblasts to 1,3-bis-(2-chloroethyl)-N-nitrosourea. *Biochem J*. 2000, 351: 439-447.
- Mangold U. Antizyme inhibitor: mysterious modulator of cell proliferation. *Cell Mol Life Sci*. 2006, 63: 2095-2101.
- Mangold U, Hayakawa H, Coughlin M, Munger K, Zetter BR. Antizyme, a mediator of ubiquitin-independent proteasomal degradation and its inhibitor localize to centrosomes and modulate centriole amplification. *Oncogene*. 2008, 27: 604-613.
- Mangold U, Leberer E. Regulation of all members of the antizyme family by antizyme inhibitor. *Biochem J*. 2005, 385: 21-28.
- Mann BJ. *Entamoeba histolytica* Genome Project: an update. *Trends Parasitol*. 2002, 18: 147-148.
- Marinets A, Zhang T, Guillen N, et al. Protection against invasive amebiasis by a single monoclonal antibody directed against a lipophosphoglycan antigen localized on the surface of *Entamoeba histolytica*. *J Exp Med*. 1997, 186: 1557-1565.
- Marton LJ, Pegg AE. Polyamines as targets for therapeutic intervention. *Annu Rev Pharmacol Toxicol*. 1995, 35: 55-91.
- Marty C, Mori G, Sabini L, Rivarola V. Effects of  $\alpha$ -difluoromethylornithine on the cyclin A expression in Hep-2 cells. *Biocell*. 2000, 24: 49-52.
- Matsufuji S, Matsufuji T, Miyazaki Y, Murakami Y, Atkins JF, et al. Autoregulatory frameshifting in decoding mammalian ornithine decarboxylase antizyme. *Cell*. 1995, 80: 51-60.

- Mayhoub AS, Khaliq M, Botting C, Li Z, Kuhn RJ, et al. An investigation of phenylthiazole antitrypanosomal agents. *Bioorg Med Chem* 2011, 19: 3845-3854.
- McCann PP, Bacchi CJ, Clarkson AB Jr, Seed JR, Nathan HC, et al. Further studies on difluoromethylornithine in African *trypanosomes*. *Med Biol*. 1981, 59: 434-440.
- McKerrow JH, Sun E, Rosenthal PJ, Bouvier J. The proteases and pathogenicity of parasitic protozoa. *Annual Review of Microbiology* 1993, 47: 821-853.
- Meyer LJ, Becker MA. Human erythrocyte phosphoribosylpyrophosphate synthetase. dependence of activity on state of subunit association. *J Biol Chem*. 1977, 252: 3919-3925.
- Mitchell JL, Judd GG, Bareyal-Leyser A, Ling SY. Feedback repression of polyamine transport is mediated by antizyme in mammalian tissue-culture cells. *Biochem J*. 1994, 299: 19-22.
- Mitchell JL, Carter DD, Rybski JA. Control of ornithine decarboxylase activity in *Physarum* by polyamines. *Eur J Biochem*. 1978, 92: 325-331.
- Mitchell JLA, Rynning MD, Hong HJ, Hicks HF. Interaction between the charge isoforms of mammalian ornithine decarboxylase. *Arch Biochem Biophys*. 1988, 264: 585-594.
- Miyazaki Y, Matsufuji S, Hayashi S. Cloning and characterization of a rat gene encoding ornithine decarboxylase antizyme. *Gene*. 1992, 113: 191-197.
- Momany C, Ernst S, Ghosh R, Chang NL, Hackert ML. Crystallographic structure of a PLP-dependent ornithine decarboxylase from *Lactobacillus* 30a to 3.0 Å resolution. *J Mol Biol*. 1995, 252: 643-655.
- Morgan DM. Polyamines. An overview. *Mol Biotechnol*. 1999, 11: 229-250.
- Mukherjee C, Majumder S, Lohia A. Inter-cellular variation in DNA content of *Entamoeba histolytica* originates from temporal and spatial uncoupling of cytokinesis from the nuclear cycle. *PLoS Negl Trop Dis*. 2009, 3: e409.
- Müller S, Dadara A, Lüersen K, Wrenger C, Gupta RD, et al. In the human malaria parasite *Plasmodium falciparum*, polyamines are synthesized by a bifunctional ornithine decarboxylase, S-adenosylmethionine decarboxylase. *J Biol Chem*. 2000, 275: 8097-8102.

- Murakami Y, Tanahashi N, Tanaka K, Omura S, Hayashi SI. Proteasome pathway operates for the degradation of ornithine decarboxylase in intact cells. *Biochem J*. 1996, 317: 77-80.
- Murakami Y, Matsufuji S, Kameji T, Hayashi S, Igarashi K, Ornithine decarboxylase is degraded by the 26S proteasome without ubiquitination. *Nature*. 1992, 360: 597-599.
- Murakami Y, Suzuki J, Samejima K, Oka T. Developmental alterations in expression and subcellular localization of antizyme and antizyme inhibitor and their functional importance in the murine mammary gland. *Amino Acids*. 2010, 38: 591-601.
- Murzin AG, Brenner SE, Hubbard T, Chothia C. SCOP: a structural classification of proteins database for the investigation of sequences and structures. *J Mol Biol*. 1995, 247: 536-540.
- Myers DP, Jackson LK, Ipe VG, Murphy GE, Phillips MA. Long-range interactions in the dimer interface of ornithine decarboxylase are important for enzyme function. *Biochemistry*. 2001, 40: 13230-13236.
- Nilsson J, Gritli-Linde A, Heby O. Skin fibroblasts from spermine synthase-deficient hemizygous gyro male (G/Y) mice overproduce spermidine and exhibit increased resistance to oxidative stress but decreased resistance to UV irradiation. *Biochem J*. 2000, 352: 381-387.
- Nilsson J, Grahn B, Heby O. Antizyme inhibitor is rapidly induced in growth-stimulated mouse fibroblasts and releases ornithine decarboxylase from antizyme suppression. *Biochem J*. 2000, 346: 699-704.
- North ML, Looockwood BC, Bremner AF, Coombs GH. Polyamine biosynthesis in *Trichomonas*. *Mol Biochem Parasitol*. 1986, 19: 241-249
- North TW, Wyler DJ. DNA synthesis in promastigotes of *Leishmania major* and *L. donovani*. *Mol Biochem Parasitol*. 1987, 22: 215-221.
- Ogier G, Chantepie J, Deshayes C, et al. Contribution of 4-methylthio-2-oxobutanoate and its transaminase to the growth of methionine dependent cells in culture. Effect of transaminase inhibitors. *Biochem Pharmacol*. 1993, 45: 1631-1644.



- Ondarza RN, Hurtado G, Iturbe A, Hernández E, Tamayo E, et al. Identification of trypanothione from the human pathogen *Entamoeba histolytica* by mass spectrometry and chemical analysis. *Biotechnol Appl Biochem*. 2005, 42: 175-181.
- Ondarza RN, Tamayo EM, Hurtado G, Hernández E, Iturbe A. Isolation and purification of glutathionyl-spermidine and trypanothione from *Entamoeba histolytica*. *Arch Med Res*. 1997, 28: 73-75.
- Oredsson SM. Polyamine dependence of normal cell-cycle progression. *Biochem Soc Trans*. 2003, 31: 366-370.
- Osterman AL, Brooks HB, Jackson L, Abbott JJ, Phillips MA. Lysine-69 plays a key role in catalysis by ornithine decarboxylase through acceleration of the Schiff base formation, decarboxylation, and product release steps. *Biochemistry*. 1999, 38: 11814-11826.
- Osterman A, Grishin NV, Kinch LN, Phillips MA. Formation of functional cross-species heterodimers of ornithine decarboxylase. *Biochemistry*. 1994, 33: 13662-13667.
- Osterman AL, Kinch LN, Grishin NV, Phillips MA. Acidic residues important for substrate binding and cofactor reactivity in eukaryotic ornithine decarboxylase identified by alanine scanning mutagenesis. *J Biol Chem*. 1995, 270: 11797-11802.
- Osterman AL, Brooks HB, Rizo J, Phillips MA. Role of Arg-277 in the binding of pyridoxal 5'-phosphate to *Trypanosoma brucei* ornithine decarboxylase. *Biochemistry*. 1997, 36: 4558-4567.
- Osterman AL, Lueder DV, Quick M, Myers D, Canagarajah BJ. Domain organization and a protease-sensitive loop in eukaryotic ornithine decarboxylase. *Biochemistry*. 1995, 34: 13431-13436.
- Palavan-Unsal N, Aloglu-Senturk SM, Arsan D. The function of polyamine metabolism in prostate cancer. *Exp Oncol*. 2006, 28: 178-186.
- Pantazaki AA, Anagnostopoulos CG, Lioliou EE, Kyriakidis DA. Characterization of ornithine decarboxylase and regulation by its antizyme in *Thermus thermophilus*. *Mol Cell Biochem*. 1999, 195: 55-64.
- Parchment RE, Pierce GB. Polyamine oxidation, programmed cell death, and regulation of melanoma in the murine embryonic limb. *Cancer Res*. 1989, 49: 6680-6686.

- Park MH, Lee YB, Joe YA. Hypusine is essential for eukaryotic cell proliferation. *Biological Signals* 1997, 6: 115-123.
- Parsons M. Glycosomes: Parasites and the divergence of peroxisomal purpose. *Mol. Microbiol.* 2004, 53: 717-724.
- Pegg AE. Investigation of the turnover of rat liver S-adenosylmethionine decarboxylase using a specific antibody. *J Biol Chem.* 1979, 254: 3249-3253.
- Pegg AE. Recent advances in the biochemistry of polyamines in eukaryotes. *Biochem. J.* 1986, 234: 249-262.
- Pegg AE, Madhubala R, Kameji T, Bergeron RJ. Control of ornithine decarboxylase activity in alpha-difluoromethylornithine-resistant L1210 cells by polyamines and synthetic analogues. *J Biol Chem.* 1988, 263: 11008-11014.
- Persson L, Oredsson SM, Anehus S, Heby O. Ornithine decarboxylase inhibitors increase the cellular content of the enzyme: implications for translational regulation. *Biochem Biophys Res Commun.* 1985, 131: 239-245.
- Petri WA Jr. Therapy of intestinal protozoa. *Trends Parasitol.* 2003, 19: 523-526.
- Petri WA Jr. Protozoan parasites that infect the gastrointestinal tract. *Curr Opin Gastroenterol.* 2000, 16: 18-23.
- Phillips R, Press MC, Bingham L, Grimmer G. Polyamines in cultured artichoke explants: effects are primarily on xylogenesis rather than cell division. *J Exp Bot.* 1988, 39: 473-480.
- Piacenza L, Peluffo G, Radi R. L-arginine-dependent suppression of apoptosis in *Trypanosoma cruzi*: Contribution of the nitric oxide and polyamine pathways. *Proc Natl Acad Sci USA.* 2001, 98: 7301-7306.
- Pilz RB, Steglich C, Scheffler IE. Molecular and genetic characterization of an ornithine decarboxylase-deficient Chinese hamster cell line. *J Biol Chem.* 1990, 265: 8880-8886.
- Pineda E, Encalada R, Rodríguez-Zavala JS, Olivos-García A, et al. Pyruvate: ferredoxin oxidoreductase and bifunctional aldehyde-alcohol dehydrogenase are essential for energy metabolism under oxidative stress in *Entamoeba histolytica*. *FEBS J.* 2010, 277: 3382-3395.

- Pfeffer LM, Yang CH, Pfeffer SR, Murti A, McCormack SA, et al. Inhibition of ornithine decarboxylase induces STAT3 tyrosine phosphorylation and DNA binding in IEC-6 cells. *Am J Physiol Cell Physiol.* 2000, 278: 331-335.
- Poulin R, Ackermann LB, Bey P, Pegg AE. Mechanism of the irreversible inactivation of mouse ornithine decarboxylase by  $\alpha$ -difluoromethylornithine. Characterization of sequences at the inhibitor and coenzyme binding sites. *J Biol Chem.* 1992, 267: 150-158.
- Preeti, Tapas S, Kumar P, Madhubala R, Tomar S. Biochemical, Mutational and *in silico* structural evidence for a functional dimeric form of the ornithine decarboxylase from *Entamoeba histolytica*. *PLoS Negl Trop Dis.* 2012, 6: e1559.
- Qian J, Luscombe NM, Gerstein, M. Protein family and fold occurrence in genomes: power-law behaviour and evolutionary model. *J Mol Biol,* 2001, 313: 673-681.
- Que X, Reed SL. The role of extracellular cysteine proteinases in pathogenesis of *Entamoeba histolytica* invasion. *Parasitology Today.* 1997, 13: 190-193.
- Raso V, Stollar BD. The antibody-enzyme analogy. Comparison of enzymes and antibodies specific for phosphopyridoxyltyrosine. *Biochemistry.* 1975, 14: 591-599.
- Raso V, Stollar BD. The antibody-enzyme analogy. Characterization of antibodies to phosphopyridoxyltyrosine derivatives. *Biochemistry.* 1975, 14: 584-591.
- Rathaur S, Wittich RM, Walter RD. *Ascaris suum* and *Onchocerca volvulus*: S-adenosylmethionine decarboxylase. *Exp Parasitol.* 1988, 65: 277-281.
- Ravanko K, Järvinen K, Paasinen-Sohns A, Hölttä E. Loss of p27Kip1 from cyclin E/cyclin-dependent kinase (CDK) 2 but not from cyclin D1/CDK4 complexes in cells transformed by polyamine biosynthetic enzymes. *Cancer Res.* 2000, 60: 5244-5253.
- Ren L, Qin X, Cao X, Wang L, Bai F, et al. Structural insight into substrate specificity of human intestinal maltase-glucoamylase. *Protein Cell.* 2011, 2: 827-836.
- Reeves RE. Metabolism of *Entamoeba histolytica* Schaudinn, 1903. *Adv Parasitol.* 1984, 23: 105-142.
- Robertson JG. Mechanistic basis of enzyme-targeted drugs. *Biochemistry.* 2005, 44: 5561-5571.

- Rosas-Arreguín P, Arteaga-Nieto P, Reynoso-Orozco R, Villagómez-Castro JC, Sabanero-López M, et al. *Bursera fagaroides*, effect of an ethanolic extract on ornithine decarboxylase (ODC) activity in vitro and on the growth of *Entamoeba histolytica*. *Exp Parasitol*. 2008, 119: 398-402.
- Rose PP, Hanna SL, Spiridigliozzi A, Wannissorn N, Beiting DP, et al. Natural resistance-associated macrophage protein is a cellular receptor for sindbis virus in both insect and mammalian hosts. *Cell Host Microbe*. 2011, 10: 97-104.
- Rosenberg-Hasson Y, Bercovich V, Kahana C. Cis-Recognition and degradation of ornithine decarboxylase subunits in reticulocyte lysate. *Biochem J*. 1991, 277: 683-685.
- Riekenberg S, Flockenhaus B, Vahrman A, Müller MC, Leippe M, et al. The beta-N-acetylhexosaminidase of *Entamoeba histolytica* is composed of two homologous chains and has been localized to cytoplasmic granules. *Mol Biochem Parasitol*. 2004, 138: 217-225.
- Russell DH. Posttranslational modification of ornithine decarboxylase by its product putrescine. *Biochem Biophys Res Commun*. 1981, 99: 1167-1172.
- Saavedra E, Encalada R, Pineda E, Jasso-Chavez R, Moreno-Sanchez R. Glycolysis in *Entamoeba histolytica*. Biochemical characterization of recombinant glycolytic enzymes and flux control analysis. *FEBS J*. 2005, 272: 1767-1783.
- Sali A, Blundell TL. Comparative protein modelling by satisfaction of spatial restraints. *J Mol Biol*. 1993, 234: 779-815.
- Sanchez CP, Sidrauski C, Menezes-Freire S, Gonzalez NS, Algranati D. Ornithine decarboxylase from *Leishmania mexicana* promastigotes: interaction with pyridoxal 5'-phosphate and  $\alpha$ -difluoromethylornithine. *Biochem Biophys Res Commun*. 1995, 212: 396-403.
- Sandmeier E, Hale TI, Christen P. Multiple evolutionary origin of pyridoxal-5'-dependent amino acid decarboxylases. *Eur J Biochem*. 1994, 221: 997-1002.
- Sarakatsannis JN, Duan Y. Statistical characterization of salt bridges in proteins. *Proteins*. 2005, 60: 732-739.

- Sauve DM, Anderson HJ, Ray JM, James WM, Roberge M. Phosphorylation-induced rearrangement of the histone H3 NH<sub>2</sub>-terminal domain during mitotic chromosome condensation. *J Cell Biol.* 1999, 145: 225-235.
- Seely JE, Pösö H, Pegg AE. Effects of androgens on turnover of ornithine decarboxylase in mouse kidney. *J Biol Chem.* 1982, 257: 7549-7553.
- Seely JE, Pegg AE. Effect of 1,3-diaminopropane on ornithine decarboxylase enzyme protein in thioacetamide-treated rat liver. *Biochem J.* 1983, 216: 701-707.
- Seiler N. Oxidation of polyamines and brain injury. *Neurochem Res* 2000, 25: 471-490.
- Seiler N. Thirty years of polyamine-related approaches to cancer therapy. Retrospect and prospect. Part 1. Selective enzyme inhibitors. *Curr Drug Targets.* 2003, 4: 537-564.
- Seiler N. Thirty years of polyamine-related approaches to cancer therapy. Retrospect and prospect. Part 2. Structural analogues and derivatives. *Curr Drug Targets.* 2003, 4: 565-585.
- Seo M, Kim JD, Neau D, Sehgal I, Lee YH. Structure-based development of small molecular PFKFB3 inhibitors: a frame work for potential cancer therapeutic agents targeting agents targeting the Warburg effect. *PLoS One.* 2011, 6: e24179.
- Sertich GJ, Pegg AE. Polyamine administration reduces ornithine decarboxylase activity without affecting its mRNA content. *Biochem Biophys Res Commun.* 1987, 143: 424-430.
- Sharma V, Visen PK, Katiyar JC, Wittich RM, Walter RD, et al. Polyamine metabolism in *Ancylostoma ceylanicum* and *Nippostrongylus brasiliensis*. *Int J Parasitol.* 1989, 19: 191-198.
- Shayovits A, Bachrach U. Immunohistochemical detection of ornithine decarboxylase in individual cells: potential application for in vitro chemosensitivity assays. *J Histochem Cytochem.* 1994, 42: 607-611.
- Shayovits A, Bachrach U. Ornithine decarboxylase: An indicator for growth of NIH 3T3 fibroblasts and their c-Ha-ras transformants. *Biochim Biophys Acta.* 1995, 1267: 107-114.
- Shibayama M, Campos-Rodríguez R, Ramírez-Rosales A, Flores-Romo L, Espinosa-Cantellano M, et al. *Entamoeba histolytica*: liver invasion and abscess production



- by intraperitoneal inoculation of trophozoites in hamsters, *Mesocricetus auratus*. *Exp Parasitol*. 1998, 88: 20-27.
- Shirahata A, Pegg AE. Regulation of S-adenosylmethionine decarboxylase activity in rat liver and prostate. *J Biol Chem*. 1985, 260: 9583-9588.
- Shur O, Wu J, Cropek DM, Banta S. Monitoring the conformational changes of an intrinsically disordered peptide using a quartz crystal microbalance. *Protein Sci*. 2011, 20: 925-930. doi: 10.1002/pro.625.
- Singh AK, Pandey N, Sinha M, Kaur P, Sharma S, et al. Structural evidence for the order of preference of inorganic substrates in mammalian heme peroxidases: crystal structure of the complex of lactoperoxidase with four inorganic substrates, SCN, I, Br and Cl. *Int J Biochem Mol Biol*. 2011, 2: 328-339.
- Silverman RB, Hawe WP. SAR studies of fluorine-substituted benzylamines and substituted 2-phenylethylamines as substrates and inactivators of monoamine oxidase B. *J Enzyme Inhib*. 1995, 9: 203-215.
- Sistonen L, Hölttä E, Lehväslaiho H, Lehtola L, Alitalo K. Activation of the neu tyrosine kinase induces the fos/jun transcription factor complex, the glucose transporter and ornithine decarboxylase. *J Cell Biol*. 1989, 109: 1911-1919.
- Sistonen L, Hölttä E, Mäkela TP, Keski-Oja J, Alitalo K. The cellular response to induction of the p21 c-Ha-ras oncoprotein includes stimulation of jun gene expression. *EMBO J*. 1989, 8: 815-822.
- Solano F, Peñafiel R, Solano ME, Lozano JA. Equilibrium between active and inactive forms of rat liver ornithine decarboxylase mediated by L-ornithine and salts. *FEBS Lett* 1985, 190: 324-328.
- Stanley SL Jr. Amoebiasis. *Lancet*. 2003, 361: 1025-1034.
- Stanley SL Jr, Huizenga H, Li E. Isolation and partial characterization of a surface glycoconjugate of *Entamoeba histolytica*. *Mol Biochem Parasitol*. 1992, 50: 127-138.
- Stevens BC. Preventing fatal overdose. *Nurs Mirror*. 1977, 145: 47-48.
- Stevens L, McKinnon IM, Turner RM, North MJ. The effects of 1,4-diaminobutanone on polyamine metabolism in bacteria, a cellular slime mould and rat tissues. *Biochem Soc Trans*. 1978, 6: 407-409.

- Stockis A, Allemon AM, De Bruyn S, Gengler C. Nitazoxanide pharmacokinetics and tolerability in man after single ascending doses. *Int J Clin Pharmacol Ther.* 2002, 40: 213-220.
- Su KL, Liao YF, Hung HC, Liu GY. Critical factors determining dimerization of human antizyme inhibitor. *J Biol Chem.* 2009, 284: 26768-26777.
- Suorsa A, Hietala O, Pajunen A. Developmental expression of ornithine and S-adenosylmethionine decarboxylases in mouse brain. *Biochem Biophys Res Commun.* 1992, 184: 1114-1118.
- Suzuki T, He Y, Kashiwagi K, Murakami Y, Hayashi S, Igarashi K. Antizyme protects against abnormal accumulation and toxicity of polyamines in ornithine decarboxylase-overproducing cells. *Proc Natl Acad Sci U S A.* 1994, 91: 8930-8934.
- Swanson T, Brooks HB, Osterman AL, O'Leary MH, Phillips MA. Carbon-13 isotope effect studies of *Trypanosoma brucei* ornithine decarboxylase. *Biochemistry.* 1998, 37: 14943-14947.
- Szczepanowska J, Malinska D, Wieckowski MR, Duszynski J. Effect of mtDNA point mutations on cellular bioenergetics. *Biochim Biophys Acta.* 2012, Epub ahead of print
- Tabor CV, Tabor H. Polyamines. *Annu Rev Biochem.* 1984, 53: 749-790.
- Tabor H, Tabor CW, Irreverre F. Quantitative determination of aliphatic diamines and polyamines by an automated liquid chromatography procedure. *Anal Biochem.* 1973, 55: 457-467.
- Tabor CW, Tabor H. Polyamines in microorganisms. *Microbiol Rev.* 1985, 49: 81-99.
- Takemoto T, Nagamatsu Y, Oka T. The study of spermidine-stimulated polypeptide synthesis in cell-free translation of mRNA from lactating mouse mammary gland. *Biochem Biophys Acta.* 1983, 740: 73-79.
- Takeuchi J, Chen H, Coffino P. Proteasome substrate degradation requires association plus extended peptide. *EMBO J.* 2007, 26: 123-131.
- Tanyuksel M, Petri WA Jr. Laboratory diagnosis of amebiasis. *Clin Microbiol Rev* 2003, 16: 713-729.

- Tatusov R L, Koonin EV, Lipman DJ. A genomic perspective on protein families. *Science*. 1997, 278: 631-637.
- Tatusov RL, Natale DA, Garkavtsev IV, Tatusova TA, Shankavaram UT, et al. The COG database: new developments in phylogenetic classification of proteins from complete genomes. *Nucleic Acids Res*. 2001, 29: 22-28.
- Terán-Figueroa Y, Arteaga-Nieto P, Bethancourt-Rodríguez A, Labra-Barrios ML, Luna-Arias JP, et al. *Entamoeba histolytica*, heterologous expression and in situ immunolocalization of ornithine decarboxylase (*EhODC*). *Exp Parasitol*. 2009, 123: 99-104.
- Thomas T, Thomas TJ. Polyamines in cell growth and cell death: molecular mechanisms and therapeutic applications. *Cell Mol Life Sci*. 2001, 58: 244-258.
- Thomas T, Kulkarni GD, Gallo MA, Greenfield N, Lewis JS, et al. Effects of natural and synthetic polyamines on the conformation of an oligodeoxyribonucleotide with the estrogen response element. *Nucleic Acids Res* 1997, 25: 2396-2402.
- Thompson JD, Higgins DG, Gibson TJ. CLUSTAL W: improving the sensitivity of progressive multiple sequence alignment through sequence weighting, position-specific gap penalties and weight matrix choice. *Nucleic Acids Res* 1994, 22: 4673-4680.
- Tibayrenc M, Kjellberg F, Ayala FJ. A clonal theory of parasitic protozoa: the population structures of *Entamoeba*, *Giardia*, *Leishmania*, *Naegleria*, *Plasmodium*, *Trichomonas*, and *Trypanosoma* and their medical and taxonomical consequences. *Proc Natl Acad Sci USA*. 1990, 87: 2414-2418.
- Tillack M, Biller L, Irmer H, Freitas M, Gomes MA, et al. The *Entamoeba histolytica* genome: primary structure and expression of proteolytic enzymes. *BMC Genomics*. 2007, 8: 170.
- Tiburcio AF, Gendy CA, Tran Thanh Van K. Morphogenesis in tobacco subepidermal cells: Putrescine as a marker of root differentiation. *Plant Cell Tiss Org Cult*. 1989, 19: 43-54.
- Tiburcio AF, Kaur-Sawhney R, Galston AW. Polyamine metabolism. In Intermediatory Nitrogen Metabolism. *The Biochemistry of Plants*. Miflin B, Lea PJ. 1990, 16: 283-325.

- Tobias KE, Mamroud-kidron E, Kahana C. Gly387 of murine ornithine decarboxylase is essential for the formation of stable homodimers. *Eur J biochem.* 1993, 218: 245-250.
- Tobias KE, Kahana C. Intersubunit location of the active site of mammalian ornithine decarboxylase as determined by hybridization of site-directed mutants. *Biochemistry*, 1993, 32: 5842-5847.
- Tomar AK, Sooch BS, Yadav S. Computational analysis of Concanavalin A binding glycoproteins of human seminal plasma. *Bioinformation.* 2011, 7: 69-75.
- Toney M. Reaction specificity in pyridoxal phosphate enzymes. *Arch Biochem Biophys.* 2005 433: 279-287.
- Tosaka Y, Tanaka H, Yano Y, Masai K, Nozaki M, et al. Identification and characterization of testis specific ornithine decarboxylase antizyme (OAZ-t) gene: expression in haploid germ cells and polyamine induced frameshifting. *Genes Cells.* 2000, 5: 265-276.
- Tovar J, Fischer A, Clark CG. The mitosome, a novel organelle related to mitochondria in the amitochondriate parasite *Entamoeba histolytica*. *Mol Microbiol.* 1999, 32: 1013-1021.
- Tsirka SE, Turck CW, Coffino P. Multiple active conformers of mouse ornithine decarboxylase. *Biochem J.* 1993, 293: 289-295.
- Tsirka S, Coffino P. Dominant negative mutants of ornithine decarboxylase. *J Biol Chem.* 1992, 267: 23057-23062.
- Vagin AA, Steiner RA, Lebedev AA, Potterton L, McNicholas S, et al. REFMAC5 dictionary: organization of prior chemical knowledge and guidelines for its use. *Acta Crystallogr D Biol Crystallogr.* 2004, 60: 2184-2195.
- Vagin A, Teplyakov A. MOLREP: an automated program for molecular replacement. *J Appl Cryst.* 1997, 30: 1022-1025.
- Vannier-Santos MA, Menezes D, Oliveira MF, de Mello FG. The putrescine analogue 1,4-diamino-2-butanone affects polyamine synthesis, transport, ultrastructure and intracellular survival in *Leishmania amazonensis*. *Microbiology.* 2008, 154: 3104-3111.

- Vertino PM, Bergeron RJ, Cavanaugh PF Jr., Porter CW. Structural determinants of spermidine-DNA interactions. *Biopolymers*. 1987, 26: 691-703.
- Vicente JB, Ehrenkaufer GM, Saraiva LM, Teixeira M, Singh U. *Entamoeba histolytica* modulates a complex repertoire of novel genes in response to oxidative and nitrosative stresses: implications for amebic pathogenesis. *Cell Microbiol*. 2009, 11: 51-69.
- Vlastos AT, West LA, Atkinson EN, Boiko I, Malpica A, et al. Results of a phase II double-blinded randomized clinical trial of difluoromethylornithine for cervical intraepithelial neoplasia grades 2 to 3. *Clin Cancer Res*. 2005, 11: 390-396.
- Wallace HM, Fraser AV, Hughes A. A prospective of polyamine metabolism. *Biochem J*. 2003, 376: 1-14.
- Wang Y, Ashkenazi YJ, Bachrach U. In vitro chemosensitivity testing of hematological cancers: immunohistochemical detection of ornithine decarboxylase. *Anticancer Drugs* 1999, 10: 797-805.
- Wang JY, McCormack SA, Viar MJ, Wang H, Tzen CY, et al. Decreased expression of protooncogenes c-fos, c-myc, and c-jun following polyamine depletion in IEC-6 cells. *Am J Physiol* 1993, 265: 331-338.
- Wang TW, Lu L, Wang D, Thompson JE. Isolation and characterization of senescence-induced cDNAs encoding deoxyhypusine synthase and eucaryotic translation initiation factor 5A from tomato. *J Biol Chem*. 2001, 276: 17541-17549.
- Wang Y, Devereux W, Stewart TM, Casero RA, Jr. Cloning and characterization of human polyamine-modulated factor-1, a transcriptional cofactor that regulates the transcription of the spermidine/spermine N(1)-acetyltransferase gene. *J Biol Chem*. 1999, 274: 22095-22101.
- Wang Y, Devereux W, Stewart TM, Casero RA Jr. Characterization of the interaction between the transcription factors human polyamine modulated factor (PMF-1) and NF-E2-related factor 2 (Nrf-2) in the transcriptional regulation of the spermidine/spermine N1-acetyltransferase (SSAT) gene. *Biochem J*. 2001, 355: 45-49.
- Wang J, Cao Z, Zhao L, Li S. Novel Strategies for Drug Discovery Based on Intrinsically Disordered Proteins (IDPs). *Int J Mol Sci*. 2011, 12: 3205-3219.



- Watanabe S, Kusama-Eguchi K, Kobayashi H, Igarashi K. Estimation of polyamine binding to macromolecules and ATP in bovine lymphocytes and rat liver. *J Biol Chem*. 1991, 266: 20803-20809.
- Wetlaufer DB, Malik SK, Stoller L, Coffin RL. Nonpolar group participation in the denaturation of proteins by urea and guanidinium salts. Model compound studies. *J Am Chem Soc*. 1964, 86: 508-514.
- Wiederstein M, Sippl MJ. ProSA-web: interactive web service for the recognition of errors in three-dimensional structures of proteins. *Nucl Acids Res*. 2007, 35: 407-410.
- Wilson CA, Kreychman J, Gerstein M. Assessing annotation transfer for genomics: quantifying the relations between protein sequence, structure and function through traditional and probabilistic scores. *J Mol Biol*. 2000, 297: 233-249.
- Wine Y, Cohen-Hadar N, Freeman A, Frolov F. Elucidation of the mechanism and end products of glutaraldehyde crosslinking reaction by X-ray structure analysis. *Biotechnol Bioeng*. 2007, 98: 711-718.
- Wittich RM, Kilian HD, Walter RD. Polyamine metabolism in filarial worms. *Mol Biochem Parasitol*. 1987, 24: 155-162.
- Wu F, Gehring H. Structural requirements for novel coenzyme-substrate derivatives to inhibit intracellular ornithine decarboxylase and cell proliferation. *FASEB J*. 2009, 23: 565-574.
- Yarlett N, Goldberg B, Moharrami MA, Bacchi CJ. *Trichomonas vaginalis*: characterization of ornithine decarboxylase. *Biochemical Journal*. 1993, 293: 487-493.
- Young ND. Plant Stress and Polyamine Metabolism: Induction of Arginine Decarboxylase in Stressed Oat Leaves. Ph.D. Thesis, Yale University. 1984.
- Young ND, Galston AW. Putrescine and acid stress: induction of arginine decarboxylase activity and putrescine accumulation by low pH. *Plant Physiol*, 1983, 71: 767-771.
- Yoshida M, Meksuriyen D, Kashiwagi K, Kawai G, Igarashi K. Polyamine stimulation of the synthesis of oligopeptide-binding protein (OppA). Involvement of a structural change of the Shine-Dalgarno sequence and the initiation codon aug in oppa mRNA. *J Biol Chem* 1999, 274: 22723-22728.

- Zhang Z, McCormick DB. Uptake and metabolism of N-(4'-pyridoxyl) amines by isolated rat liver cells. *Arch Biochem Biophys*. 1992, 294: 394-397.
- Zhang Z, McCormick DB. Uptake of N-(4'-pyridoxyl) amines and release of amines by renal cells: a model for transporter-enhanced delivery of bioactive compounds. *Proc Natl Acad Sci U S A*. 1991, 88: 10407-10410.
- Zheliaskova A, Naydenova S, Petrov AG. Interaction of phospholipid bilayers with polyamines of different length. *Eur Biophys*. 2000, 29: 153-157.
- Zhou C, Gee-Wan Wong O, Masters JR, Williamson M. Effect of Cancer-associated Mutations in the PlexinB1 Gene. *Mol Cancer*. 2012, 11: 11.
- Zou T, Mazan-Mamczarz K, Rao JN, Liu L, Marasa BS, et al. Polyamine depletion increases cytoplasmic levels of RNA-binding protein HuR leading to stabilization of nucleophosmin and p53 mRNAs. *J Biol Chem*. 2006, 281: 19387-19394.

